Experimental Characterisation of the Compressive Permanent Deformation Behaviour in Asphaltic Mixtures

by

Hasan Taherkhani

Thesis submitted to the University of Nottingham for the degree of Doctor of Philosophy

September 2006

DEPARTMENT OF CIVIL ENGINEERING

To my family

Abstract

In UK, rutting of flexible pavements is one of the most common forms of road failure. Permanent deformation of asphaltic layers has a significant contribution to the rutting. The main objective of this study is to improve current understanding of the permanent deformation behaviour of asphaltic mixtures. The research has focused on the compressive deformation behaviour of asphaltic mixtures under conditions that the loading time is considerably longer than that for the typical traffic loading. The approach used for this project was to experimentally investigate the steady-state viscous deformation and recovery behaviour and volumetric response of two typical asphaltic mixtures used in the UK; namely HRA30/10 and 10 mm DBM. These mixtures are representative of gap graded and continuously graded mixtures respectively. After investigation of the steady-state viscous deformation and recovery behaviour of the pure bitumen used in the mixtures as binder, the following tests were conducted on the mixtures:

- Uniaxial constant stress creep tests over a range of temperatures and stress levels.
- Uniaxial constant strain rate tests over a range of temperatures and strain rates.
- Uniaxial single creep recovery tests over a range of stress levels and temperatures.
- Uniaxial repeated creep recovery tests over a range of loading and recovery times.
- Triaxial creep tests over a range of deviatoric stresses and stress ratios.

The test results have been used for determination of the parameters of a non-linear viscoelastic constitutive model. The formulations of the model have been derived using the Burger's mechanical model comprising elastic, delayed elastic and viscous elements. The elastic and delayed elastic components are linear and the viscous component is stress-based non-linear and sensitive to confinement, temperature and damage accumulation. Using the parameters determined from test results the model is verified by simulating the creep and creep recovery test results.

Acknowledgements

I would like to express my appreciation to all persons and institutions who contributed to this research project through providing assistance, advice, encouragement, and financial and spiritual support during the course of my research. I would like to particularly thank the following:

- Professor Andrew Collop, my supervisor, for suggesting the research project, his guidance, invaluable advice and comments on my work, encouragement, friendship, and enthusiasm towards this project. I benefited from his great experience and knowledge throughout my studies.
- Professor Stephen Brown, for his invaluable guidance and advice on my project plan and research reports.
- Dr Salah Zoroob for the valuable discussions with him on my experimental work and reports during the course of this research work.
- Mr Barry Brodrick who provided valuable technical support during the course of my experimental work. In spite of his own heavy workload, he provided assistance to solve the problems with the machines and instruments.
- The staff of the NCPE laboratory, especially Murray Parry, Michael Winfield, Kevin Gilbert, Jon Watson, Laurence Pont, Neil Parkers, Michael Pepper and Richard Blakemore, for their assistance for providing the materials and making the specimens for this research.
- The researchers of the Nottingham Centre for Pavement Engineering, particularly, Joel, Alex, James, York, Ted, Joe, Wahab and Sami, with whom I had lots of long discussions from which I learned a lot to apply in my work and use in my future careers.
- The Ministry of Science, Research and Technology of Iran for funding the project and its financial support for paying my maintenance fees.
- Finally, very special thanks to my wife Mehrnaz and my son Kiarash for their patience, support and understanding throughout my studies.

Contents

Page

Declaration

The research described in this thesis was conducted at the University of Notingham, School of Civil Engineering between October 2002 and June 2005. I declare that the work is my own and has not been submitted for a degree of another university.

Hasan Taherkhani

Nottingham

July 2006

Introduction

1.1 A Brief History of Pavement Construction

An effective transport system is essential for the economic and social development of any nation. Roads are the most popular form of transportation system. Early roads were made for carriages, which in some cases, were paved and had drainage systems to keep them passable in wet weather. However, they were still weak and easily damaged and were not suitable for heavy traffic. Most of the ancient roads were constructed for governments to transport information and troops. The Silk Road from China to Rome and roads established by Persians, Egyptians, Romans and Incas are good examples of ancient roads. The Romans constructed a lot of roads with an overall length of approximately 85,000 km. The roman roads were built on a well-constructed embankment, using locally available materials in different layers, to produce well drained strong roads. They used a wooden mattress in marshy areas to prevent the roads from sinking. After the fall of the Rome Empire, these road networks were not maintained properly and deteriorated gradually. In the 18th Century, as a response to an increase in traffic volume and weight, more development in road construction occurred in France by Tresaguet, and in the UK by Thomas Telford

(1757-1834) and John Loudon McAdam (1756-1836) [Read, 1996]. Telford placed an emphasise on providing a strong foundation, using large stones and thick layers, whereas McAdam favoured a thinner construction of smaller angular materials watered to assist granular interlock, relying on the native soil strength [Croney *et al.*, 1998]. Asphaltic materials became popular at the end of the 19th Century, when automobiles started to become available to the public, and the need increased for dust free hard surfaces. At first, tar and naturally occurring asphalts were used to make mixtures for road surfaces. Later, bitumen refined from petroleum was mainly used in pavement construction.

1.2 Pavement Structure

Roads are constructed to carry traffic safely, economically and conveniently throughout their design life. A road pavement structure consists of a series of layers, and its function is to provide a dry, skid resistant, hard and even surface for vehicles. In terms of the materials used in the different layers, pavements are divided into three general types: rigid, flexible and composite pavements. In rigid pavements, concrete slabs are used as the main load-carrying layer, whereas in flexible pavements the load carrying layers are composed of asphaltic materials. A composite pavement is a combination of both flexible and rigid pavements. A typical flexible pavement in the UK is shown in Figure 1.1. Using the new European Committee for Standardisation (CEN) terminology, the asphaltic layers are referred to as surface course, binder course and base respectively [Read, 1996] (see Figure 1.1).

Surface Course

The role of the surface course is to provide a safe and smooth surface for vehicles, with adequate skid resistance. It also protects the sub-layers from ingress of water. Skid resistance depends on the microtexture and macrotexture of the surface layer. Microtexture refers to fine-scale “grittiness” on the pavement’s surface produced by coarse aggregates, which depends on the resistance of exposed aggregates to polishing from traffic loads. Macrotexture refers to the large-scale roughness obtained through the arrangement of aggregate particles. The shape, size, gradation and resistance to abrasion of coarse

aggregates determine this texture. Other important characteristics for the surface course are durability, defined as resistance to weathering and abrasive action of traffic, workability during laying, impermeability, resistance to cracking, low noise generation, load spread ability and resistance to permanent deformation.

Binder Course

The role of the binder course is to provide a level surface for laying the surface course, and to distribute traffic loads over the sub-layers. The important properties for the asphalt mixtures used in this layer are resistance to permanent deformation and fatigue cracking, high stiffness for satisfactorily spreading the traffic load to lower layers, durability, workability and impermeability.

Base

The base is the main structural layer, and its function is to distribute the traffic load to the sub-layers and to prevent them becoming overstressed. This layer must be strong enough to resist the stresses without suffering permanent deformation and fatigue cracking.

Sub-Base

This layer is a part of road foundation in a flexible pavement structure that is usually made with granular materials. Its function is distribution of traffic load to the subgrade, providing a platform for construction of upper asphaltic layers, protecting the subgrade from frost and providing drainage of water from pavement.

Capping Layer

In the cases where the natural soil is weak and a thick sub-base is required, part of the sub-base can be replaced by a capping layer. It is cheaper than sub-base material and its quality is between that of the natural soil of the subgrade and sub-base material. This layer can be made by treating the natural soil with lime, and/or cement.

Subgrade

Subgrade is the compacted natural soil in the fill or cut. It must carry the stresses due to the wheel loads transferred through the pavement layers without deforming excessively.

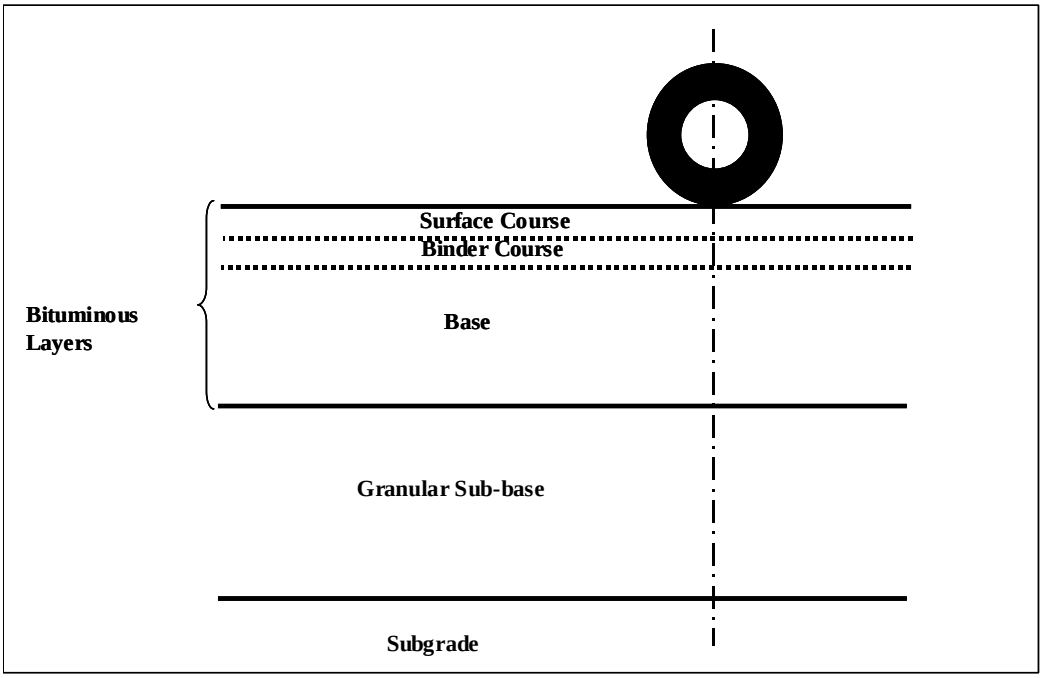

Figure 1.1 A typical UK flexible pavement.

The thicknesses of the pavement layers are determined by a pavement design method. The pavement is designed to ensure that the traffic loads are distributed such that the stresses and strains developed in the layers and the subgrade don't induce premature failure.

1.3 Asphaltic Mixtures

As explained above, asphaltic mixtures are used as a surface course, binder course and base layer in a flexible pavement structure. These layers distribute stresses caused by loading and protect the underlying unbound layers from the effects of water. To perform both of these functions adequately over the pavement design life, the mixture must withstand the effects of air and water, resist permanent deformation, and resist cracking caused by loading and the environment. Many factors including mixture design, construction practice, and

properties of constitute materials play a role in the mixture's characteristics to meet the above-mentioned structural requirements. Various types of asphaltic mixtures are used in pavement construction. The composition of an asphaltic mixture depends on a variety of factors, such as the layer being used (surface course, binder course or base), cost (availability of material and construction equipment), environmental conditions and traffic loads. Typical hot-mixed asphaltic mixtures used in the UK pavement industry are Dense Bitumen Macadam (DBM), Hot Rolled Asphalt (HRA) and Stone Mastic Asphalt (SMA). These mixtures will be explained in the following sections.

1.3.1 Dense Bitumen Macadam (DBM)

DBM is an example of a continuously graded mixture. A typical grading and an idealised section through this mixture are shown in Figure 1.2. The specifications for this mixture are given in BS 4987: Part 1 [British Standard Institution, 2003]. The strength of this mixture is mostly provided by aggregate interlock. The VMA (Voids in Mixed Aggregates) and the bitumen content are relatively low, which result in relatively thin binder films around the aggregates. This mixture does not have good workability and requires good compaction to achieve a durable material, which results in a surface with low texture which is not suitable as surface course for high speed roads. This kind of mixture is typically used for lower layers such as the binder course and base in major roads. It is not used for the surface course except on minor roads. Asphaltic concrete, commonly used in the USA, is also a continuously graded mixture, similar in nature to the DBM. Asphaltic concrete is designed by the Marshall method while the DBM is designed based on a recipe defined in the standards.

1.3.2 Hot Rolled Asphalt (HRA)

Hot Rolled Asphalt is a gap-graded mixture with very little medium-sized aggregate. This mixture consists of a matrix of sand, fine mineral filler and bitumen, into which a relatively single sized coarse aggregate is incorporated. Figure 1.3 shows a typical aggregate grading curve, and a cross section of the HRA mixture. The figure shows the distribution of coarse aggregate particles in a

mortar of bitumen, fine aggregate and filler. Compared to the DBM, HRA has more binder and filler content with generally a lower Penetration grade bitumen (e.g. 50 Pen). Specifications for Hot Rolled Asphalt can be found in BS594: Part1 [British Standard Institution, 2003].

In HRA, there is a lack of direct contact between the coarse aggregate particles, so the load is primarily transmitted by the mortar. Hence, the stiffness of mortar is very important to the stability of this mixture. The main role of the coarse aggregate is to extend the mortar and reduce bitumen consumption although it also increases the stiffness of mixture. Therefore, where HRA applications require more stability (the binder course and base) a higher volume of coarse aggregate is usually used (up to 60%).

HRA is an asphaltic product with a very good durability compared to many asphaltic mixtures. It has a wide range of applications. It is used as a surfacing in the UK and also commonly used in base and binder courses of all types of roads until the last decade of twentieth century [Read *et al*., 1996]. To give the required friction and skid resistance to the surface, coated chippings are applied separately but as a concurrent operation during the laying of the mixture.

1.3.3 Stone Mastic Asphalt (SMA)

Due to the problems related to the chippings in HRA and the relatively low resistance to permanent deformation of the mixture, it is rapidly being replaced by Stone Mastic Asphalt (SMA) in the UK as a surfacing material. SMA is a dense gap-graded asphaltic mixture with a high content of coarse aggregate (>70%) and a binder rich mortar (filler and bitumen). It was developed in Germany in the 1960s and offers a more attractive solution than the chipped Gussasphalt (a type of mastic asphalt) for the reduction of wear caused by studded tyres. As a result of its improved performance (excellent resistant to deformation and cracking, high durability, wearing and ravelling resistance, insensitivity to water, good skid resistance, low surface noise and superior surface finish), SMA rapidly gained acceptance in many countries, especially in

Europe. The use of SMA in the UK has provided the highway engineer with a further option in the choice of surfacing materials.

1.4 Mechanical Properties of Asphaltic Mixtures

To perform satisfactorily in pavement systems, asphaltic mixtures must exhibit: (a) the ability to distribute stresses; (b) resistance to permanent deformation; (c) resistance to cracking (fatigue, thermal, reflective, and construction cracking); (d) resistance to freeze-thaw and moisture damage. The ability to meet these requirements is related to the fundamental mechanical properties of the mixture which are, in turn, affected by numerous factors related to the constituent materials (binders, aggregates and additives and their proportions), load (loading rate, loading and rest times, load level, stress state etc.), environmental conditions (temperature, moisture etc.) and construction (compaction method, quality control etc.). There are three mechanical properties which are particularly important [Preston, 1991]:

- Stiffness
- Resistance to fatigue cracking
- Resistance to permanent deformation

Stiffness is simply defined as the ability of a material to resist deflection by an applied load. Analogous to Young modulus for perfectly elastic materials, the stiffness modulus is defined as the ratio of stress to the corresponding strain. The stiffness of an asphaltic mixture in the pavement is an indication of its ability to spread the load-induced stress to the lower layers. Figure 1.4 shows schematically the relation between load spreading and the stiffness of pavement materials.

Fatigue can be defined as "the phenomenon of fracture under repeated or fluctuating stress having a maximum value generally less than the tensile strength of the material" [Whiteoak, 1991]. This property of asphaltic mixtures is related to fatigue cracking failure, which is not under study in this research.

Permanent deformation of asphaltic mixtures in combination with the permanent deformation of other materials in pavement layers manifests as rutting in the wheel track, which is one of the main load associated modes of failure of the flexible pavements in UK. Figure 1.5 shows structural and non-structural rutting. Non-structural rutting is associated with permanent deformation in the asphaltic layers which is usually accompanied by shoulders at road surface. Structural rutting includes rutting in the lower pavement layers.

For conditions which usually occur *in situ*, an asphaltic mixture typically behaves as a viscoelastic material. In this region of behaviour, the response of an asphaltic mixture to a simple creep recovery test is as shown schematically in Figure 1.6. As a stress is applied and held constant for a certain time, the resulting strain comprises an instantaneous component (typically divided into elastic and plastic strains), a delayed elastic component (also known as viscoelastic strain) and a steadily increasing viscous component. When the load is removed the elastic and delayed elastic components are recovered leaving a permanent viscous strain. Permanent deformation in asphaltic material due to the passage of a single vehicle is typically small, but, with a large number of vehicles, the resulting permanent deformation can be considerable. The permanent deformation behaviour of asphaltic mixtures is the main subject of this thesis and will be discussed in detail in the following chapters.

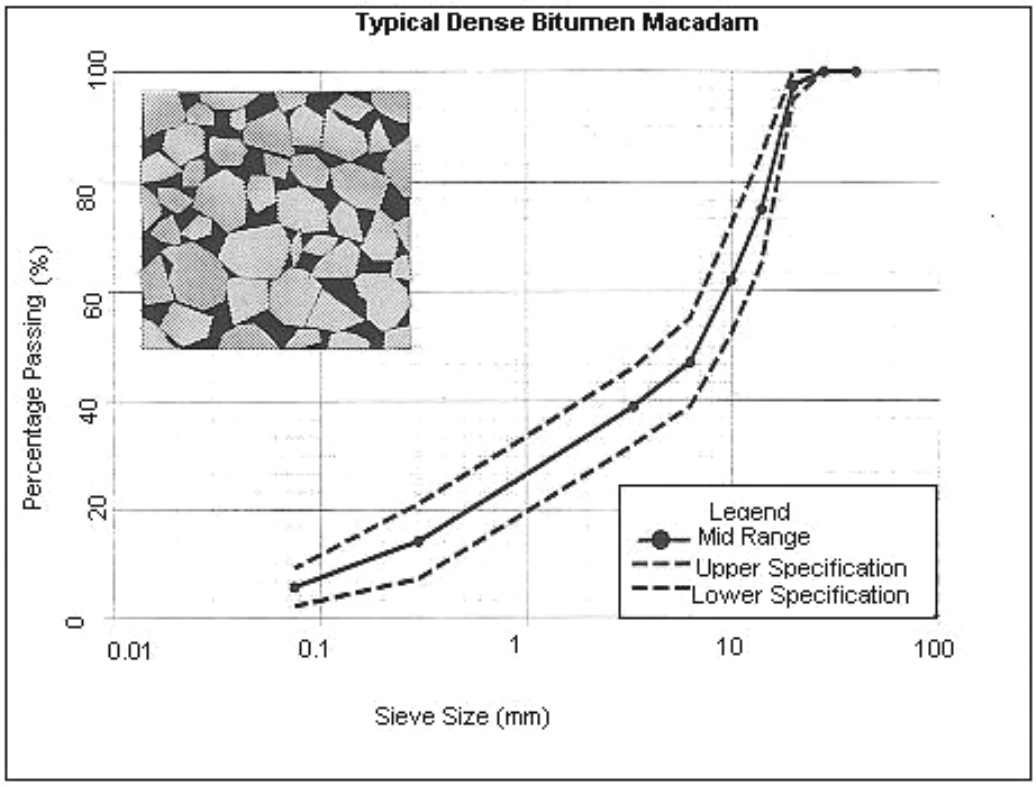

Figure 1.2 A typical grading and cross section of a 20 mm DBM [Read, 1996].

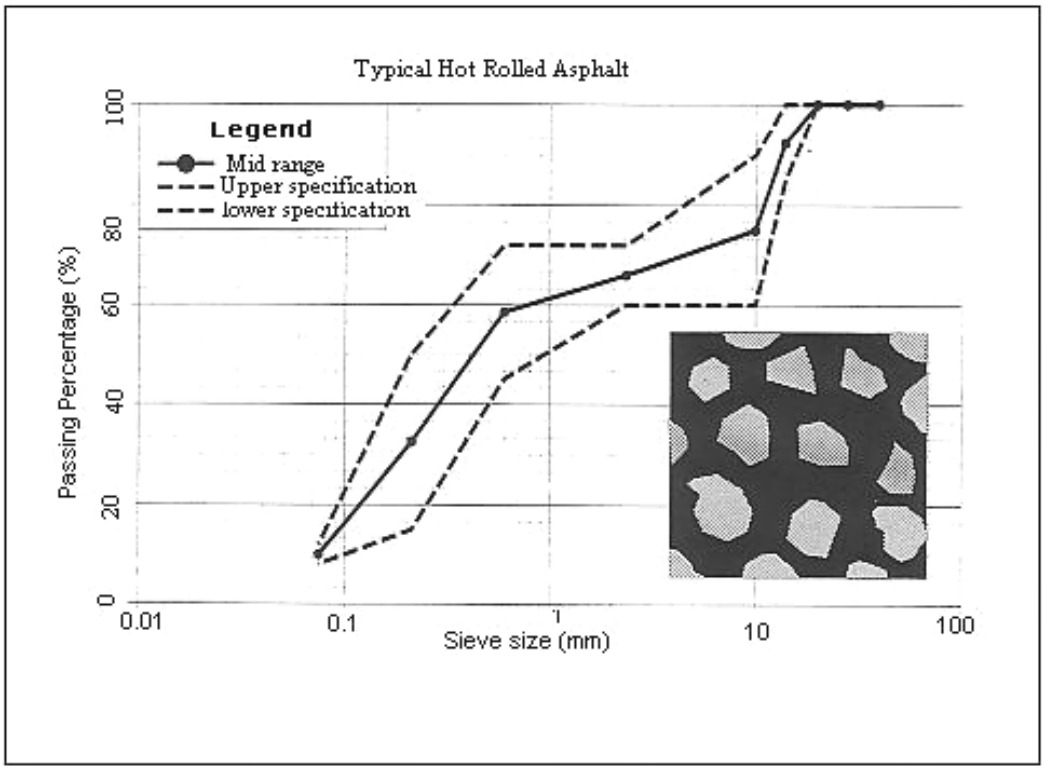

Figure 1.3 A typical grading and cross section of a HRA30/14 [Read, 1996].

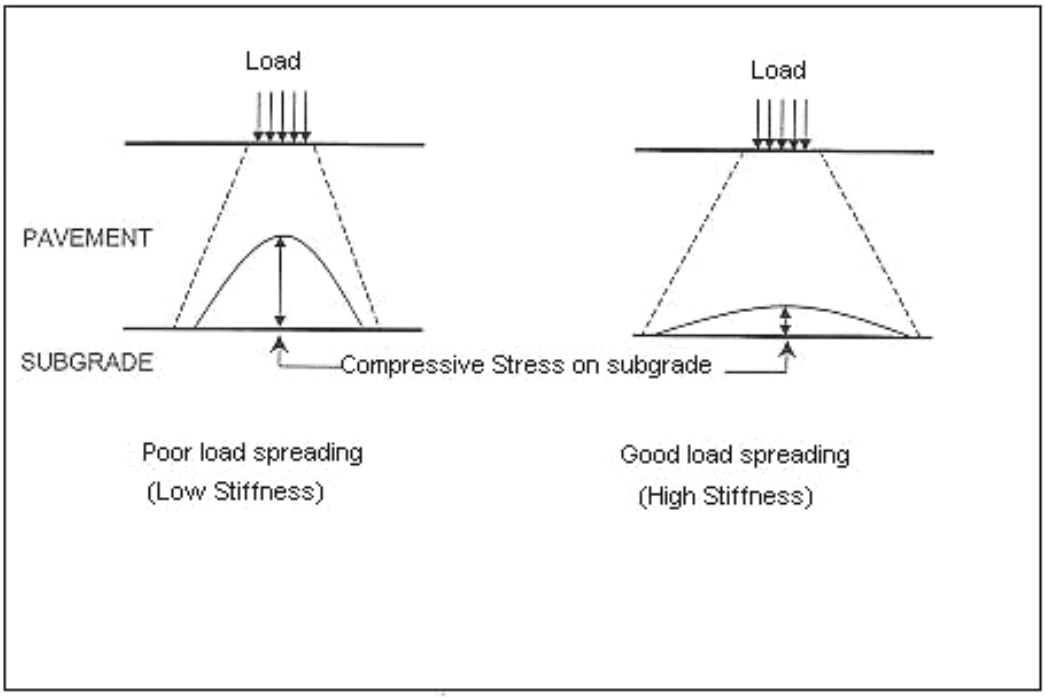

Figure 1.4 Pavement stiffness and load spreading [Anon, 2000].

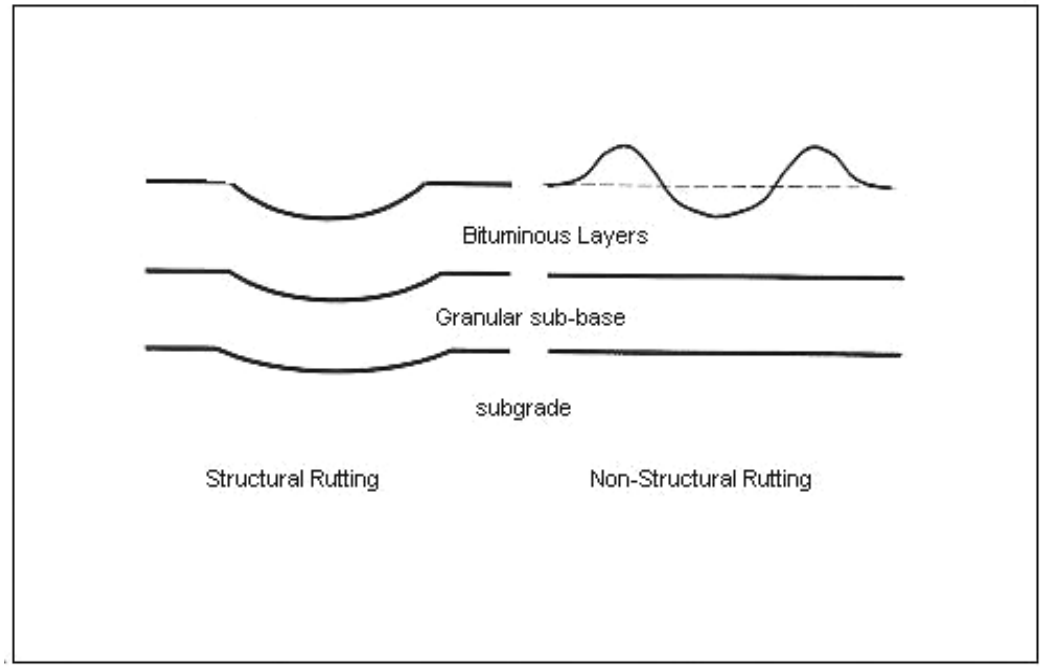

Figure 1.5 Structural and non-structural rutting [Khanzada, 2000].

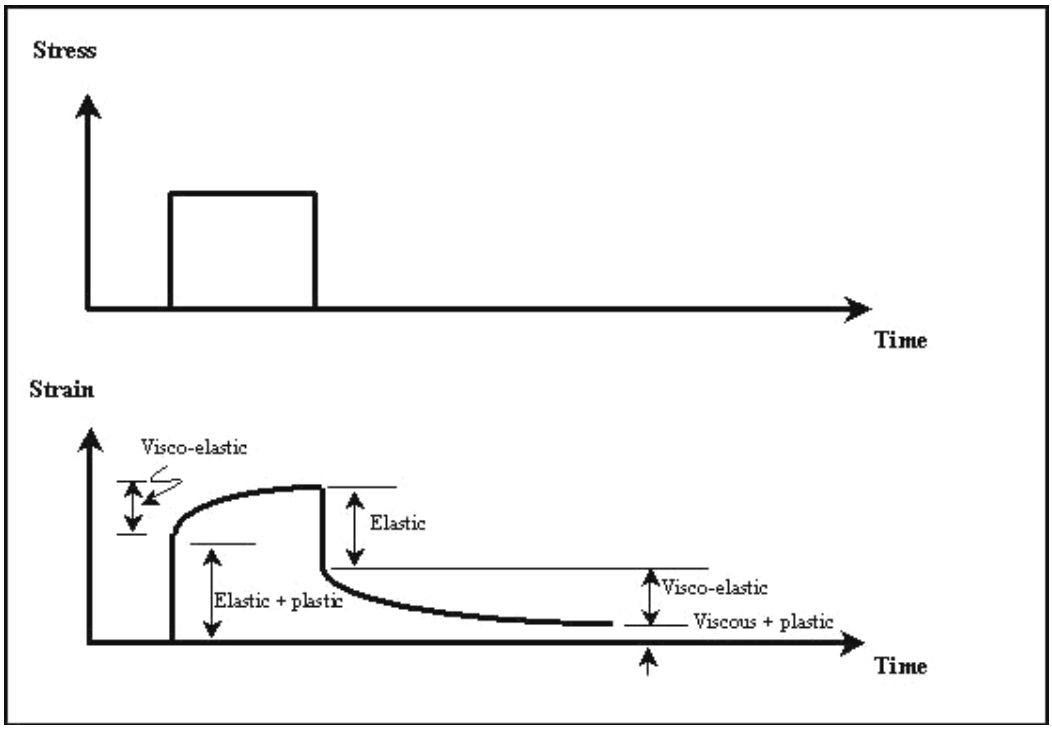

Figure 1.6 Viscoelastic response to static loading [Gibb, 1996].

1.5 Problem Definition

Premature rutting of asphalt pavements can be a serious problem for heavily trafficked roads, particularly under high temperature conditions. While the incidence of wheel track ruts in the highway does not typically imply failure in the case of non-structural rutting, it does represent a serviceability failure. Rutting causes loss of ride comfort for drivers, and can make it difficult to change lane at high speeds. Rutting also results in the collection of water on the pavement surface, which can cause aquaplaning as a result of water film between the tyre and road surface. In cold weather, the water collected in ruts can result in icing which can be dangerous for road users. The presence of non-structural rutting can also lead to other modes of failure such as cracking which results in ingress of water into the pavement structure and reduces the strength of under-laying layers.

To ensure that a pavement fulfils its functions, rutting is typically limited to specified critical levels after which the pavement surfacing must be renewed using appropriate maintenance treatments. In the UK, a rut depth of 20 mm or

extensive cracking is considered as pavement failure. The 'critical life' of a pavement is defined as the point at which the deterioration starts to accelerate rapidly, which, in the UK, is when the rut depth reaches 10 mm or the onset of cracking in the wheel path [Brown *et al.*, 1986]. Pavements are designed to ensure that, throughout their design life, the level of the failures remain below the critical values. Pavement design methods are typically divided into two broad categories: (1) empirical design methods, like the method described in Road Note 29 [Department of the Environmental and Road Research Laboratory, 1970], utilize relationships between traffic loading, environmental conditions and pavement performance obtained from experience and field testing; and (2) mechanistic design methods analytically evaluate the stresses and strains or deflections in the pavement which are used to predict the pavement damage.

For analytical evaluation of stress and strain in the pavement, functional relationships between stress and strain in the pavement materials, known as constitutive models, are used. Most mechanistic pavement design methods use multilayer linear elastic theory for structural analysis of the pavement and determination of the pavement response [Shell International Petroleum Company Limited, 1978; Brown *et al.*, 1986]. Multilayer linear elastic theory is widely used because of its easy implementation and fast execution. However, linear elastic theory is only an approximation to real pavement material behaviour which can be quite complex. Inappropriate analysis of a pavement may result in an uneconomic design. Therefore, improvement of pavement design methods needs an appropriate analysis method, which, in turn, requires accurate constitutive models for simulation of the material performance.

An important aspect of the performance of asphaltic materials is the resistance to permanent deformation. Permanent deformation of asphaltic mixtures can contribute significantly to pavement rutting, particularly in pavements with thick asphaltic layers under high temperatures. Due to their complex physical structure, the response of asphaltic materials to load is complex. Therefore, unlike many materials in civil engineering, they have become a difficult medium to be modelled by engineers. The majority of constitutive models for permanent deformation of asphaltic mixtures do not reflect the realistic behaviour of the

materials. It is well documented that asphaltic mixtures are both loading rate and temperature dependent and exhibit elastic, plastic and viscous behaviour [Dunhill, 2002]. Development and application of accurate constitutive models for asphaltic materials need intensive simulations, which has been prohibited because of the required processing time and storage space. However, increased computing power and advanced numerical techniques have facilitated the implementation of complex constitutive models into incremental numerical techniques such as the Finite Element (FE) methods. Moreover, the development of a constitutive model for prediction of the permanent deformation of asphaltic material relies, at least in part, on understanding the constitutive behaviour of the materials over a range of conditions, which, in turn, requires undertaking extensive experimental work over the conditions.

1.6 Background of Research

Under quasi-static conditions, the viscous deformation of asphaltic mixtures is dominant. In order to investigate the deformation behaviour of asphaltic mixtures under quasi-static conditions, a series of ongoing research studies have been undertaken in Cambridge and Nottingham Universities. The steady-state viscous deformation behaviour of pure bitumen over a range of conditions was studied at Cambridge University [Cheung, 1995; Cheung *et al.*, 1997a; Cheung *et al.*, 1997b]. The research was followed by investigation of the steady-state viscous deformation and volumetric behaviour of idealised asphaltic mixtures (sand asphalts) [Collop *et al.*, 1999; Collop *et al.*, 2001; Deshpande, 1997; Deshpande *et al.*, 1999; Ossa, 2004].

In an ongoing collaboration between the University of Nottingham and Delft University of Technology, based on the studies at the Cambridge and Nottingham Universities, a three-dimensional constitutive model was developed for permanent deformation of asphaltic mixtures under quasi-static loading [Collop *et al.*, 2003]. It is a non-linear viscoelastic constitutive model with viscous damage, and comprises elastic, delayed elastic and viscous components. The model was implemented in a FE program known as CAPA-3D, developed at Delft University of Technology [Scarpas, 1992]. The nature of stress-based non-

linearity and sensitivity to confinement of the viscous component were determined based on quasi-static compressive experimental data for the idealised asphaltic mixtures [Collop *et al.*, 1999].

1.7 Research Objectives

The aim of this project is to extend the above-mentioned research to experimentally investigate the quasi-static compressive permanent deformation behaviour of realistic asphaltic mixtures. This work is complementary to other research work that is currently being undertaken at Nottingham University where tensile behaviour is being investigated. The results from these two research studies are used for further development of the constitutive model developed by Collop *et al.* [2003]. Two generic types of asphaltic mixtures were chosen; a continuously graded 10 mm Dense Bitumen Macadam (DBM) and a gap graded 30/10 Hot Rolled Asphalt (HRA). The objectives of this project can be listed as follows:

1. To investigate the compressive steady-state deformation behaviour and volumetric response of these mixtures under uniaxial and triaxial loading conditions. The effect of temperature, deviatoric and confining stress on the steady-state deformation and volumetric response of the mixtures is studied.
2. To study the recovery behaviour in compression of the asphaltic mixtures over a range of axial stresses, temperatures and accumulated damage in the mixtures.
3. Determination of the parameters for the viscoelastic constitutive model developed by Collop *et al.* [2003] using the experimental results from the realistic asphaltic mixtures.
4. Verification of the model using the experimental data.

1.8 Scope of Research

This Thesis consists of 9 chapters with each chapter detailing one aspect of the research work. Chapter 2 reviews the literature concerning the deformation behaviour of bitumen, idealised and realistic asphaltic mixtures and permanent deformation testing. In Chapter 3, the literature concerned with the constitutive

modelling of pavement rutting and permanent deformation of asphaltic mixtures is reviewed. Chapter 4 describes creep and creep recovery tests carried out on bitumen using the Dynamic Shear Rheometer (DSR). The steady-state deformation and recovery behaviour of the pure bitumen used in the asphaltic mixtures are investigated. Chapter 5 describes the experimental work such as development of specimen, test equipment, instrumentation and friction reduction system for the research. It also covers the static uniaxial constant stress creep and constant strain rate tests performed on the asphaltic mixtures over a range of stress levels, strain rates and temperatures. The steady-state deformation behaviour and volumetric response of the mixtures have been characterised and compared. Chapter 6 describes uniaxial single creep recovery tests carried out on the mixtures over a range of stress levels and temperatures for a series of total strains before unloading. This chapter also explains repeated creep recovery tests performed on the mixtures at selected loading and rest times. Chapter 7 describes development of the triaxial test set-up and its results on the mixtures over a range of deviatoric stresses and stress ratios. The steady-state deformation behaviour and volumetric response of the mixtures under triaxial stress state are discussed in this chapter. Determination of the non-linear viscoelastic constitutive model parameters using the experimental data on the mixtures is explained in Chapter 8. The procedure for determination of each parameter from tests data is described, and for each mixture a relationship is developed to present the parameter as a function of variables such as temperature, deviator stress level and stress ratio. In order to verify the capabilities of the constitutive model, using the experimentally determined model parameters, the uniaxial creep and creep recovery tests are simulated by the model. In the final chapter, a summary, the main conclusions from the research work and the recommendations for future research are presented.

2 Permanent Deformation of Asphaltic Mixtures

2.1 Introduction

This chapter provides a review of permanent deformation in asphaltic mixtures. The review is divided into four sections. The first section reviews the mechanisms of permanent deformation in asphaltic mixtures followed by a section in which the resistance to permanent deformation of the mixtures is reviewed. In the third section, recent studies at Cambridge and Nottingham universities into the steady-state deformation behaviour of bitumen, and idealised and realistic asphaltic mixtures are reviewed. Finally, a review of testing methods used for investigation of the deformation behaviour of asphaltic mixtures is presented.

2.2 Mechanisms of Permanent Deformation in Asphaltic Mixtures

Permanent deformation in asphaltic mixtures is due to the combination of densification and shear deformation. Newcomb *et al.* [1997] found that the majority of densification of asphalt by traffic occurs within the first year of

construction. Shear deformation in asphaltic mixtures occurs because of the viscous behaviour of the material which will be explained later in this chapter.

When a wheel load is applied to an element of asphaltic material in the pavement, it causes some deformation in the material. The magnitude of the deformation depends on the material properties, load level, temperature and loading time. After removing the load, part of the deformation will be recovered, and some permanent deformation will remain in the material. The recovered deformation is related to the elastic and delayed elastic properties, and the permanent deformation is related to the plastic and viscous properties of the material. The value of permanent deformation for each passing load may not be high, but accumulation of these small deformations results in high deformations in the asphaltic material (see Figure 2.1).

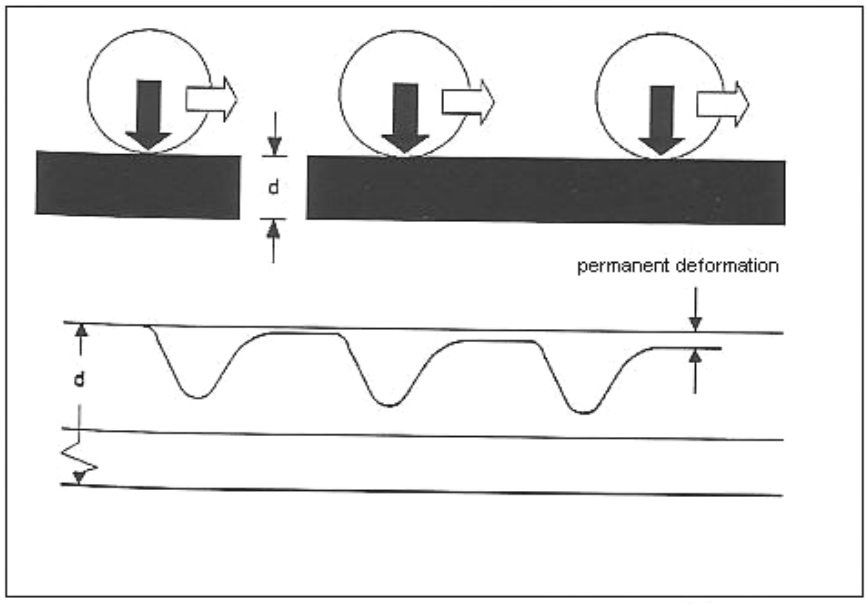

Figure 2.1 Accumulation of permanent deformation under repeated loading [Dunhill, 2002].

For asphaltic mixtures, well compacted during construction, it has been found that the shear deformation is the primary cause of rutting [Eisenmann *et al.*, 1987; Hofstra *et al*, 1972; Collop *et al*., 1995]. Eisenmann *et al.* [1987] concluded that rutting was mainly caused by deformation without volume change. Hofstra *et al.* [1972], in their study of flexible pavements in a laboratory

test track, measured the asphalt density in the wheel track and outside the wheel track. It was observed that the densities were equal, and they concluded that the deformation was due to transverse flow of material not densification.

2.3 Resistance to Permanent Deformation of Asphaltic Mixtures

Resistance to permanent deformation in asphaltic mixtures is influenced by the properties of bitumen and aggregate, their proportions in the mixture, compaction level and environmental conditions.

An important property of bitumen for resistance to permanent deformation is the grade or hardness of bitumen. However, the extent of the effect depends on the type of mixture. Hofstra *et al.* [1972] compared rutting in sections of asphalt concrete with various grades of bitumen and concluded that the hardest bitumen gave the smallest rut depth. In Hot Rolled Asphalt (HRA), in which resistance to deformation relies on the stiffness of the bitumen/filler/fine mortar, this effect is more important. In DBM or SMA, where the resistance relies on particle interlock, binder stiffness has less effect on the resistance to deformation. Brown *et al.* [1984], using the repeated load triaxial test on Dense Bitumen Macadam (DBM) at 30°C, found that the resistance to deformation was not influenced by the grade of binder. A similar response was observed for both a 100 Pen and a 200 Pen bitumen used in the mixture.

Gibb [1996] investigated the role of aggregate and bitumen in the resistance to permanent deformation of asphalt mixtures using the Nottingham Asphalt Tester (NAT). He conducted compressive cyclic uniaxial tests on DBM and HRA mixtures over a range of temperatures. Both mixtures were made with two different constituent bitumens (50 Pen and 200 Pen). He found that at low binder stiffnesses (all temperatures with the 200 Pen bitumen and 40°C with the 50 Pen bitumen), the aggregate structure is more important than the binder in providing resistance to permanent deformation. Under these conditions, the DBM showed better performance than the HRA. At high binder stiffnesses (the 50 Pen at 20°C and 30°C), the HRA showed more resistance to permanent deformation than the DBM. The higher permanent deformation in the continuously graded mixture

(DBM) was attributed to the plastic strain related to movement of the aggregate particles under the action of repeated loading. From the test results it was concluded that, up to a certain level of binder stiffness, the deformation resistance of the mixtures is dominated by the binder. Below that level the binder is not able to contribute significantly to deformation resistance, and the role of the aggregate structure is dominant. It was also found by Brown *et al.* [1974] that the viscosity of bitumen is effective in the relative contribution of aggregate and bitumen to resistance to permanent deformation. At high temperatures, the binder viscosity is low and aggregate interlock is more important in providing resistance to deformation. Under these conditions, a high bitumen content reduces aggregate interlock and, therefore, the resistance to deformation is reduced, and a low bitumen content will result in more aggregate interlock and, therefore, the resistance to permanent deformation is increased. At lower temperatures, a medium bitumen content will give the maximum contribution of both aggregate interlock and binder viscosity to resistance to deformation.

The properties of aggregates which are important in producing resistance to permanent deformation are: gradation, surface texture, shape and size. A mixture with more resistance to aggregate movement generally has more resistance to permanent deformation. A compacted mixture with its aggregate particles in intimate contact with each other provides more load bearing and resistance to permanent deformation. Brown *et al.* [1984] concluded that aggregate grading has a significant influence on resistance to permanent deformation. At the temperature that they carried out their tests (30°C), continuously graded mixtures had more resistance to permanent deformation than the gap graded mixtures. However, gap graded mixtures with a high volume fraction of coarse aggregate, like SMA, which has a coarse aggregate content greater than 70%, can have a high deformation resistance due to more aggregate contact. Aggregate shape and surface texture are important factors in the performance of asphaltic mixtures; especially where aggregate contact is prevalent. In terms of resistance to permanent deformation, angular crushed rock and rough surface textured aggregate are preferable to smooth surface texture and rounded shape aggregate.

To study the interaction of aggregate and binder in permanent deformation, Gibb [1996] carried out static and repeated load creep tests both with a static confining stress equal to 70 kPa. Unbound and bound specimens were used, in which two aggregates, different in shape and texture but similar in structure (both single size), were used. Under static and repeated loading conditions, both the aggregate's shape and texture showed a significant effect on the resistance to permanent deformation. Angular and rough aggregates proved superior to smooth aggregates. Under static creep loading, in both cases of angular and smooth, the bound specimens showed more permanent deformation than the unbound specimens. Meanwhile, bound specimens with round and smooth aggregates showed more deformation than those with angular aggregates. In the repeated load tests, the unbound specimens showed more permanent deformation than in the static creep tests. This was related to the deformation which occurs due to the movement of aggregates in contact under repeated load. Specimens of bound mixtures with round and smooth aggregates showed less permanent deformation under repeated load tests than under static creep test.

The volumetric composition of mixtures quantified using parameters such as VMA (voids in mineral aggregates), VFB (degree of the VMA filled with bitumen) and air void content of mixture are important factors in the resistance to permanent deformation [Gibb, 1996]. Decreasing the VMA results in an increased number of aggregate contacts, which is desirable for enhanced resistance to permanent deformation. However, a very low VMA or very dense graded asphaltic mixtures are susceptible to permanent deformation. This is because, in these kinds of mixtures, the bitumen/filler mortar is forced between coarse aggregate particles and reduces the number of contact points and therefore, resistance to permanent deformation is reduced [Gibb, 1996]. VMA is also influenced by bitumen content and the degree of compaction. There is a bitumen content, which results in minimum VMA, the maximum number of particle contact points and maximum resistance to permanent deformation. After that, the bitumen film around the aggregates becomes thicker and the void content is decreased to zero, which results in decreased resistance to permanent deformation. A low air void content causes a reduction in the resistance to permanent deformation and this is the reason that the mixture design methods

have limited the minimum air void content for asphaltic mixtures. Mixture design methods use the maximum VFB (voids filled by bitumen) criterion to control the permanent deformation of asphaltic mixtures.

In terms of environmental conditions, temperature is the most important factor in permanent deformation of asphaltic mixtures. Hofstra *et al.* [1972] compared the deformation of mixtures in wheel tracking tests at temperatures between 20 and 60°C. It was found that, over this range of temperatures, the permanent deformation increased by a factor of 250-350. This shows that temperature is a very important factor in permanent deformation of asphaltic mixtures.

2.4 Steady-state Deformation Behaviour of Asphaltic Mixtures

2.4.1 Introduction

Much research has been directed at the study of the mechanisms of permanent deformation in the bitumen and asphaltic mixtures. Viscous deformation of bitumen and asphaltic mixtures is a major component of the permanent deformation, especially for static and/or slow moving loads, high temperatures and high stress levels. During the last decade, as a part of an overall effort to understand rutting of asphaltic pavements, the deformation behaviour of bitumen, idealised and realistic asphaltic mixtures has been studied at the Universities of Cambridge and Nottingham. In this research, the steady state viscous deformation of these materials has been studied over a range of loading and temperature conditions. A review of this research is given in the following sections.

2.4.2 Steady-state Deformation Behaviour of Bitumen

Bitumen is a material which can be naturally occurring or is manufactured from crude oil. Bitumen is produced as a result of processes on organic materials over several millions of years. Natural bitumen has been used as an adhesive and waterproofing material from as early as 3800 B.C. [Whiteoak, 1991]. Extensive

use of bitumen in pavement construction started in the early nineteenth century [Cheung, 1995]. Systematic research to understand the behaviour of bitumen as an engineering material was started in the 1920s by oil companies. Research on bitumen was started with a simple colloidal model and its corroboration by mechanical tests. This was followed by Van der Poel's work [Van der Poel, 1954], in which the stiffness of bitumen was correlated with two experimental parameters, namely the *penetration*[1] and the ring and ball *softening point*[2] obtained from routine tests on bitumen. After 1960, a wide range of experimental tools were developed to study the chemical composition and mechanical behaviour of bitumen. A more detailed review on progress in research on bitumen since the 1920s can be found in Cheung [1995].

Understanding the mechanical behaviour of asphaltic mixtures relies on an understanding of the behaviour of the constituent materials and their interaction. The mechanical properties of bitumen can play an important role in the deformation behaviour of asphaltic mixtures. Bitumen is a viscoelastic material and its deformation under stress depends on temperature, strain level and loading time. Bitumens behave as a viscous liquid at high temperatures and/or long loading times, whereas at low temperatures and/or short loading times they behave as an elastic solid. The behaviour at intermediate temperatures and loading times is viscoelastic [Whiteoak, 1991]. The quasi-static deformation behaviour of bitumen, defined as the response under static loading, has been described by several theories such as the time dependent modulus, correspondence principles, molecular theories and mechanical analogies. Most of the theories have concentrated on small strains in which the bitumen behaviour is nearly linear. The behaviour at higher strains where the non-linearity is dominant has not been studied very much. A comprehensive review of these theories can

[1] The penetration of bitumen is the distance which a standard needle penetrates into a sample of bitumen under a known load (100g), at a fixed temperature (25°C), for a known time (5 seconds) [Whiteoak, 1991].

[2] Softening point is the temperature at which the bitumen sample, contained in a brass ring, under the load of a steel ball (3.5g) softens, flows and touches a base plate 25 mm below the ring when the bath temperature is raised at 5°C per minute [Whiteoak, 1991].

be found in Cheung [1995] and Ossa [2004]. Some of the theories relevant to this research will be discussed in this section.

By undertaking a number of monotonic tests in tension, compression and shear, over a range of loading and temperature conditions, Cheung [1995] and Cheung *et al.* [1997] developed various physical models for the steady-state behaviour of a 50 Pen bitumen.

From the results of tensile tests undertaken at ambient temperatures (-10°C to 30°C) and stress levels greater than 100 kPa on two nominal 50 Pen bitumens, taken from two different batches (same source), Cheung [1995] concluded that the steady-state behaviour of the bitumen at a particular temperature can be represented by a power law equation. He also found that the temperature dependence of the steady-state deformation behaviour of the bitumen at ambient temperatures can be well described by the Arrhenius equation. By combining these two theories, the Power Law Model (PLM) was presented as:

$$\frac{\dot{\varepsilon}}{\dot{\varepsilon}_{op}} = \left(\frac{\sigma}{\sigma_{op}}\right)^{n} \exp\left(-\frac{Q_p}{RT}\right), \qquad \textbf{(2.1)}$$

where $\dot{\varepsilon}$ = uniaxial strain rate

σ = uniaxial stress

n = creep exponent

$\dot{\varepsilon}_{op}$ = reference strain rate at a reference stress σ_{op}

Q_p = thermal activation energy, which was determined to be 228 kJ/mol

R = universal gas constant with a value 8.13 J $mol^{-1}K^{-1}$

T = temperature in degree Kelvin

By fitting this model to test results, the creep exponent, *n*, was found to be 2.3, which indicates that the behaviour of the bitumen at these stress levels is non-linear.

The steady-state deformation behaviour of the bitumen at high temperatures was found to be well described by the WLF equation, which is based on the concept that molecular mobility at any temperature depends primarily on the free volume [Cheung, 1995].

In order to observe the deformation behaviour of the bitumen at lower stress levels, constant strain rate tests were carried out at ambient temperatures (-10°C to 30°C). It was found that the behaviour at lower stress levels is linear (power law creep with a creep exponent of 1). For all temperatures, the transition from linear to non-linear behaviour took place at approximately the same stress level (100 kPa). The change in deformation behaviour from linear at low stress levels to non-linear at high stress levels was attributed to the rupture of the molecular network formed by the association of asphaltens. He proposed the modified Cross model (MCM) for describing the uniaxial steady-state deformation behaviour of the bitumen. Based on this model, the steady-state deformation behaviour changes from linear at low stress levels to non-linear at high stress levels, and from free volume dependent deformation at higher temperatures (T≥20°C for his bitumen), described by WLF equation, to diffusional deformation at lower temperatures (T≤20°C), described by Arrhenius equation. The modified Cross model is given by:

$$\eta = \frac{\eta_{0T}}{1 + \left(\frac{\eta_{0T}\,\dot{\varepsilon}}{\sigma_{0c}} \right)^{m}} \quad , \qquad \textbf{(2.2)}$$

where η = the viscosity of bitumen

σ_{0c} = failure strength of the structural linkages, which reflects the change from linear to non-linear behaviour and was determined by fitting the MCM model to the test results.

$$\eta_{0T} = \eta_{0c} \exp\left(\frac{Q_C}{RT} \right) \qquad T > T_g \ , \qquad \textbf{(2.3)}$$

$$\eta_{0T} = \eta_s \exp\left[-\frac{2.303 c_1^s (T - T_s)}{c_2^s + (T - T_s)}\right] \quad T >> T_g \ , \tag{2.4}$$

and

$$m = \frac{n - 1}{n} \ , \tag{2.5}$$

where η_{0T} = the limiting viscosity when $\dot{\varepsilon} \to 0$

η_{0c} = pre-exponential for viscosity with value 5.66×10^{-34} Pa.s

Q_C = thermal activation energy with value 2.28×10^3 J mol^{-1}

η_s = reference viscosity with value 214×10^3 Pa.s at a reference temperature T_s with value 35.2°C

c_1^s, c_2^s = universal constants with the values 8.86 and 101.6.

n = creep exponent

T_g = the glass transition, which divides low temperature behaviour (glassy behaviour) from the high temperature behaviour.

For bitumen, the glass transition temperature varies between -40°C and 0°C [Cheung, 1995]. The values of the above-mentioned constants and parameters for the bitumen can be found in Cheung [1995]. Cheung applied the MCM to the data for many types of bitumen from previous research. It was found that the stress level at which the viscous behaviour changes from linear to non-linear power law creep lies between 0.1 and 0.5 MPa. The value of creep exponents in the power law regime was found to be between 2 and 2.5.

Cheung also investigated the effects of ageing on the steady-state deformation behaviour of bitumen. By applying the MCM to previous research data for more than 50 types of bitumen, it was found that ageing generally increases the creep exponent and viscosity, and decreases the transition stress level. By carrying out creep tests in tension and compression at temperatures from –35°C to -20°C on

the 50 Pen bitumen, a model was also proposed for describing the bitumen behaviour at temperatures in the vicinity of and below the glass transition.

Using the experimental results, deformation-mechanism maps were constructed for the bitumen which were divided into 6 fields all of which were described by a physical model. It was claimed that these kinds of map can be used for different bitumens, but the material parameters for the physical models may be different.

From an extensive set of tensile, shear and compression tests, Cheung [1995] showed that the 3-Dimensional steady-state deformation behaviour of pure bitumen above the glass transition, which corresponds to most practical conditions, could be approximated by the following model:

$$\left(\frac{\dot{\varepsilon}_{ij}}{\dot{\varepsilon}_0}\right) = \frac{3}{2}\left(\frac{\sigma_e}{\sigma_0}\right)^n \frac{\sigma'_{ij}}{\sigma_0}, \qquad \textbf{(2.6)}$$

where $\dot{\varepsilon}_{ij}$ = strain rate tensor

$\dot{\varepsilon}_0$ = reference strain rate

σ_0 = reference stress

σ_{ij}' = the deviatoric stress tensor given by:

$$\sigma_{ij}' = \sigma_{ij} - \frac{1}{3}\delta_{ij}\sigma_{kk}, \qquad \textbf{(2.7)}$$

where δ_{ij} is Kronecker delta

for which:

$$\delta_{ij} = \begin{cases} 0 & if \quad i \neq j \\ 1 & if \quad i = j \end{cases} \qquad \textbf{(2.8)}$$

σ_{kk} = is a stress invariant in the multiaxial stress state,

$$\sigma_{kk} = \sigma_{xx} + \sigma_{yy} + \sigma_{zz}\ , \qquad \textbf{(2.9)}$$

σ_e = the Von Mises effective stress as:

$$\sigma_e = \left(\frac{3}{2} \sigma_{ij}' \sigma_{ij}' \right)^{\frac{1}{2}}, \qquad \textbf{(2.10)}$$

n = creep exponent, which for low stress levels is 1 and for high stress levels is greater than 1 (2.3 for the bitumen tested).

For characterisation of two 50 Pen and 100 Pen bitumens, Collop *et al.* [2002], using a Dynamic Shear Rheometer (DSR), carried out constant stress creep tests over a range of shear stress levels at 20°C. They found that at low stress levels (< 70 kPa) the deformation behaviour of the bitumens was linear, whereas at higher stress levels the deformation behaviour was non-linear, and the effective creep exponent was found to be 2.4. They developed a model for describing the deformation behaviour of the bitumen subjected to shear loading in the DSR. The model related the steady-state shear stress to the steady-state shear strain rate. In this model it was assumed that the behaviour is linear at low stress levels (<50 kPa) and power law creep at high stress levels (>100 kPa) and a transition from linear to non-linear behaviour for the stress levels between 50 and 100 kPa. It was concluded that the creep tests performed by a DSR with parallel plate geometry can be used for characterisation of the value of the power law creep exponent at high stress levels and the shear viscosity at low stress levels in the linear regions. Using correlation factors, the DSR model in the linear and non-linear region agreed well with the uniaxial tensile model. Equations 2.1 and 2.11, for uniaxial stress and pure shear, respectively, derived from Equation 2.6, were used to correlate the DSR model to the uniaxial tensile model developed by Cheung [1995] for the same 50 Pen bitumen.

$$\left(\frac{\dot{\gamma}}{\dot{\varepsilon}_0} \right) = \sqrt{3}^{n+1} \left(\frac{\tau}{\sigma_0} \right)^n, \qquad \textbf{(2.11)}$$

where τ and $\dot{\gamma}$ are the shear stress and shear strain rate, respectively, and the rest are the same material constants, as defined before. It can be seen that the behaviour in tension and shear is related by the correlation factor of $\sqrt{3}^{n+1}$, which equals 3 in the linear region (n=1), and 6.47 in the non-linear region (n=2.4).

Ossa *et al.* [2003] investigated the deformation behaviour of pure bitumen and polymer-modified bitumen by performing static constant stress, monotonic constant strain rate, creep recovery, continuous cyclic and pulse train tests in tension (see Figure 2.2). Similar to the findings of Cheung *et al.* [1997], they found that the steady-state deformation behaviour of the bitumen is non-linear viscous at high stress levels and linear at low stress levels. Over the range of temperatures they performed the tests ($-5^{\circ}C \le T \le 20^{\circ}C$), the temperature dependence of the steady-state behaviour of the bitumens was well captured by the Arrhenius relation. The monotonic and creep tests revealed that the steady-state stress and strain rate of pure bitumen occurs at a strain level of about 0.15, which is consistent with results from Cheung *et al.* [1997].

The creep recovery behaviour of the bitumens was studied by performing a series of single load/unload tests (see Figure 2.2a) over a range of temperatures and stress levels. In the creep recovery tests, a stress was applied rapidly to the specimen and was held constant until a specified total strain ε^T was achieved. At this strain level, the stress was released and the tensile strain was monitored until the recovered strain rate was approximately zero, where the strain at this point was assumed to be plastic or irrecoverable ε^{pl}. At each stress level and temperature, the tests were repeated for a series of total strain ε^T. Results from their experiments showed that the recovered strain $\varepsilon^r (= \varepsilon^T - \varepsilon^{pl})$ increased linearly with the total strain prior to unloading ($\varepsilon^r = \psi \varepsilon^T$). Over the range of temperatures and stress levels, the slope of the line ψ ($0 \le \psi \le 1$) was found to be independent of the shear stress level and temperature. The recovered strain was found to be temperature dependent and over the range of temperatures tested, $-5^{\circ}C \le T \le 20^{\circ}C$, the temperature dependency of the bitumens was captured by the Arrhenious relation.

Continuous stress controlled cyclic tests were carried out over a range of mean stresses $\sigma_m = (\sigma_{\max} + \sigma_{\min})/2$, load ratios $R = \sigma_{\min} / \sigma_{\max}$ (see Figure 2.2b), frequencies f and temperatures. It was shown that the response of the bitumens in this test, in terms of strain versus time, was similar to the static creep response

with primary, secondary and tertiary regimes of behaviour (see Section 2.5.2). The mean gradient of the strain versus time history in the secondary regime of behaviour was defined as the cyclic steady-state strain rate. It was found that the effect of load ratio *R* and frequency on the steady-state strain rate was negligible, and the behaviour was mainly governed by the mean stress σ_m. The cyclic steady-state behaviour was found to follow the steady-state behaviour in static creep with the creep stress interpreted as the cyclic mean stress.

Cyclic pulse train tests (see Figure 2.2c) were carried out over a range of temperatures, stress levels σ_p and time period ratios Δ_p/Δ_g (see Figure 2.2c). It was shown that, for a fixed value of σ_p, the accumulated permanent deformation decreased with decreasing Δ_p/Δ_g, because larger fractions of the creep strain recovered during zero-load gaps between the pulses.

Based on experimental observations and expressing the monotonic and recovered strain of the bitumens by an extended modified Cross model, a general 3D phenomenological model was proposed to characterise the monotonic, continuous cyclic and pulse train loading response of bitumen.

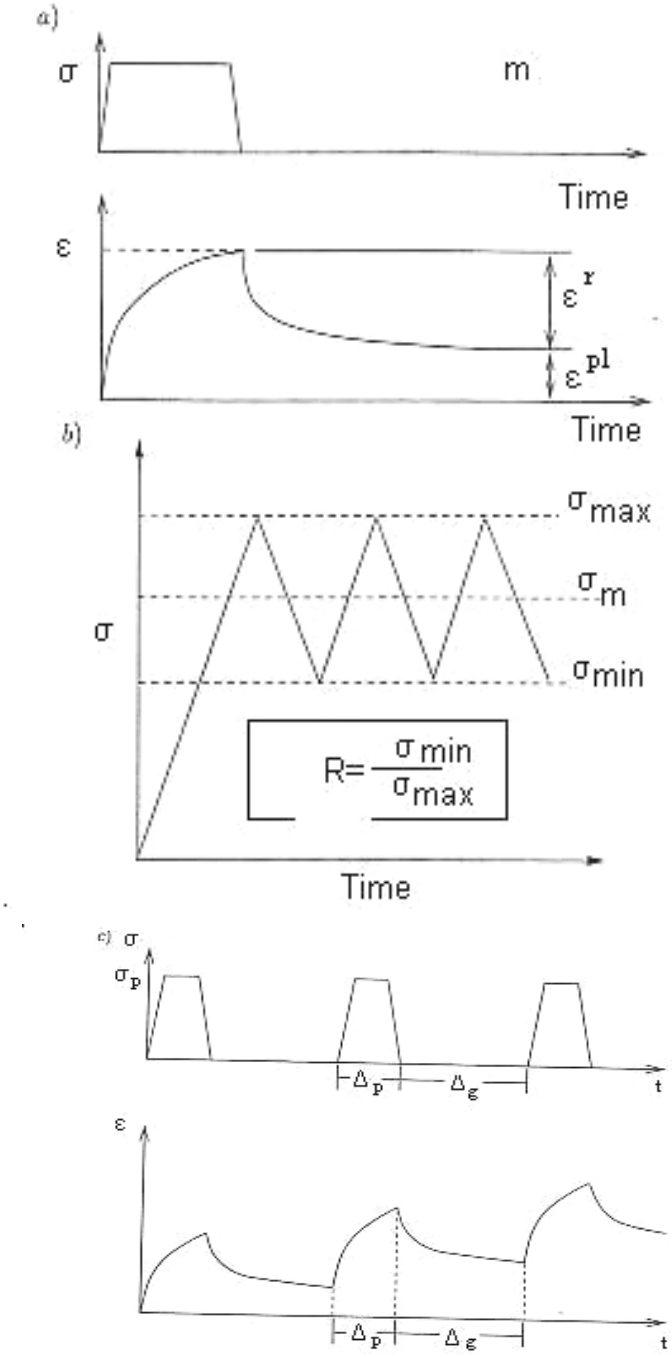

Figure 2.2 a) Creep recovery test b) Continuous cyclic tests c) Cyclic stress controlled pulse test [Ossa, 2004].

2.4.3 Steady-state Deformation Behaviour of Idealised Asphaltic Mixtures

As a first step towards understanding the deformation behaviour of realistic asphaltic mixtures, which are complex multi-phase composites consisting of a graded aggregate, air voids and bitumen, the deformation behaviour of idealised asphaltic mixtures (bitumen and aggregate with a simplified grading) has been investigated [Deshpande, 1997; Collop *et al.*, 1999; Khanzada, 2000; Ossa, 2004].

Deshpande [1997] and Deshpande *et al.* [1999] investigated the deformation behaviour of idealised asphaltic mixtures with various volume fractions (low and high volume fraction) of different types of inclusion (in terms of size and shape). The mixtures were made using the same bitumen as used by Cheung [1995], and compressive static uniaxial and triaxial creep and constant strain rate tests were conducted on the mixtures over a range of deviatoric stress levels, stress ratios (mean stress/deviatoric stress), strain rates and temperatures. It was found that the steady-state deformation behaviour of the idealised mixtures and the temperature dependency was of the same form as that of the constitutive bitumen with the aggregates acting as a stiffener (see Figure 2.3). Therefore, to describe the steady-state deformation behaviour of the idealised mixtures, the model developed by Cheung [1995] for bitumen was modified by introducing a stiffening factor S giving:

$$\frac{\sigma}{\sigma_0} = \frac{S\dot{\varepsilon}}{\dot{\varepsilon}_0}\left(\frac{1}{1+\left(\frac{S\dot{\varepsilon}}{\dot{\varepsilon}_0}\right)^m}\right), \qquad \textbf{(2.12)}$$

where σ_0, $\dot{\varepsilon}_0$, m = material constants, as defined before

S = the stiffening factor, which describes the amount by which the mixture is stiffer than the pure bitumen.

The stiffening factor was found to depend on the volume fraction of aggregates in the idealised mixture, temperature, air void content and stress ratio, but is independent of aggregate size. They found that the stiffening factor was the same in the linear and non-linear viscous regimes of behaviour. The shape of the aggregate particles was found not to have a strong effect on the deformation behaviour of the mixtures. However, it was noted that this may not extend to aggregates with high angularity in mixtures with wide distribution of particle sizes where friction between aggregates will increase the stiffening.

The radial strain of the specimens was also measured in the uniaxial and triaxial tests. For each test, the volumetric strain (Equation 2.13) and the shear strain (Equation 2.14) were calculated and plots of the volumetric strain versus the shear strain were produced. It was found that the volumetric strain varies linearly with the shear strain. The slope of the relation, known as the dilation ratio, was found to be independent of temperature, stress ratio and deviatoric stress, strain rate and type of the test (constant strain rate or constant stress creep test). The test results showed that the mixtures with high volume fraction of aggregates dilate under uniaxial and triaxial compressive loading (dilation ratio more than 1). However, the mixtures with low volume fraction of aggregate deformed at constant volume.

$$\varepsilon_V = 2\varepsilon_{11} + \varepsilon_{33} , \tag{2.13}$$

$$\varepsilon_S = \frac{2}{3}(\varepsilon_{11} - \varepsilon_{33}) , \tag{2.14}$$

where ε_V = volumetric strain

ε_S = shear strain

ε_{11} and ε_{33} = the radial and axial strains, respectively, with negative sign for the axial strain and positive for the radial strain values.

With the aim of extending the work done by Deshpande *et al.* [1999], Collop *et al.* [1999] investigated the relationship between the rutting performance of the

idealised mixtures, measured by simulative wheel tracking tests, and the mechanical properties of two idealised mixtures, measured by simplified uniaxial quasi-static and uniaxial repeated load tests. One idealised mixture comprised a single size sand (between 1.18 mm and 2.36 mm) and the other comprised two different sizes of sand (between 1.18-2.36 mm and 150 μm-300 μm). Both mixtures were made with a 50 Pen bitumen. Uniaxial constant stress creep and constant strain rate tests were performed over a range of stresses and strain rates at 20°C and 30°C. Consistent with the findings of Deshpande *et al.* [1999], their experimental work showed that the steady-state deformation behaviour of the idealised mixtures mirrored that of the constitutive bitumen with the stiffening effect of the aggregates. At high stress levels (>500 kPa), the steady-state deformation behaviour was non-linear, following power law creep with a creep exponent of approximately 2.4, and at low stress levels (<70 kPa), the behaviour was linear with a power exponent of approximately 1. Between 70 kPa and 500 kPa, there was a transition from non-linear behaviour to linear viscous behaviour.

Collop *et al.* [1999] also investigated the deformation behaviour of the idealised mixtures under uniaxial repeated loading over a range of temperatures and stress levels between 50 kPa and 100 kPa. The variation of the axial strain with the number of cycles was found to be similar to that from static creep tests with three distinctive regions of primary, secondary and tertiary creep (see Section 2.5.2). The slope of the curve in the secondary creep region, which is almost constant, was characterised as the steady-state strain rate and was plotted against stress level. They found that the steady-state deformation behaviour of the mixtures under repeated load followed power law creep with creep exponent values varying between 1.1 and 1.5. Lower values of the creep exponents compared with those calculated from static uniaxial and triaxial creep tests were attributed to the low stress level operation of the test equipment, where the deformation behaviour of bitumen and asphaltic mixtures is essentially linear. It was noted that the repeated load axial test (RLA) may be sufficient to rank the rutting potential of mixtures. However, the test was not sufficient to fully characterise the deformation behaviour of mixtures, as the stress levels applied by the equipment was not enough to reach the non-linear behaviour.

By performing laboratory scale wheel tracking tests on the idealised mixtures over a range of temperatures and stress levels (between 500 kPa and 1500 kPa), rut depth against the number of load passes was plotted for each test condition. Similar to the patterns from static uniaxial and repeated load tests, after an initial period where the rutting rate decreased, the rut depth increased linearly in proportion to the number of cumulative load passes. The constant rutting rate was used to characterise the steady-state rutting rate of the mixtures. It was found that, over the range of stress levels applied in the tests, the rutting rate varied non-linearly with stress level. The non-linearity followed the power law creep with the creep exponent values from 1.9 to 2.4 which is similar to the creep exponent of static creep tests.

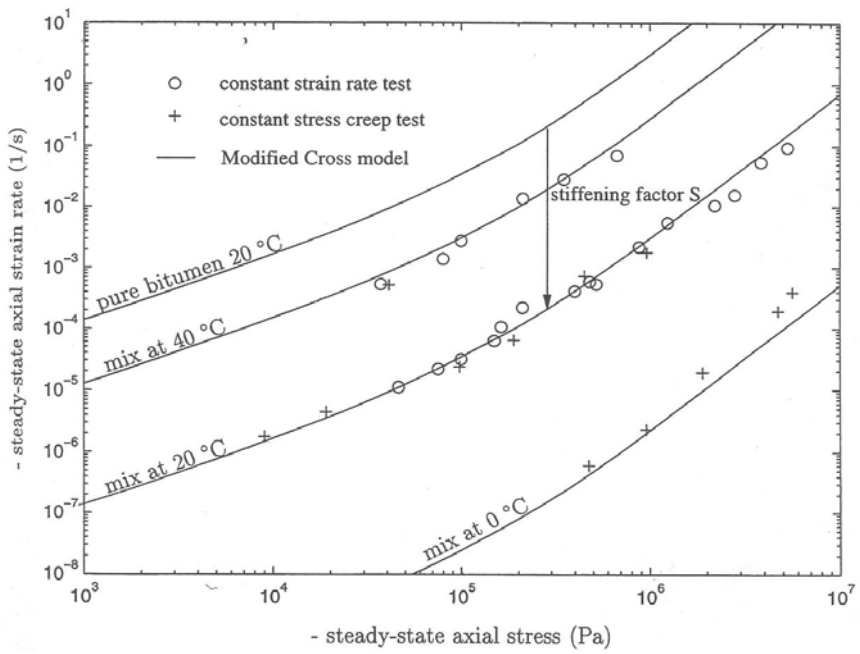

Figure 2.3 Steady-state deformation behaviour of an idealised mixture with 64% by volume sand and 50 Pen pure bitumen at different temperatures [Deshpande, 1997].

2.4.4 Steady-state Deformation Behaviour of Realistic Asphaltic Mixtures

Khanzada [2000] investigated the steady-state deformation behaviour of two realistic asphaltic mixtures, Hot Rolled Asphalt (HRA) and Dense Bitumen Macadam (DBM). Compressive static uniaxial and triaxial tests, uniaxial

repeated load tests and laboratory scale wheel tracking tests were carried out on the mixtures. Khanzada designed both realistic mixtures with a binder content of 7% and target air void content of 7% with intention of making the specimens close to the idealised mixtures he had used.

To study uniaxial steady-state deformation behaviour, uniaxial tests under constant stresses and constant strain rates were carried out at 20°C. The steady-state strain rate from the uniaxial creep test results and the steady-state stress from constant strain rate tests were used to characterise the steady-state deformation behaviour of the mixtures. The experimental results showed that the uniaxial steady-state deformation behaviour of the HRA30/10 and 10 mm DBM mixtures had the same form as that of pure bitumen and the idealised mixtures with linear behaviour at low stress levels and non-linear power law creep behaviour at high stress levels. However, the mixtures were stiffer than the idealised mixtures which had the same constituent bitumen and different volume fractions of aggregate. At the stress levels greater than 700 kPa, viscous deformation of the mixtures was non-linear with creep exponent of 2.4. The DBM was found to be stiffer than the HRA with the same constituent bitumen. Comparison of the uniaxial test results on the 10 mm DBM made by 100 Pen grade bitumen with the results on the mixtures made by 50 Pen bitumen, showed that the form of the steady-state deformation behaviour of the two mixtures was similar, but the mixture with 100 Pen bitumen reduced the stiffening effect by approximately 6 times.

To investigate the triaxial steady-state deformation behaviour of the realistic mixtures, triaxial creep tests were carried out on the HRA30/10 with 50 Pen bitumen and the 10 mm DBM with 100 Pen bitumen, over a range of deviatoric stresses and stress ratios at 40°C. It was found that the triaxial steady-state deformation behaviour of the mixtures had the same form as that of the pure bitumen with a stiffening effect of aggregates and confining stress. Like the idealised mixtures, both the HRA30/10 and 10 mm DBM mixtures were observed to dilate under triaxial stress states. The volumetric strain for both mixtures was found to vary linearly with the shear strain. The dilation ratio was observed to be independent of the stress ratio and deviator stress, but dependent

on the volume fraction of aggregates. The values of dilation ratio for the HRA and DBM were observed to be higher than those for the idealised mixtures at corresponding stress ratio.

Khanzada [2000] also studied the steady-state deformation behaviour of realistic mixtures under repeated loading. Uniaxial repeated load tests were conducted over a range of stress levels (between 50 and 100 kPa) at 40°C. The creep exponent for the mixtures were found to be between 0.8 and 0.9, which was attributed to the low applied stress levels, since, the existing Repeated Load Axial (RLA) test machine could not operate at high stress levels. The laboratory scale wheel tracking tests were carried out over a range of temperatures and stress levels, and the steady-state rutting rate was used for characterisation of the permanent deformation behaviour of the mixtures. Due to the high values of applied stresses in these tests in comparison with the repeated load axial creep test (RLA), the non-linear creep exponent values were found to be between 1.9 and 2.4. This was attributed to the fact that at these stress levels the binder viscous properties is non-linear.

2.5 Permanent Deformation Testing

2.5.1 Introduction

Principally, the objective of pavement material testing is to investigate their behaviour under conditions as close to *in situ* as possible. The first stage in the development of a constitutive model for characterisation of the material being modelled is the availability of experimental data for determination of the model constants, calibration and verification of the model. A typical stress condition for an element in a pavement under a moving load, including vertical, horizontal and shear stresses and their variation with the load movement is shown schematically in Figure 2.4. Reproducing *in situ* conditions in the laboratory is not easy to do, and needs complex equipment. Over the years, simplified tests have been used for investigation of the permanent deformation behaviour asphaltic materials and the development of constitutive models. The most common tests are listed below.

- Static uniaxial and triaxial tests
- Cyclic uniaxial and triaxial tests
- Shear tests
- Laboratory and full scale wheel tracking tests

2.5.2 Static Uniaxial and Triaxial Tests

Static uniaxial tests are the simplest tests used for characterisation of the deformation behaviour of viscoelastic materials like asphaltic mixtures. They are typically conducted at either a constant stress (creep test) or a constant strain rate in tension or compression. In the more common compressive tests, cylindrical specimens with a friction reduction system between the loading platens and specimen are used to prevent specimen barrelling due to the friction.

In a static uniaxial creep test, a vertical stress is applied rapidly to the specimen and then held constant and the strains (usually axial and radial) and axial load are measured as a function of time. Figure 2.5 shows schematically a typical creep curve of strain versus time for a viscoelastic material. The curve comprises of the instantaneous strain (elastic and plastic), also known as time-independent strain, that occurs upon load application followed by time dependent strain (delayed elastic and viscous) which occurs over time. The creep curve can be divided into three regions. A primary creep region in which the strain rate leading to the secondary (steady-state) creep region, in which the strain rate is constant followed by the tertiary creep region in which there is an accelerating strain rate.

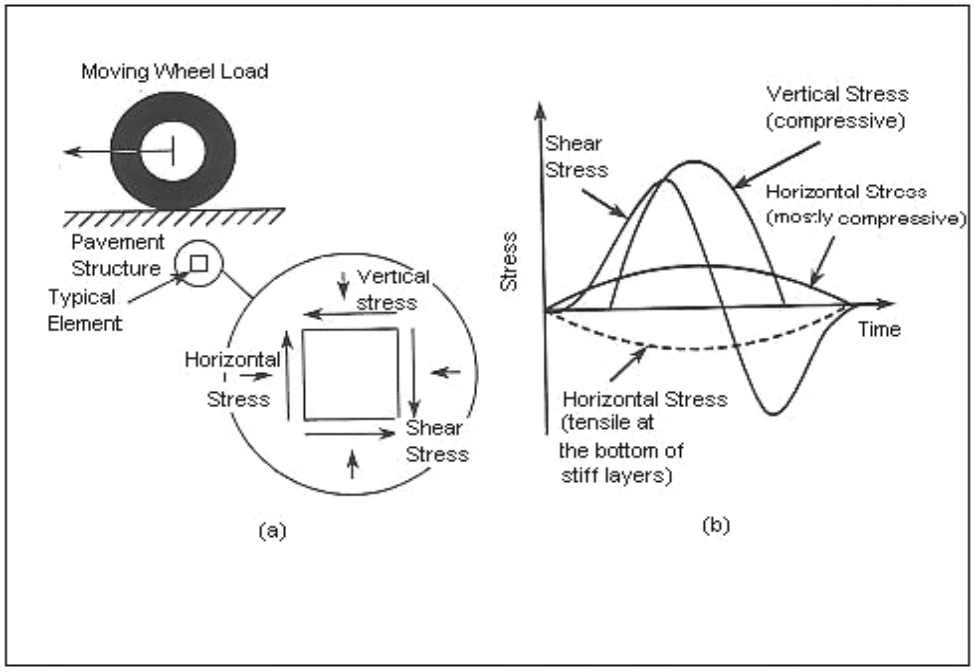

Figure 2.4 Stresses induced by a moving wheel load on a pavement element [Brown, 1978a].

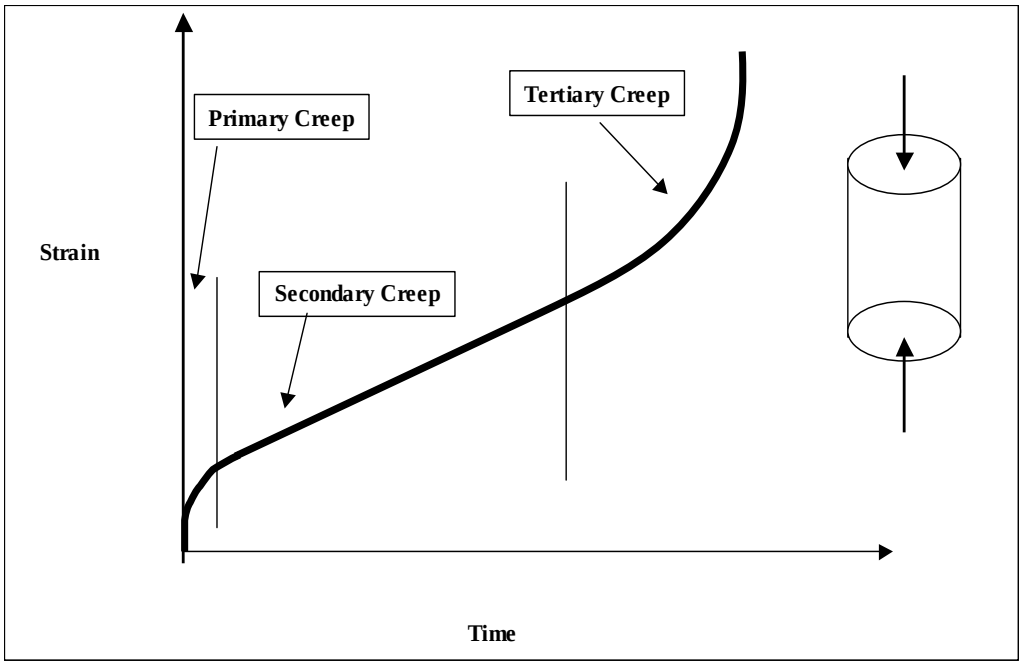

Figure 2.5 Schematic creep curve (Reproduced from [Gibb, 1996]).

In an attempt to develop a test method to judge the stability of asphalt mixtures in terms of resistance to permanent deformation and to permit prediction of the rut depth in the pavement, the Shell organisation developed the static uniaxial

creep test for asphaltic materials [Hills, 1973]. Hills [1973] used equipment in which the upper platen was fixed and the lower platen was loaded by a dead weight through a system of levers. Experimental results were presented in plots of stiffness modulus of the mixture S_{mix} against stiffness modulus of bitumen S_{bit}. The stiffness of the mixture was defined as constant stress divided by nominal strain in the mixture ($S_{mix} = \sigma / \varepsilon_{mix}$). The stiffness of bitumen was obtained from the Van der Poel nomograph [Van der Poel, 1954] using loading time, temperature and the penetration and softening point of the bitumen. For short loading times and/or low temperatures, it was found that the stiffness modulus of a mixture was a function of the stiffness modulus of bitumen and volume fraction of aggregate. However, at higher temperatures and/or higher loading times, in addition to the effect of aggregate volume concentration, the gradation, shape, surface texture and compaction level were found to be important in determining the stiffness of the mixture. The Shell researchers used the uniaxial creep test for prediction of rut depth in asphaltic pavements, which will be explained later in Chapter 3.

There are some differences between the static uniaxial creep test and realistic loading conditions. In the pavement, the materials are confined and loaded dynamically, whilst in the static uniaxial creep test the specimen is unconfined and loaded statically. For the same accumulated loading time, the permanent deformation of asphaltic mixtures under dynamic loading has been found to be greater than that under static loading [Bolk *et al*., 1978; Monismith *et al*., 1988; Gibb, 1996; Brown *et al.*, 1980]. This difference increases with increasing the number of load passes [Gibb, 1996; Brown *et al.*, 1974]. It has been attributed to the contact between aggregate particles, which causes the plastic deformation in each load pass. The difference in the behaviour under static and dynamic loading conditions varies with the type of mixture [Van de Loo, 1974] and confining stress level [Monismith *et al.*, 1988] with the difference typically decreases as the confining stress increases.

Another difference between the static uniaxial creep test and realistic loading conditions is that the mixtures *in situ* are confined whilst the specimens in the

static uniaxial creep test are unconfined. In the static uniaxial creep test, the deformation mostly depends on the bitumen and filler properties (bitumen content, viscosity, type of filler and filler/bitumen ratio) and the internal friction of the aggregates has little influence on the deformation [Gibb, 1996]. In triaxial stress conditions, in addition to the properties of bitumen and filler, aggregate interlock has a major influence on the deformation behaviour of the mixture. Brown *et al.* [1984] compared the static uniaxial and triaxial creep test with the cyclic triaxial creep test. The cyclic triaxial creep tests were carried out with both deviator and confining stresses cycled sinusoidally. The comparison was based on the stiffness evaluated from each test for four types of mixtures. They used the plots of mixture stiffness obtained from each test versus the stiffness of bitumen. They concluded that the static uniaxial creep test distinguished well between mixtures with different deformation resistance, as good correlation was observed between the unconfined creep test results and the cyclic triaxial creep test results. However, the static uniaxial creep test resulted in lower mixture stiffness values compared to the cyclic triaxial creep test. They found that the confining stress has a significant influence on resistance to permanent deformation of the continuously graded mixtures, while the influence is at a minimum for gap-graded mixtures.

The constant stress static creep test has been used by some researchers for the evaluation of resistance to permanent deformation of asphaltic mixtures. Van de Loo [1974] suggested that the creep test should be carried out in the linear range of behaviour where the stiffness is independent of stress level. The reason for this suggestion was that the *in situ* loading time is small compared with the loading time in the creep test and the permanent deformation per wheel pass remains in the linear range. The creep test conditions were chosen to be 40°C temperature, 1-hour loading time and the stress level equal to 0.1 MPa. Rowe *et al*. [1988] proposed the standard unconfined creep test to be undertaken at a stress level of 100 kPa, 30°C and 5.5 hours loading time. In the US, Hadipour *et al.* [1988] and Monismith *et al.* [1988] conducted the uniaxial creep test at 103-207 kPa and 40°C. Based on realistic loading and climatic conditions, Brown *et al.* [1994] proposed the test conditions for the static uniaxial creep test of 138 kPa vertical

stress at 40°C. The triaxial creep tests were suggested to be performed with 828 kPa vertical stress, 138 kPa confining stress at 60°C.

To determine the parameters of an elasto-visco-plastic constitutive model, developed by Scarpas *et al.* [1997], Scarpas *et al.* [1998], Erkens [2002] and Dunhill [2002] performed stain-controlled monotonic uniaxial tests in compression and tension over a range of temperatures and displacement rates. The asphaltic mixtures were subjected to a constant strain rate and the axial and radial strains and the axial stress values were recorded with time. Figure 2.6 shows schematically a typical result of a constant strain rate test where the axial stress is plotted against the strain (radial or axial strain). Erkens [2002] developed expressions to represent the strength and stiffness modulus of a Dutch sand asphalt mixture. Equations 2.15 and 2.16 show the relationship for the compressive strength and stiffness, respectively. These relationships were also successfully used by Dunhill [2002] to describe the strength response and elastic stiffness of the UK HRA30/10 and 10 mm DBM.

$$f_c = a\left(1 - \frac{1}{1 + \left[\dot{\varepsilon}\exp^{(b+c/T)}\right]^d}\right), \qquad \textbf{(2.15)}$$

$$E = a'\left(1 - \frac{1}{1 + \left[\dot{\varepsilon}\exp^{(b'+c'/T)}\right]^{d'}}\right), \qquad \textbf{(2.16)}$$

where f_c = compressive strength in MPa

E = elastic stiffness in MPa

T = temperature in degrees Kelvin

$\dot{\varepsilon}$ = strain rate in s^{-1}

a, b, c and *d* = compressive strength non-linear regression parameters

a', b', c' and *d'* = compressive stiffness non-linear regression parameters.

The strength and stiffness of the mixtures were found to increase with decreasing temperature and increasing strain rate. Dunhill's experimental results showed higher compressive strength values for the HRA compared to the DBM [Dunhill, 2002]. It was concluded that the strength of asphalt mixtures is sensitive to both binder content and binder hardness (penetration grade).

As explained earlier, the monotonic constant strain rate test was used in combination with the constant stress creep test to study the steady-state deformation behaviour of bitumen, idealised and realistic asphaltic mixtures [Deshpande *et al.*, 1999; Collop *et al.*, 1999]. Cheung [1995] and Deshpande [1997] found that the constant strain rate test and the constant stress creep test are complementary experimental tools for investigation of the steady-state deformation behaviour of bitumen and idealised asphaltic mixtures. This can also be seen in Figure 2.3, where the results from constant stress creep tests and constant strain rate tests are consistent. Therefore, for investigation of the steady-state deformation behaviour of asphaltic mixtures the more convenient test can be used at a given test conditions.

Single and/or cyclic creep recovery tests have been used by researchers for characterisation of the strain components for asphaltic materials (elastic, plastic, delayed elastic and viscous strains) [Drescher *et al.*, 1993; Lu, 1998; Sides *et al.*, 1985]. The strain components can be studied as a function of stress level, temperature, loading time, unloading time and number of cycles. In a single creep recovery test, a stress is applied rapidly to the specimen and then held constant. The specimen is allowed to creep for a certain time and the stress is released rapidly to allow the elastic and delayed elastic components of the deformation recover. In cyclic creep recovery tests (see Figure 2.7), the loading

and unloading is repeated for a certain number of cycles which allows study of the deformation components as a function of number of cycles.

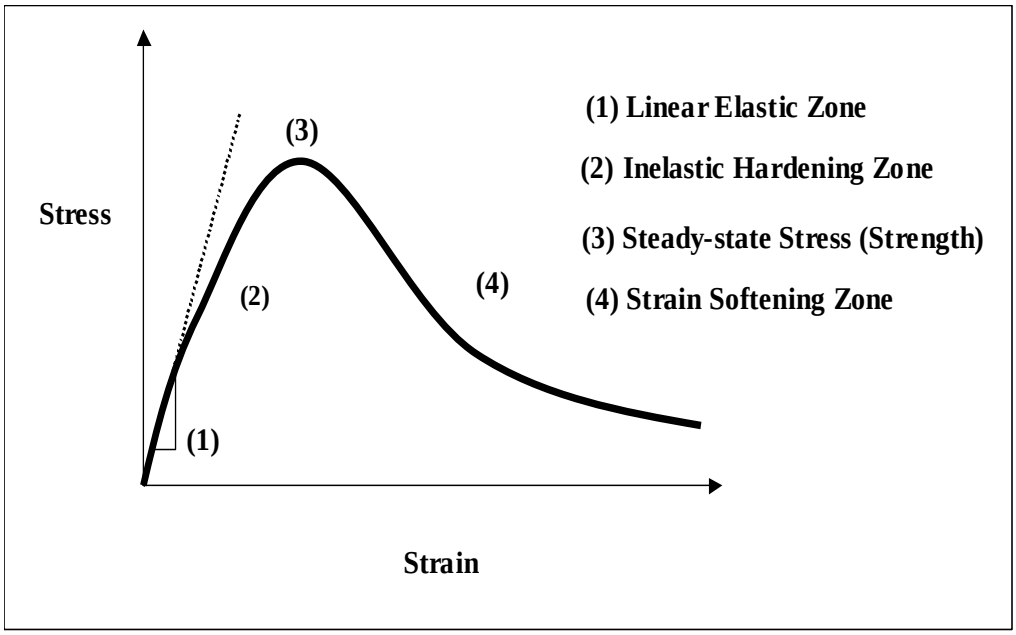

Figure 2.6 A typical monotonic constant strain rate test result (Reproduced from [Dunhill, 2002]).

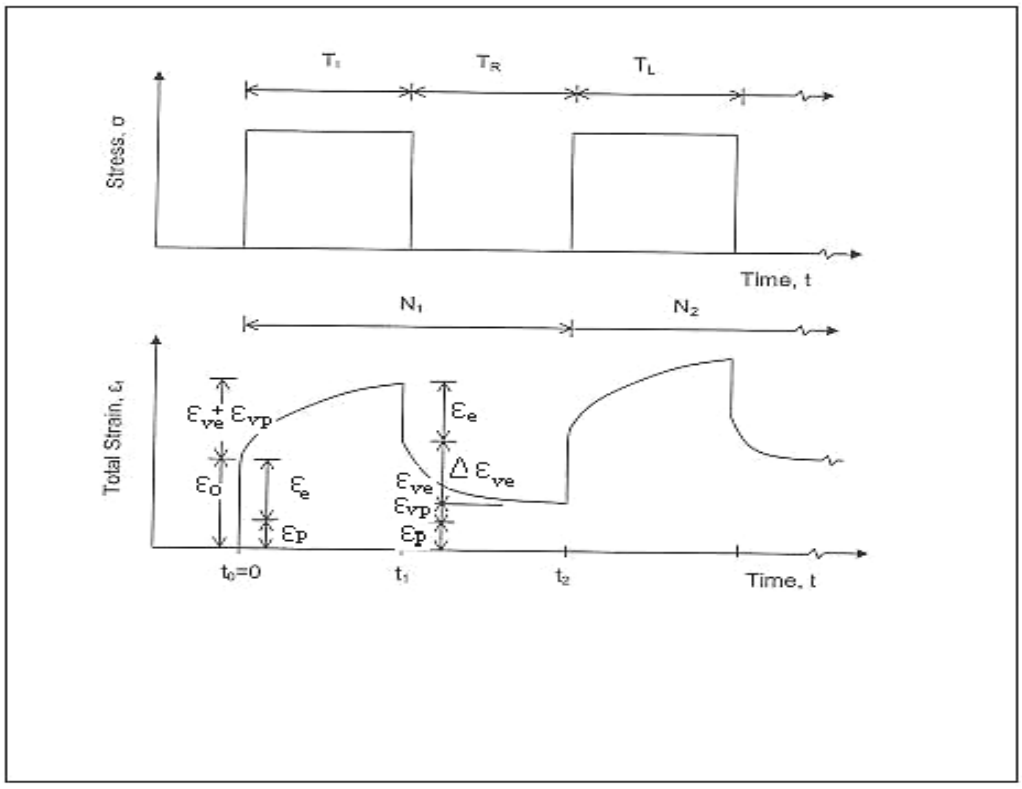

Figure 2.7 Strain components in a creep recovery test [Sides *et al.*, 1985].

By performing uniaxial and triaxial single creep recovery tests over a range of deviatoric stresses, temperatures, stress ratios and total strains before unloading, Ossa [2004] investigated the recovery behaviour of low volume fraction and fully dense idealised mixtures. Similar to bitumen, it was observed that, for both uniaxial and triaxial conditions, the recovered strain increases linearly with increasing the total strain before unloading. The slope of the line, named as recovery constant, was found to be independent of temperature, deviator stress level and stress ratio. However, the recovery constant was observed to decrease with increasing the volume fraction of aggregate. A model was developed to capture the recovery strain versus time history of the mixtures. By measuring the radial strain of the specimens and calculation of the shear and volumetric strains, it was found that the volumetric strain varied linearly with the shear strain with the same slope during creep and recovery.

Stress-controlled cyclic uniaxial and triaxial pulse tests, (see Figure 2.2c), were performed on the idealised mixtures, over a range of temperatures, deviatoric stresses, stress ratios and time period ratios Δ_p/Δ_g. The uniaxial test results revealed that, for a fixed value of axial stress, the accumulated permanent deformation decreased with decreasing Δ_p/Δ_g because larger fractions of the creep strain were recovered during the zero-load gaps between the pulses. The triaxial test results showed that for a fixed deviator stress and time period ratio, the accumulated permanent strain decreases with increasing stress ratio.

2.5.3 Cyclic Uniaxial and Triaxial Tests

Cyclic creep tests have been used to study the deformation behaviour of pavement materials under more realistic loading conditions [Brown, 1978a]. In the cyclic uniaxial tests, an axial load is applied repeatedly with or without a rest period between the pulses. The maximum deformation from each load pulse is recorded and plotted against the number of cumulative cycles. The creep curve for the cyclic creep test is similar to that of the static creep test (see Figure 2.5) including the primary, secondary and tertiary creep regions. The deformation of the mixture during each cycle can also be plotted (see Figure 2.7). In the cyclic

triaxial creep test, the vertical load is applied repeatedly along with a static or dynamic confining stress. Depending on the equipment, the vertical and lateral loads can be applied in various shapes such as sinusoidal, square, triangular and trapezoidal. Sinusoidal loading, although requiring more complex equipment, is the best for simulating *in situ* loading conditions [Brown, 1976]. The loading time is chosen to represent that of the material under passing traffic in the pavement. Barksdale [1971] has presented data with which the duration of load pulse in a repeated load test, corresponding to vehicle speed and depth in the pavement, can be determined. Various loading systems, from simple pneumatic or mechanical systems to more sophisticated servo-controlled electro-hydraulic systems, have been used to apply repeated loading, [Brown, 1976].

The cyclic uniaxial creep test does not directly simulate *in situ* loading conditions. However, for the ranking of different mixtures, in terms of resistance to permanent deformation, it has been shown that is more suitable than the static creep test [Gibb, 1996]. Nunn *et al.* [1999] demonstrated that the cyclic uniaxial test could not discriminate mixtures with different aggregate gradings in terms of resistance to permanent deformation. For mixtures with different gradings, the cyclic triaxial creep test results have shown good correlation with simulated wheel tracking tests results [Nunn *et al.*, 1999]. Zhang *et al.* [2000] compared the cyclic triaxial creep test with a simulated rut test; the asphalt pavement analyser (APA), in evaluating of permanent deformation and found good correlation between the tests. The cyclic triaxial creep tests were conducted for 1 hour (3600 cycles), with 0.1-second load duration and 0.9-second rest period intervals. The axial load was 827 kPa and the confining stress was 138 kPa. The test was carried out at 60°C. After 3600 cycles, the load was removed and the recovery was measured for 15 min. The strain after this period was reported as permanent strain, which is an indicator of the rutting potential.

Brown *et al* [1980] investigated the deformation behaviour of a continuously graded mixture under static and cyclic triaxial conditions at 25°C. In the cyclic tests, both the deviatoric and confining stresses were cycled in a square waveform with 0.5 second loading and 0.5 second rest time. The stress levels in the static triaxial creep tests were equal to the peak values in the cyclic tests.

They presented their results as plots relating the volumetric strain (Equation 2.13) and the shear strain (Equation 2.14) to the deviatoric and mean normal stresses, which were defined as follows.

$$\sigma_m = \frac{1}{3}(2\sigma_{11} + \sigma_{33}), \quad \textbf{(2.17)}$$

$$\sigma = (\sigma_{11} - \sigma_{33}) \ , \quad \textbf{(2.18)}$$

where σ_m = mean normal stress

σ = deviatoric stress

σ_{11} and σ_{33} = the confining and axial stress respectively.

Various stress conditions in compression and extension were used. For extension conditions, they applied confining stresses higher than the axial stresses. They concluded that the volumetric strains and strain rates depended only on the mean normal stress, while the shear strains and strain rates depended on both the deviator stress and the mean normal stress. For the cyclic triaxial creep tests, both the extension and compression tests with equal deviatoric stresses produced similar volumetric and shear strains. However, for the static triaxial creep test, the strains were different in extension and compression. Volumetric strains in extension and compression, and shear strains in compression, for the cyclic tests, were higher than those for the static creep tests while the shear strains in extension were similar in both tests.

Brown *et al* [1974] investigated the effects of vertical stress, temperature, confining stress, frequency of the vertical stress pulse, rest period and binder content on deformation of a dense bitumen macadam in a cyclic triaxial creep test. The vertical stresses were applied dynamically and the confining stresses were static. They found that the level of the static confining stress, which gave the same strain as the dynamic confining stress was approximately equal to the mean level of the dynamic stress amplitude. It was also concluded that an increase in temperature and vertical stress increases the strain and an increase in confining stress decreases the strain. At frequencies above 1 Hz, the strain was

found to be time, rather than frequency dependant. The rest period between pulses was found to have negligible effect on the accumulation of strain.

2.5.4 Wheel Tracking Tests

The wheel-tracking test is used as a simulator of *in situ* conditions for pavement materials. Its simplicity and simulative nature have made it a popular test for many years throughout the world. Various kinds of wheel trackers have been developed, such as the Georgia loaded wheel tester, the asphalt pavement analyser (APA), the Hamburg wheel tracking device, the Laboratoire Central des Ponts et Chaussees (LCPC), the Nottingham pavement testing facility (PTF) etc. (for details see [Zhang *et al.*, 2000]). Wheel trackers are used as a small scale wheel tracking test, as shown in Figure 2.8, half scale testing facility like Nottingham Pavement test Facility (PTF) [Brodrick, 1977] or full scale Accelerated Pavement Test facilities (APT). The specimens in these tests range from full pavement sections in APT to half scale pavement sections in the half scale wheel tracking test through to small slabs or cores in the small scale wheel tracking test. The specimens are loaded by full size tyres through to small tyres depending on the test scale. The specimen in wheel-tracking tests is loaded repeatedly by moving the wheel on the specimen and, in small scale wheel tracking tests, by moving the specimen to and fro under the wheel. The specimens are usually loaded in one direction and some wheel tracking tests have the facility of traversing to simulate lateral wander of wheels. The test is carried out at specified temperatures by placing the apparatus in temperature-controlled room (in small scale and half scale tests), or in realistic climatic conditions by making pavement sections in outside. The specimen is loaded at predetermined passes and the rut depth at the centre of the loaded region and/or transverse section profile is monitored against time or the number of load passes. In addition to the assessment of mixtures, it is also used for validation of the rutting prediction methods, which will be described in the next chapter. The wheel-tracking test is also used as a reference for the evaluation of element testing methods [Nunn *et al.*, 1999; Gibb *et al.*, 1996; Gibb, 1996; Zhang *et al.*, 2000]. The LCPC mixture design method in France uses the LCPC wheel tracker test

for evaluation of mixture resistance to permanent deformation in conditions where the risk of rutting is high.

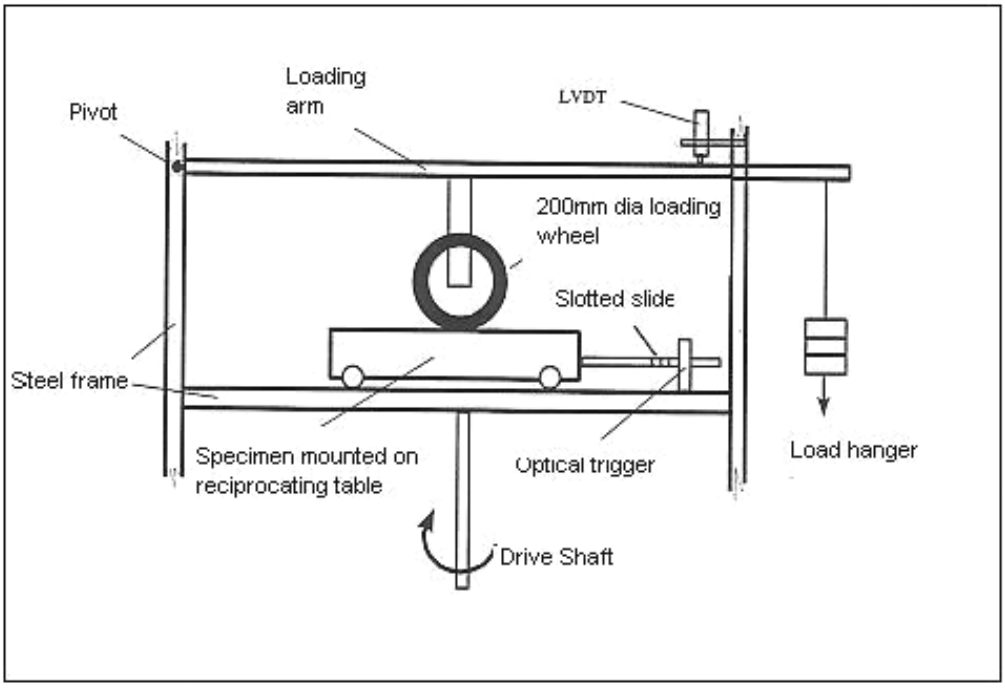

Figure 2.8 Schematic of a small-scale wheel-tracking test [Gibb, 1996].

2.5.5 Repeated Simple Shear Test (RSST)

The Strategic Highway Research Program (SHRP) developed the Universal Testing Machine (UTM), which had the capability of testing for fatigue, permanent deformation and stiffness [Sousa *et al.*, 1993]. One piece of the equipment was the simple shear tester, which was used to measure the deformation properties of asphaltic mixtures. A measure of the primary mechanism contributing to rutting, i.e. shear distortion, is provided by the Simple Shear Test. The testing system consists of two orthogonal tables connected to two perpendicular load actuators and an environmental chamber unit, which can provide accurate temperature and air pressure control. The specimen is held on the shear table, which is actuated to impart a shear load. Linear Variable Differential Transformers (LVDTs) are used to measure vertical and shear deformations. The applied loads can be controlled from the LVDT's feedback. Various modes of loading can be applied using the Simple Shear Test (SST). A very brief description of two tests using this equipment for evaluation of rutting

performance of asphaltic mixtures follows. A detailed explanation of the tests can be found in Harvey *et al.* [2001].

Repeated Simple Shear Test at Constant Height (RSST-CH)

The repeated simple shear test at constant height (RSST-CH) is used to predict the rutting performance of asphaltic mixtures. Cylindrical specimens, cored from the field or compacted in the laboratory are used in the test. The diameter of the specimen is 150 mm or 200 mm, and their height should be less than 1/3 of the diameter, and also depends on the maximum aggregate size [Harvey *et al.*, 2000]. The test is conducted at specified temperatures. The specimen is loaded by repeated haversine shear stress followed by a rest period. The magnitude of the shear stress, loading duration and rest period can be varied. The typical loading conditions that have been used for highway applications are: a shear stress of 68.9 kPa, a load duration of 0.1 seconds and a rest period of 0.6 seconds [Harvey *et al.*, 2002]. The deformations during the test are measured by LVDTs. The specimen will dilate under shear stress, which increases the specimen height. Hence, a variable axial stress, which is controlled by LVDTs' feedback, is applied continually to maintain the specimen height constant. The intention is to obtain pure shear distortion and eliminate volume change. Using the LVDTs' output the resilient and permanent shear deformations during the test are calculated. The test is typically run for 5,000 to 10,000 repetitions. The permanent shear strain versus load repetition is plotted, which again has three regions similar to the static and cyclic creep tests. Resilient shear stiffness for the given load condition and test temperature can also be calculated [Harvey *et al.*, 2002]. The results of the RSST-CH can be used to rank mixtures for expected performance, or to estimate their performance.

Shear Frequency Sweep (FS-S)

In terms of specimen dimensions, constant height condition, instrumentation and testing equipment, the shear frequency sweep test (FS-S) is the same as the RSST-CH test. The differences are in the loading and temperatures. This test is performed at a series of frequencies and temperatures. The loading is a shear

stress adjusted to provide a sinusoidal shear strain wave and a variable axial load to maintain a constant specimen height. The data obtained from the test are shear stress amplitude; shear strain amplitude and the shear phase angle for each frequency. These are used to determine the linear viscoelastic properties of the material (i.e. storage modulus, loss modulus, complex modulus and phase angle). A master curve of shear stiffness can be developed using the results of the test at multiple temperatures.

2.6 Summary

The permanent deformation of asphaltic mixtures in the upper pavement layers can be a significant contribution to rutting. Therefore, development of a model to explain the rutting relies, at least in part, on the understanding of the deformation behaviour of the asphaltic mixtures.

Permanent deformation of asphaltic mixtures, after initial densification, occurs mainly due to shear viscous deformation. Shear deformation of the asphaltic mixtures depends on the properties of constituent materials, their composition, stress state and environmental conditions.

Steady-state deformation behaviour of bitumen, idealised mixtures and some realistic mixtures, investigated at the Universities of Nottingham and Cambridge, were reviewed. The research showed that the steady-state deformation behaviour of the asphaltic mixtures mirror that of the bitumen which is non-linear creep law at high stress levels, linear at low stress levels and is temperature and confinement dependent.

The review of the test methods for measurement of permanent deformation properties showed the limitation of existing test methods in terms of their ability to replicate *in situ* conditions. A test method that can apply varying shear, axial and radial stresses, whilst controlling temperature and moisture content needs very complex equipment. The static uniaxial and triaxial creep tests and creep recovery test are suitable for capturing elastic, delayed elastic and viscous deformation of asphaltic mixtures. The cyclic tests can be applied to study the

effect of loading rate and rest time on permanent deformation of asphaltic mixtures. Moreover, cyclic tests have been found to be suitable for discrimination of deformation behaviour of mixtures with different aggregates structure. The wheel tracking test can better simulate actual pavement, and is used for validation of constitutive models for pavement material performance, mixture design purposes, and evaluation of element testing methods.

Review of Constitutive Modelling of Rutting

3.1 Introduction

For successful analysis and design of a pavement, it is necessary to determine a functional relationship between stress and strain for the pavement materials at different working conditions. This relationship is called a constitutive model. Constitutive modelling is well established in many fields of engineering such as soil and rock mechanics, concrete technology, etc. However, asphaltic materials are more difficult to model because of their complex behaviour. Ideally, a constitutive model for predicting the permanent deformation of asphaltic mixtures should include the following features [Cheung, 1995 and Sousa *et al.*, 1993]:

- the inelastic, non-homogeneous, non-linear, anisotropic, time, loading rate and temperature dependent behaviour of the mixtures
- dilatancy
- different properties in tension and compression
- existence of residual deformations at the end of loading cycles

- the effect of ageing, moisture and air voids content on the permanent deformation.

These requirements make constitutive modelling complex and difficult to implement. Despite this difficulty, developments in computer technology and advances in numerical techniques in recent years have made easier the implementation of complex constitutive models. An important application of the constitutive modelling of the permanent deformation of asphaltic mixtures is for prediction of pavement rutting to be included in the design methods and used by pavement management systems. Therefore, this chapter reviews the constitutive models for describing the deformation behaviour of asphaltic mixtures and their application for prediction of flexible pavement rutting. As an introduction the earlier work dealing with the rutting of flexible pavements is explained in the following section.

3.2 Early Work on Rutting

Earlier work to prevent rutting in flexible pavements focused on limiting the vertical compressive stress or strain at the top of the subgrade. Many analytical pavement design methods and their empirical rutting relationships, often called 'rutting subgrade failure criteria' can be found in the literature. Based on the subgrade failure criterion, rutting is controlled by using materials with adequate stiffness and sufficient thickness in the pavement layers so that the strain or stress levels typically at the top of the subgrade do not exceed permissible values [Monismith *et al.*, 1962]. The use of the subgrade strain criterion to control permanent deformation was based on the hypothesis that plastic strains in pavement materials are proportional to elastic strains. Thus, by limiting the elastic strains on the subgrade, the elastic strains in the other layers of the pavement will be controlled; hence, the permanent deformation of the pavement will be controlled [Huang, 1993].

Various subgrade strain failure criteria have been proposed [Monismith *et al.*, 1962 and Pidwerbesky *et al*., 1997]. In these methods, strains at the subgrade surface are usually converted to failure using a failure criterion of the form:

$$N = \left[\frac{k}{\varepsilon_s}\right]^b, \quad \textbf{(3.1)}$$

Where N = the predicted repetitions of compressive strain level ε_s

k = a material constant

b = the damage exponent of the material

Dormon *et al.* [1965] developed a relationship between vertical compressive strain in the subgrade, induced by a single standard axle load, and the number of load repetitions. They used an elastic analysis of pavements from the AASHO road test sections designed by the CBR design method, and produced asphalt pavement thickness design charts for various design traffic loads. Their approach gained popularity for use in analytical pavement design methods.

By analysis of a representative selection of test sections in the AASHO road test using the BISAR program, Claessen *et al* [1977] proposed the following relationship between the number of standard axle load repetitions and the permissible compressive strain in the subgrade:

$$\varepsilon_s = 2.8 \times 10^{-2} \times N^{-0.25}, \quad \textbf{(3.2)}$$

where, ε_s is the permissible compressive strain in the subgrade, and N is number of load repetitions. They checked candidate designs, selected by their method, for acceptability in terms of permanent deformation of asphalt layers during the design life of the pavement.

Pidwerbesky *et al.* [1997] measured strains in the unbound granular layer and subgrade using an electronic-based system and observed that, for the same number of load repetitions, the measured values were substantially greater than the values predicted by the models presented by the Shell and others, as mentioned earlier. They developed a new subgrade strain criterion as:

$$\varepsilon_s = 0.012 \times N^{-0.145} \quad \textbf{(3.3)}$$

It should be noted that this method of limiting rutting protects the pavement against the structural rutting and does not preclude rutting due to compaction and shear deformation of the materials in pavement layers.

3.3 Elastic Models

Elastic theory was used first by Westergaard [1927] for analysis of Portland cement concrete pavements, after which the principles of elasticity were widely used in the analysis and design of flexible and rigid pavements. Burmister [1943] developed elastic layer theory for a two-layer pavement, which later was used for three and more layers. In this theory, it is usually assumed that the materials comprising the pavement layers are homogeneous, isotropic and linear elastic and characterised by time independent constants of proportionality between stress and strain [Huang, 1967].

For a linear elastic material, the proportionality between stress and strain follows Hooke's Law. For three-dimensional bodies the relationship between stress and strain can be written as follows [Sluys *et al.*, 2002]:

$$\{\sigma\} = [K]\{\varepsilon\}, \tag{3.4}$$

where $\{\sigma\}$ and $\{\varepsilon\}$ are the stress and strain tensors, respectively, and $[K]$ is the stiffness matrix of elasticity. For a homogenous linear elastic isotropic material, the stiffness matrix is defined as:

$$[K] = \frac{E}{(1+\nu)(1-2\nu)} \begin{bmatrix} 1-\nu & \nu & \nu & 0 & 0 & 0 \\ 0 & 1-\nu & \nu & 0 & 0 & 0 \\ 0 & 0 & 1-\nu & 0 & 0 & 0 \\ 0 & 0 & 0 & 0.5-\nu & 0 & 0 \\ 0 & 0 & 0 & 0 & 0.5-\nu & 0 \\ 0 & 0 & 0 & 0 & 0 & 0.5-\nu \end{bmatrix}, \tag{3.5}$$

where E = Young's modulus

ν = Poisson's ratio.

In order to account for the effect of loading time and temperature on the response of asphaltic mixtures, it was suggested that Young's modulus of elasticity E be replaced by a stiffness modulus [Lu, 1998]. The stiffness of asphalt mixtures will be described in Section 3.5.

The number of independent constants increases for anisotropic linear elastic materials. For non-linear elastic materials, the stress-strain relationship is non-linear and the material parameters are dependent on the stress and or strain level. Hence, for non-linear elastic analysis, material behaviour is approximated using piecewise linear elastic theory and an incremental approach like finite element (FE) method is used. The following paragraphs explain the research studies which have used elastic theory for prediction of the rutting in flexible pavements.

The layer-strain method calculates the rut depth in flexible pavements using linear or non-linear elastic analysis together with the permanent deformation properties of pavement materials typically evaluated using the repeated load triaxial test. To predict the amount of permanent deformation after a given number of load applications, each layer of the pavement structure is divided into several sub layers (Figure 3.1). Following that, using appropriate linear or non-linear elastic layered theory, the stress state at the centre of each sub layer beneath the wheel load is calculated. The axial plastic strain corresponding to the average stress state at the centre of each sublayer is determined from the results of repeated load triaxial tests performed for the desired number of load repetitions. The total rut depth beneath the wheel load is obtained from following equation [Barksdale, 1972]:

$$\delta_{total}^{p} = \sum_{i=1}^{N} (\varepsilon_i^p h_i), \qquad \textbf{(3.6)}$$

where δ_{total}^{p} = total rut depth

N = number of sublayers

ε_i^p = average plastic strain in the *ith* sublayer

h_i = thickness of ith sublayer

In this method, the effects of moving loads are considered indirectly by using pulse loading in the repeated load triaxial test. This is a limitation of this method because varying speed traffic loading cannot be simulated in this way.
The following paragraphs describe some of the studies that have used the layer-strain method for prediction of rut depth in flexible pavements. A more complete review of this research can be found in [Khanzada, 2000 and Monismith, 1976].

Using the layer-strain method, Romain [1972] developed a computer program for prediction of rut depth in flexible pavements. Each layer of pavement was divided into an adequate number of sublayers, and each sublayer was divided horizontally. The produced elements dimensions were chosen such that each element can be considered in a homogeneous state of stress. From the stresses in each element, evaluated by elastic analysis theory, and experimental stress-strain laws the expected deformation of each element after a given number of vehicle passages was calculated. Finally by summing up the partial deformations of the elements, the total rut depth at the pavement surface was calculated.

McLean *et al.* [1977] used elastic layer theory for calculation of permanent deformation for a two-layer system consisting of asphaltic concrete directly on subgrade. They subdivided the asphalt layer at 2.5 cm intervals, and assumed constant stiffness modulus for the asphalt layer. Using elastic layer theory, they calculated stress states at the centre of each sublayer beneath the axle of load. To obtain permanent deformation for each sublayer, the stress values were used in the empirical equation obtained from the results of triaxial repeated load tests. The total deformation was the sum of all sublayers' permanent deformation. For evaluation, stress, elastic strain and permanent strain distribution with depth were obtained and compared with the test track used by Hofstra *et al.* [1972]. The distribution of permanent strain observed in the test track was different from their results. This difference was related to the assumption of constant stiffness modulus values with depth, while because of increasing loading time with depth the stiffness in reality is reduced. By examining the influence of various factors on rut depth, they found that asphalt concrete stiffness had a significant influence on rutting, and the stiffness of subgrade had little influence on the accumulation of permanent deformation in the asphalt layer.

Based on the layer strain method, Morris *et al* [1974] proposed a method for prediction of rut depth in flexible pavements. They considered the permanent strain in an asphalt element to be dependent on vertical and horizontal stresses (σ_1, σ_3), temperature T and the number of load repetitions N, which was expressed as:

$$\varepsilon_p = f(\sigma_1, \sigma_3, T, N) \pm e, \qquad \textbf{(3.7)}$$

where e is an error. They carried out triaxial tests in tension and compression over a range of stresses and temperatures. Two equations were obtained which related permanent strain in tension and compression to the above-mentioned factors. For prediction of rut depth, the pavement was divided into sublayers, and the average stresses and temperatures were calculated beneath the centre of wheel load on elements of each sublayer. Using the obtained equations, the permanent strain in the elements was determined. By summation of the permanent deformations of the elements, they obtained the total permanent deformation or the rut depth of the pavement. They compared their predicted values of rut depth with the actual rut depth in a full-depth section of a test road, and obtained good agreement between the predicted and measured values. They concluded that almost all of the permanent deformation occurs in the tension zone due to lateral distortion.

The repeated load triaxial tests, used for the layer-strain method, reproduced the *in situ* principal stress conditions occurring beneath the centre line of wheel load only for compressive stress conditions, which occur in the upper part of the asphalt layer. Proposed repeated load triaxial tests, which could apply tension stresses in one direction, were also reasonable only for locations on the centre line of the wheel load, where principal planes are vertical and horizontal [Brown, 1975]. For off-axis locations, stresses acting on vertically oriented elements in the pavement are typically as shown before in Figure 2.4, in which principal planes are not vertical and horizontal, and shear stresses act on the elements. Ignoring the shear stresses in the simulation of stress conditions results in underestimation of the permanent deformation in the pavement surface [Brown *et al.*, 1977].

In dealing with these problems, Brown [1975] introduced a mean normal stress and a shear stress invariants, p and q, respectively, the same as σ_m and σ, respectively, as were defined in Equations (2.17) and (2.18). These invariants are used to describe the stress conditions at a point in the pavement, and are dependent on the principal stresses. In the triaxial test program the combination of p and q for the sample should be the same as the *in situ* combinations for the point concerned. The *in situ* vertical strain is assumed to be equal to the major principal strain in the triaxial test. This assumption is on the safe side for design purposes [Brown *et al.*, 1977].

In addition to the inability to reproduce the *in situ* stress conditions in the triaxial repeated load tests, the layer-strain method does not predict the lateral plastic flow of material from beneath the wheel load and the formation of the characteristic shoulders adjacent to the wheel path (Figure 3.2). This is because the interaction of lateral plastic deformation in adjacent elements is not considered. The approaches based on this method generally found that most strains occurred in the tensile zone in asphaltic layers.

Researchers from Shell [Hills, 1973; Hills *et al.*, 1974; Van de Loo, 1974, 1976 & 1978 and Bolk *et al.*, 1978] used elastic layer theory together with uniaxial static creep tests on asphaltic materials to calculate the rut depth of asphaltic layers in flexible pavements. It was assumed that the deformations in the unbound layers underneath can be avoided by proper thickness design [Van de Loo, 1978]. They determined the deformation properties of asphaltic mixtures by static uniaxial creep tests, as described earlier in Section 2.6.2. The stiffness modulus of the mixture S_{mix} was derived as a function of stiffness modulus of the bitumen S_{bit}. It was assumed that permanent deformation was a function of only the irrecoverable component of the bitumen stiffness $S_{bit,vis}$, which was obtained as [Van de Loo, 1978]:

$$S_{bit,vis} = 3\frac{\eta}{wt_0}, \qquad \textbf{(3.8)}$$

where w = number of wheel load passes

t_0 = time of one wheel pass (sec.)

η = bitumen viscosity (Ns/m^2)

The reduction in layer thickness or the rut depth was calculated as:

$$\text{Rut depth} = \frac{C_m h_0 \sigma_{av}}{S_{mix,vis}} \quad , \tag{3.9}$$

where h_0 = is the asphaltic layer thickness

σ_{av} = is average stress under moving wheel

$S_{mix,vis}$ = the mixture stiffness when $S_{bit} = S_{bit,vis}$

C_m is a correction factor for dynamic effects, to account for the actual response of mixtures under dynamic loading. The reason is that in the static creep tests, used in this method, the load is applied statically and the deformation behaviour under static and dynamic conditions are different. The order of difference between deformation under dynamic and static loading depends on the mixture type and was suggested to be determined empirically [Van de Loo, 1974].

To calculate σ_{av}, it was assumed that the loading time was short enough for asphalt material to behave elastically. An elastic analysis model (BISAR) was used for calculation of stresses. The average stress was expressed as a portion of the contact stress σ_0 as:

$$\sigma_{av} = Z\sigma_0 , \tag{3.10}$$

where Z is the proportionality factor between the average stress and the contact stress between tyre and pavement.

The behaviour of asphaltic materials can be assumed elastic only under high speed or short loading times, and/or low temperatures [Monismith *et al.*, 1962]. For in-service conditions, asphaltic mixtures usually exhibit non-linear stress-strain behaviour, and display elastic, viscous and plastic strains. Honrych *et al.*

[2002] simulated the behaviour of subgrade soil, unbound layers and asphalt layer with different models, as follows:

1. All materials were modelled as linear elastic.
2. Asphalt concrete was modelled as linear elastic, and the subgrade and granular materials were modelled as non-linear elastic.
3. Asphalt concrete and the subgrade were modelled as linear elastic, and granular material was modelled as non-linear elastic.
4. Asphalt concrete was modelled as viscoelastic, and granular material and the subgrade were modelled as non-linear elastic.

Predictions from each modelling scheme were compared with measured strains and deflections from a full-scale pavement instrumented for measuring deflections and strains at pavement surface and various pavement layers. Among the four hypotheses, they found that the most complete was to simulate asphalt concrete with a viscoelastic model and granular and subgrade soil with a non-linear elastic model.

3.4 Elasto-plastic Models

Elasto-plastic models have been used successfully for describing the response of soils, granular materials, concrete and metals [Dunhill, 2002]. In these models, yield points in uniaxial models and yield surfaces in multiaxial models are used for separation of elastic and plastic behaviour. The material behaviour before the yield point or yield surface is elastic, and plastic thereafter. A relationship between stress and strain is formulated for describing the material behaviour under elastic conditions, i.e. before the onset of plastic deformation, and a relationship is developed for after-yielding behaviour, i.e. when the deformation is made up of both elastic and plastic deformation components [Owen *et al.*, 1980]. Tan *et al*. [1994] used an idealised elastic-perfectly plastic constitutive model, to describe the behaviour of an asphalt mixture loaded in compression until failure and well simulated the stress-strain failure curves of triaxial tests at different confining stresses.

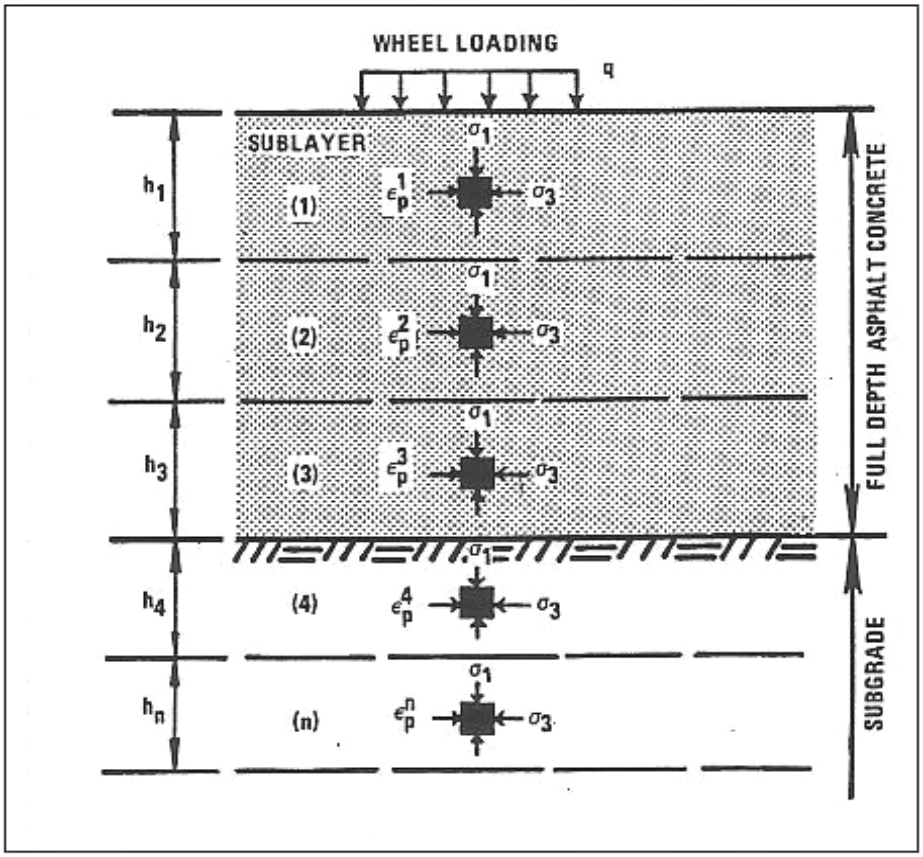

Figure 3.1 Layer-strain method of calculating rut depth using sublayers [Barksdale, 1972].

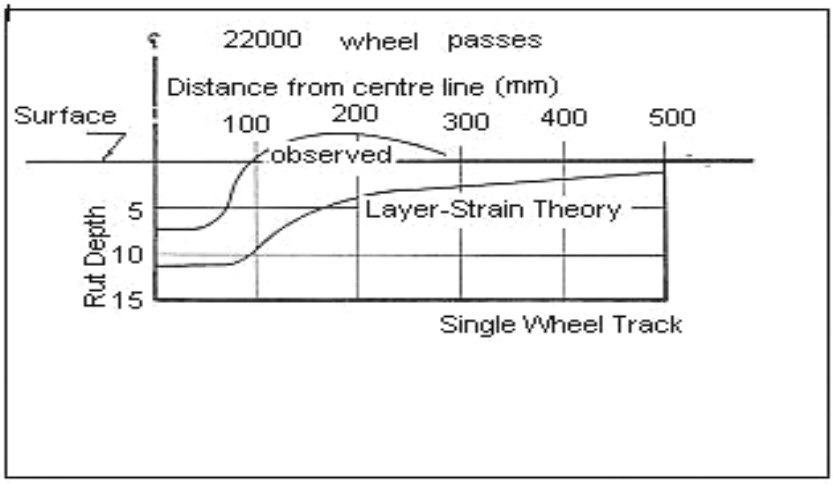

Figure 3.2 Measured and calculated rut depth [Brown *et al.*, 1977].

3.5 Viscoelastic Models

It is well documented that asphaltic mixtures behave as viscoelastic materials. These materials display elastic, delayed elastic and viscous behaviour under an applied stress. Originally, viscoelastic theory was developed to describe the mechanical behaviour of polymers. Asphalt technologists used the basic information developed in this area to explain the viscoelastic behaviour of asphaltic mixtures. Establishment of a relationship between stress and strain for bitumen and asphaltic mixtures as a viscoelastic material has been undertaken in various ways. For example, Van der Poel [1954] assessed the viscoelastic behaviour of bitumen by defining a stiffness modulus. He developed a nomograh for determination of the stiffness of bitumen. Analogous to the elastic modulus of solids, the stiffness was defined as a relationship between the stress and strain under a given condition of loading time and temperature. When a stress is applied to an elastic material an instant strain occurs which does not increase with loading time. The stress strain relation for an elastic material obeys Hook's, as follows:

$$E = \frac{\sigma}{\varepsilon}, \tag{3.11}$$

where, E is the elastic modulus of the material, and σ and ε are stress and strain, respectively. In the case of viscoelastic materials like an asphaltic mixture, when a load is applied, an instantaneous strain occurs is the material, followed by viscous strain that increase with time. The stiffness modulus S_{tT} is defined as the relation between the applied stress and the resulting strain at a certain time t and temperature T given by:

$$S_{tT} = \frac{\sigma}{\varepsilon_{tT}} . \tag{3.12}$$

Van der Poel [1954] tested over forty bitumens at different temperatures and frequencies using creep and dynamic tests, resulting in the so-called Van der Poel nomograph. From the nomograph, the stiffness of bitumen can be predicted

for any condition of temperature and loading time using only penetration and softening point.

The stiffness of asphaltic mixtures has been presented by empirical relationships [Heukelom *et al.* 1964 and Brown *et al.* 1978b] and nomographs [Bonnaure *et al.* 1977] as a function of the bitumen stiffness, volume fraction of aggregate and bitumen.

Mechanical models based on springs and dashpots are commonly used to establish a relationship between the stress and strain as a function of time for viscoelastic materials. Application of mechanical models for characterisation of asphaltic mixtures, have yielded reasonable agreement with experimental results for specific conditions, at low strain and stress levels (see Ossa [2004] for a literature review on the subject).

The mechanical models are comprised of purely elastic elements (springs) and purely viscous elements (dashpots). Deflection of the purely elastic springs depends upon stress and their stiffness, and is independent of time, and deflection of the viscous dashpots (Newtonian elements) depends upon stress, viscosity and time. These elements are combined in series (Maxwell model), parallel (Voigt element) or combinations of both in various configurations, such that they simulate the desired elastic, viscoelastic and viscoplastic strains in the material. Examples of these combinations, used by researchers for modelling bitumen and asphaltic mixtures behaviour, are shown in Figure 3.3. Theoretically, any viscoelastic behaviour of asphalt mixtures can be modelled by combining the springs and dashpots in different ways [Lu, 1998].

The simplest models for representation of the viscoelastic behaviour of bitumen and asphaltic mixtures are the two-element models, i.e. Maxwell and Voigt models (Figure 3.3 a(1), a(2)). Figure 3.4 shows schematically the creep and recovery response of the Maxwell and Voigt models compared with the realistic behaviour of asphaltic mixtures. As can be seen, neither the Maxwell nor the Voigt models can represent realistic behaviour of the asphaltic mixtures. The Maxwell model does not capture the retarded viscoelastic strain, and the Voigt

model does not represent the permanent strain of the asphaltic mixtures. Better approximations to the realistic behaviour can be obtained by increasing the number of elements in the models [Monismith *et al.*, 1966]. However, as the number of elements increases the mathematical expressions become more complex. Therefore, selection of a mechanical model for simulation of asphaltic mixtures needs to balance the required accuracy in approximation and simplicity of formulation. Figure 3.4 also shows the creep and recovery behaviour of the Van der Poel model (Voigt model in series with a spring), and the Burger's model (Voigt element in series with the Maxwell model). As can be seen, the Burger's model can simulate the creep recovery of the asphaltic mixture better than the other models in the figure. Generalised models (see Figure 3.3d) are options to better simulate the realistic behaviour of asphaltic mixtures. Papazian [1962] claimed that good approximation to the behaviour of asphalt concrete can be obtained by a generalised Kelvin model (Figure 3.3 d(1)) with five Voigt elements. By fitting the generalised Kelvin model with 1, 3 and 5 Voigt elements to test results, Uzan [1996] concluded that the model with one Voigt element was inadequate to fit test results. The models with 3 and 5 Voigt elements slightly improved the fitting. However, it was argued that the model with five Voigt elements was acceptable for low and medium temperatures, and unacceptable for high temperatures. This was attributed to the fact that at high temperatures the deformation is mostly plastic and viscoplastic, and at low and medium temperatures the deformation is mostly viscoelastic, and the generalised Kelvin model does not predict the plastic deformation. It was found that the model fitted well the results of the first cycle only, and became poor when it was applied to several cycles. From this, he concluded that repetitive loading tests with as many cycles as possible were needed.

Based on the cumulative effects of the elements in the mechanical models, mathematical relationships are proposed to describe the material stress-strain relation as a function of time. The relationships contain a number of parameters, which depend on the properties of the material, and are usually determined by experiments. As an example, mathematical expressions of the Maxwell model (Figure 3.3a(1)), for i) creep response ε (t) in response to a unit step change in

stress σ, ii) the creep compliance J(t) under constant stress of σ, and iii) the relaxation function σ (t), which is the stress response to a step change of strain are given by:

$$\varepsilon(t) = \frac{\sigma}{E} + \frac{\sigma}{\eta}(t - t_\circ), \tag{3.13}$$

$$J(t) = \frac{1}{E} + \frac{1}{\eta}(t - t_\circ), \tag{3.14}$$

$$\sigma(t) = \varepsilon_0 E \exp\left(\frac{(t - t_0)}{\tau}\right), \tag{3.15}$$

where E and η are elastic modulus of spring and viscosity of dashpot respectively and $\tau = \frac{\eta}{E}$ is relaxation time constant, which is a measure of the time required for stress relaxation.

For the case of Van der Poel's model (Figure 3.3 b(1)), which consists of a spring in series with a Voigt Model, the strain response to a step change in stress σ and the stress response to a step change in strain $\varepsilon_\circ$ are written as:

$$\varepsilon(t) = \left[\frac{1}{E_2} + \frac{1}{E_1}\left\{1 - \exp(-\frac{t}{\lambda_1})\right\}\right]\sigma, \tag{3.16}$$

$$\sigma(t) = \frac{E_2}{E_1 + E_2}\left\{E_1 + E_2 \exp(\frac{-t}{\lambda_2})\right\}\varepsilon_\circ, \tag{3.17}$$

where, $\lambda_1 = \frac{\eta_1}{E_1}$ and $\lambda_2 = \frac{\eta_1}{E_1 + E_2}$.

This model exhibits delayed elastic strain but the ultimate strain is limited to a finite value, which is equal to $\frac{\sigma}{E_1} + \frac{\sigma}{E_2}$. Such mathematical relationships can be presented for the other mechanical models.

The behaviour of asphaltic mixtures may be characterised as linear or non-linear viscoelastic. In linear viscoelastic materials, the ratio of stress and strain is a function of time and temperature but not of stress magnitude [Rahimzadeh, 2002]. Based on Schapery's definition, the mechanical behaviour of a material is considered to be linear viscoelastic if two conditions are satisfied [see Cheung, 1995]:

1. The proportional change in input causes the same proportional change in response. This condition can be expressed mathematically as:

$$\sigma(k.\varepsilon) = k.\sigma(\varepsilon), \tag{3.18}$$

2. The response due to independent inputs acting simultaneously is equal to the sum of responses due to each input acting separately. This superposition condition can be expressed as:

$$\sigma(\varepsilon_1 + \varepsilon_2) = \sigma(\varepsilon_1) + \sigma(\varepsilon_2). \tag{3.19}$$

The stress/strain behaviour of asphaltic mixtures is generally non-linear at high stresses, with the stiffness modulus decreasing as the stress is increased. However, at small stress or strain levels the behaviour is linear [Rahimzadeh, 2002]. Characterising the behaviour of asphaltic mixtures, as linear viscoelastic is a means of simplifying the mathematical modelling, because modelling of non-linear viscoelastic behaviour needs generally complicated calculation.

Linear viscoelastic models have been used in many studies for characterisation of asphaltic mixtures, analysis of stresses and strains, and prediction of rutting in flexible pavements e.g. [Papazian, 1962; Pagen, 1964, 1968 & 1972; Sayegh, 1967; Huang, 1967; Thrower, 1975; Huschek, 1977; Kenis, 1977; Nunn, 1986; Hopman *et al.* 1992 and Blab *et al.* 2002]. Notable among these works, Huang [1967] analysed two and four-layer viscoelastic systems based on the elastic-viscoelastic correspondence principle developed by Schapery [1984]. This principle transforms the viscoelastic problem into an associated elastic problem. More details about this principle can be found in [Huang, 1967&1993].

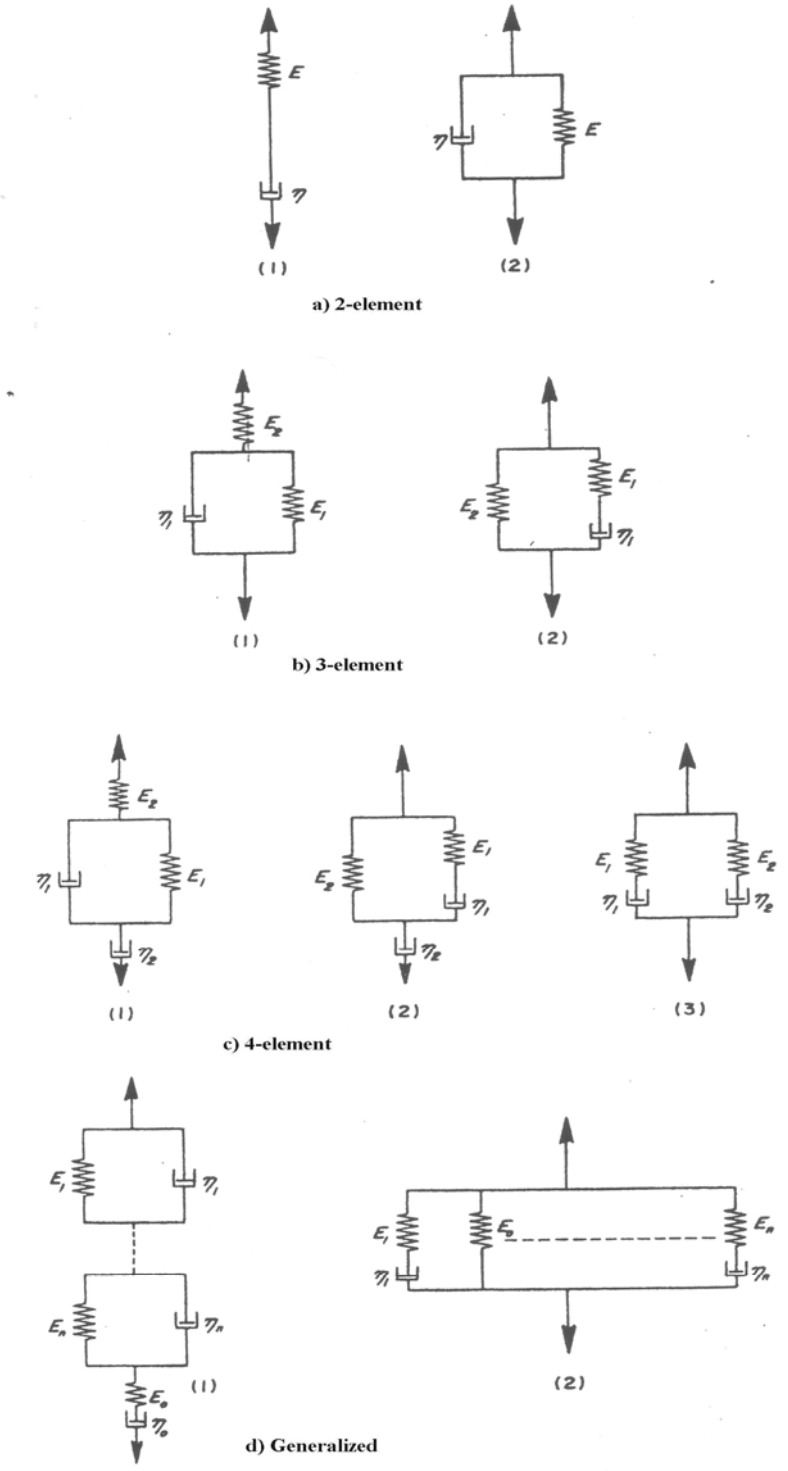

Figure 3.3 Some typical mechanical models used by researchers [Monismith *et al.*, 1966].

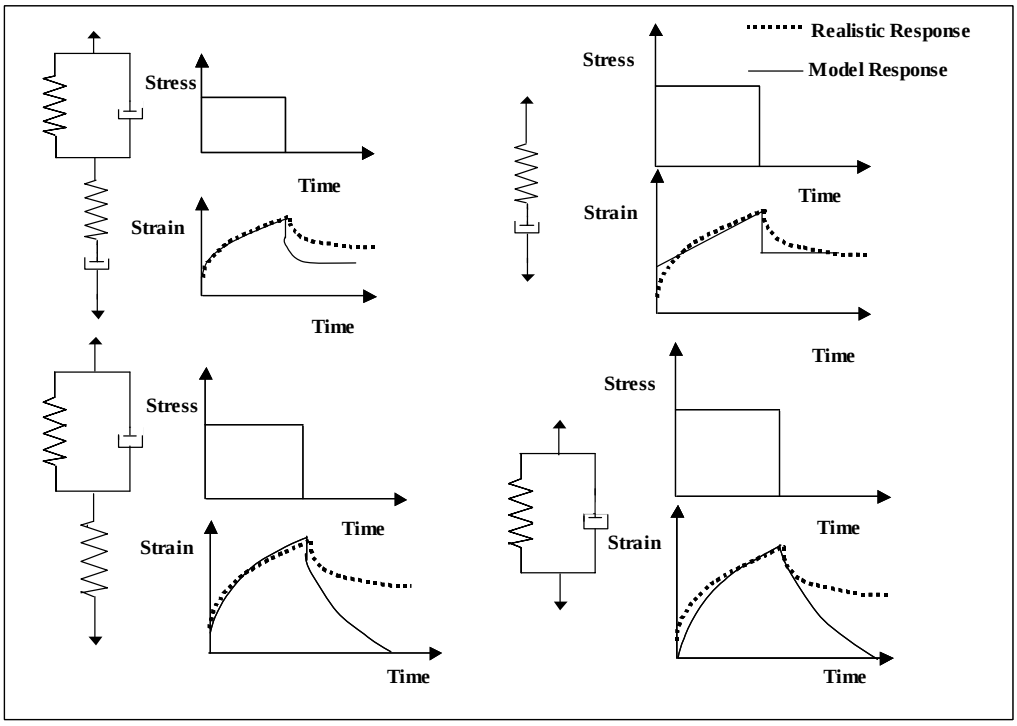

Figure 3.4 Schematic responses for the mechanical models and real material.

Some researchers have extended linear viscoelastic models to include non-linear effects e.g. [Fitzgerald *et al*., 1973; Lai *et al.*, 1973 and Vakili, 1983]. However, due to complexity, the uniaxial nature and number of required constants for the models, the non-linear viscoelastic models have not been widely used for modelling the deformation behaviour of real pavements. Some researchers, based on a non-linear extension of the corresponding principle, have developed non-linear viscoelastic models to model the behaviour of asphaltic mixtures under large strains or stresses under monotonic or repeated load conditions e.g. [Kim *et al.*, 1990 & 1995].

Both linear and non-linear viscoelastic theories have been used for prediction of rutting in asphaltic pavements. In viscoelastic methods, unlike the elastic methods described earlier, time-dependent behaviour of asphaltic mixtures is incorporated in analysis of the pavement and calculation of stresses, strains and deformations. Permanent deformation of asphaltic mixtures in this method is assumed to be due to viscous flow of material and independent of elastic properties. Mechanical models, as described before in this section, represent the behaviour of asphaltic mixtures and the viscoelastic properties of the mixtures

are determined by creep tests. Unlike the layer-strain approach, viscoelastic approaches can predict development of the shoulders adjacent to the rut path as it incorporates viscous flow of the asphaltic mixtures in permanent deformation. Due to simplicity in modelling and laboratory work, most of the methods in the literature have used linear viscoelastic theory, whereas the behaviour of asphaltic mixtures, in general, is non-linear. Using linear viscoelastic theory is a serious disadvantage of this approach. The following paragraphs explain some research works which have used the viscoelastic theory for prediction of permanent deformation of asphaltic pavements.

Assuming linear viscoelastic properties for asphaltic materials and elastic properties for non-asphaltic materials in the pavement, Huschek [1977] developed a method for prediction of the permanent deformation in a pavement. It was assumed that every load application causes a deformation comprised of reversible and irreversible deformations. The asphaltic material was modelled using a Maxwell model, in which the spring represented reversible and the dashpot represented irreversible deformation of the mixture. Static and cyclic uniaxial creep tests were used to characterise the material. With respect to speed, stress and strains at every point were evaluated as a function of time. Permanent deformation in one layer was calculated and the total rut depth was obtained by summation of the irreversible deformations of all viscoelastic layers.

Hopman *et al.* [1992] proposed a linear viscoelastic approach for calculation of vertical strain and stresses for a moving point load *(v=20m/s)* on a half space consisting of a viscoelastic material. They used Burger's model to characterise asphalt concrete behaviour. Using the Nottingham Asphalt Tester (NAT), repeated load uniaxial creep tests at 40°C were carried out on dense asphalt concrete made by Marshal compaction procedure. The axial permanent deformation as a function of the number of pulses and the response under each individual pulse were obtained. The latter was used for determination of the Burger's model parameters. They studied the change of Burger's model parameters as a result of repeated loading, and pointed out that the parameters should be readjusted as a function of time. They found that the viscosity of the dashpot in the Voigt element and both the stiffness of the spring in series and in

the Voigt element remain constant, whereas the viscosity of the dashpot in series was increases with increasing the number of load application. It was also argued that the parameters of the model are dependent on the type of loading (compression or tension).

Using linear viscoelastic theory, Collop *et al.* [1995] presented a method for prediction of permanent deformation in flexible pavements. To obtain the rate of deformation of pavements, a relation was developed in terms of load, vehicle speed and an influence function. A linear elastic layer model was used for calculation of the influence function for rate of permanent deformation. For this calculation, instead of elastic material parameters, viscous equivalents of Young's modulus E_V and Poisson's ratio v_V were used, which were presented as functions of bulk and shear viscosity. The permanent deformation was assumed to be limited to shear flow with no change in volume; therefore, the bulk viscosity was taken as infinite in value. They presented a relationship for asphalt mixture viscosity in terms of bitumen viscosity and mixture composition as voids in mixed aggregates (VMA). Creep behaviour of bitumen was modelled by a Burger's model with two retardation times. For determination of the viscosity of bitumen at a certain temperature the creep compliances of this model were fitted to data deduced from the Van der Poel nomograph. The unbound granular material and subgrade were assumed to have high effective viscosity and minor effect in rutting. The model was validated by simulation of a full-scale test track section in France. The model predicted satisfactorily the permanent deformation beyond 0.25×10^6 load passes. The discrepancies in results for traffic levels less than 0.25×10^6 were attributed to the densification of granular and asphalt layer that could not be modelled by their linear viscoelastic model. It was concluded that the permanent deformation is independent of material elasticity, and only the viscosity of pavement layers affects permanent deformation. The ridge adjacent to the wheel path was also simulated by their model. It was also argued that using a linear viscoelastic model is not suitable for asphalt materials at large strains.

Blab *et al.* [2002] proposed a 3-dimensional finite element model for a pavement, in which, for the sake of simplification, the behaviour of asphaltic mixtures was

assumed to be linear viscoelastic. The elastic and viscous parameters of the model were determined based on the results of dynamic shear tests. They used a frequency sweep shear test in which specimens undergo sinusoidal shear strain, yielding complex shear modulus and phase angle as a function of load frequency for different load magnitudes (shear strains) and temperatures. In addition to vertical stress, longitudinal and transverse stresses between tyre and pavement were taken into account. They evaluated their model by simulation of rutting on a controlled temperature test section trafficked by Heavy Vehicle Simulator (HVS) at Pavement Research Centre of the UC Berkeley. The unbound materials behaviour was assumed to be linear elastic and the permanent deformation development after specified load cycles was predicted by the model. Their simulation showed that most deformation occurs in the top asphalt layer. This was attributed to high viscous deformation due to the high shear stresses in this area. Comparison of predicted and measured deformation after certain loading cycles showed good agreement up to 10000 cycles but much discrepancy at higher cycles. This was attributed to the assumption of linear viscoelastic behaviour for the asphaltic materials, and errors in determination of material parameters.

As a part of Strategic Highway Research Program (SHRP), Sousa *et al.* [1993] presented a non-linear elastic viscous constitutive model with damage to capture the permanent deformation behaviour of asphalt aggregate mixtures. One year later, Sousa *et al.* [1994] stated that the proposed non-linear viscoelastic model failed to provide a good representation of the asphalt aggregate mixtures behaviour under cyclic loading, as the model exhibited more strain recovery in unloading in comparison with test results. Hence, they enhanced the non-linear viscoelastic constitutive model to include a simple elastoplastic component.

Long *et al.* [2002] developed a non-linear viscoelastic constitutive model for describing permanent deformation behaviour of asphalt concrete. It was focused on the dependency of permanent deformation on the rate of loading and temperature, and non-linearity of the deformation behaviour at high strain levels. The non-linear model was developed for shear deformation because of its significant influence on the permanent deformation of asphalt concrete. Their

model comprised Maxwell elements and a free spring in parallel. Simulation of Heavy Vehicle Simulator (HVS) with the non-linear model showed a rutting profile with "shoulders" on the side of the wheel paths close to the actual profile. It was found that the maximum shear strains occurred in the upper part of the pavement underneath and at the edge of the tyre. Their model did not account for densification and hence some discrepancy was observed for the rutting of the gap-graded mixture.

Collop *et al.* [2003] developed a non-linear viscoelastic constitutive model for prediction of permanent deformation in asphaltic materials under quasi-static loading. They used the Burger's mechanical model comprising elastic, delayed elastic and viscous elements, for which the strains and strain rates were additive and the stress was the same for the elements. The elastic and delayed elastic components were linear, and the viscous component was stress-based non-linear and sensitive to confinement, temperature and damage accumulation in the mixture. To account for the accumulation of damage in the viscous deformation, a Continuum Damage Mechanics (CDM) formulation was introduced in the formulation of the viscous component. This constitutive model is used in this study for characterisation of deformation behaviour of HRA and DBM mixtures which the detailed explanation of the model and its formulations can be found in Chapter 8.

Mathematical expressions for the elastic, delayed elastic and viscous strains were presented as three-dimensional incremental equations to be adapted to the CAPA-3D software. CAPA-3D is a three-dimensional finite element program, developed at the Delft University of Technology (The Netherlands) [Scarpas, 1992], which is based on an incremental formulation. A change in stress is calculated from a change in displacement. They focused on the viscous deformation which is the major deformation of asphaltic mixtures under quasi-static loading.

Using the constitutive model, the response of a typical industrial pavement structure under container loading was simulated. All materials were assumed to be linear elastic except the asphalt. The pavement response was simulated under

a uniform vertical constant stress of 10.6 MPa which was applied over 1 second, held at constant level for 24 seconds, unloaded over 1 sec and held at zero for 25 seconds. The parameters in the viscous, elastic and delayed elastic formulations were determined by fitting the test results on an idealised asphalt mixture. The results of the finite element implementation were presented as distribution of, Von Mises equivalent stress, stress ratio, equivalent viscosity of viscous component, damage variable (calculated just before unloading), and permanent strain (calculated after unloading) in the asphalt layer. The permanent strain of the asphalt layer for stress dependent and non-stress dependent models were compared. In the non-stress dependent model, the equivalent viscosity was assumed to be constant. It was concluded that the permanent vertical strains in non-stress dependent cases were significantly lower than those in the stress-dependent cases. This was attributed to the reduction of the equivalent viscosity due to the accumulation of viscous damage and local stress condition in the stress dependent cases. It was also found that, in the stress dependent case, the area of high permanent strain was localised, and for non-stress dependent case, it was more evenly distributed. The surface deformation showed reduction in thickness under load and increase in thickness outside the loaded area, which showed that the deformation occurred due to material flow under load.

Researchers like Papazian [1962] and Nair *et al.* [1962] have used vibratory tests over a range of load frequencies for assessment of viscoelastic behaviour of asphaltic mixtures. Sinusoidally varying stresses or deformations were applied, and the strain was related to stress by complex modulus or compliance. When a sinusoidally varying stress, $\sigma = \sigma_{\circ} \sin \omega t$, is applied to a linear viscoelastic material the resulting strain response will be sinusoidal as $\varepsilon = \varepsilon_{\circ} \sin(\omega t - \phi)$. Where, $\sigma_{\circ}$ and $\varepsilon_{\circ}$ are the stress and strain amplitudes, respectively, and ϕ is the phase angle. The complex modulus is a complex number in which the argument is the angle φ and the absolute value is the ratio of the amplitude the stress to that of strain. The phase angle indicates how much of the total complex modulus is attributable to viscous behaviour and/or elastic behaviour. For a completely elastic material, the phase angle is zero and for a completely viscous material the phase angle is equal to 90°. If the complex modulus is denoted by E^{*} and

written as a complex number, $E^* = E' + iE''$ where E' and E'' are the real and imaginary parts of the complex modulus, called storage modulus (relates to elastic response) and loss modulus (relates to viscous response) respectively. Then, by definition:

$$\left|E^*\right| = \frac{\sigma_\circ}{\varepsilon_\circ} = \sqrt{E''^2 + E'^2}\ , \qquad \textbf{(3.20)}$$

$$E' = \frac{\sigma_\circ}{\varepsilon_\circ}\cos\phi\ , \qquad \textbf{(3.21)}$$

$$E'' = \frac{\sigma_\circ}{\varepsilon_\circ}\sin\phi\ , \qquad \textbf{(3.22)}$$

$$\phi = \tan^{-1}\frac{E'}{E''}\ , \qquad \textbf{(3.23)}$$

Linear viscoelastic materials are thermorheologically simple. Frequency and temperature have a reciprocal effect on their characteristics, and the time-temperature superposition principle is applicable. Thus, a viscoelastic function for a temperature T can be derived from those obtained for a temperature T_1 through a horizontal translation of the curve. If various isotherms are so transformed up to a reference temperature T_s a unique curve will be obtained which is called "master curve". The shift bringing the isotherm T to T_s is called the shifting factor a_T. The WLF equation has been used for computation of shift factor as [Cheung, 1995]:

$$Loga_T = -\frac{C_1(T - T_s)}{C_2 + (T - T_s)}\ , \qquad \textbf{(3.24)}$$

where C_1 and C_2 are constants to be determined experimentally.

Using this principle for linear viscoelastic materials, the viscoelastic functions, which have two variables (temperature and frequency), are transformed into functions of only one variable (reduced frequency), and the experimental results can be extrapolated outside experimental limits, which may be difficult to achieve by direct measurements. Comparison of the viscoelastic behaviour with

this method has shown good agreement with the results from the Van der Poel nomograph [Papazian, 1962].

3.6 Elasto-visco-plastic Models

Under a load application, asphaltic materials usually show elastic, plastic, viscoelastic (delayed elastic) and viscoplastic (viscous) deformations. An elasto-visco-plastic constitutive model usually comprises formulations for each of these components. A flow law formulation is used to describe the viscoplastic deformation of the material. In viscoplastic behaviour, after initial yielding of the material, the material has time dependent plastic deformation. This behaviour is always present, to some degree, in all materials, but depending on the physical situation of the material may not be significant for some of them [Owen *et al.*, 1980]. The following paragraphs describe some of the elasto-visco-plastic constitutive models developed for characterisation of asphaltic mixtures.

Abdulshafi *et al.* [1968], using a mechanical model composed of a frictional slider element in series with a Burger's model, developed a one-dimensional combo-visco-elastic-plastic constitutive model for describing the deformation behaviour of asphalt mixtures. The total strain of the asphalt mixtures was resolved into two groups of the time-independent response in an elastic-plastic component and the time-dependent response in a visco-elastic component. Two separate models were proposed, the first for describing the elastic-plastic and the second for visco-elastic strain. The former was made up of time independent elastic and plastic strains, and the latter was made up of viscoelastic and viscoplastic strains. For calculation of permanent deformation, they developed a model comprised of three components including permanent deformation due to densification, time dependent viscous permanent deformation and time independent plastic permanent deformation. The mathematical expression of the model can be found in [Abdulshafi *et al.*, 1968]. The parameters of the models were determined by fitting to creep test results. Based on creep test results performed at 21°C, they found a true yield surface. In compression, the yielding occurred at 0.52 MPa (75 Psi), and in tension, it occurred at 0.021 MPa (3 Psi). Based on these results, they proposed that as actual pavement stress levels

exceed 0.52 MPa, plastic strains should be accounted for in characterisation of asphaltic materials.

Uzan [1996] analysed test results on asphalt concrete to study its response to load application. Total strain at a specified time was resolved into four components as:

$$\varepsilon_t = \varepsilon_e + \varepsilon_p + \varepsilon_{ve} + \varepsilon_{vp}, \quad \textbf{(3.25)}$$

where ε_e = elastic strain (recoverable and time independent)

ε_p = plastic strain (irrecoverable and time independent)

ε_{ve} = viscoelastic strain (recoverable and time dependent)

ε_{vp} = viscoplastic strain (irrecoverable and time dependent)

The viscoelastic and viscoplastic components are active during loading and only the viscoelastic part of the deformation recovers during unloading. In a loading and unloading sequence, the elastic deformation was obtained from the unloading sequence, while the plastic deformation was obtained by subtracting the elastic part from the instantaneous deformation under loading. As the recovered strain in the unloading paths represents only a portion of the viscoelastic strain (see Figure 2.7), the viscoelastic and viscoplastic components could not be separated from tests results. Therefore, it was attempted to develop a material model for separating these two components. The intention was to obtain the viscoplastic component by fitting the model to the recovery strain in unloading sequences, and then subtracting the plastic, elastic and viscoelastic components from the loading sequence. To determine the deformation components, the elasto-visco-plastic model developed by Sides *et al.* [1985] was improved as:

$$\varepsilon(t)/\sigma = D_e + D_p + D_{ve} \times t^m/(1+at^m) + D_{vp}t^n, \quad \textbf{(3.26)}$$

where D_e = elastic compliance (time independent)

D_p = plastic compliance (time independent)

D_{ve}, a, m = viscoelastic parameters

D_{vp}, n = viscoplastic parameters.

In this model, under cyclic loading, the accumulated plastic and viscoplastic strains increase with number of cycles N as:

$$\varepsilon_p(N) = \varepsilon_P(1) \times N^{\alpha} \quad \textbf{(3.27)}$$

and

$$\varepsilon_{vp}(t_n = T_L, N) = \varepsilon_{vp}(t_n = T_L, 1) \times N^{\beta} \quad \textbf{(3.28)}$$

where α, β = material properties

T_L = duration of loading time during one cycle

t_n = time measured from the beginning of cycle N.

It was found that the predominant components of the deformation depended on temperature and loading rate. At high temperatures and fast loading rates, the plastic component constituted the major part of the permanent deformation and, at low and medium temperatures, and slow loading rates, the plastic deformation was negligible. The residual deformations were found to be mainly composed of irrecovered viscoelastic and viscoplastic components. It was also indicated that the asphalt concrete behaviour was non-linear at all conditions higher than a low temperature threshold, below which the behaviour can be assumed to be linear.

Chehab *et al.* [2003] used a uniaxial viscoelastoplastic constitutive model for asphalt concrete for prediction of the response of asphaltic mixtures subjected to uniaxial tensile loading. The constitutive model comprised elastic, viscoelastic, plastic and viscoplastic components. Effects of temperature, loading rate, stress and strain amplitude, and damage were accounted for in the model formulation. Separate models for the strain components were developed and integrated to form a viscoelastoplastic continuum damage model. The viscoelastic (VE) behaviour, including the time-independent elastic component, was modelled

using continuum damage and work potential theory along with the elastic-viscoelastic correspondence principle. A formulation was also developed for the viscoplastic behaviour. The predicted values of the viscoelastic behaviour were subtracted from total strains measured in monotonic tests to obtain the viscoplastic strains. The resulting viscoplastic strains were then used for determination of the coefficients in the viscoplastic behaviour formulation. The viscoelastic and viscoplastic models were then added to form the Viscoelastoplastic continuum damage model.

A more detailed review of research work dealing with simulation of the permanent deformation behaviour of asphaltic mixtures by elasto-visco-plastic models can be found in Lu [1998].

3.7 Summary

Early methods to control rutting were to limit the stress or strain at the surface of the subgrade to a permissible level corresponding to the predicted traffic load repetitions. These methods were included in many analytical pavement design methods as a criteria to preclude rutting. Permanent deformation of asphaltic layers, that is independent of subgrade strain or stress, is not precluded in this method.

For successful analysis and design of pavements, it is necessary to establish a relationship between stress and strain for the pavement materials over a wide range of working conditions. The behaviour of asphaltic mixtures has been characterised by linear or non-linear elastic, linear or non-linear viscoelastic and elasto-visco-plastic models.

In the layer-strain method for prediction of rut depth, pavement materials are considered to be elastic. The pavement is analysed by a linear or non-linear elastic method to obtain the stress state on the elements of the materials in the pavement. Repeated load triaxial creep tests are used to determine the permanent deformation of the elements in the calculated stress state. The flexibility in using linear or non-linear elastic analysis has made this methodology attractive for

engineers to be used for prediction of rut depths. Moreover, using the triaxial test method, which better simulates in *situ* stress conditions, is an advantage for this method. However, the inability of the triaxial test to replicate the stress state in off-axis and tensile zones, the impossibility of simulating varying weight and speed vehicles in the triaxial test, considering the asphaltic mixtures as a elastic material in analysis and inability to characterise the formation of shoulders adjacent to wheel path, are disadvantages of this method.

Considering the asphaltic mixtures as viscoelastic materials, which takes into account the temperature and time dependency of deformation behaviour, is more realistic. The effect of moving load can be considered directly, and the formation of shoulders adjacent to a rut, which is a result of shear viscous deformation can be characterised in this method. Because of complexity in implementation of non-linear viscoelastic models, most of the researchers have used linear viscoelastic theory in pavement analysis and prediction of rutting. However, asphaltic mixtures have non-linear behaviour at high stress and strain levels. Ignoring the non-linear behaviour is a disadvantage of the linear viscoelastic method. Collop *et al.* [26] developed and implemented a non-linear viscoelastic constitutive model for permanent deformation of asphaltic mixtures taking into account many realistic properties of asphaltic mixtures as stress-based non-linearity, confinement and temperature dependency and the effect of damage accumulation on the viscous deformation. The model was developed for quasi-static loading conditions and was based on the static uniaxial and triaxial creep test results on idealised asphaltic mixtures. This model is currently undergoing further development at the University of Nottingham, to be used for prediction of permanent deformation in realistic asphaltic mixtures.

Elasto-visco-plastic constitutive models for asphaltic mixtures consider the plastic and/or viscoplastic deformation of the materials and are more appropriate for characterisation of the permanent deformation behaviour of asphaltic mixtures.

4 Binder Testing

4.1 Introduction

The deformation behaviour of bitumen has a significant influence on the behaviour of the mixture. Therefore, understanding the deformation behaviour of bitumen is very important to ensure good and long-term performance of the pavement when designing the pavement and the mixture. As explained earlier, one of the objectives of this study is to investigate the quasi-static deformation and recovery behaviour of two mixtures with different aggregate gradings and the same bitumen. For a better understanding of the effect of different aggregate structures on the deformation behaviour, in this chapter, the quasi-static deformation and recovery behaviour of the bitumen used in the mixtures is investigated. Constant stress shear creep tests over a range of stress levels and temperatures, and single creep recovery tests over a range of stress levels and temperatures for a series of total strains before unloading are described in this chapter. The tests were performed using a Bohlin Gemini200 Dynamic Shear Rheometer (DSR).

4.2 Dynamic Shear Rheometer (DSR)

Dynamic Shear Rheometers (DSRs) are used to measure rheological characteristics of bitumen, such as complex modulus and phase angle, from which viscoelastic properties can be defined [Airey, 1997; Khanzada, 2000]. Figure 4.1 shows the principles involved in the DSR test. The bitumen is sandwiched between a spindle and a base plate. The spindle, which can be either disc-shaped or conical, is allowed to rotate while the base plate remains fixed during testing. The test is performed by oscillating the spindle about its own axis such that a radial line through point A moves to point B, then reverses direction and moves past point A to point C, followed by a further reversal and movement back to point A. This oscillation which is smooth and continuous, as illustrated in Figure 4.2, comprises one cycle which can be continuously repeated during the test. Normally DSR tests are carried out over a range of frequencies and temperatures.

DSR tests can be carried out in controlled stress or controlled strain mode. In controlled stress mode, a specified magnitude of shear stress at a specified radius on the disc is applied to the bitumen by application of a torque to the spindle. The resultant spindle rotation is measured, from which the magnitude of the shear strain is calculated at the edge of the disc (R). In the controlled strain mode, the magnitude of spindle rotation (i.e., magnitude of shear strain at the edge of the disc) is specified and the required torque needed to achieve this is measured. In a DSR test, assuming a sinusoidal shear stress of the form:

$$\tau = \tau_0 e^{i\omega t}\ , \qquad \textbf{(4.1)}$$

where τ = shear stress

τ_0 = shear stress amplitude

i = $\sqrt{-1}$

ω = angular frequency, rad/sec.

The resulting shear strain, for a linear material, will be of the form:

$$\gamma = \gamma_0 e^{i(\omega \cdot t - \delta)}, \quad \textbf{(4.2)}$$

where γ = shear strain

γ_0 = shear strain amplitude

δ = phase angle, degrees.

Consequently, a complex shear modulus can be defined as:

$$G^* = \frac{\tau}{\gamma} = \frac{\tau_0}{\gamma_0} e^{i\delta} = \frac{\tau_0}{\gamma_0}(\cos\delta + i\sin\delta). \quad \textbf{(4.3)}$$

The real and imaginary parts in the above equation are related to the elastic (storage modulus) and viscous (loss modulus) responses, respectively, which are given by:

$$G' = \frac{\tau_0}{\gamma_0}\cos\delta = \left|G^*\right|\cos\delta, \quad \textbf{(4.4)}$$

$$G'' = \frac{\tau_0}{\gamma_0}\sin\delta = \left|G^*\right|\sin\delta, \quad \textbf{(4.5)}$$

where G' = storage modulus, Pa

G'' = loss modulus, Pa.

The magnitude of the complex shear modulus is given by:

$$\left|G^*\right| = \sqrt{G'^2 + G''^2} = \frac{\tau_0}{\gamma_0}. \quad \textbf{(4.6)}$$

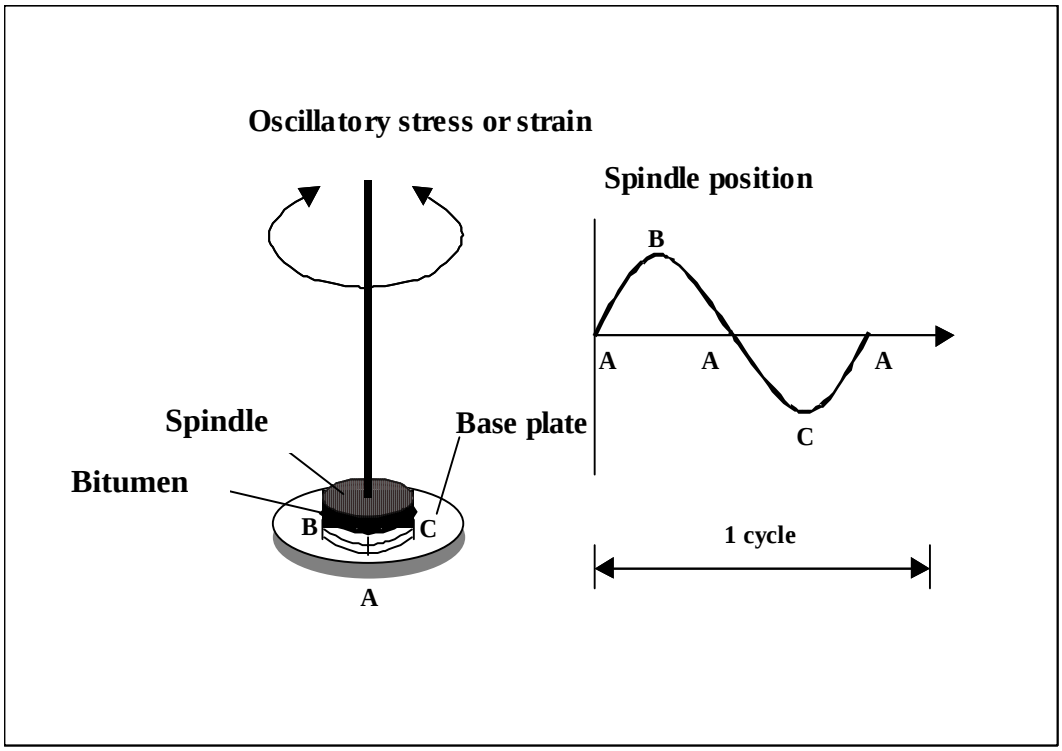

Figure 4.1 Principle of Dynamic Shear Rheometers (DSRs).

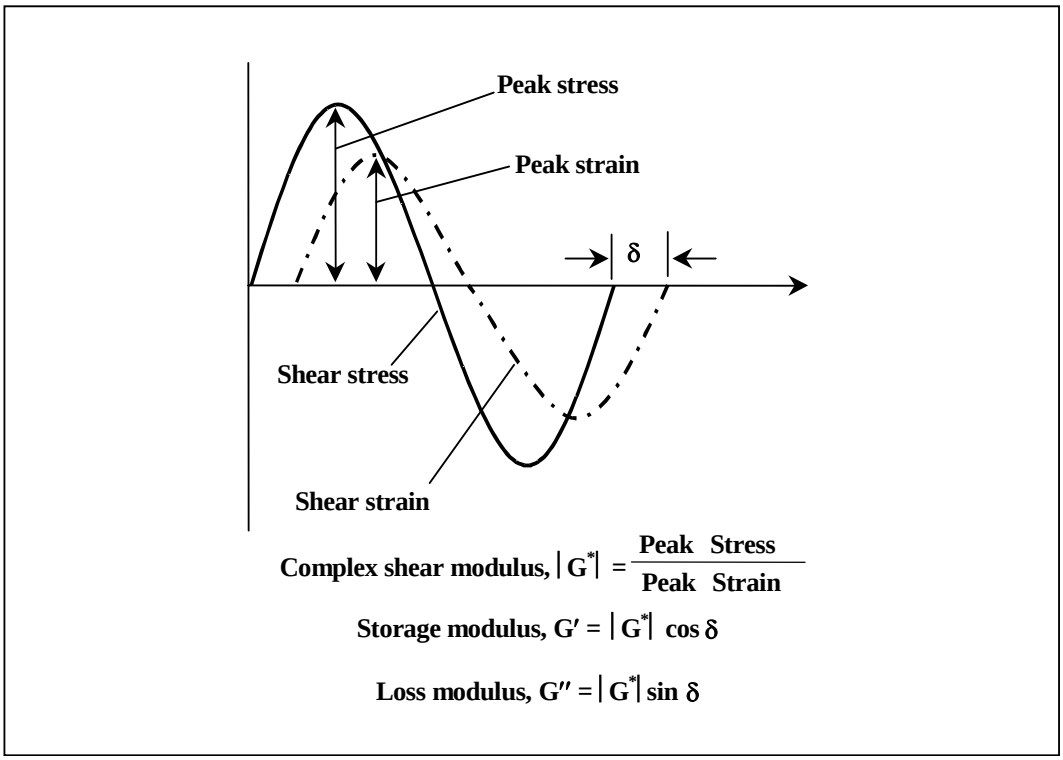

Figure 4.2 Definitions of moduli obtained from DSR tests.

4.3 Apparatus

The DSR test set-up consists of parallel metal plates, a temperature control chamber, a loading device and a control and data acquisition system (see Fig.4.3). The metal plates are typically 8 or 25 mm in diameter with smooth polished surfaces. A temperature-controlled water chamber controls the temperature of the specimen. Water is pumped through the test chamber by a separate circulating bath temperature control unit. The temperature control chamber and the circulating bath temperature control unit control the temperature of the specimen to an accuracy of ±0.1°C [Airey, 1997].

The temperature-controlled chamber completely encloses the specimen between the top and bottom plates to minimise thermal gradients. The loading device typically applies a sinusoidal oscillatory torque to the specimen at various frequencies. When the load is stress controlled, the loading device applies a cyclic torque accurate to within 10 mN.m of the specified torque. When the load is strain controlled, the loading device applies a cyclic torque sufficient to cause an angular rotational strain accurate within 100 μrad of the specified strain. The test temperature, frequency, angular rotation and torque are recorded by the control and data acquisition system. The DSR can also be used for creep tests in which a constant level of torque is applied to the specimen and the accumulation of the resulting angular rotation is monitored.

4.4 Preparation of Apparatus

An 8 mm diameter spindle was firmly mounted as the upper test plate of the DSR. By using the control buttons on the equipment or the software controlling the machine, a zero gap between the movable upper and lower test plates was established. This was done by lowering the upper spindle to touch the lower plate. For the tests at low temperatures (≤10°C), the temperature of the environmental chamber was set at 50°C. This was done because pouring the bitumen on the bottom plate at low temperatures does not give sufficient adhesion and results in separation and incorrect creep results.

Figure 4.3 Dynamic Shear Rheometer (DSR).

4.5 Test Specimen Preparation and Test Procedure

The creep and creep recovery properties of 70/100 penetration grade bitumen, used in the HRA30/10 and 10 mm DBM mixtures as binder, were studied over a range of temperatures and shear stress levels. The bitumen was heated, stirring occasionally (to ensure homogeneity and to remove air bubbles), and then poured into small containers to be used for testing when required. To use the bitumen for testing, the container of bitumen was placed in an oven set at 140°C for about 15 minutes. As noted earlier, by setting the temperature of the environmental water chamber, the lower and upper plates were heated to a temperature of approximately 50°C. The cover of the environmental water chamber was removed and the upper plate was raised by manually pressing the buttons on the equipment to provide enough room for pouring the bitumen on the lower plate.

Before pouring the bitumen onto the lower plate, the surfaces of the upper and lower plates were dried to ensure that the bitumen specimen adhered to both the plates uniformly.

A sufficient amount of heated bitumen from the container was poured onto the centre of the bottom fixed plate such that the bitumen was uniformly squeezed out between the plates for trimming. The gap between the upper and lower plates was set at 2.05 mm and the loading mechanism along with the upper plate was lowered to the required gap of 2.05 mm. The excess bitumen, squeezed out between the lower and upper plates, was trimmed from the specimen by moving a heated trimming tool around the upper and lower plate perimeters. When the trimming was completed, the gap between the lower and upper plates, which in this stage was 2.05 mm, was set at 2 mm. The cover of the environmental water chamber was then replaced, ensuring that both the upper and lower plates and the bitumen specimen were immersed in water. The temperature of the environmental water chamber was set to the test temperature, and once the desired test temperature was achieved, it remained at that temperature for at least 10 minutes to ensure uniform test temperature in the bitumen specimen [Airey, 1997]. Then the test was started.

Shear creep tests were performed by applying the desired shear stress to the outside of the disc-shaped specimen which is then held constant for a specified time. The tests were conducted over a range of shear stress levels from 400 Pa to 1000 kPa at 10°C and 20°C. The creep recovery behaviour of the pure bitumen was investigated by performing a series of single load/unload tests as shown in Figure 4.4. In these tests, a shear stress τ was quickly applied to the specimen and then held constant. The material was allowed to creep to a specified total shear strain γ^T, at which the stress was removed and the shear strain was monitored until the strain rate was zero $\dot{\gamma} \approx 0$. The strain at this point $\gamma^{pl} = \gamma^T - \gamma^r$ is the permanent shear strain, as shown schematically in Figure 4.4. These tests were repeated for a series of strains γ^T and shear stresses τ at 10°C and 20°C.

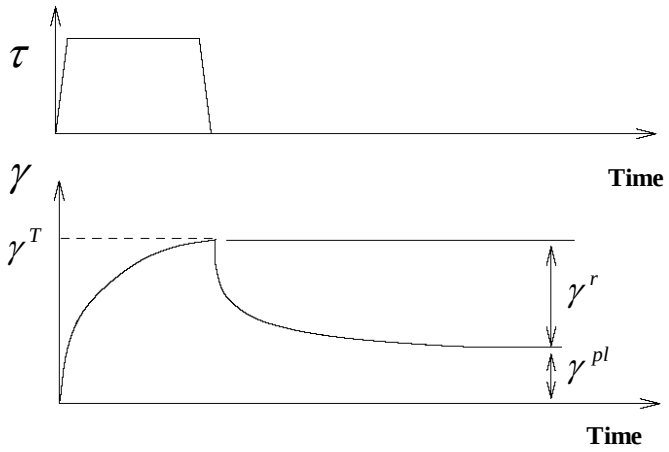

Figure 4.4 Schematic showing of the stress and strain time histories in a creep recovery test.

4.6 Test Results

A typical static shear creep test result for the 70/100 penetration grade of bitumen, at 20°C for two selected stress levels, is shown in Figure 4.5, where the creep shear strain at the outside of the disc is plotted against the time elapsed after the application of the stress. It should be noted that in these DSR tests the shear strain, shear strain rate and shear stress are calculated at the outside of the disc-shaped plates using:

$$\gamma_d = \frac{\theta R}{h}\ , \tag{4.7}$$

$$\dot{\gamma}_d = \frac{\dot{\theta} R}{h}\ , \tag{4.8}$$

$$\tau_d = \frac{2T_r}{\pi R^3}\ , \tag{4.9}$$

where γ_d = shear strain

$\dot{\gamma}_d$ = shear strain rate

τ_d = shear stress

T_r = torque

R = the radius of parallel disks

θ = angular rotation

$\dot{\theta}$ = angular velocity

h = the gap between the lower and upper plates (2 mm in these tests).

The creep curve can be divided into three regions: a primary creep region where the strain rate decreases, a secondary creep region where the strain rate is approximately constant and a tertiary creep region where the strain rate increases. The secondary and tertiary creep regions can clearly be seen in Figure 4.5. The creep behaviour of bitumen in the primary region is shown in a separate plot (Figure 4.6). The slope of the secondary creep region, in which the strain varies linearly with time, is defined as the steady-state strain rate at the prescribed stress, in line with the prescription of Cheung *et al.* [1997], Collop *et al.* [1999] and Ossa [2004].

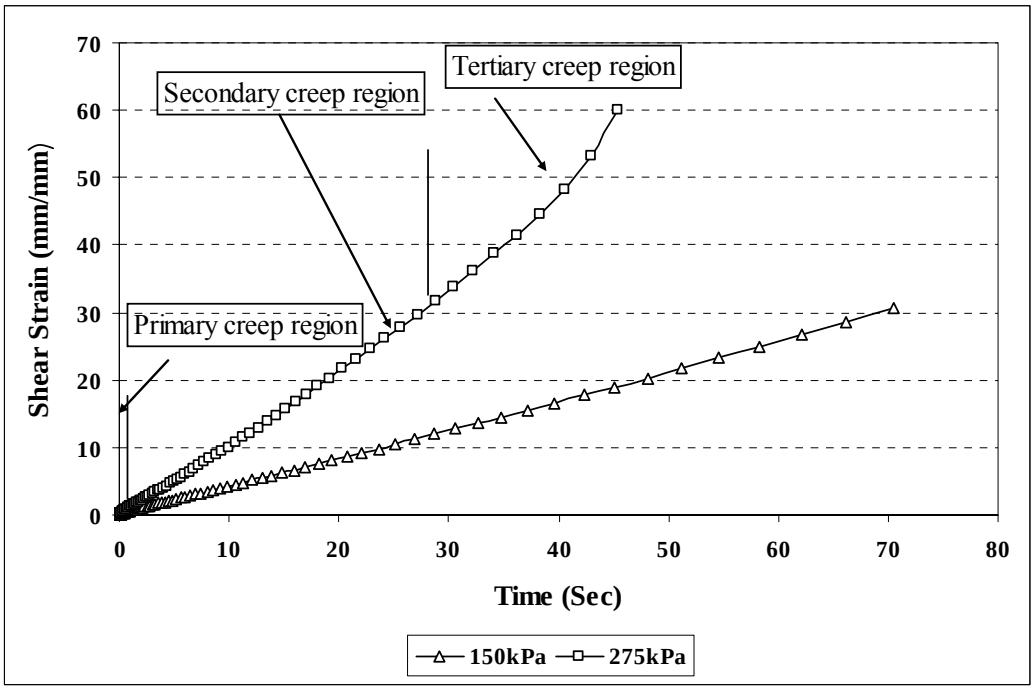

Figure 4.5 Typical creep test results for the 70/100 Pen grade bitumen.

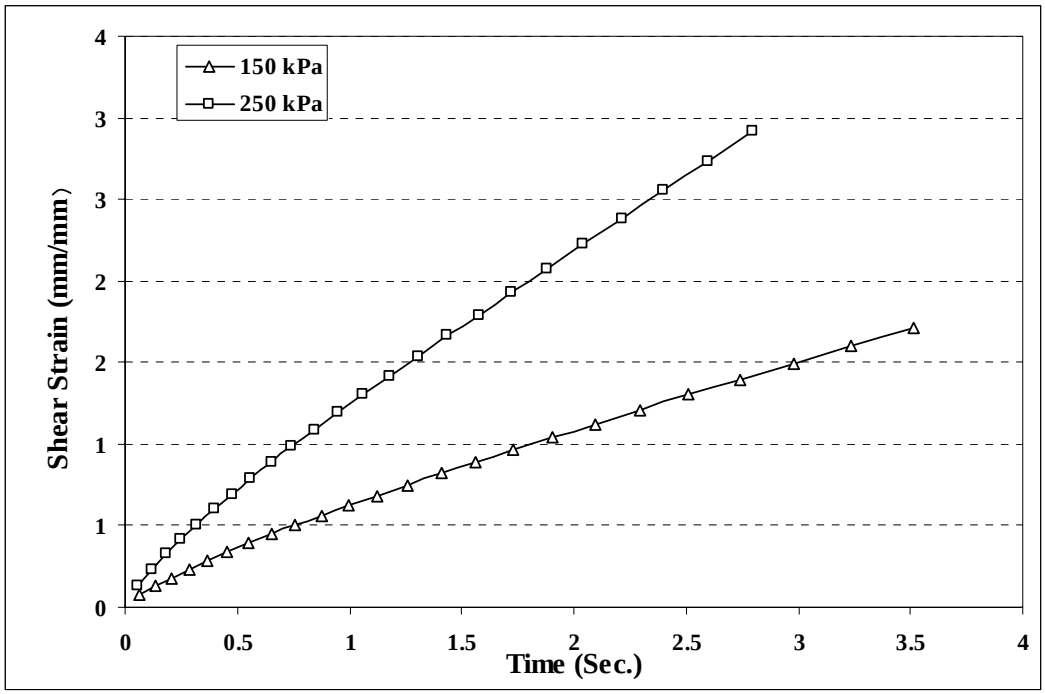

Figure 4.6 The creep behaviour of bitumen in primary creep region.

Figure 4.7 summarises the steady-state deformation behaviour of the bitumen over a range of stress levels at 10°C and 20°C on double logarithmic scales, where the shear strain rate is plotted against the steady-state creep shear stress. It can be seen from the figure that the steady-state deformation behaviour of the binder at both temperatures is similar in shape, with higher strain rates at 20°C for a particular stress level. As can be seen in the figure, there is a lack of data points for 20°C at high stress levels. This is because at those conditions the specimens fails very quickly and there were not enough data points to determine the steady-state strain rate. However, similar behaviour is anticipated at high stress levels for both temperatures.

It can be seen that at low stress levels (<approximately 100 kPa) the experimental data points tend to lie on a straight line with a slope of approximately 1. This indicates that the steady-state deformation behaviour of the bitumen in this region is linear viscous ($\dot{\gamma} \propto \tau$). At the stress levels just above 100 kPa the slope of the line tends to increase, indicating a transition from linear viscous behaviour to non-linear viscous behaviour. At the stress levels greater than approximately 500 kPa, the experimental data points tend to lie on a

straight line again with a slope of approximately 2.6 indicating non-linear power law creep viscous behaviour ($\dot{\gamma} \propto \tau^{2.6}$). The linear and non-linear behaviour of the binder can also be seen in Figure 4.8 where the shear viscosity of the binder ($\eta = \tau / \dot{\gamma}$) is plotted against the shear stress. At low stress levels, the viscosity is constant indicating linear behaviour and tends to decrease as the stress level increases which indicates that the behaviour is non-linear at high stress levels.

Figure 4.9 shows the creep recovery behaviour of the bitumen subject to a shear stress level of 1000 Pa, at 20°C for a series of γ^T, with shear strain plotted against the time elapsed after the stress application.

Figure 4.10 shows a summary of the results from all the creep recovery tests performed on the bitumen, where the recovered strain γ^r is plotted against the total strain prior to unloading γ^T. The figure shows that the recovered strain increases with increasing total strain before unloading. This continues up to a certain level of the total strain prior to unloading after which the recovered strain remains approximately constant.

It can be seen from Figure 4.10 that the level of the total strain before unloading, after which the recovered strain is constant, increases with increasing the stress level. For a viscoelastic material, an increase in applied stress will increase the elastic deformation and therefore increase the elastic recovery [Henderson, 2005]. Limited data points for the stress level of 1000 Pa at 10°C and 20°C show that the temperature does not significantly affect the recovered strain.

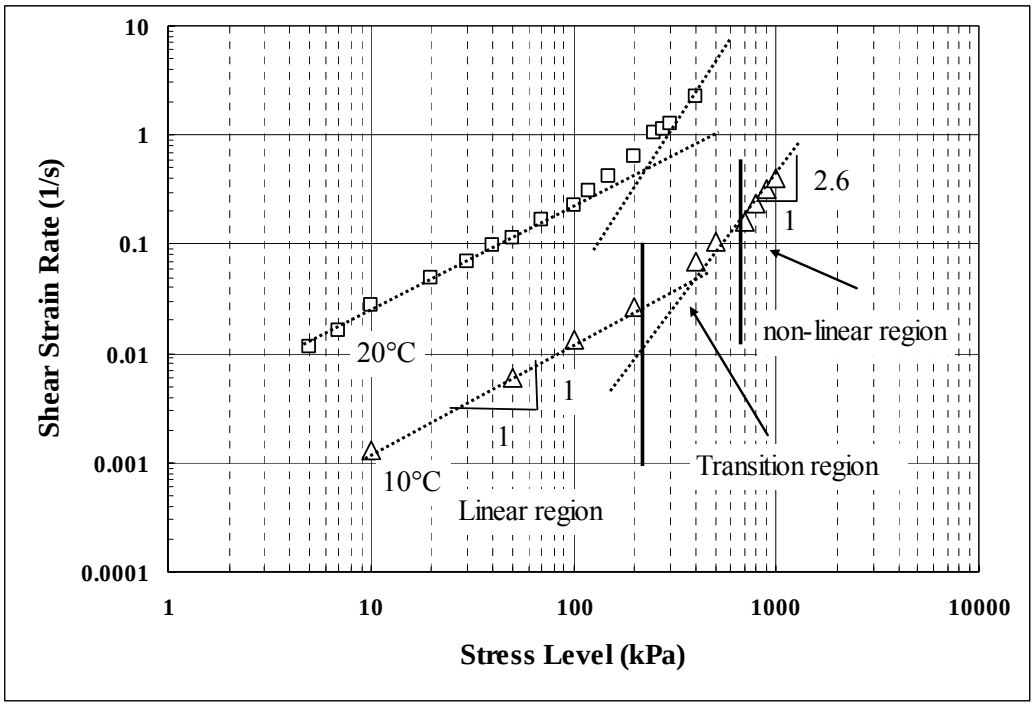

Figure 4.7 The steady-state deformation behaviour of the 70/100 Pen grade bitumen.

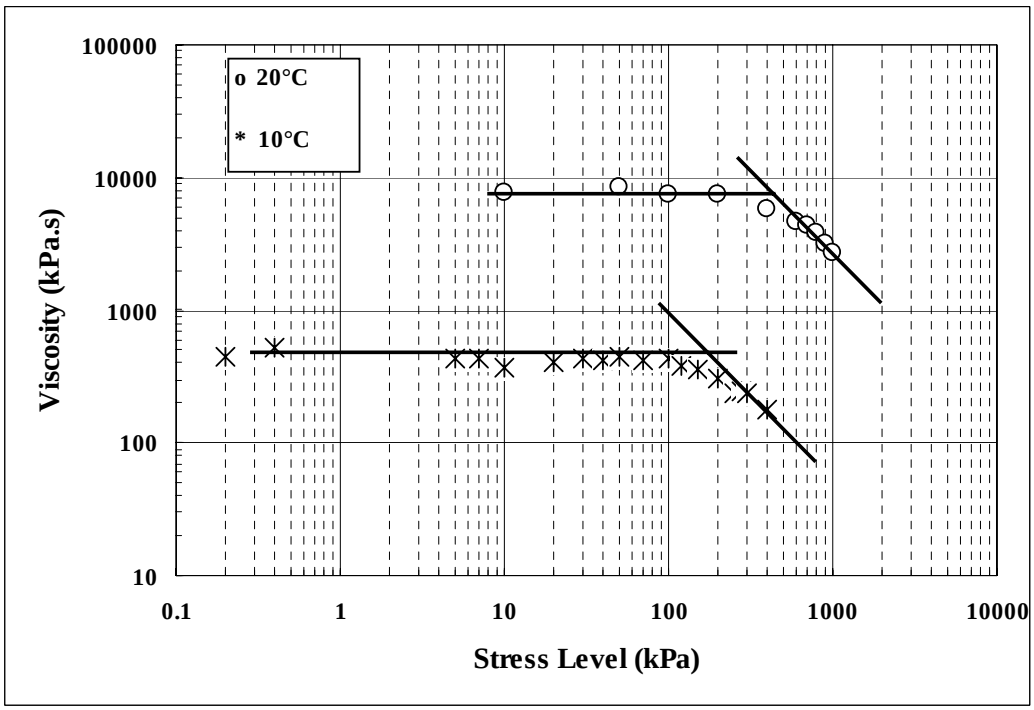

Figure 4.8 Linear and non-linear behaviour of the 70/100 Pen grade bitumen.

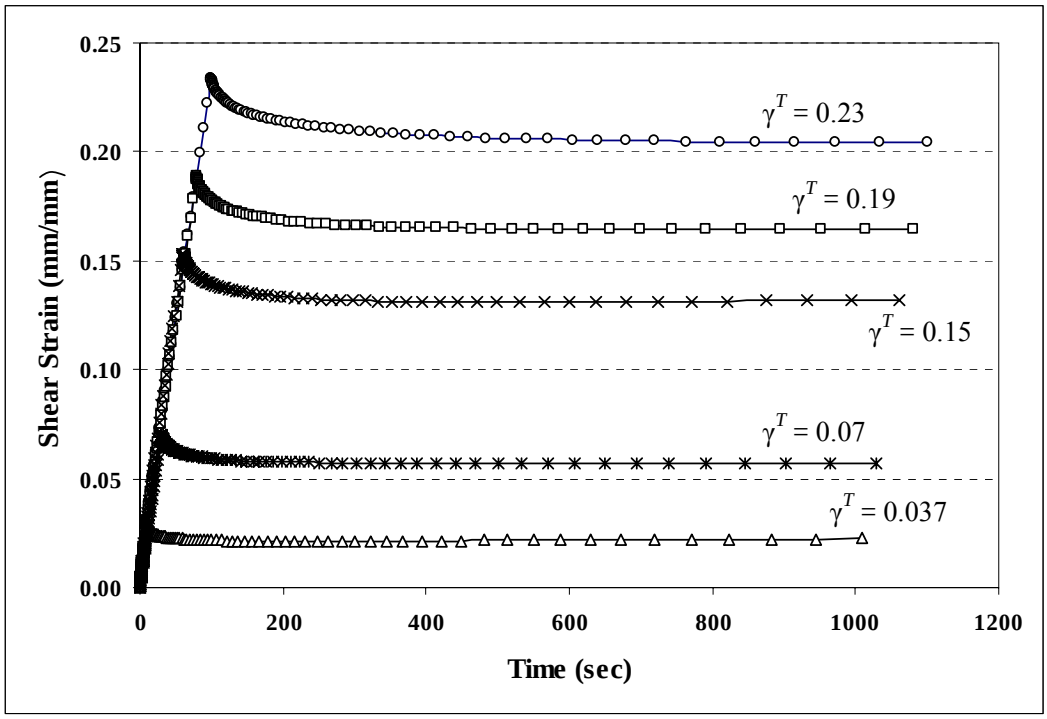

Figure 4.9 Creep recovery test results for 70/100 grade bitumen.

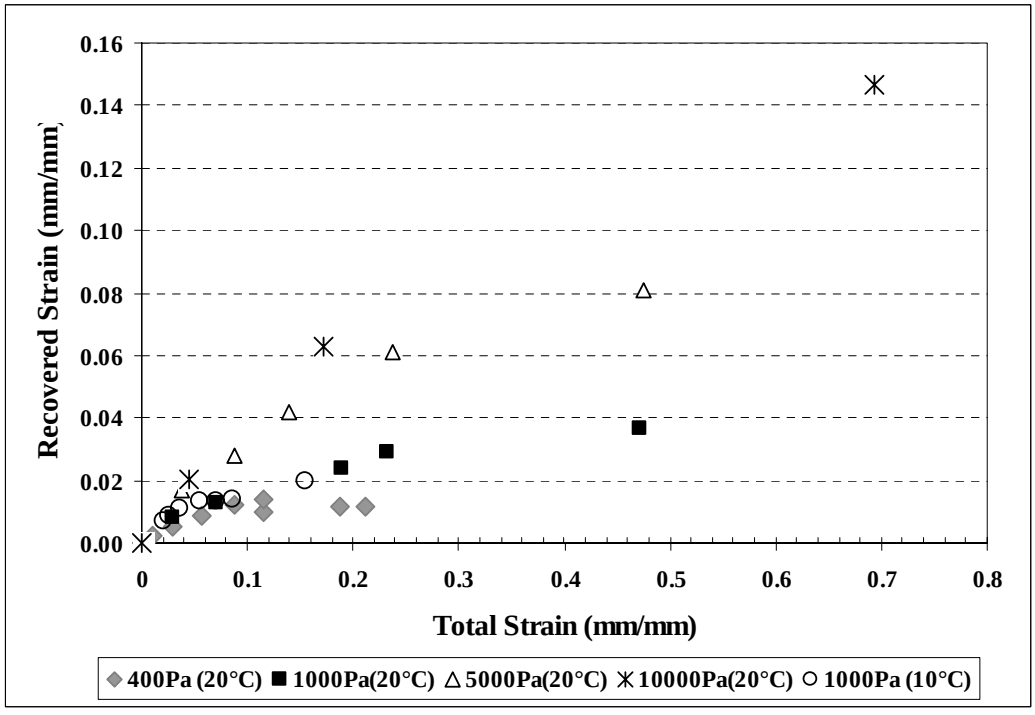

Figure 4.10 Summary of the creep recovery test results.

These results seem to be in contradiction with some of the findings of Ossa [2004]. Firstly, Ossa found that, for the total strain before unloading in the range of 0.02 to 0.2, the recovered strain increases linearly with the total strain before unloading with a slope, termed as the recovery constant, which was found to be independent of stress level (see also Section 2.5.2 for details). This contradiction is attributed to the narrow range of stress levels and total strains before unloading utilised by Ossa. As can be seen in Figure 4.9, over a narrow range of stress levels (e.g. 5 kPa and 10 kPa), the data points before the total strain level of 0.2 can be assumed on a straight line. However, for higher levels of the total strain the data points diverge, and also, the recovered strain decreases with decreasing stress level. Another contradiction is that Ossa found the recovery constant, for the 50 Pen and 100 Pen bitumens, to be 0.7 and 0.47, respectively, which are higher than the ratio of recovered strain to total strain for the experimental data summarised in Figure 4.9. This difference is attributed to the lower stress values applied in this research compared to the stress levels applied by Ossa, and the test method. Adhesion of the bitumen to the plates in the DSR prevents full recovery of the bitumen, while Ossa performed tensile creep tests on the bitumen and measured the strain at the middle half of the specimen, in which the bitumen was allowed to recover.

4.7 Conclusions

The following conclusions can be drawn from this chapter:

- Constant stress creep tests performed on the 70/100 Pen bitumen indicated that the steady-state deformation behaviour of the pure bitumen can be characterised by power law creep with the creep exponent of 1 at low stress levels (<100kPa), indicating linear behaviour, and the creep exponent of approximately 2.6 at high stress levels (>500 kPa), indicating non-linear viscous behaviour. At the intermediate stress levels (100 kPa> and <500 kPa) the behaviour is transition from linear to non-linear behaviour.

- Creep recovery tests on the bitumen revealed that, at the same test conditions (temperature and stress level), the recovered strain increases with increasing the total strain before unloading. This continues up to a level of the total strain before unloading after which the recovered strain tends towards a constant value.

- The level of the total strain before unloading after which the recovered strain is constant increases with increasing the applied shear stress level.

- The recovered strain in the creep recovery test was found to increase with increasing applied stress level independent of temperature.

5 Uniaxial Tests on Asphaltic Mixtures

5.1 Introduction

In general, asphaltic mixtures are three phase composites consisting of a high volume fraction of graded aggregate, bitumen and air voids. The physical properties and proportions of these three phases influence the deformation behaviour of the mixtures. The main load-carrying mechanisms of asphaltic mixtures are inter-particle friction and interlocking of the aggregates and the stiffness of the bitumen.

As discussed earlier in Chapter 2, the steady-state deformation behaviour of pure bitumen and idealised asphaltic mixtures has been studied by a series of researchers at the Universities of Cambridge and Nottingham. Cheung [1995] found that at temperatures above glass transition, the steady-state deformation behaviour of bitumen was linear viscous at low stress levels and non-linear power law creep at high stress levels with a creep exponent of between 2 and 2.5. Cheung's work was extended by Deshpande [1997], Khanzada [2000] and Ossa [2004] by performing static uniaxial creep and constant strain rate tests on idealised asphaltic mixtures over a wide range of stress levels, strain rates and temperatures. The steady-state deformation behaviour of the idealised mixtures

was found to mirror that of the bitumen with linear behaviour at low stress levels and power law creep at high stress levels. Using idealised mixtures composed of various volume fractions of both rounded and angular aggregate, Ossa [2004] and Deshpande found that the idealised mixtures with high volume fractions of aggregate (more than 64%) dilated under uniaxial compression. The volumetric strain varied linearly with shear strain with a slope, known as the dilation ratio. The dilation ratio was found to be independent of the applied stress level and temperature and increased with the volume fraction of aggregate in the mixture. Investigating the steady-state deformation behaviour and volumetric behaviour of realistic mixtures is an important step towards improving the understanding of the mechanisms of permanent deformation in flexible pavements.

This chapter presents experimental work and results from compressive static uniaxial creep and constant strain rate tests conducted over a range of temperatures, stress levels and strain rates on two types of asphaltic mixtures in the UK. This chapter is broadly divided into two main sections. In the first section, the experimental work, specimen manufacture, test equipment, instrumentation, friction reduction system and test procedure are discussed. In the second section the results of the tests are detailed and the steady-state deformation behaviour and volumetric response of the mixtures are discussed.

5.2 Experimental Work

In this section the experimental procedure for performing static uniaxial creep and constant strain rate tests on the mixtures is detailed.

5.2.1 Selection of Mixtures

Two generic types of asphaltic mixture, which are commonly used in UK pavements, were selected for this investigation. These two mixtures were a hot rolled asphalt (HRA) and a close graded dense bitumen macadam (DBM) surfacing. These mixtures are representatives of a gap graded and continuously

graded asphaltic mixture which allows comparison of their deformation behaviour.

To study the effect of different aggregate structures on the deformation behaviour of mixtures, without the influence of different bitumen types, the same 70/100 penetration grade bitumen was used in both mixtures. The measured Ring and Ball softening point and Penetration value of the bitumen were 45°C and 88 dmm Pen respectively. A Granite aggregate supplied by Bardon Hill quarry was used to produce the DBM specimens. The sand supplied by the quarry was not fine enough to give a satisfactory design grading for the HRA mixture. Therefore, the HRA mixture was made using the granite aggregates along with a fine sand supplied by Tarmac from Hint quarry.

5.2.2 Mix Design

The mix designs for the HRA30/10 and 10 mm DBM are shown in Tables 5.1 and 5.2, respectively, and represented schematically in Figure 5.1. The binder content by mass for the DBM and HRA mixtures were selected at 5.5% BS: 4987, Part 1 [2003] and 8% BS: 594, Part 1 [2003] respectively.

The air void content of asphaltic mixtures has a significant effect on their performance. High air void content leads to increased permeability resulting in water damage, oxidation, ravelling, and cracking. Low air void content leads to plastic flow and rutting. Since the air void content of the mixture varies throughout its life, research work has shown that the initial in-place voids should be no more than approximately 8 percent and the minimum in-place voids should never fall below approximately 3 percent during the life of the pavement [Brown, 1990]. The objective of this research was to study the deformation behaviour of realistic asphaltic mixtures after initial compaction by traffic. Therefore, the target air void content for both mixtures was set at 4%.

The design aggregate grading for the DBM and HRA are shown in Figures 5.2 and 5.3, respectively. The figures also show the grading limits recommended in

BS: 4987, Part 1 [British Standards Institution, 2003] and BS: 594, Part 1 [British Standards Institution, 2003] for the HRA 30/10 and 10 mm DBM, respectively.

The constituent aggregates were graded individually and then the percentage of each was calculated, such that their combined target grading was located in the middle of the recommended limits. Using the calculated percentages for the constituent aggregates and the design bitumen content, a sample of each mixture was produced to measure the maximum theoretical density. The maximum theoretical densities of the mixtures were used for calculation of the bulk density of the mixtures required in the mixture design.

Table 5.1 HRA mixture design

Constituent	Percentage by Mass %	Percentage by Volume %
10 mm Aggregate	27.6	23.5
Sand	57.9	49.3
Filler	6.44	5.48
Bitumen	8	17.6
Air Voids	-	4

Table 5.2 DBM mixture design

Constituent	Percentage by Mass %	Percentage by Volume %
10 mm Aggregate	29.3	25.76
6 mm Aggregate	27.4	24.1
Dust	37.3	32.82
Filler	0.47	0.41
Binder	5.5	12.8
Air Voids	-	4

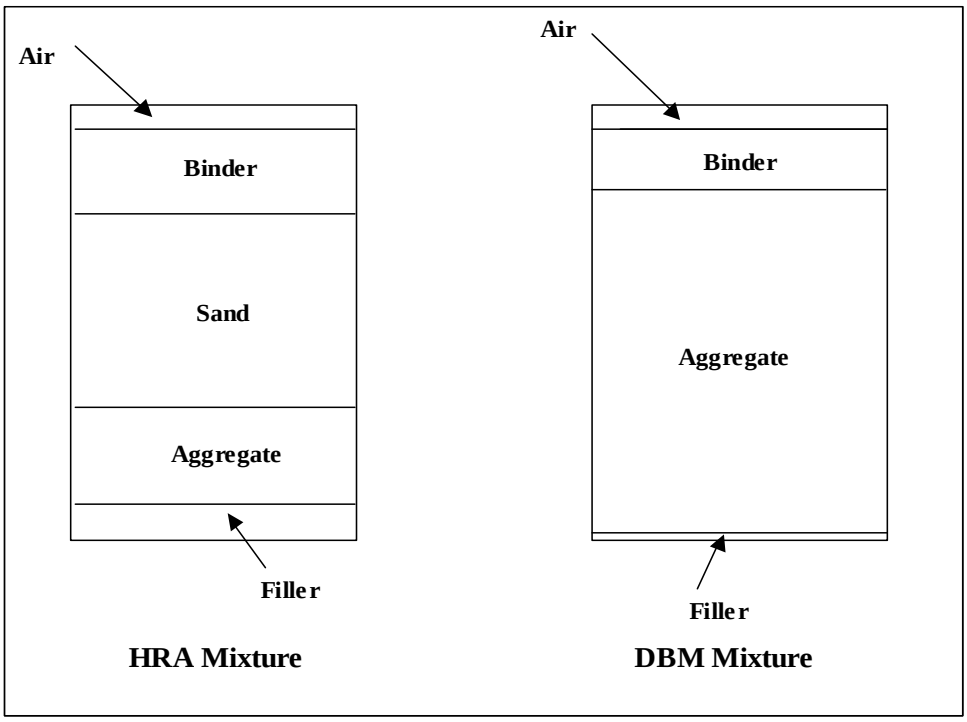

Figure 5.1 Schematic representation of the DBM and HRA materials.

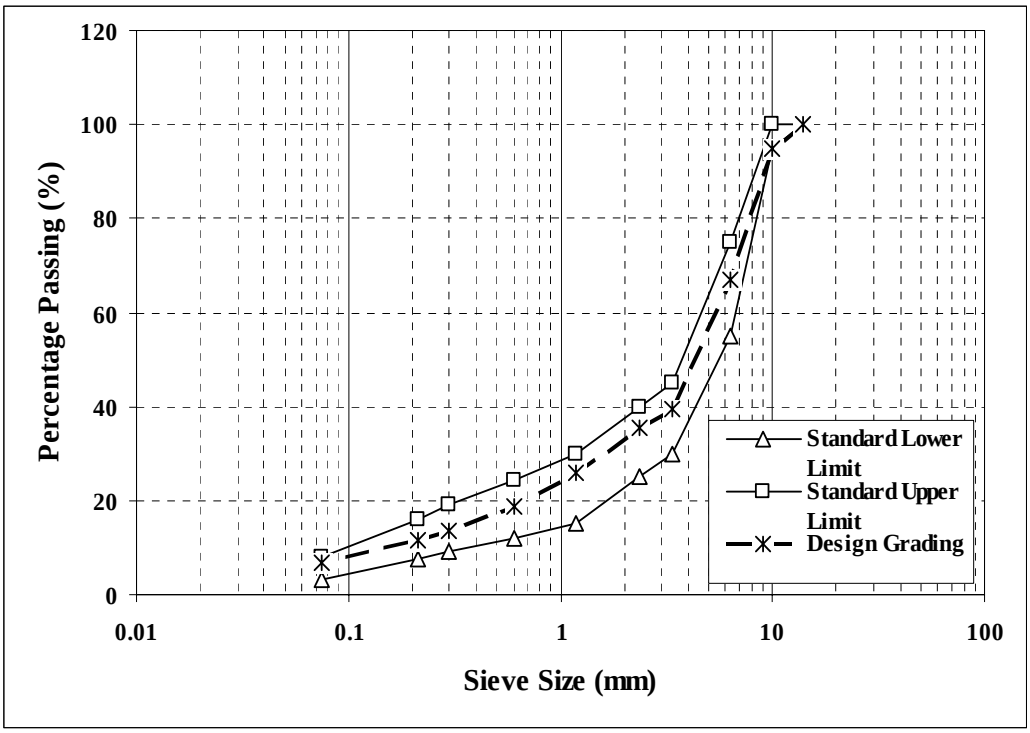

Figure 5.2 Aggregate gradation of the 10 mm DBM.

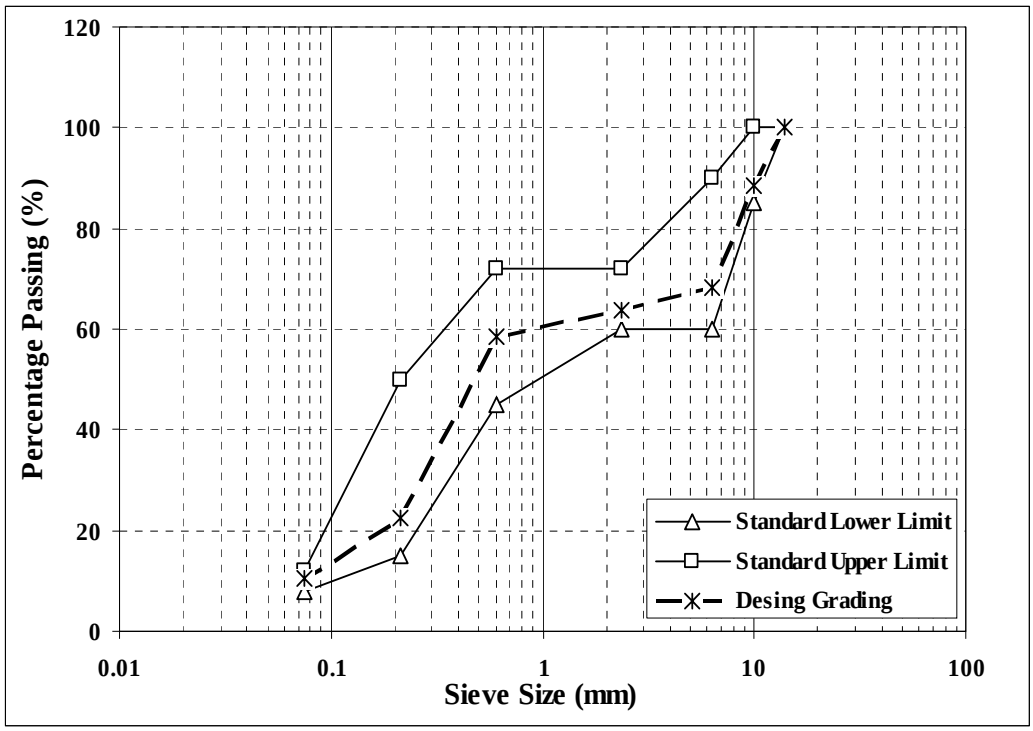

Figure 5.3 HRA30/10 aggregate gradation.

5.2.3 Mixing

Asphalt mix design procedures use equiviscous temperature ranges for selecting laboratory mixing and compaction temperatures. The purpose of using equiviscous mixing and compaction temperatures is to normalise the effect of bitumen stiffness on mixture volumetric properties. This means that, a particular asphalt mixture of the same aggregate gradation will exhibit very similar volumetric properties following compaction with a softer bitumen as with a harder bitumen. Based on the Asphalt Institute recommendation [Hinsley, 1998], which defines the viscosity ranges of 0.17±0.02 Pa.s for mixing temperature, and the viscosity data of the bitumen used in this research, as shown in Figure 5.4, the mixing temperature for both mixtures was set within 155±5˚C. To prepare a mixture for manufacturing a specimen, the required aggregate batches were placed in a tray and heated in a thermostatically controlled oven to within the pre-selected temperature range. At the same time the bitumen was also heated to within the required mixing temperature range. The aggregate and bitumen were maintained at the required temperature for approximately four hours. For mixing the aggregate and bitumen, the heated aggregate was placed in a preheated sun-

and-planet mixer. The required mass of bitumen was then added to the aggregate. The aggregates and the bitumen were then mixed for approximately two minutes.

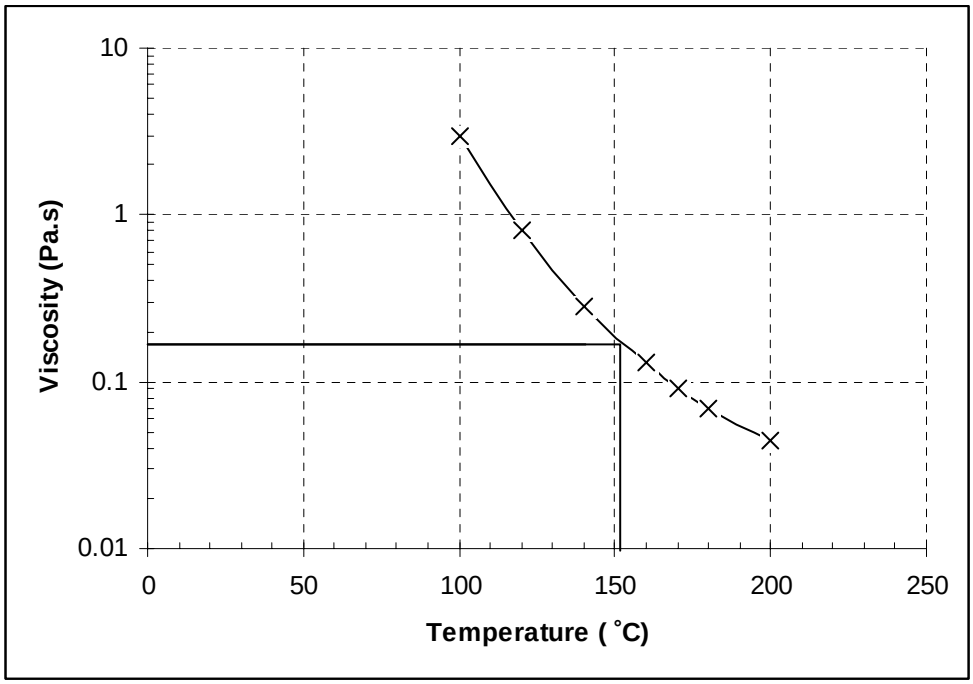

Figure 5.4 Viscosity of the 70/100 Pen grade bitumen against temperature.

5.2.4 Specimen Development

For the compressive tests in this research (uniaxial and triaxial tests), cylindrical specimens were used. The procedure for selection of specimen dimensions is explained in the following paragraphs. For the specimens made in the laboratory to be representative of *in situ* mixtures and to allow preferential orientation of aggregates in the mixture, the dimensions of the specimens must be large relative to the largest aggregate particle size. Following a general rule, commonly used in asphalt, soil and concrete technology, test specimens compacted in the laboratory, must have a specimen dimensions 4 to 6 times the maximum aggregate size [Harvey *et al.*, 2000]. Therefore the minimum dimension of the specimens of the mixtures with nominal maximum aggregate size of 10 mm must be 40 mm.

Based on the dimensions of the triaxial cell and available membranes for triaxial tests, the collar for measuring the radial deformation (see Section 5.2.8), and the

diameter of available coring drills in the laboratory, the diameter of all specimens was set to 100 mm. With the selected diameter for specimen and based on the testing program, the hydraulic machine loading capacity (±100 kN) was checked to ensure that it can apply the required loads for the tests.

To avoid confinement effects in the specimen due to the friction between specimen and loading platens, the aspect ratio (ratio of height to diameter) of the specimen in creep tests is usually chosen to equal a value of 2 [Erkens, 2002]. When the aspect ratio is 2, it is assumed that there is no confinement in the middle third of the specimen and that part is under pure uniaxial compression. Therefore, reliable values of strain and strength can be obtained. For a specimen of diameter 100 mm, to have an aspect ratio equal to 2, the height of the specimen must be 200 mm. Unfortunately, the gyratory compaction method used for making the specimens for this research (see Section 5.2.5) did not allow compaction of specimens with heights more than about 105 mm. However, Erkens [2002] found that by using an effective friction reduction system the specimens with an aspect ratio of 1 have a stress-strain response reasonably close to those with the aspect ratio of 2 (see Figures 5.5 and 5.6). In this research, an effective friction reduction system, similar to that used by Erkens [2002], is used (see Section 5.2.9), and hence the height of 100 mm for the specimen, which gives an aspect ratio of 1 seemed to be acceptable. Therefore, the dimensions of the specimen for all the tests in this research were chosen to be 100 mm in diameter by 100 mm height.

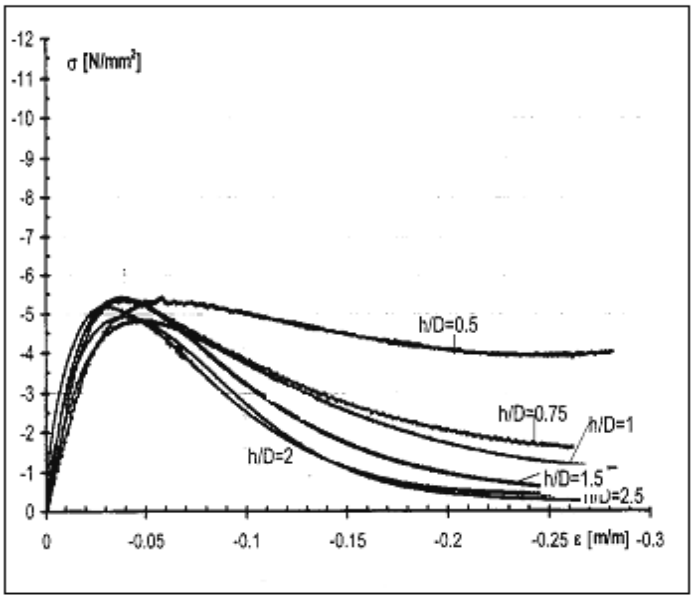

Figure 5.5 The effect of the h/D ratio on the overall stress-strain relation for tests with friction reduction [Erkens, 2002].

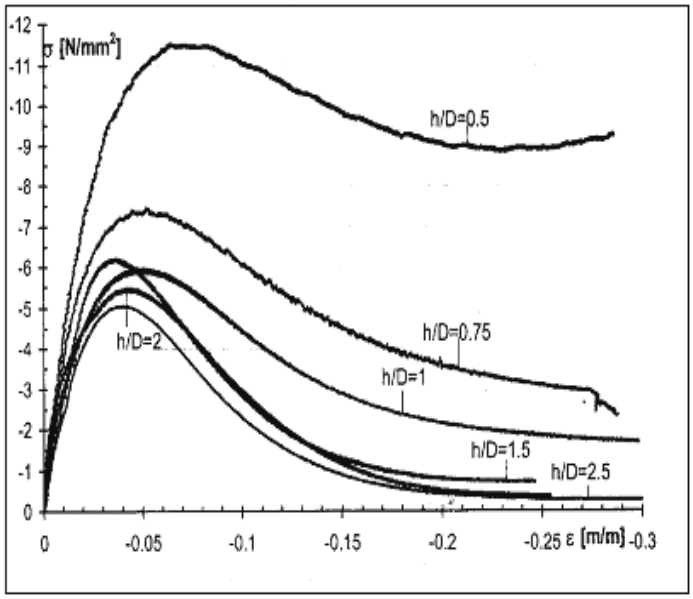

Figure 5.6 The effect of the h/D ratio on the overall stress-strain relation for tests without friction reduction [Erkens, 2002].

5.2.5 Specimen Manufacture

An ideal specimen for this research would be a specimen with a uniform air void distribution and an aggregate orientation similar to that found in the real pavement. Homogeneity of a mixture is controlled by the compaction effort,

method of compaction, viscosity of bitumen, aggregate gradation and aggregate shape [Tashman *et al.*, 2002].

An initial decision was made to make the specimens by coring from slabs compacted by a laboratory roller compactor. Therefore, three slabs of the 10 mm DBM mixture were made. The finished asphalt slabs had the dimensions of 305 mm by 305 mm in plan and the thickness of 120 mm. The roller compactor used for compaction (Figure 5.7) consists of a sector of roller wheel of diameter 900 mm, which is loaded vertically by a pneumatic actuator, and a trolley which is powered by a horizontal actuator. The slab of mixture is placed on the trolley, which moves to and fro at a constant speed of travel. The vertical roller sector compacts the mixture in the slab. After compaction, the slabs were allowed to cool before removal from the moulds. Using a masonry saw the slabs were trimmed at the ends. The specimens were cored through the thickness of the slabs using a wet diamond tipped core drill. The bulk density of the specimens was measured and using Equation 5.1 the air void content of the specimens was calculated.

$$V_v = \left(1 - \frac{\rho}{\rho_{\max}}\right) \times 100 \,, \qquad \textbf{(5.1)}$$

where V_v = the percentage volume of voids %

ρ = bulk density of the specimen

$\rho_{\max}$ = the theoretical maximum density of mixture, which was measured by a standard method, explained in BS 598, Part 104 [British Standards Institution, 1989] for the 10 mm DBM mixture.

Using the following equation, the bulk density ρ of the specimens was calculated by weighing them in air and water:

$$\rho = \frac{M_a \times \rho_w}{M_a - M_w} \,, \qquad \textbf{(5.2)}$$

where M_a = mass of the specimen in air

M_w = mass of the specimen in water

ρ_w = density of water (998 kg/m^3)

The variation in the air void content, characterised by a mean value, minimum, maximum and the standard deviation (S.D.), for the 10 mm DBM specimens were as follows:

Number of samples = 24

Minimum air void content = 3.4 %

Maximum air void content = 6.1 %

Mean air void content = 4.84 %

Standard Deviation = 0.64 %

Some of the specimens were utilised for the uniaxial creep tests, where a constant load was applied to the specimen until failure. It was observed that the deformation of the specimens was not uniform with more deformation in one end compared to the other (Figure 5.8) and also more deformation on one side compared to the other side (Figure 5.9). This non-uniform deformation was thought to be due to non-homogeneity of the specimens. As a result, it was decided to study more accurately the air void distribution in the slab.

To investigate the distribution of air voids, a slab of the 10 mm DBM mixture was made, trimmed and sub-sectioned into 27 equal cube specimens (Figure 5.10). Following the above-mentioned procedure, the air void content of the cubical specimens was calculated, as shown in Figure 5.10. It can be seen in this figure that there was an approximate 4.7% variation in the air void content between top and bottom specimens with more air voids in the specimens at the bottom of slab. This variation of air void content in the slab did not allow coring of homogenous specimens through the thickness. The figure also shows variation of air void content in the direction of compaction. Higher air voids were also

observed in the specimens near the mould walls than the specimens in the middle. This indicated that coring through the thickness in this direction results in specimens with different air void content at two ends. The complex air void distribution in the slab can be explained by the effect of contact between the mixture and the solid surfaces of the mould during compaction. The bottom of the slab, the surface of roller compactor and the mould walls all restrain the mobility of aggregates and reduce compaction at these locations.

It was anticipated that the gyratory compacted mixtures would yield more homogenous specimens. Gyratory compaction attempts to reproduce on-site compaction of hot asphalt mixtures by applying a vertical compressive stress and a gyratory action at the same time. The gyratory action generates horizontal shear stresses in the mixture as applied by the moving road rollers. The principle of gyratory compaction is to rotate a mould on an axis eccentric to the vertical and apply a fixed pressure to the material inside the mould through parallel end plates (Figure 5.11). The 150 mm diameter moulds were used for gyratory compaction, and the specimens were cored from the centre of the compacted mixture, as shown in Figure 5.12.

Figure 5.7 Laboratory roller compactor.

Figure 5.8 Specimen with more deformation in one end.

Figure 5.9 Specimen with more deformation on one side.

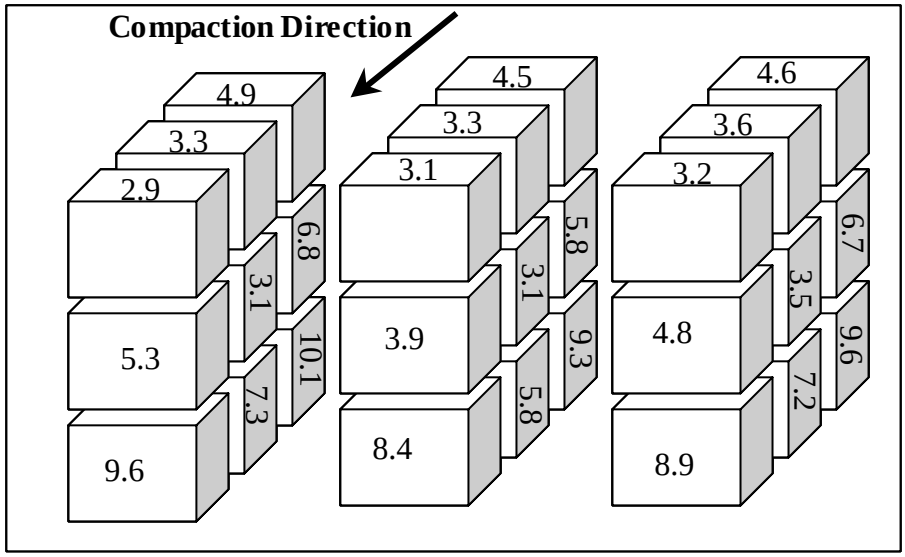

Figure 5.10 Air voids distribution in a slab compacted by roller compactor.

To produce a specimen using the gyratory compactor, after preparing the mixture, as explained in Section 5.2.3, the mix was placed into the preheated mould after lubrication of the internal surfaces with silicone grease. A preheated plate was then put on the mixture in the mould and the whole assembly was then placed in the gyratory compactor (Figure 5.13). After clamping, the mould was tilted to 1.25 degrees while the upper and lower plates were maintained parallel and perpendicular to the original axis of the mould. The mould was clamped to prevent its rotation during the gyration process and was gyrated at 30 rpm while a 600 kPa fixed axial pressure was applied on the mixture by a pneumatic ram. As the specimen was being compacted its height was automatically measured after each gyration. Knowing the mass of the specimen being compacted and the specimen height, measured at each gyration, the density of the mixture was plotted against the number of gyration by the software in the computer connected to the machine. The compaction process was automatically stopped when a pre-set number of gyrations or a target density was achieved. After compaction, the mixture was allowed to cool, and was then removed from the mould by extrusion. Typically, a compacted mixture had a height of about 115 mm which was trimmed at both ends with a masonry saw to produce a specimen with a height of about 100 mm. The specimens were then cored from the centre of the trimmed gyratory compacted mixture by a 100 mm diameter coring drill (Figure 5.12).

A specimen of the DBM mixture was compacted in the 150 mm mould and was sliced into three equal cylindrical pieces. The air void content of the pieces was determined which yielded a relatively uniform air void distribution along the height with more air voids in the pieces cut from top and bottom compared to the piece cut from the middle. This is similar to the air voids distribution in the field cores [Tashman *et al.*, 2002]. As the specimens were cored from the centre of a cylindrical compacted mixture (Figure 5.12), it could be assumed that the specimen was uniform diametrically. This results in a uniform deformation across the diameter and prevents sliding of the specimen during testing. Therefore, it was decided to make the specimens by coring from gyratory compacted mixtures.

The specimens made using the gyratory compactor showed less variation in air void content. As an example, for 30 specimens of the DBM mixture, manufactured for testing, the variation in the air void content was as follows:

Number of specimens= 30

Minimum air void content = 3.2 %

Maximum air void content = 5.3 %

Mean value of air void content = 4 %

Standard Deviation = 0.53 %

As can be seen, there is a marked reduction in the variation in air void content in specimens produced by gyratory compactor compared with the specimens from slab compaction. Figure 5.14 shows typical HRA and DBM specimens, in which the DBM is ready for instrumentation and testing.

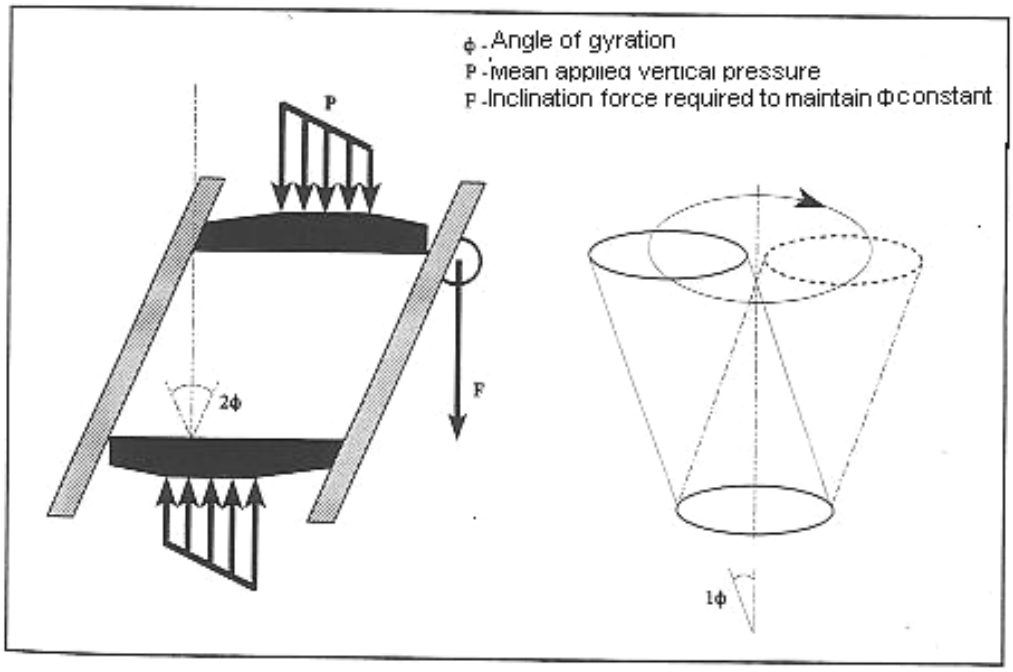

Figure 5.11 Principles of compaction in gyratory compactor [Gibb, 1996].

Figure 5.12 A typical cored specimen.

Figure 5.13 Nottingham laboratory gyratory compactor.

To prevent aging and distortion at ambient temperatures, all the specimens were stored at a cold room set at 5°C until required for testing.

5.2.6 Specimen Preparation

Prior to testing, the end surfaces of each specimen were sanded to minimise any surface roughness, and the height and diameter were measured accurately. To avoid sliding of the specimen during testing, any specimen with a non-uniform height as measured around the circumference was not used in the test. The mid-height of each specimen was marked diametrically opposite each other and two pips were carefully glued at the marked points (Figure 5.14). The pips were used to hold the collar onto which the LVDT for measuring the radial deformation was mounted.

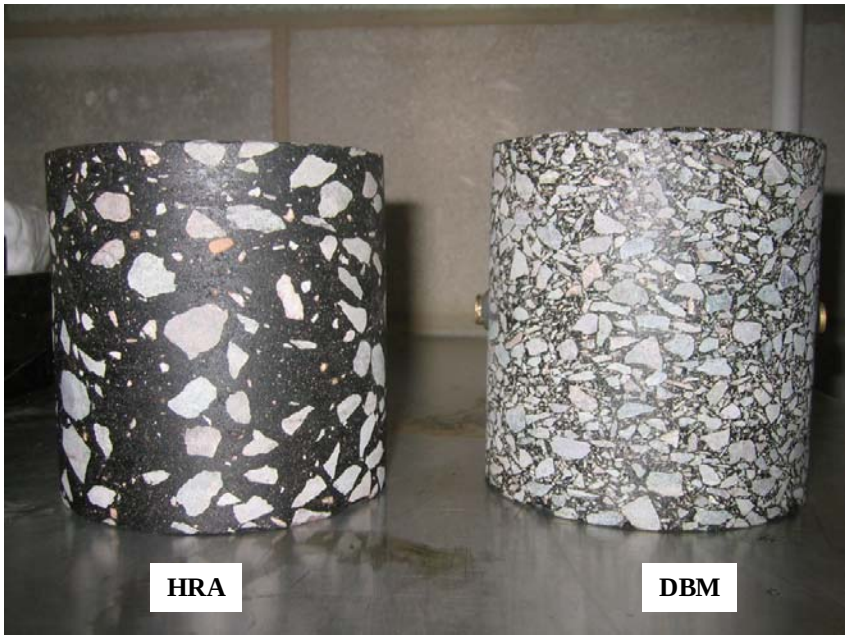

Figure 5.14 Typical HRA30/10 and 10 mm DBM specimens.

5.2.7 Test Equipment

Figure 5.15 shows a photograph of the equipment used for the uniaxial tests undertaken in this study. The equipment consists of a temperature-controlled cabinet, with a -5˚C to 50˚C operating range, mounted on an INSTRON loading frame, a 100 kN servo-hydraulic actuator with ±50 mm movement, an axially mounted load cell, the specimen and its instrumentation. The loading frame is operated by a 'Rubicon' digital servo-control system. An external pump supplies

the hydraulic power for the equipment. A desktop computer is used for data acquisition.

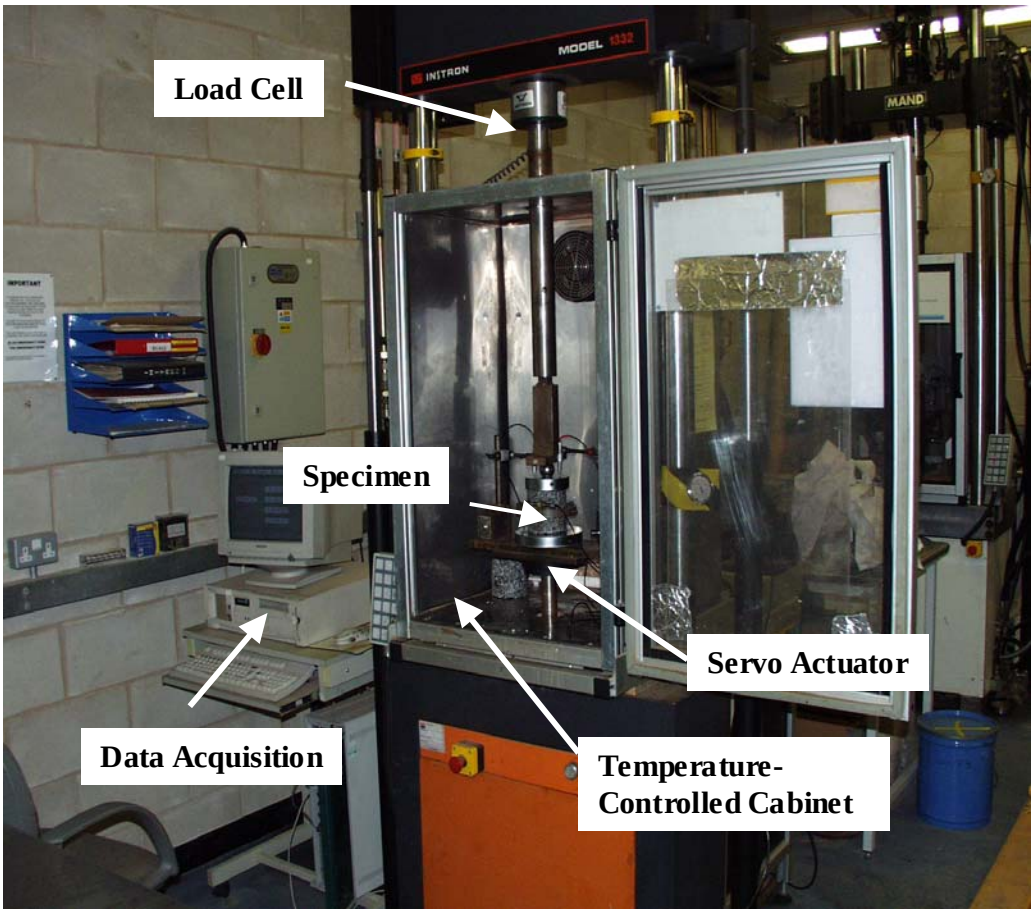

Figure 5.15 Uniaxial tests equipment.

For a uniaxial creep test, a constant load is quickly applied to the specimen through movement of the hydraulic actuator which passes through an opening in the underside of the temperature-controlled cabinet. The axially mounted load cell is connected to the specimen through a ram passing through an opening through the roof of the temperature-controlled cabinet. The load cell monitors the load applied to the specimen and provides a feedback signal for the control system. The control system compares this feed back signal with the input command signal and the difference is fed to the servo-valve, which reduces the difference between the input and output signals by adjusting the oil flow to the actuator. For a constant strain rate test, a monotonically increasing displacement is applied to the specimen through the actuator. A Linear Variable Differential Transformer (LVDT), connected to the actuator piston, monitors the movement

of the crosshead stroke and provides a feedback signal for the control system. The control system compares the signal with the input command signal and the difference is fed to the servo-valve, which reduces the difference by adjusting the oil flow.

5.2.8 Specimen Instrumentation

In both uniaxial creep and constant strain rate tests, the axial and radial deformations were measured at pre-set intervals during testing by the axial and radial LVDTs mounted on the specimen.

Linear Variable Differential Transformers (LVDTs) are inductive sensing devices that produce an AC output voltage proportional to the mechanical displacement of a small iron core. They can measure movements as small as a few millionths of a millimetre up to a few centimetres. Figure 5.16 shows schematically the structure of a typical LVDT. One primary and two secondary coils are symmetrically arranged to form a hollow cylinder. A magnetic core, moves axially within the cylinder in response to mechanical displacement of the probe tip. With excitation of the primary coil by an AC source, induced voltages will appear in the secondary coils. Because of the symmetry of the magnetic coupling to the primary coil, the induced voltages in secondary coils are equal when the core is in the central or null position. If, however, the core is displaced from central position in either direction, one secondary voltage will increase, while the other decreases, which results in a net output voltage exactly proportional to the magnitude of the displacement. Because the device relies on the coupling of magnetic flux, an LVDT can have a high resolution and the smallest fraction of movement (a few millionths of a millimetre) can be detected by suitable signal conditioning hardware and high-resolution data acquisition system.

Instrumentation for Axial Deformation

For the experiments in this research, the ideal instrumentation for measuring axial deformation would be one that could accurately measure the deformation of

the specimen until failure without being damaged. After trying a number of systems, it was decided to use two LVDTs diametrically opposite each other, fixed vertically on supporting arms, and placed on the top platen to measure the axial deformation of the specimen (Figure 5.17). This system actually measures the deformation between the top and bottom plates, which includes deformation in the specimen and any deformation in the friction reduction system (two foils and the soap layers detailed in Section 5.2.9). To obtain the deformation of the specimen, that of the friction reduction system was measured separately and subtracted from the LVDT measurements. To do this, uniaxial creep tests at a series of stress levels were performed without using the specimen and the axial deformation was measured by the two vertical LVDTs. Figure 5.18 shows a typical result in which the deformation of the platens and friction reduction system is plotted as a function of time elapsed since load application. As can be seen, after an almost instantaneous deformation, there was no significant further deformation.

The range of the vertical LVDTs was ±5mm, which could not cover the total axial deformation of the specimens until failure, which was around 13 mm (see Section 5.3.1). Therefore, the load-line displacement measured using an LVDT mounted on the actuator was used for deformations beyond the range of the two vertical LVDTs. The LVDT on the actuator measures the deformation of whole set-up including the specimen, top and bottom plates, friction reduction system and the upper ram connecting the specimen to the load cell. Deformation of the set-up without any specimen was measured by the LVDT on the actuator at different stress levels. Similar to that shown in Figure 5.18, it was observed that, after a short time since load application, there was no significant deformation for the set-up. Therefore, it was concluded that the measurements of the LVDT on the actuator could be used for measuring the deformation of specimen beyond the range of the axial LVDTs.

Instrumentation for Radial Deformation

The radial deformation of the specimens was measured at the mid-height by an LVDT, mounted on a collar, as shown in Figure 5.17. This instrumentation is

usually used in triaxial tests for soil and granular materials [Brown *et al.*, 1980] therefore; it was selected for use in the triaxial cell for the triaxial tests. An LVDT with a range of ±10 mm was selected and calibrated using the set-up shown in Figure 5.19 to directly measure the radial deformation of specimen. The accuracy of the LVDT for measuring the radial deformation was checked by comparing the measurements of the LVDT with the average measurements of two LVDTs fixed horizontally on two supporting arms, diametrically opposite to each other, as shown in Figure 5.20. Good agreement was obtained between the measurements of the two systems.

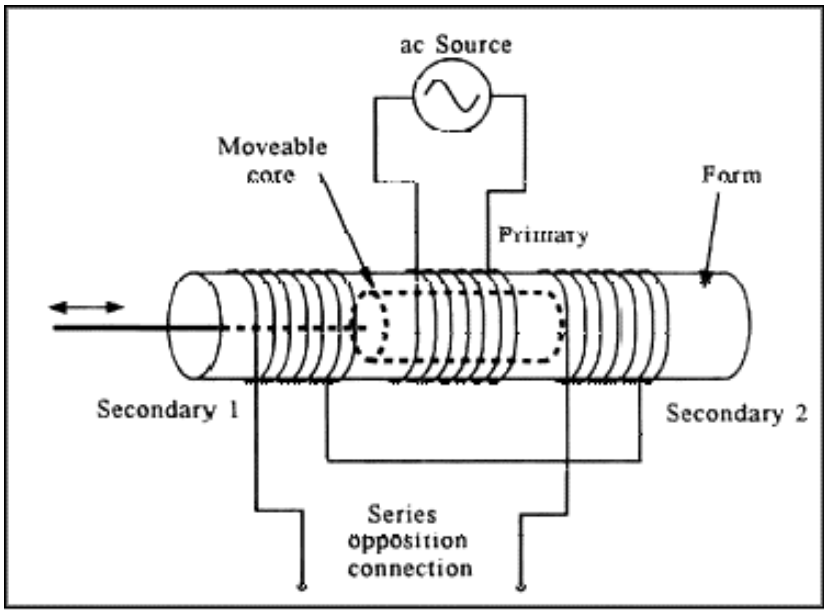

Figure 5.16 Schematic showing of an LVDT (Zone.ni.com, 2006).

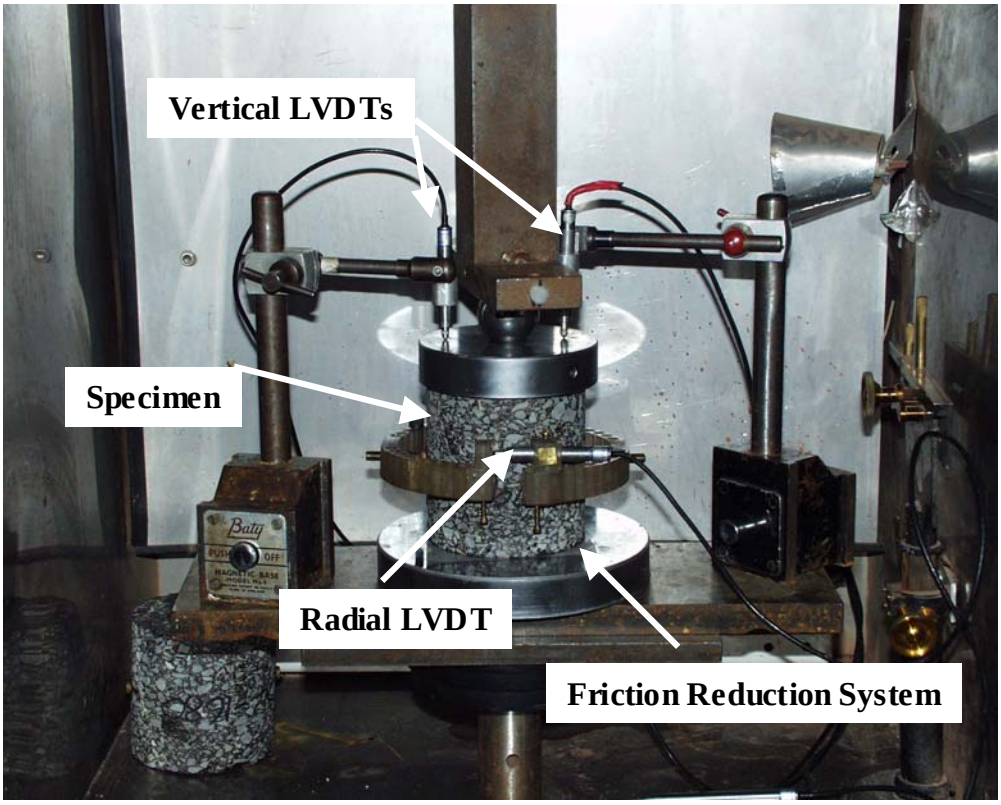

Figure 5.17 Uniaxial test set-up.

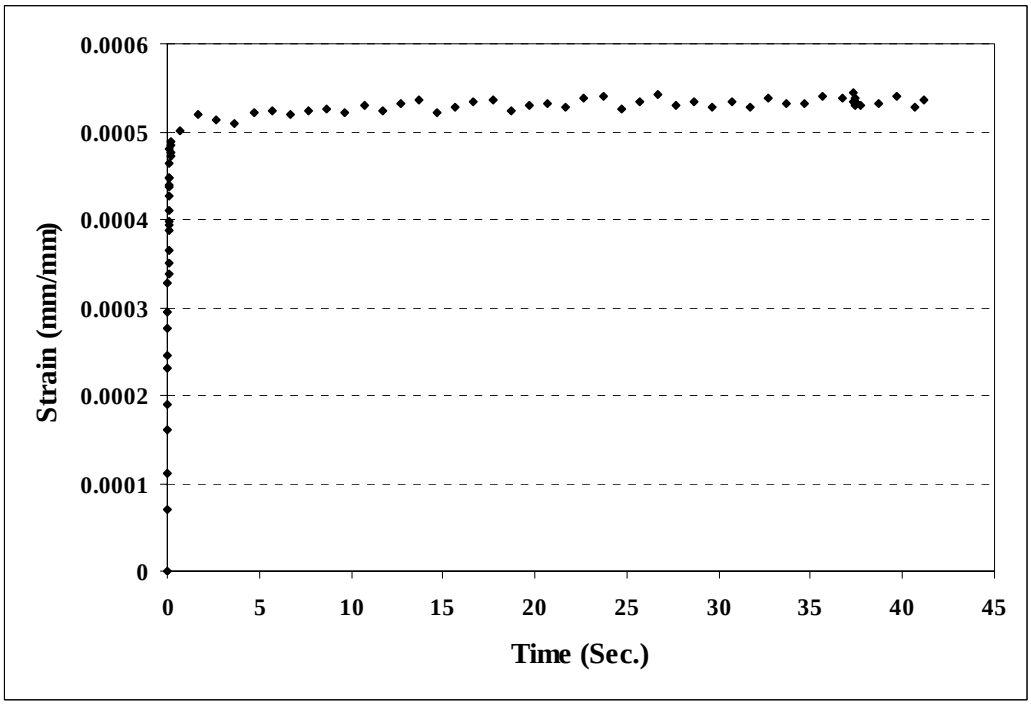

Figure 5.18 A typical deformation of the plates and friction reduction system.

Figure 5.19 The set-up for calibration of radial LVDT.

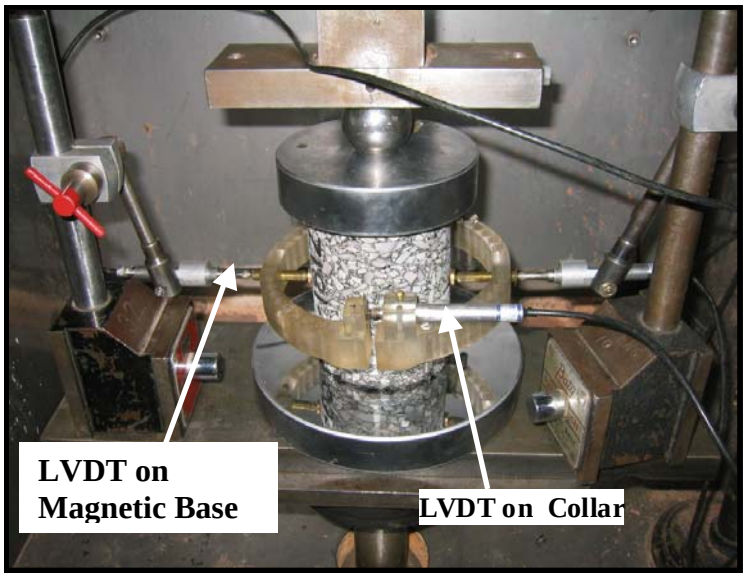

Figure 5.20 The system to check the accuracy of the LVDT on collar for measuring the radial deformation.

5.2.9 Friction Reduction System

In a compressive test, friction between the specimen and loading platens has a significant effect on the stress distribution in the specimen [Erkens, 2002].

Friction confines the specimen at the top and bottom which restrains the radial deformation and results in barrel shape deformation of the specimen. As explained earlier, for a specimen with the height to diameter ratio of 2:1, the middle third part of the specimen is considered to have no confinement and is under uniaxial compression. Therefore, when there is no friction reduction system in use, specimens with a height to diameter ratio of equal or greater than 2 are considered to result in reliable results in compressive tests.

To minimise the confinement and have uniform deformation in the specimen, the friction between specimen and the platens must be eliminated. Different materials (rubber, plastic, bitumen sheets) combined with different types of lubricant have been used by researchers to reduce or eliminate the friction (for details see [Erkens, 2002]). As a friction reduction system, Erkens [2002] and Dunhill [2002] used a plastic film of Luflexen© in combination with a thin layer of a soft soap both between the foil and the loading platen, and between the foil and the specimen. The film was used at each of the specimen and loading platen interfaces. Luflexen© was selected for its low yield strength, high ultimate strain and high resistance to rupture. For this research, a polyethylene foil, named EXCEED^{TM}, supplied by Exxon Mobil, with similar characteristics to the Luflexen© was selected. The foil with a thickness of 50 μm in combination with a thin layer of a liquid soft soap called 'Zalpon' supplied by Diverseylevler Limited was used as a friction reduction system. Figure 5.21 shows the deformation of two specimens in the uniaxial creep test, one tested using the friction reduction system (Figure 5.21a) and the other without any friction reduction system (Figure 5.21b). The barrel shape deformation of the specimen without the friction reduction system, and the almost uniform deformation of the specimen with the friction reduction system showed that the friction reduction system was effective.

A problem experienced in some of the trial uniaxial tests with the friction reduction system was sliding of the specimen during the test, which could damage the specimen instrumentations. The reasons which could lead to sliding of specimen were found to be: using a specimen which had not properly been trimmed, non-uniform air void distribution across the diameter, eccentric

loading, non-uniform temperature distribution in the specimen and using much soap for lubrication of the films [Erkens, 2003].

a)

b)

Figure 5.21 Specimen deformation (a) without the friction reduction system and, (b) with the friction reduction system

5.2.10 Testing Procedure

Using the equipment and instrumentation explained above, uniaxial constant strain rate and constant stress creep tests were undertaken at the conditions summarised in Tables 5.3 and 5.4, respectively. Each specimen was kept in a temperature-controlled cabinet and conditioned at the testing temperature, for at least 12 hours before commencement of the test to ensure that it was at a uniform temperature. When ready to start a test, the specimen was taken from the conditioning cabinet and the specimen's end surfaces were lubricated with the soap described in Section 5.2.9. The specimen was then placed on a polished chrome platen whose surface had also been lubricated with the liquid soap. A

thin layer of the plastic film, detailed in Section 5.2.9, was placed between the specimen and the polished plate. Before placing the top platen, the collar, instrumented with the radial LVDT, was fitted at mid-height of specimen. The stiffness of the spring in the Radial LVDT did not allow the collar to be held in place and therefore a rubber band was used to hold it in position. Checks were made to ensure that the rubber band imparted enough stress to hold the LVDT and the collar in place without constraining the specimen and causing depressions at the point of contact. The top platen was then placed centrally on the specimen after lubricating its surface with the liquid soap and putting the plastic film between the platen and the specimen. The axial LVDTs, mounted on two magnetic bases, were then placed on the top platen diametrically opposite each other. Alignment of the LVDTs was checked to be vertical, as any misalignment causes error in measuring the axial deformation. After placing a steel ball on the top platen, the actuator was brought into position using the Rubicon control system so that the ball was nearly touching the upper ram.

As the temperature-controlled cabinet door was open during the specimen instrumentation, therefore, before starting the test, the door was closed for 20-40 minutes, depending on the difference between the room and test temperature, to ensure that the temperature of the specimen and the cabinet were both at the testing temperature. Before starting the test, a compressive pre-load of approximately 2% of target load in uniaxial creep tests and predicted strength in constant strain rate tests, was applied to the specimen. This pre-loading was to take up any slack in the system and allow the friction reduction system to deform in order to minimise subsequent measurement errors.

Following the preloading, in a constant stress creep test, a constant load was applied quickly (over a time period of 30-40 milliseconds) to the specimen and maintained at a constant value until the end of the test. The uniaxial creep tests were continued until the specimens failed. Visual inspection of specimens in the trial tests showed that above an axial strain level of about 13% the specimen had wide vertical cracks and the axial strain increased at a high rate which could damage the instrumentation. Therefore, it was assumed that the specimens would fail at a strain level of approximately 13% and the tests were not allowed to

continue beyond this strain level. In a constant strain rate test, after the preloading phase, a constant axial displacement rate was immediately applied to the specimen and was maintained constant until an axial strain level of 13%. During the testing, the axial and radial deformations of the specimen and load measurements at pre-set time intervals were logged and saved by a desktop computer. The data were converted to ASCII files for data analysis using spreadsheet software.

Table 5.3 Uniaxial constant strain rate test conditions.

Temperature (˚C)	Strain Rate (1/s)	
	HRA30/10	10mm DBM
10	0.00005, 0.0005, 0.005	0.00005, 0.0005, 0.005
20	0.00005, 0.0005, 0.005	0.00005, 0.0005, 0.005
40	0.00005, 0.0005, 0.005	0.00005, 0.0005, 0.005

Table 5.4 Uniaxial constant stress creep test conditions.

Temperature (˚C)	Stress Level (kPa)	
	HRA30/10	10mm DBM
10	1500, 2000	2000, 2500
20	60, 100, 1000, 1500, 2000	1000, 1500, 2000
40	400, 500	300, 500, 750

5.3 Test Results

5.3.1 General Observations

Typical uniaxial creep test results for the 10 mm DBM and HRA30/10 mixtures at the same selected testing conditions are presented in Figures 5.22 and 5.23, respectively. In these figures the axial strain is plotted against the time elapsed following the application of the target load. The following general observations from the uniaxial creep tests on the mixtures can be made:

- Similar to the creep curve for bitumen, as explained in Chapter 4, the creep curve of both mixtures can be divided into three regions: a primary creep region where the strain rate decreases, a secondary creep region where the strain rate is almost constant, known as steady-state strain rate, and a tertiary creep region where the strain rate increases rapidly as the specimen approaches failure. This behaviour can also be seen in Figure 5.24, where the strain rate is plotted against time. This figure is related to the test conditions of 20°C and 1000 kPa, for the HRA mixture, for which the creep curve is shown in Figure 22.
- At the same test conditions, the DBM mixture is stiffer (i.e. the deformation is lower) than the HRA.
- For both mixtures the axial strain increases with increasing temperature and stress level.
- It was observed that the stiffness (resistance to deformation) of the HRA is more sensitive to temperature than that of the DBM. This can also be seen in Figures 5.22 and 5.23 by comparing the difference between the creep curves of the mixtures for the test conditions of 20°C and 1000 kPa, and 2000 kPa and 10°C.
- It was observed that the stiffness of the DBM is more sensitive to the applied stress level than that of the HRA. As it can be seen from Figures 5.22 and 5.23, for an increase in the stress level from 1000 kPa to 1500 kPa at 20°C, the reduction in the time until failure for the DBM is much more than that for the HRA.
- Visual inspection of the specimens during testing showed that the accumulation of damage in the specimens (development of cracks and increment of the strain rate) is dependent on the temperature and type of mixture and independent of stress level at the same axial strain developed in the specimen. At the same axial strain level, it was observed that the specimen at a lower temperature had less cracks (less damage). Moreover, at the same axial strain level, it was observed that the HRA specimens had less cracks (damage) than the DBM.

For all test conditions, Figure 5.25 shows the axial strain level at which the steady-state strain rate is reached. The data points at each temperature are for different stress levels with no stress-dependent pattern, as it was observed that this strain level is independent of stress level. The scattered values at each temperature are thought to be because of experimental errors. As can be seen in Figure 5.25, for both mixtures, the axial strain at the beginning of the steady-state region decreases with increasing temperature. This figure also shows that the values of the strain for the DBM are slightly less than those for the HRA. This is thought to be because the steady-state behaviour of the mixtures is governed by the bitumen film separating the aggregates. The results of shear creep tests on the bitumen used in these mixtures showed that the steady-state behaviour of the bitumen is reached at a shear strain level of approximately 50% (see Chapter4). The steady-state behaviour of the mixtures should therefore be reached when a shear strain of 50% occurs in the binder films. The local strain in the bitumen film is much higher than the overall macroscopic strain of the specimen and increases with increasing volume fraction of the aggregate. Therefore, it appears that the DBM, which has a thinner bitumen film between the aggregates, reaches the steady-state strain rate at a lower strain level of the specimen compared to the HRA.

Figures 5.26 and 5.27 show typical results from the constant strain rate tests for the 10 mm DBM and HRA30/10, respectively, at the same selected test conditions, where axial stress is plotted against the axial strain. In all of the experiments, the stress-stain (axial and radial) relationships were similar, consisting of an ascending portion, up to a peak stress, known as steady-state stress [Cheung, 1995], followed by a descending softening portion. The following points are the observations from the constant strain tests:

- Irrespective of temperature, strain rate and type of mixture, the plot of axial stress against the axial and radial strain can be divided into four distinct regions: an initial linear region, an inelastic strain hardening region, the peak stress and the descending strain softening region, as shown in Figure 5.28.

- Both mixtures showed an increase in the peak stress with increasing strain rate and/or decreasing temperature. Figure 5.29 shows the peak stress as a function of strain rate and temperature for the mixtures. It can also be seen that the peak stress values for the DBM are higher than those for the HRA.
- For each test conditions, Young's modulus of the mixtures was calculated from the axial stress and strain data taken at the beginning of the test (the linear region in Figure 5.28). Figure 5.30 shows Young's modulus of the mixtures as a function of strain rate and temperature. The figure shows that, in a similar manner to the peak stress, Young's modulus increases with decreasing temperature and/or increasing strain rate. It can also be seen from the figure that, for comparable test conditions, Young's modulus of the continuous graded DBM mixture is higher than that of the gap graded HRA mixture.
- Consistent with Dunhill [2002] and Erkens's [2002] findings, there is an approximately linear relationship between the peak stress (compressive strength) and Young's modulus, which can be seen in Figure 5.31.
- As can be seen in Figures 5.26 and 5.27, the stress-strain curves for the DBM show a sharper peak stress-strain response compared to a more rounded peak stress-strain response of the HRA, which means that the DBM mixture fails in a more brittle manner compared to the HRA.
- The axial strain levels corresponding to the peak stress were taken for all test conditions which are summarised in Figure 5.32. The data points at each temperature are for different strain rate levels with no strain rate dependent pattern. The scattered values are thought to be because of experimental errors. It was observed that the strain values are independent of the strain rate. Figure 5.32 shows that the magnitudes of the axial strain for the DBM mixture were generally lower than those for the HRA. As can also be seen in the figure, similar to the axial strain level at the beginning of the steady-state strain rate in creep tests, for both mixtures, the axial strain levels corresponding to the peak stress decrease with increasing temperature.

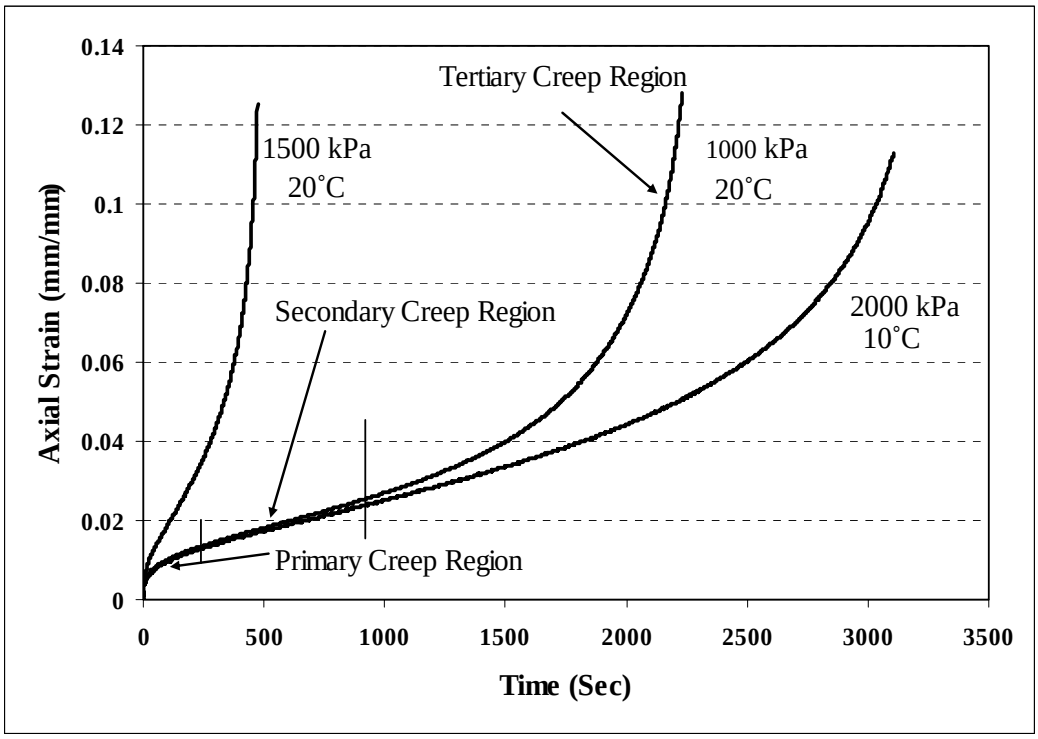

Figure 5.22 Uniaxial creep test results for the DBM at selected test conditions.

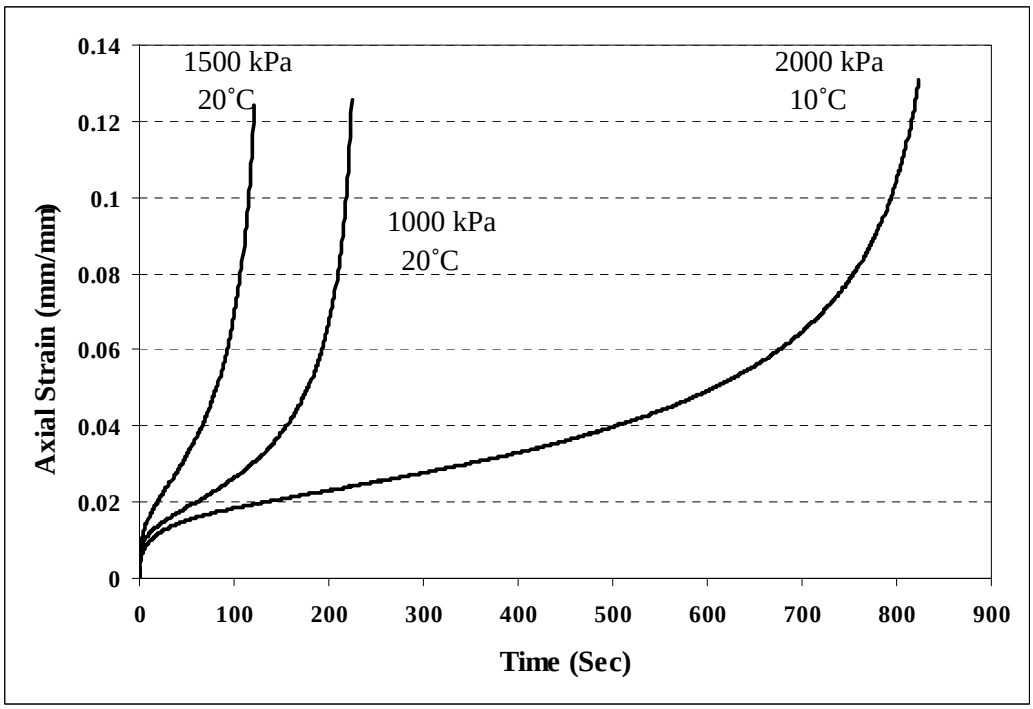

Figure 5.23 Uniaxial creep test results for the HRA at selected test conditions.

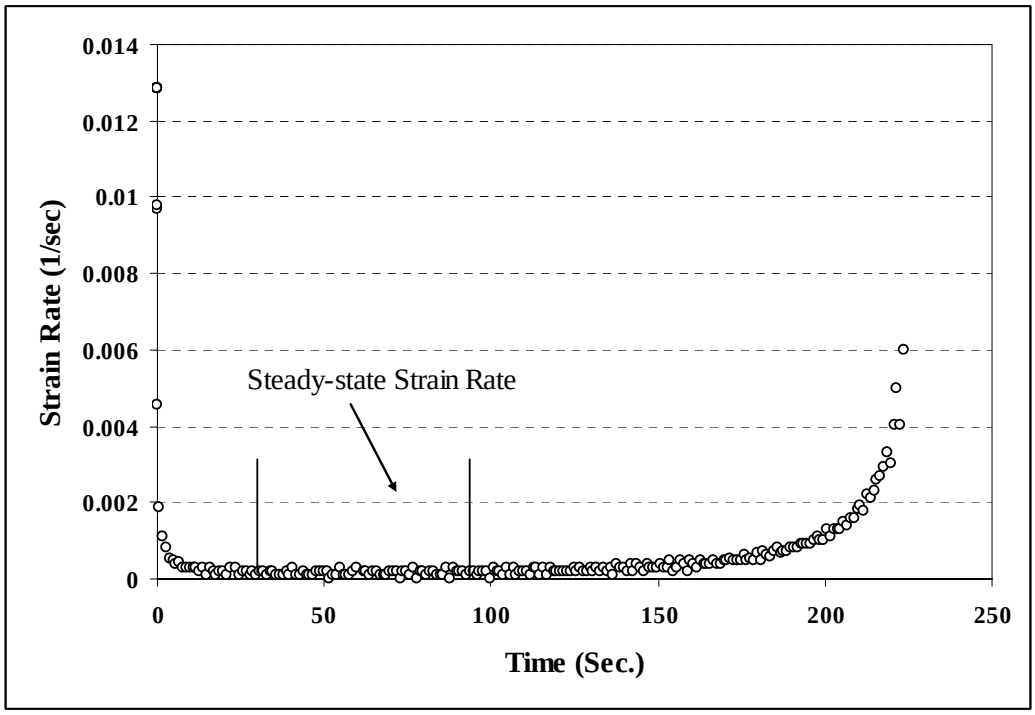

Figure 5.24 **Variation of strain rate in a uniaxial creep test** for the HRA (1000 kPa, 20°C).

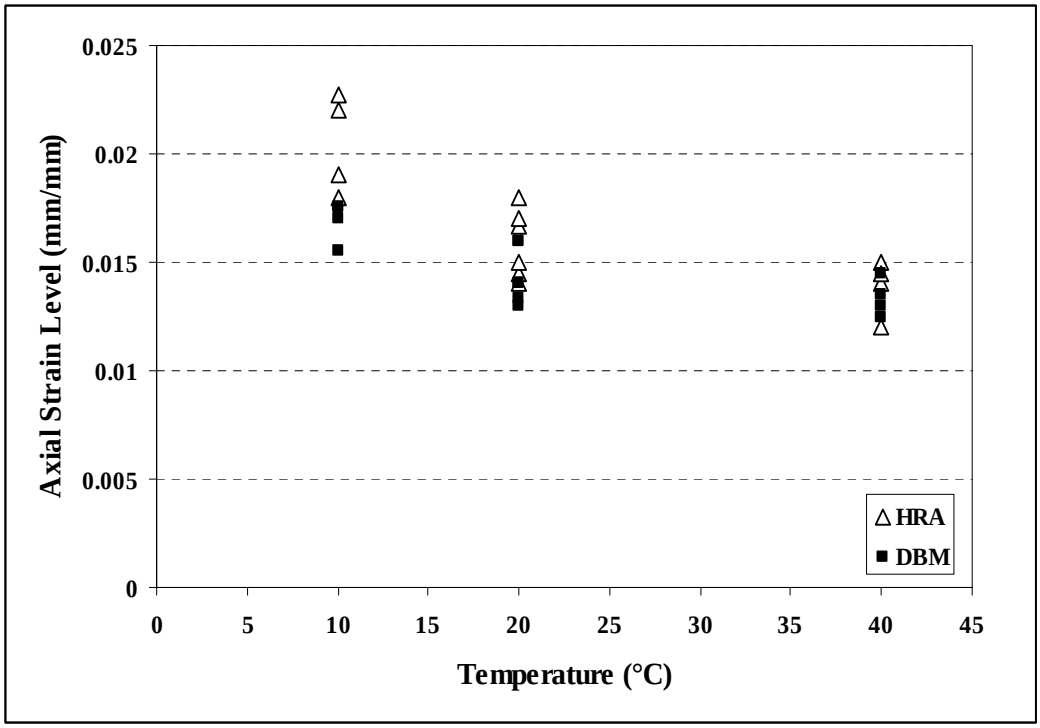

Figure 5.25 Axial strain levels at the beginning of the secondary creep region.

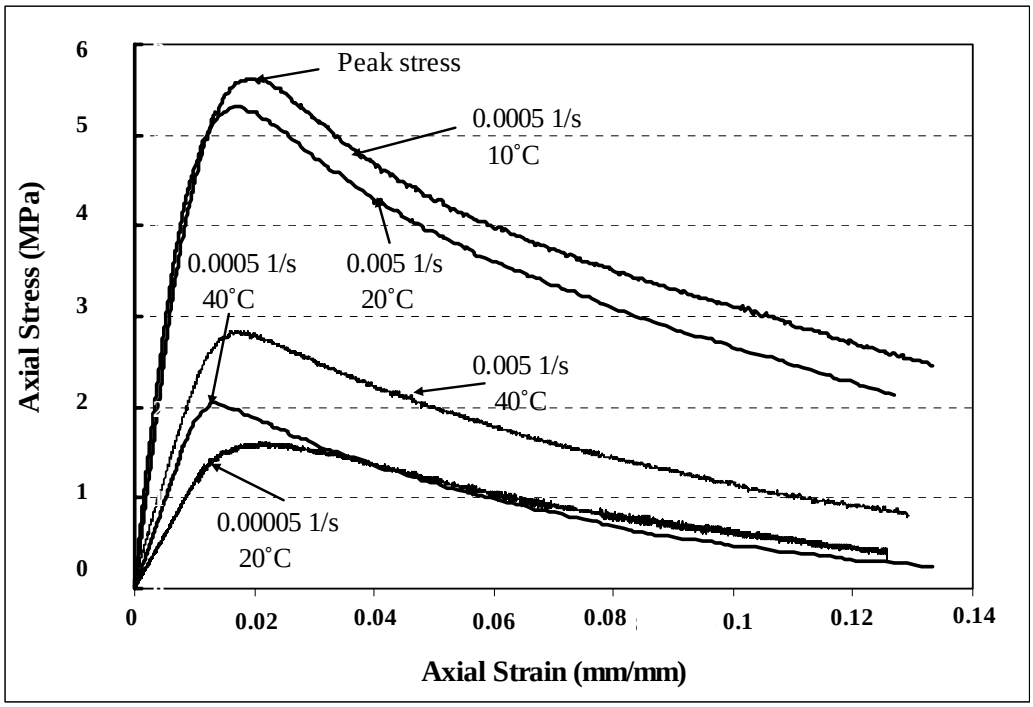

Figure 5.24 Typical constant strain rate test results for the DBM at selected test conditions.

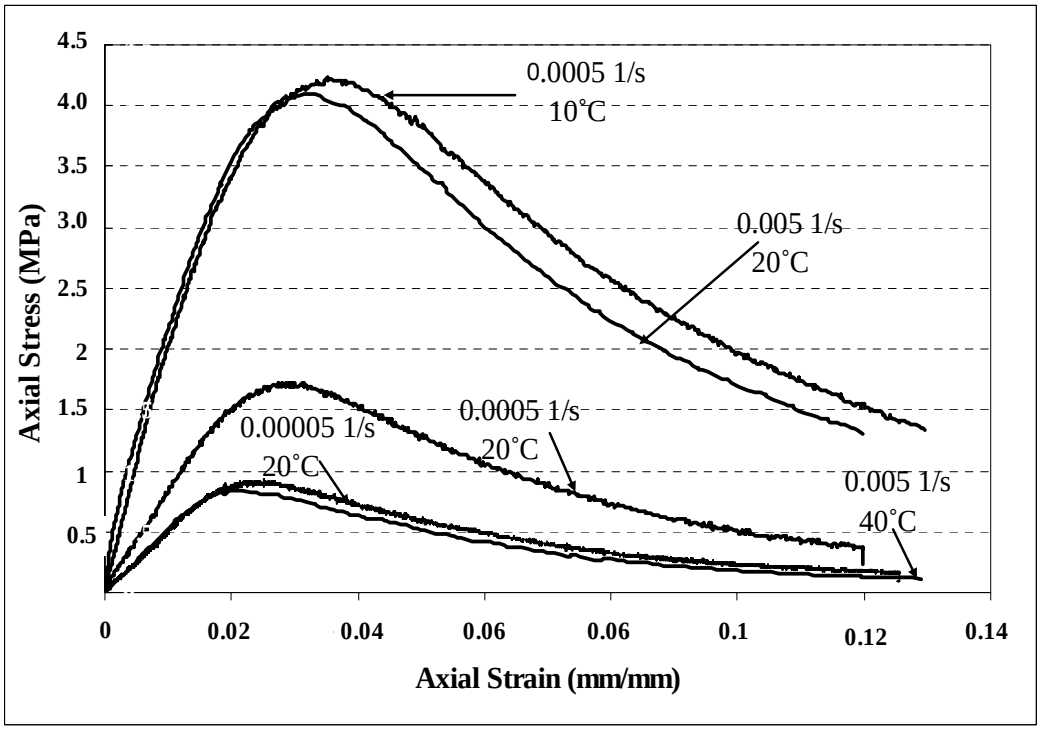

Figure 5.25 Typical constant strain rate test results for the HRA at selected test conditions.

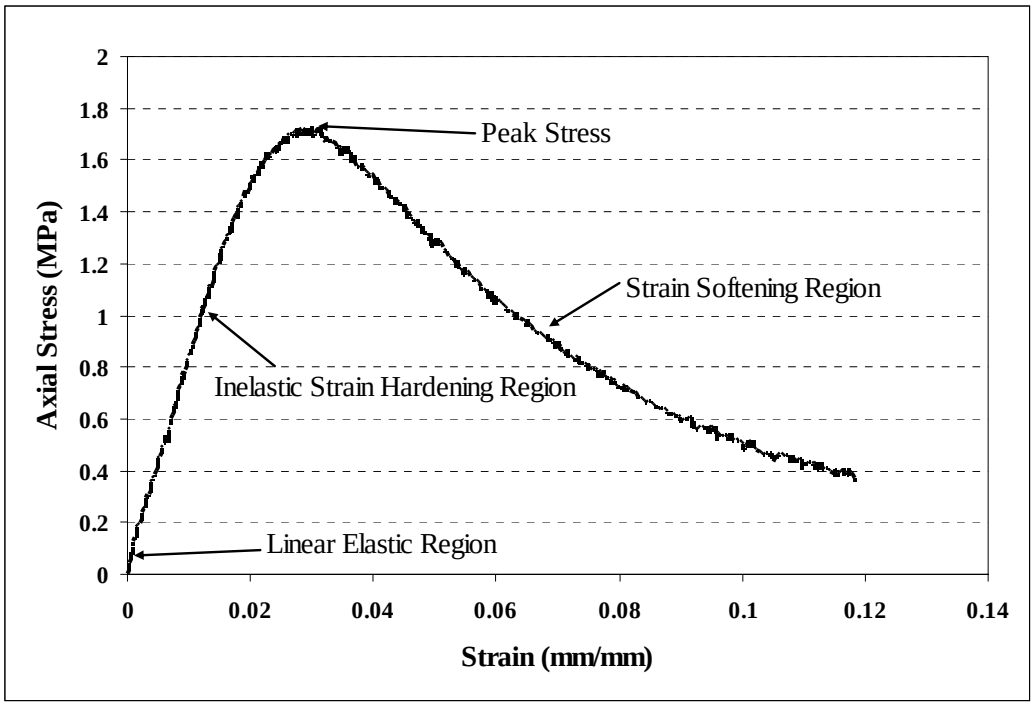

Figure 5.26 A typical constant strain rate test result for the HRA30/10.

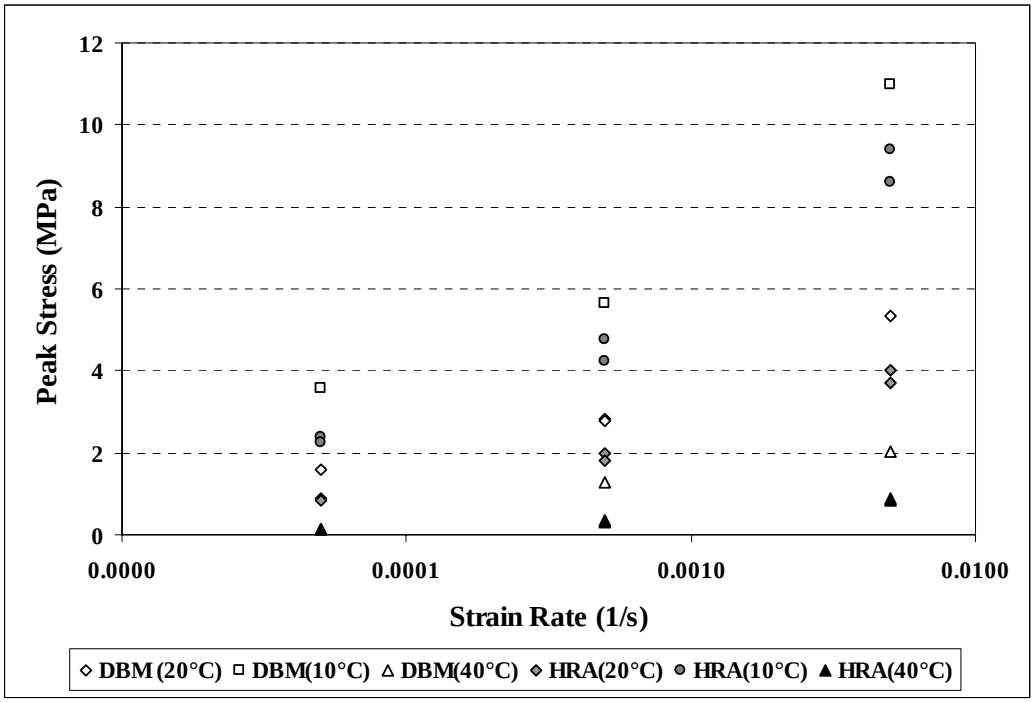

Figure 5.27 Peak stress of HRA and DBM as a function of strain rate and temperature.

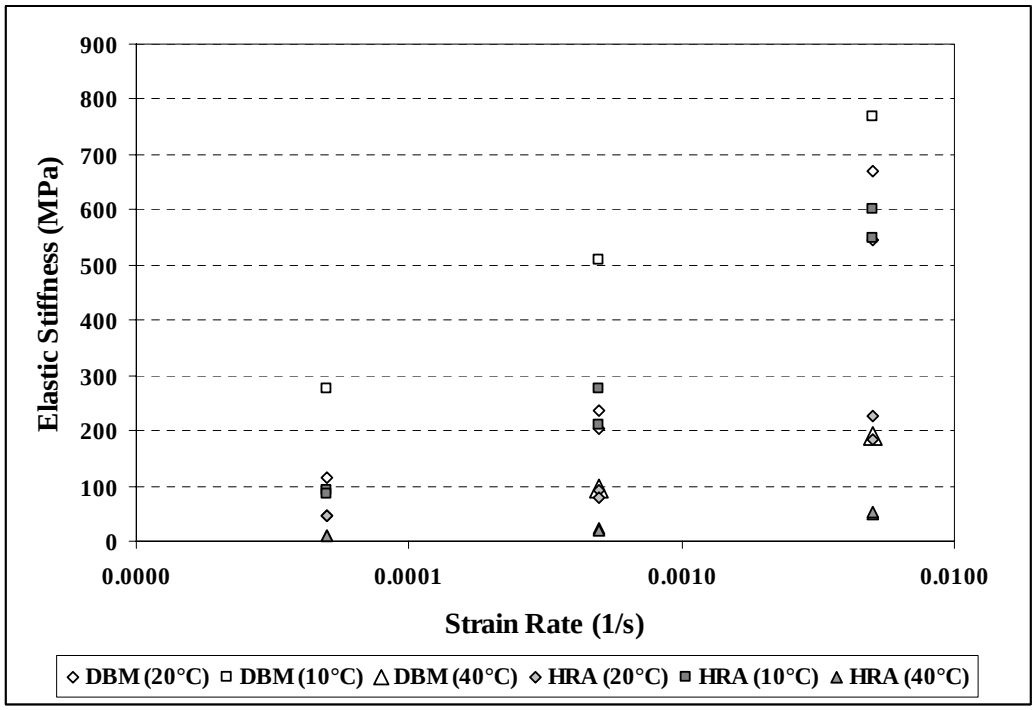

Figure 5.30 Elastic stiffness of HRA and DBM as a function of strain rate and temperature.

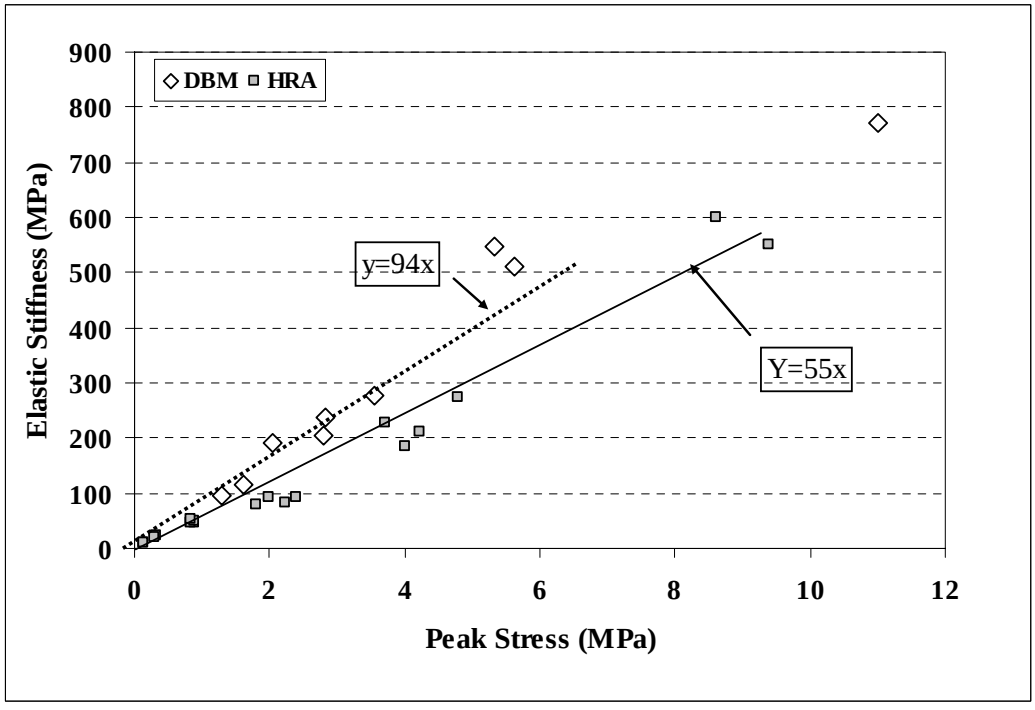

Figure 5.28 Elastic stiffness of the HRA and DBM against peak stress.

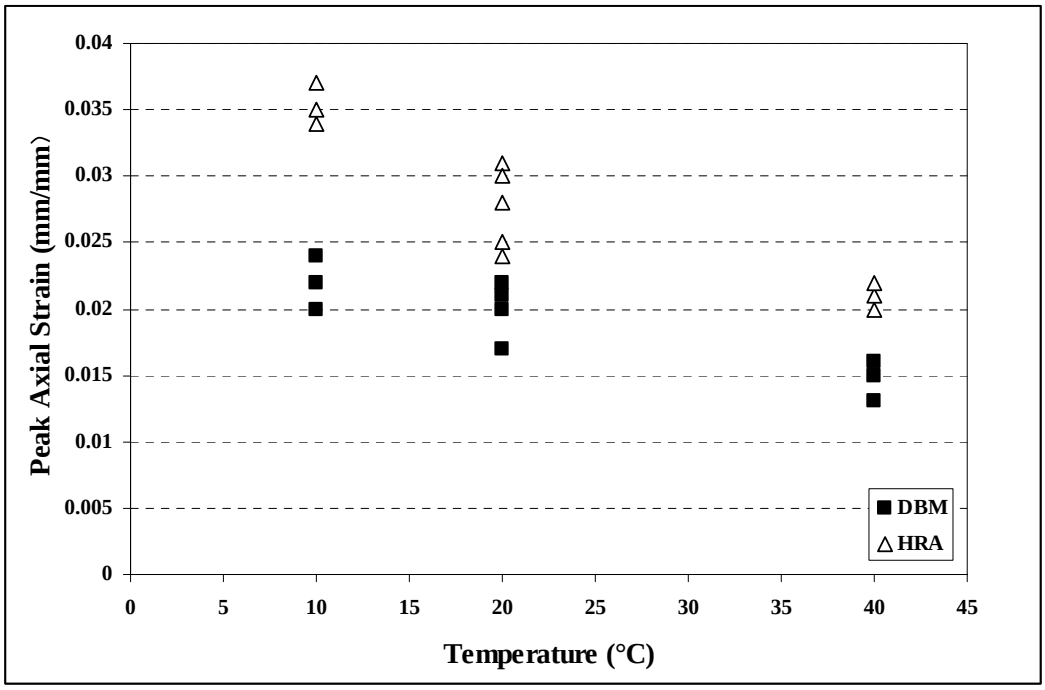

Figure 5.29 The axial strain at the peak stress for the mixtures.

5.3.2 Steady-State Behaviour

Steady-state results from the static constant stress creep and constant strain rate tests are summarised on Figures 5.33 and 5.34 for the HRA and DBM mixtures, respectively, where the steady-state strain rate is plotted against the steady-state stress on a double logarithmic scales. In the constant strain rate tests, the steady-state stress is the peak stress at the prescribed strain rate. In the constant stress creep tests, the steady-state strain rate is the slope of the secondary creep region, as shown in Figure 5.22, at the prescribed stress level.

Cheung [1995], Ossa, [2004] and Khanzada, [2000] found that the steady-state results of the constant strain rate and constant stress creep tests on bitumen and idealised mixtures are complementary. The complementary nature of the constant strain rate and constant stress creep tests can be seen in Figures 5.33 and 5.34 for the HRA and DBM mixtures respectively. This behaviour enables the use of constant stress creep test at low strain rates where it is difficult for the machines to accurately control low velocity for constant strain rate test. Conversely, at higher strain rates, where the creep tests are impractical, the constant strain rate test can be used.

The modified Cross model (Equation 5.3) proposed by Cheung [1995] and Deshpande [1997] for relating the steady-state stress to the steady-state strain rate was fitted to the steady-state experimental data of the HRA and DBM mixtures.

$$\sigma = \frac{S\sigma_0 \dot{\varepsilon}}{\dot{\varepsilon}_p} \left\{ \frac{1}{1 + \left(\frac{S\dot{\varepsilon}}{\dot{\varepsilon}_p} \right)^m} \right\}, \qquad \textbf{(5.3)}$$

where σ = uniaxial stress

$\dot{\varepsilon}$ = uniaxial strain rate

$\sigma_0, m, \dot{\varepsilon}_p$ = material constants for the mixtures (see Table 5.5 and Equation 5.4)

S = stiffening factor, which, in this equation, is the amount by which the mixture is stiffer than the mixture at 20°C.

As can be seen from Equation 5.3, for low values of $\dot{\varepsilon}$ the equation reduces to a linear viscous law where $\dot{\varepsilon} \propto \sigma$ and for high values of $\dot{\varepsilon}$ the equation reduces to a non-linear viscous law where $\dot{\varepsilon} \propto \sigma^n$ with the power law exponent of $n = 1/(1-m)$. The solid lines in Figures 5.33 and 5.34 is the fitted modified Cross model. For the DBM, as can be seen in Figure 5.34, the experimental data points tend to lie on a straight line with a slope of approximately 3.9. This means that, over the range of test conditions, the mixture exhibits non-linear viscous behaviour. It can be seen in Figure 5.34 that the modified Cross model predicts that the steady-state deformation behaviour of the DBM is linear at low stress levels (<100 kPa). Conducting the creep tests at low stress levels was found to be impractical. Trial creep tests on the DBM at a test conditions of 40°C and 250 kPa showed that after 4 days of running the test the specimen did not reach the steady-state strain rate and the strain rate was too small (almost zero). Figure

5.33 shows that the HRA mixture exhibits non-linear power law viscous behaviour at high stress levels with a power exponent of 2.9. As for the DBM, the model predicts linear viscous behaviour for the HRA at low stress levels (<41 kPa). However, because of lack of experimental data, the behaviour of material at low stress levels can not be presented.

For the three temperatures investigated in this study, the temperature dependence of the steady-state deformation behaviour of the HRA and DBM mixture was found to be well captured by the free volume model (WLF equation). The WLF equation is incorporated into Equation 5.3 through the following equation for $\dot{\varepsilon}_p$ (see Cheung [1995] for further details):

$$\dot{\varepsilon}_p = \dot{\varepsilon}_{pc} \exp\left(\frac{2.303 c_1^s (T - T_s)}{c_2^s + (T - T_s)} \right), \qquad \textbf{(5.4)}$$

where $\dot{\varepsilon}_{pc}$ = is the reference strain rate at T=0°C

c_1^s & c_2^s = universal constants with the values 8.86 & 101.6

T_s = reference temperature with the value of 30°C

As explained in the previous chapter, shear creep test results on the bitumen used in the mixtures showed that the steady-state deformation behaviour of the bitumen is linear at low stress levels and power low creep at high stress levels with a creep exponent of approximately 2.6. It was expected that the steady-state deformation behaviour of the mixtures would be dominated by the bitumen with the same creep exponent for the mixtures as that for the bitumen. However, as can be seen in Figures 5.33 and 5.34, the steady-state deformation behaviour of the mixtures is power law creep at high stress levels with creep exponent values of approximately 2.9 and 3.9 for the HRA and DBM, respectively.

As noted earlier, Cheung [1995] found that bitumen ageing generally increases the power exponent of the non-linear creep law. The difference in the steady-state behaviour of the mixtures and the bitumen was thought to be caused by the ageing of bitumen during mixing. The thin films of bitumen subjected to high temperatures during mixing undergo ageing which makes it harder than the

bitumen before mixing. The Rolling Thin Film Oven Test, which is used to simulate the short-term aging of bitumen during mixing [Anon, 2000], was used to age the bitumen. In this test, the bitumen flows continuously around the inner surface of cylindrical glass container in relatively thin films of 1.25 mm to ensure that all the bitumen is exposed to heat and air and no skin is developed to protect the bitumen. Following the same procedure explained in Chapter 4, using the DSR, a few constant stress shear creep tests were performed on the short-term aged bitumen over a range of stress levels at 5°C. Figure 5.35 shows the steady-state deformation behaviour of the short-term aged bitumen. As can be seen in the figure, the steady-state deformation behaviour of the short-term aged bitumen is similar to that of normal bitumen, as presented in Chapter 4, with linear behaviour at low stress level and non-linear power law creep at high stress level with a power exponent of 2.35. It can be therefore concluded that the aging process that occurs during the specimen manufacture does not influence the steady-state behaviour of the mixtures.

Table 5.5 The modified Cross model constants for the mixtures

Parameter	**HRA**	**DBM**
σ_0 **(MPa)**	0.041	0.1
$\dot{\varepsilon}_{pc}$ **(1/s)**	8.7×10^{-8}	8.7×10^{-9}
m	0.66	0.75

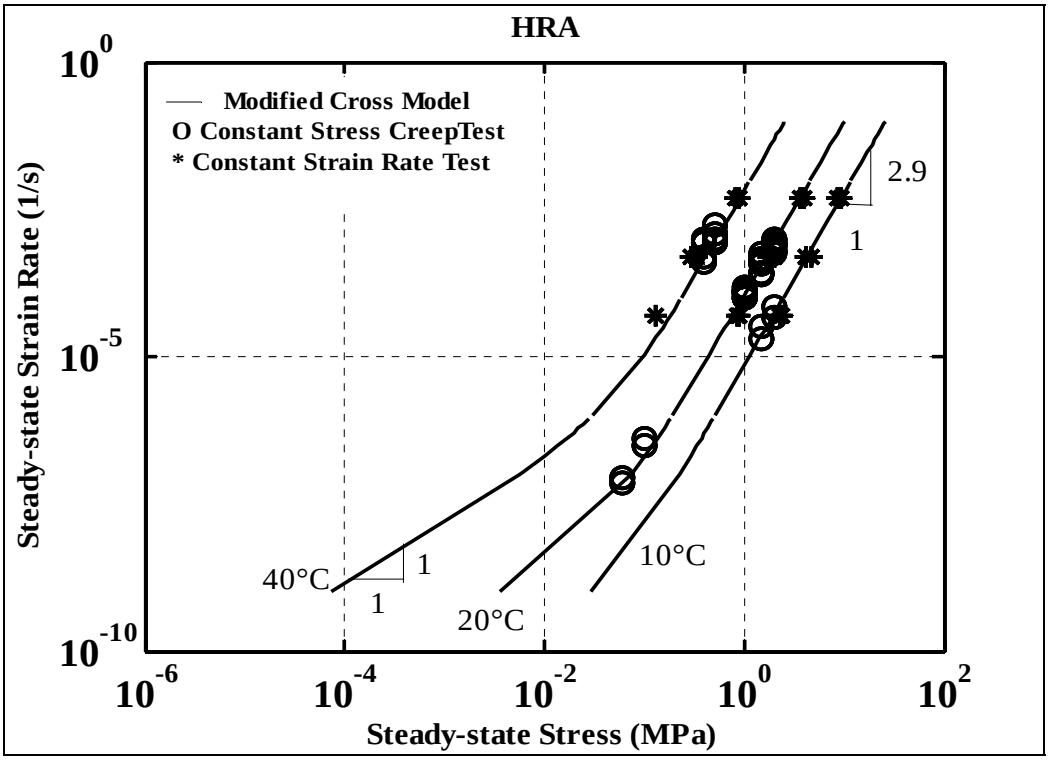

Figure 5.30 The uniaxial steady-state behaviour of the HRA30/10 at different temperatures.

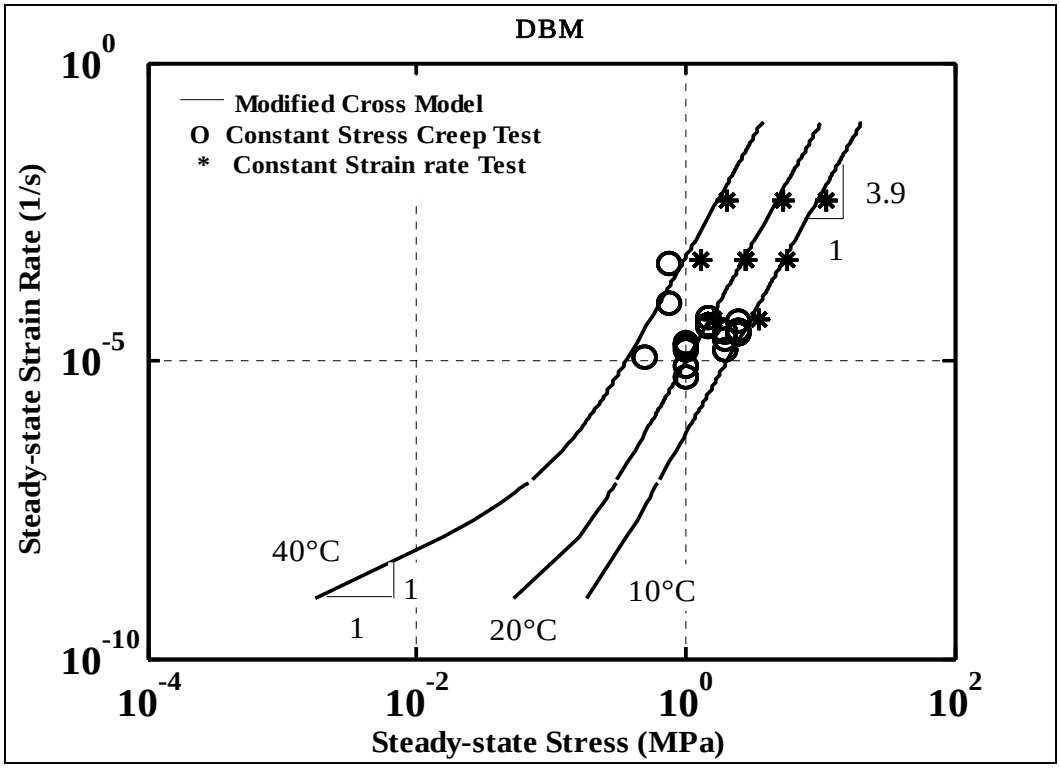

Figure 5.314 The uniaxial steady-state behaviour of the 10 mm DBM at different temperatures.

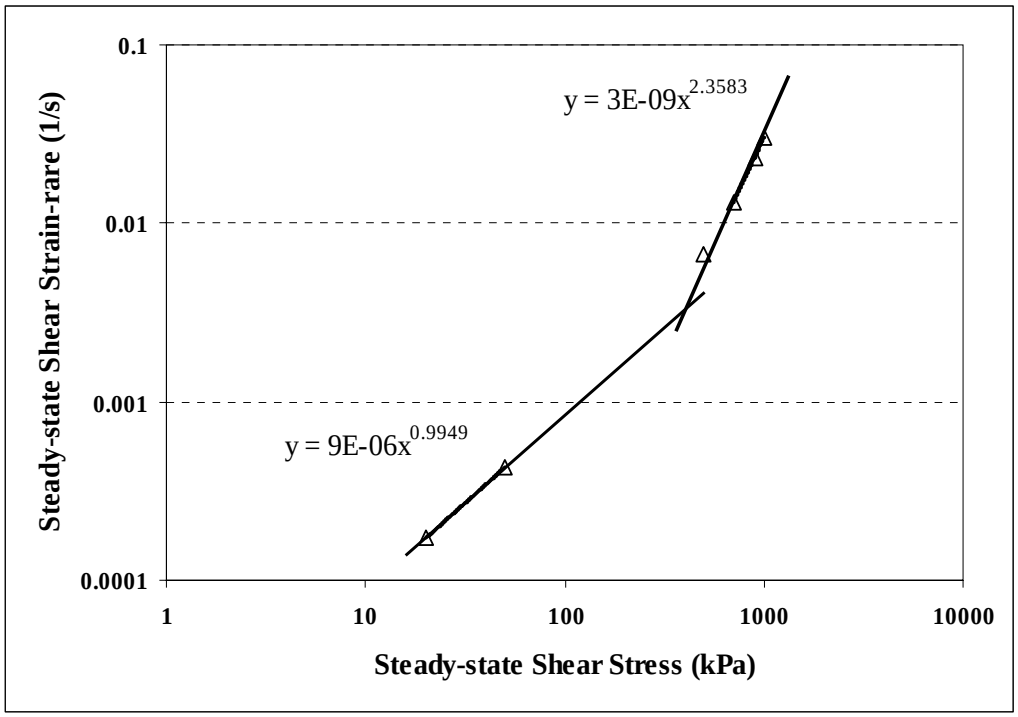

Figure 5.32 The steady-state deformation behaviour of short-term aged bitumen.

5.3.3 Volumetric Behaviour

As mentioned earlier, to study the volumetric behaviour of the mixtures, the radial deformation of the specimens was measured during the uniaxial creep and constant strain rate tests. Figure 5.36 shows a typical result of the constant stress creep tests for the HRA mixture at the test conditions of 20°C and 1000 kPa, where the radial and axial strains are plotted against time. As can be seen in this figure, the variation of the radial strain with time is similar to that of the axial strain with three distinct regions as explained in Section 5.3.1. The figure shows that, up to a level, the radial strain values are smaller than axial strain after which, due to specimen dilation, they become greater. Figures 5.37 and 5.38 show the variation of radial strain with the axial strain for the HRA and DBM mixtures, respectively, at a selected test conditions. The figures show that, up to a level, the radial strain increases with axial strain at an increasing rate after which the radial strain varies almost linearly with the axial strain. For both mixtures, over the range of temperatures in this study it was observed that the slope of the linear section, which is referred to as dilation gradient, is independent of the applied stress. Similar results were obtained by Deshpande

[1997] and Khanzada [2000] for idealised asphaltic mixtures. While the dilation gradient was observed to be almost the same at 10°C and 20°C, it increases at 40°C which implies that more dilation occurs at higher temperatures. For the DBM mixture, the dilation gradient was found to be higher than that for the HRA. For the single size and double size idealised mixtures with an aggregate volume fraction of 75%, Khanzada [2000] found that the dilation gradient is approximately 1. For the HRA and DBM mixtures in this study, as shown in Figure 5.37 and 5.38, higher values were observed.

Figure 5.39 shows the ratio of the radial strain to the axial strain as a function of time for the HRA mixture at a test conditions defined in the figure. It can be seen from this figure that, similar to the creep curve, there is an instant value for the ratio, known as Poisson's ratio, followed by a decreasing rate of the ratio up to a level after which the ratio increases approximately linearly with time. Beyond the linear region, the rate tends to increase at an increasing rate. The slope of the linear region was found to be independent of stress level and dependent on the type of mixture and temperature.

Figure 5.40 shows a typical result from the constant strain rate tests for the HRA at the test conditions of 0.0005/s and 20°C, where the axial stress is plotted against the radial and axial strains. It can be seen from this figure that, the curve for the radial strain is similar to that for the axial strain with four distinct areas as explained in Section 5.3.1. The figure shows that, as for the creep test results, the radial strain is less than the axial strain up to a level after which, because of dilation, it becomes greater in magnitude than the axial strain. Figure 5.41 shows variation of the radial strain with axial strain for the HRA at selected test conditions. As can be seen in the figure, the variation of radial strain with axial strain is similar to that for the uniaxial creep tests. Figure 5.41 also shows that, for both mixtures, the dilation gradient increases with increasing temperature. The DBM mixture showed a higher dilation gradient than the HRA. Within the experimental errors, at a specified temperature, the dilation gradient obtained from the constant strain rate and constant stress creep tests were found to be the same.

Figures 5.42 and 5.43 show the variation of the volumetric strain with the shear strain in uniaxial creep tests at selected test conditions for the HRA and DBM mixtures respectively. Figure 5.44 shows the corresponding results for the HRA in constant strain rate tests. The volumetric and shear strain for the cylindrical specimens were calculated using Equations 2.13 and 2.14. The sign convention for calculation of the volumetric and shear strain from Equations 2.13 and 2.14 is positive for extended direction and negative for contracted direction. Therefore, as the tests were in compression, the specimen is contracted in axial direction and extended in radial direction. Hence, the axial and radial strain values were taken to be negative and positive respectively.

As can be seen in Figures 5.42, 5.43 and 5.44, at all test conditions, the volumetric strain decreases slightly at the beginning of the test up to a point after which it increases approximately linearly with the shear strain. The initial reduction in volume is attributed to the densification of the mixtures. After initial densification, the mixtures dilate and the volume increases. The linear relationship between the volumetric and shear strain can be expressed as:

$$\varepsilon_V = D\left|\varepsilon_S\right|, \tag{5.5}$$

where D is the slope of the linear relation, known as dilation ratio, as shown on the figures. For the HRA mixture, over the range of test conditions utilised for the tests, it was observed that the dilation ratio is independent of the applied stress level and strain rate. Similar behaviour was observed for the DBM mixture. However, for the DBM, at the same temperature, the dilation ratio at the strain rate of 0.00005/s was clearly higher than those at 0.0005/s and 0.005/s. A summary of the values of dilation ratio, obtained from the uniaxial creep and constant strain rate tests on the HRA and DBM, are presented in Figures 5.45 and 5.46 respectively. Figure 5.45 shows that the dilation ratio for the HRA is independent of the applied stress level and strain rate. Figures 5.45 to 5.46 show that, at the same test conditions, the DBM has a higher dilation ratio. It can also be seen that, for both mixtures, the dilation ratio at 40°C is considerably higher than that at 10°C and 20°C, for which the dilation ratios are almost the same. In

Figure 5.46, the higher values of the dilation ratio at 10 and 20°C are corresponding to the low strain rate of 0.00005/s.

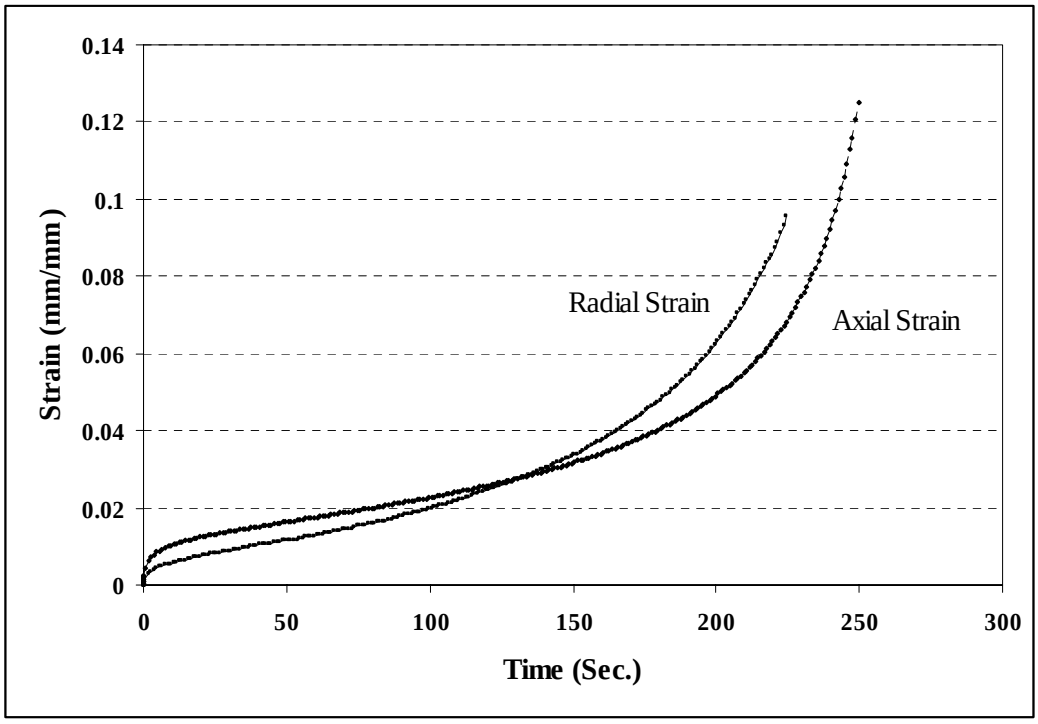

Figure 5.33 Axial and radial strain of the HRA at 20°C (axial stress of 1000 kPa).

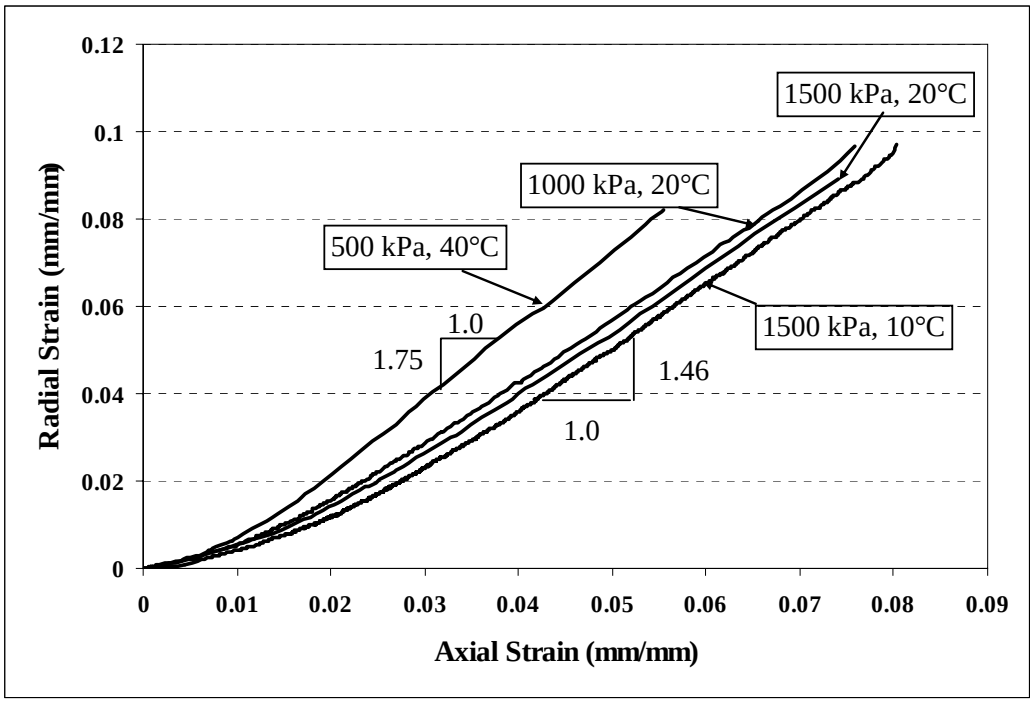

Figure 5.347 Radial strain against axial strain for the HRA at selected test conditions.

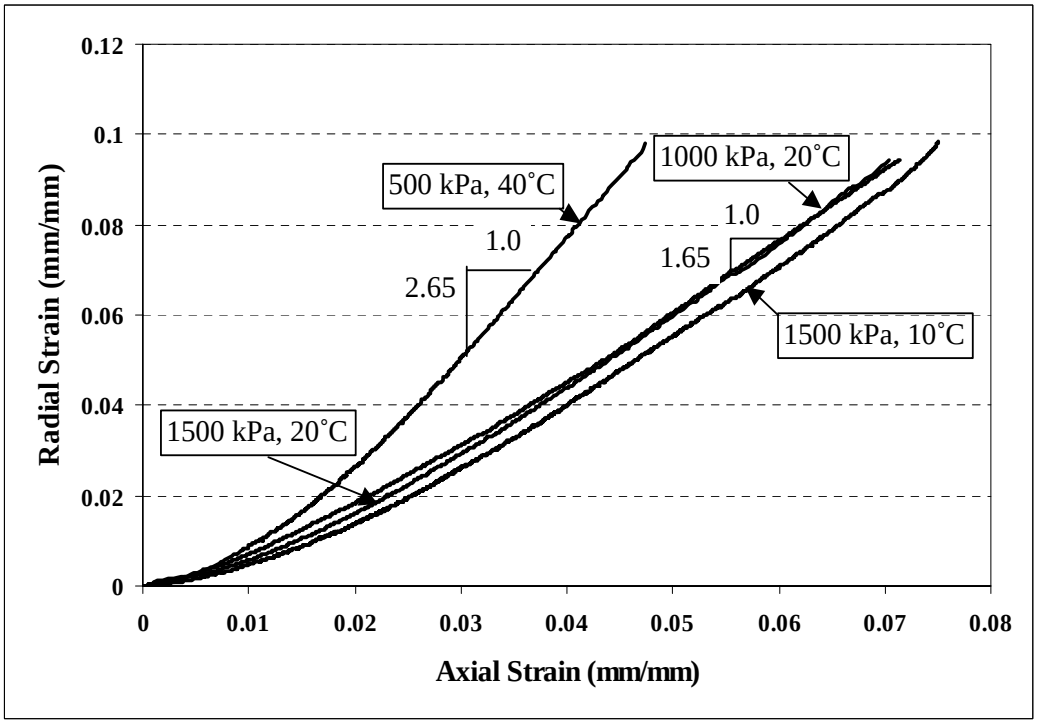

Figure 5.358 Radial strain against axial strain for the DBM at selected test conditions.

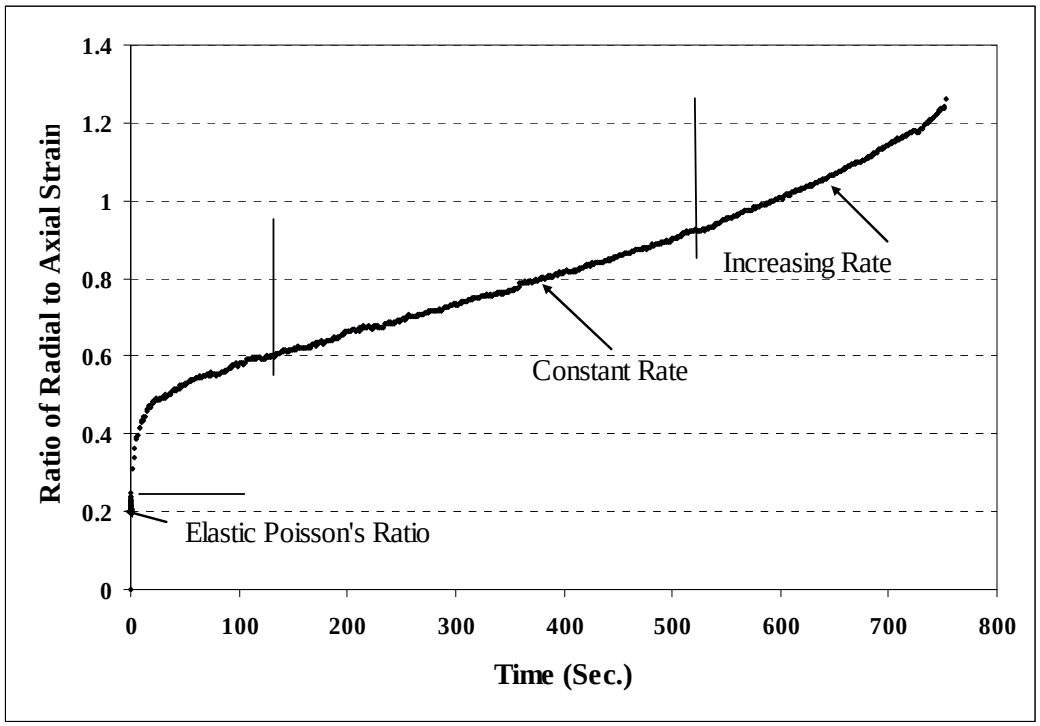

Figure 5.369 A typical result for the ratio of radial to axial strain for the HRA at 20°C.

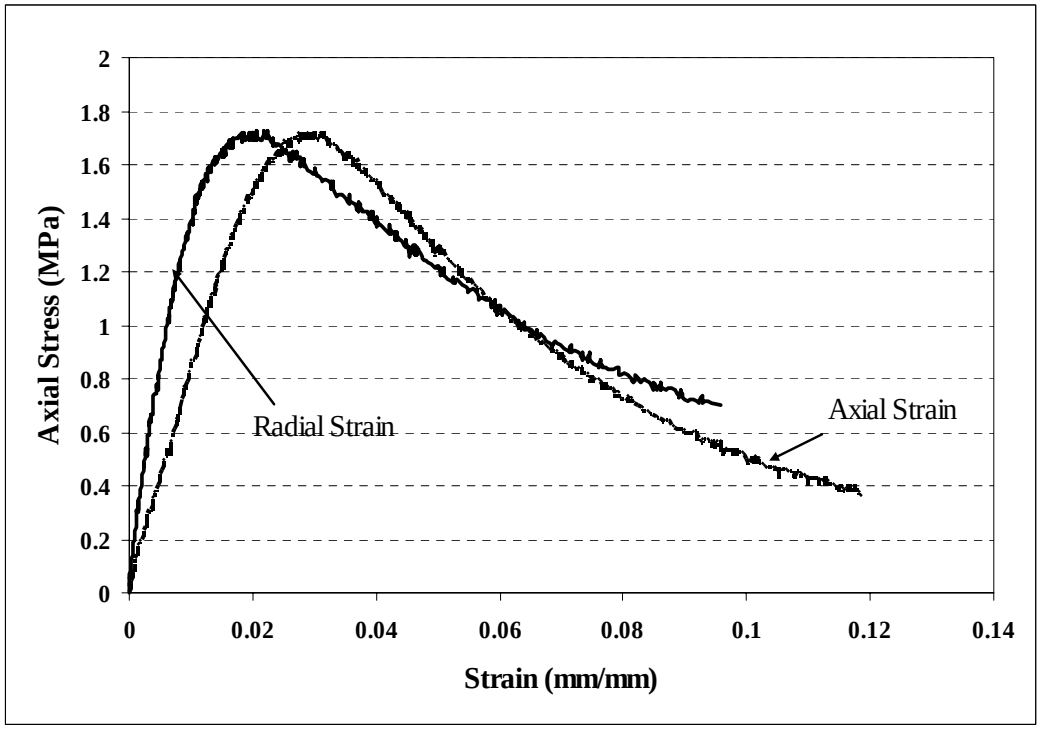

Figure 5.40 A typical constant strain rate test result for the HRA at 20°C (strain rate of 0.0005/s).

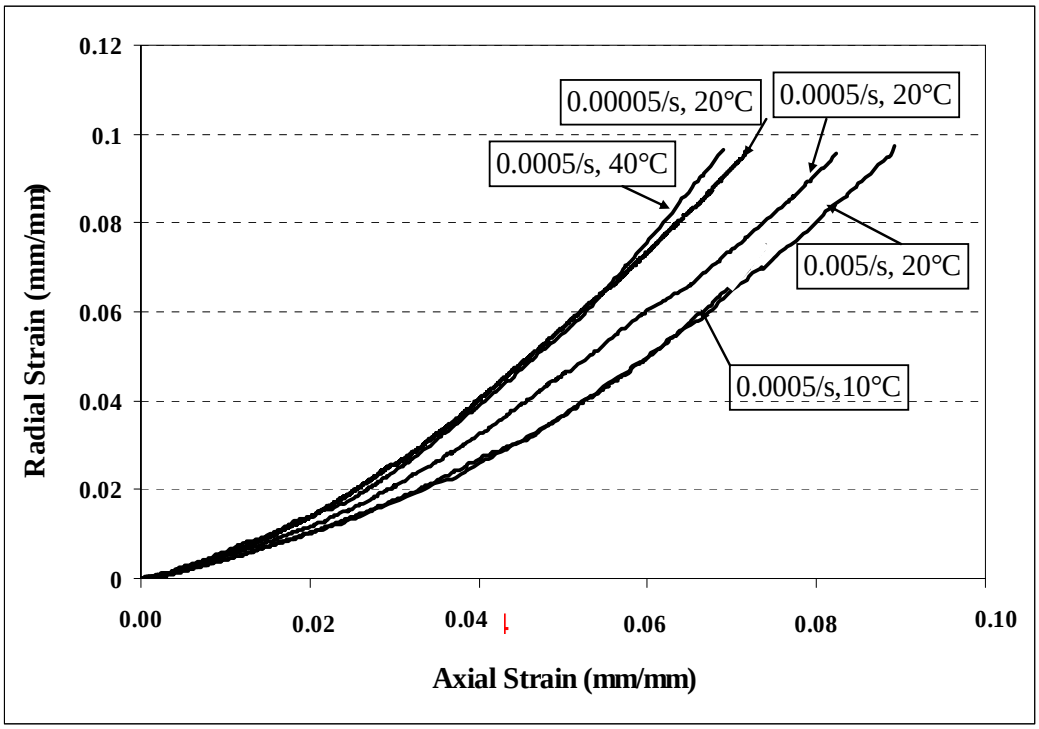

Figure 5.41 Variation of the radial strain with axial strain for uniaxial constant strain rate tests at selected test conditions (HRA mixture).

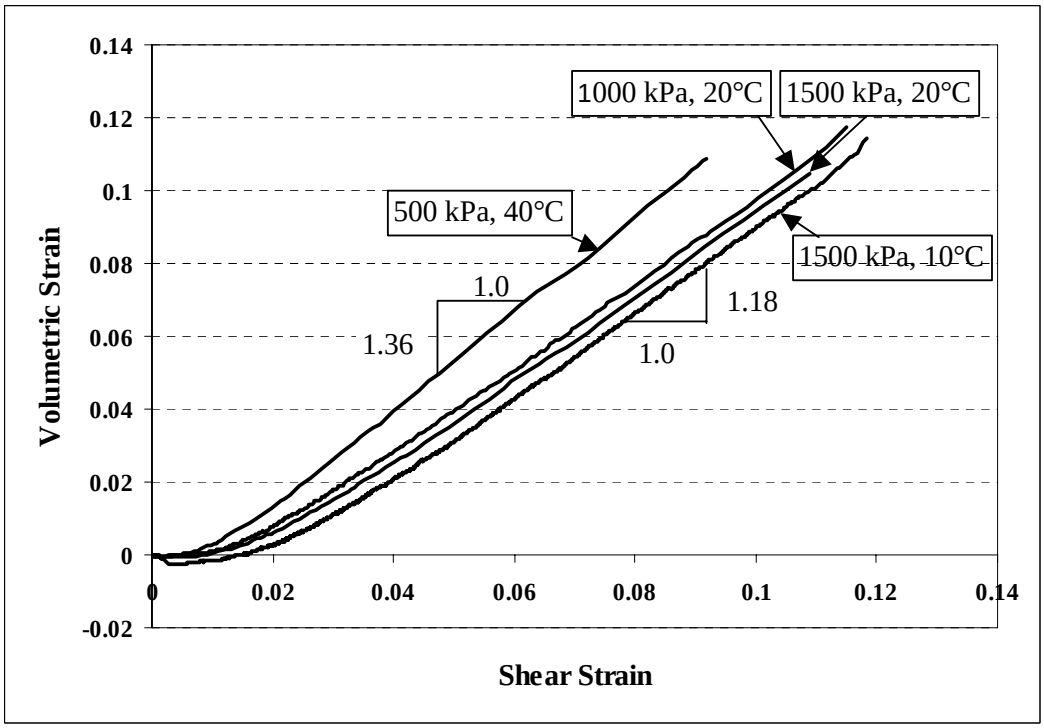

Figure 5.37 Variation of the volumetric strain with the shear strain for uniaxial creep tests at selected test conditions on the HRA.

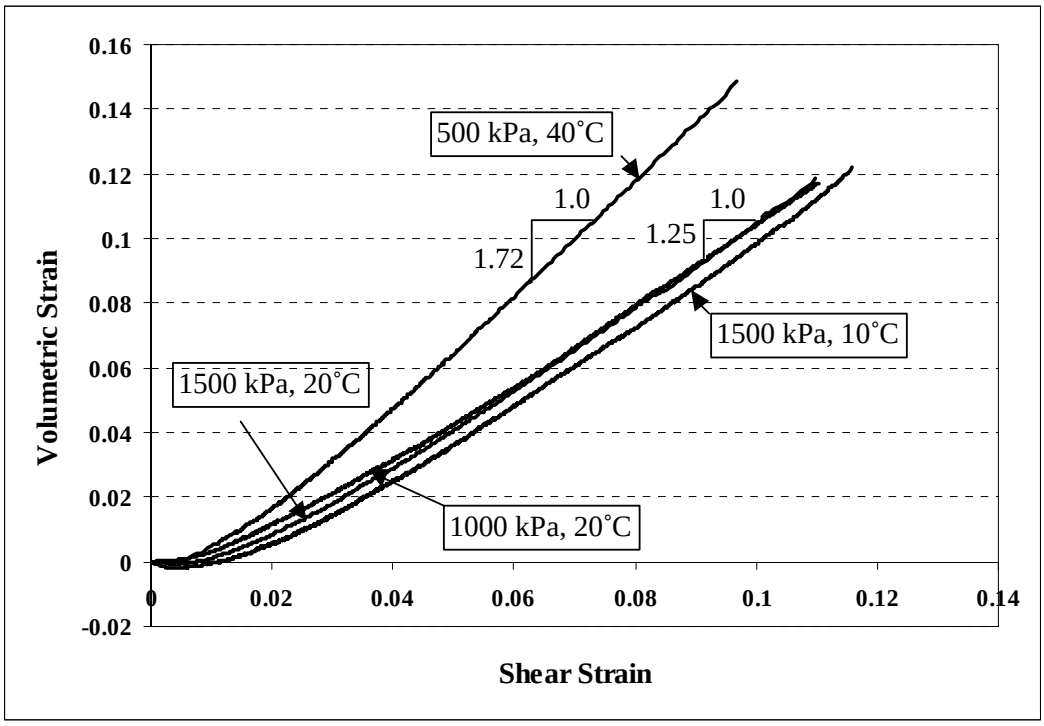

Figure 5.383 Variation of the volumetric strain with the shear strain for uniaxial creep tests at selected test conditions on the DBM.

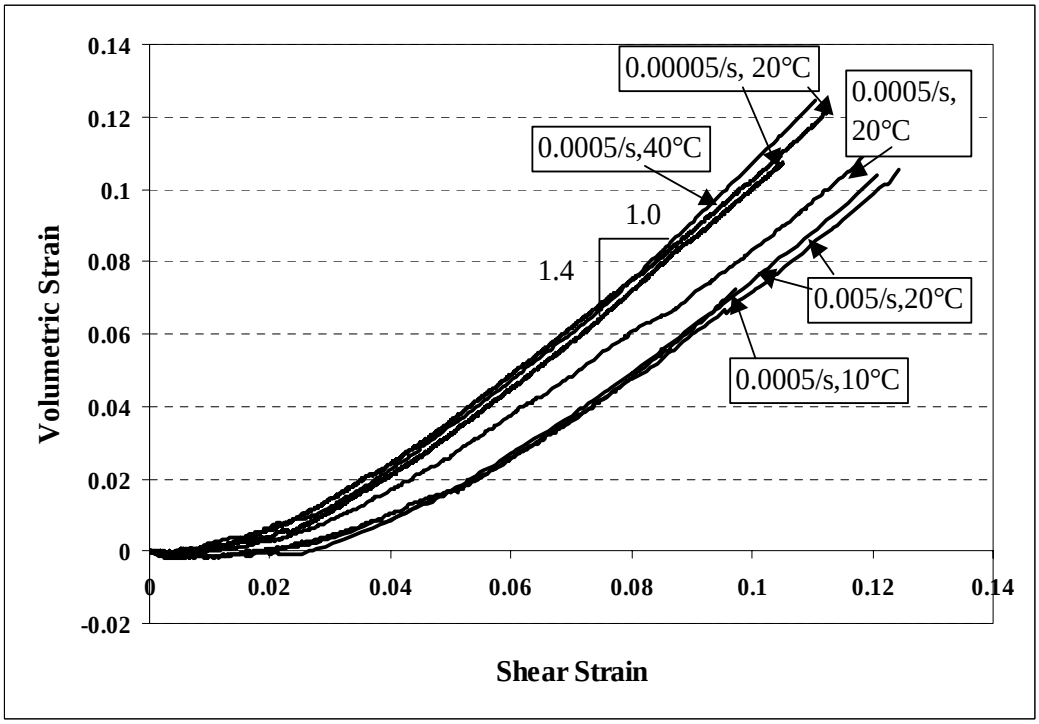

Figure 5.39 Variation of the volumetric strain with the shear strain from uniaxial constant strain rate tests on the HRA.

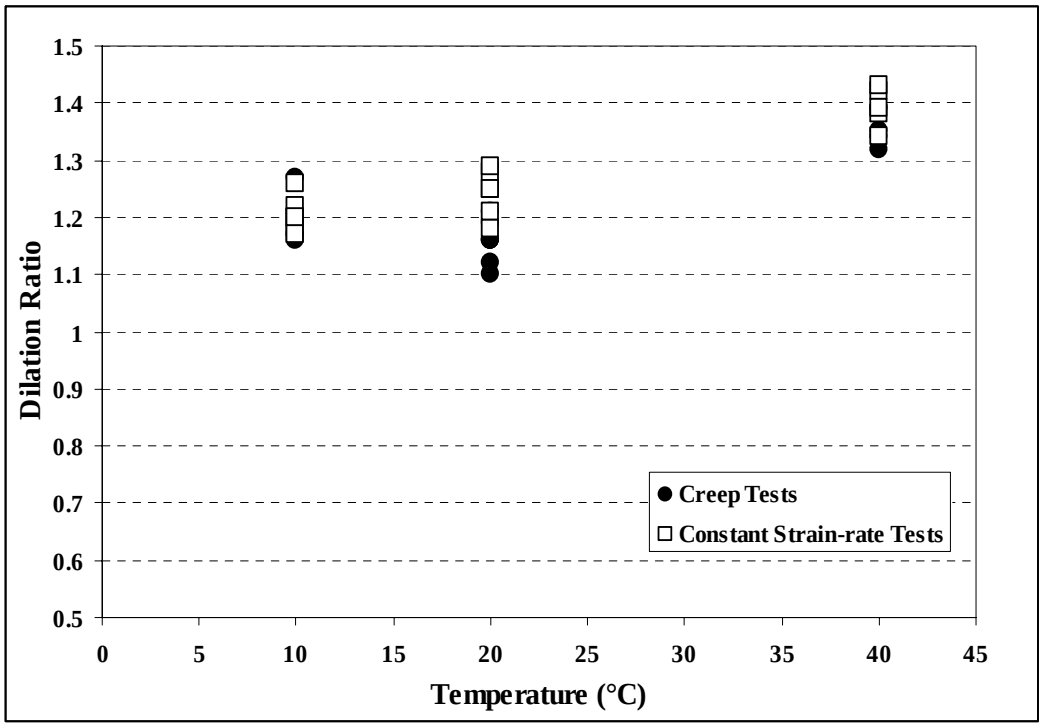

Figure 5.40 Variation of dilation ratio with temperature for the HRA.

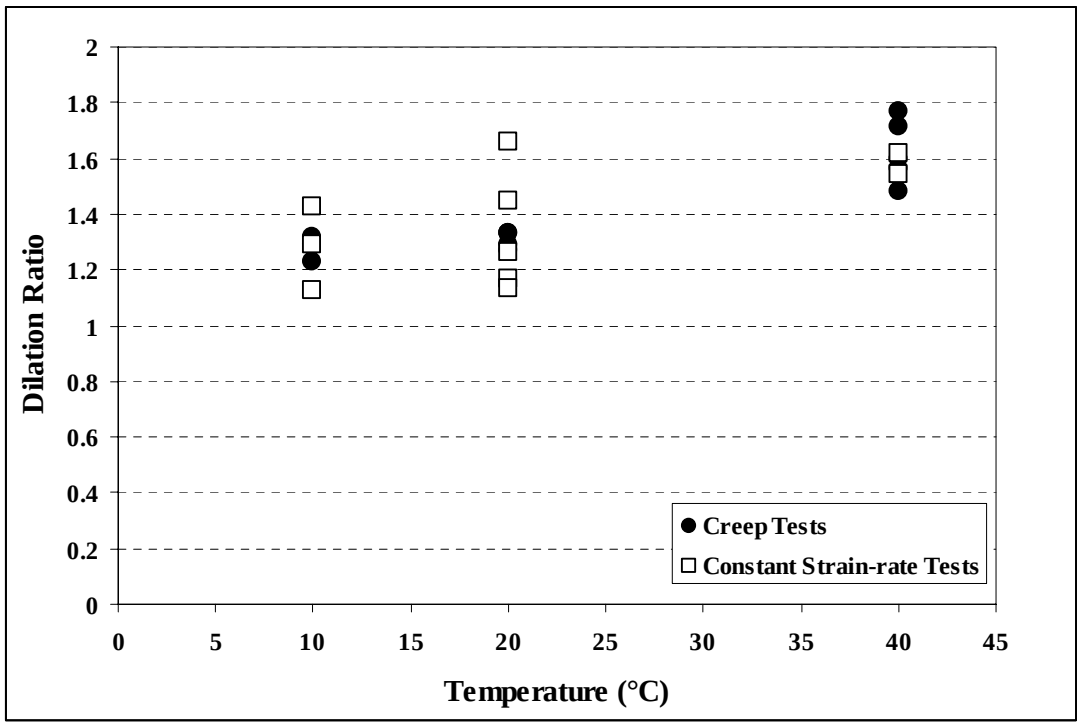

Figure 5.46 Variation of dilation ratio with temperature for the DBM.

5.3.4 Poisson's Ratio

Poisson's ratio is defined as the negative ratio of the transverse extension strain to the longitudinal contraction strain in the direction of loading in the elastic region of behaviour, as given in Equation 5.6. As tensile deformation is considered positive and compressive deformation is considered negative, therefore Poisson's ratio is a positive value.

$$\upsilon = -\frac{\varepsilon_r}{\varepsilon_a}, \tag{5.6}$$

Poisson's ratio for all elastic materials must fall in the range of 0 to 0.5. Materials with a Poisson's ratio of exactly 0.5 are incompressible, since the sum of all their strains leads to a zero volume change. Poisson's ratio in a viscoelastic material is time dependent.

Poisson's ratio of the mixtures studied in this research is one of the parameters required for the non-linear viscoelastic constitutive model developed by Collop *et al.* [2003] to be applied for analysis and prediction of permanent deformation of the mixtures. Poisson's ratio values for asphaltic mixtures have been found to lie somewhere in the range 0.1 to 0.45 [Read, 1996]. Dunhill [2002] proposed Poisson's ratio values for the HRA and DBM mixtures at different temperatures. Table 5.6 presents the temperature dependent values for the Poisson's ratio of asphalt mixtures recommended by TRL [Nunn, 1995] and the values proposed by Dunhill [2002].

Poisson's ratio of the mixtures was determined from the data at the beginning of the uniaxial creep tests. In the uniaxial creep tests, Poisson's ratio was determined as the average ratio of the radial strain to the axial strain over the short time period in the beginning of the test during which the load increases from zero to the target load (Figure 5.47). Figure 5.48 shows Poisson's ratio of the mixtures at 20°C. The scatter in the values is caused by the experimental errors in measurement of the small radial and axial strains by which the Poisson's ratio was calculated. As can be seen, Poisson's ratio of both mixtures is independent of the applied stress. A summary of the Poisson's ratio for the

mixtures is presented in Figure 5.49 as a function of temperature. As can be seen in the figure, Poisson's ratio increases with increasing temperature and is almost the same for both mixtures. Also in the figure the superimposed line refers to the values of Poisson's ratio recommended by the TRL [Nunn, 1995], as given in Table 5.6. As can be seen, the values determined in this study are consistent with the values recommended by TRL, and therefore, those values can be used as Poisson's ratio of the mixtures in the constitutive model.

Table 5.6 Values for Poisson's ratio recommended by the TRL and proposed by Dunhill [2002]

Temperature (°C)	Poisson's ratio recommended by the TRL	Poisson's ratio proposed by Dunhill [2002]
0 and less	0.25	0.3
20	0.35	0.35
30 and more	0.45	0.4

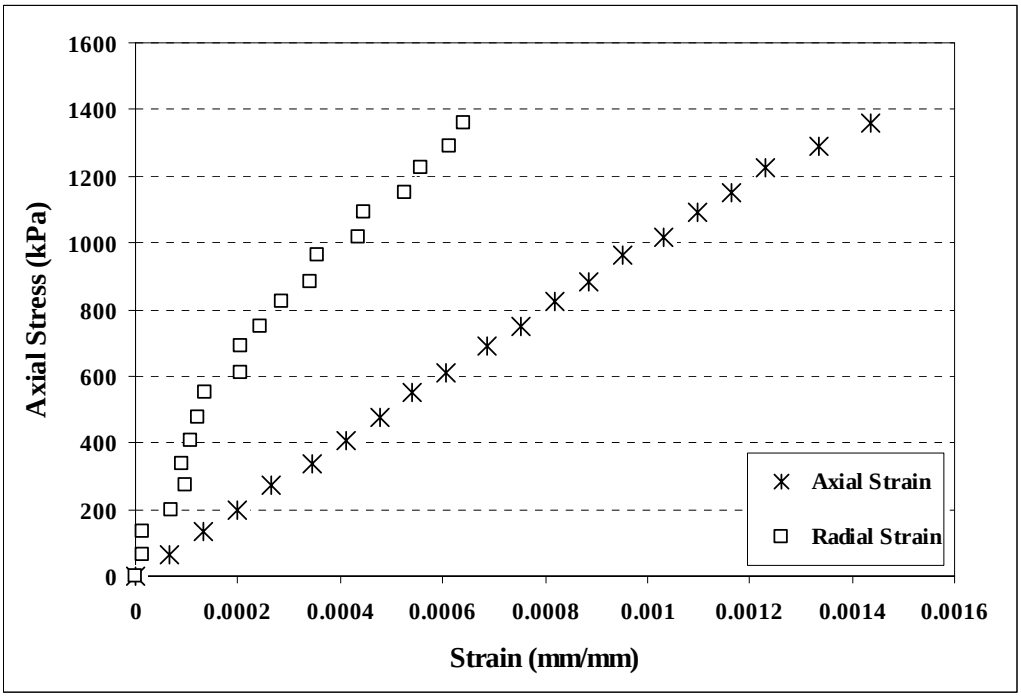

Figure 5.47 The axial and radial strain at the short period of load application for the HRA30/10 (20°C, 1500 kPa).

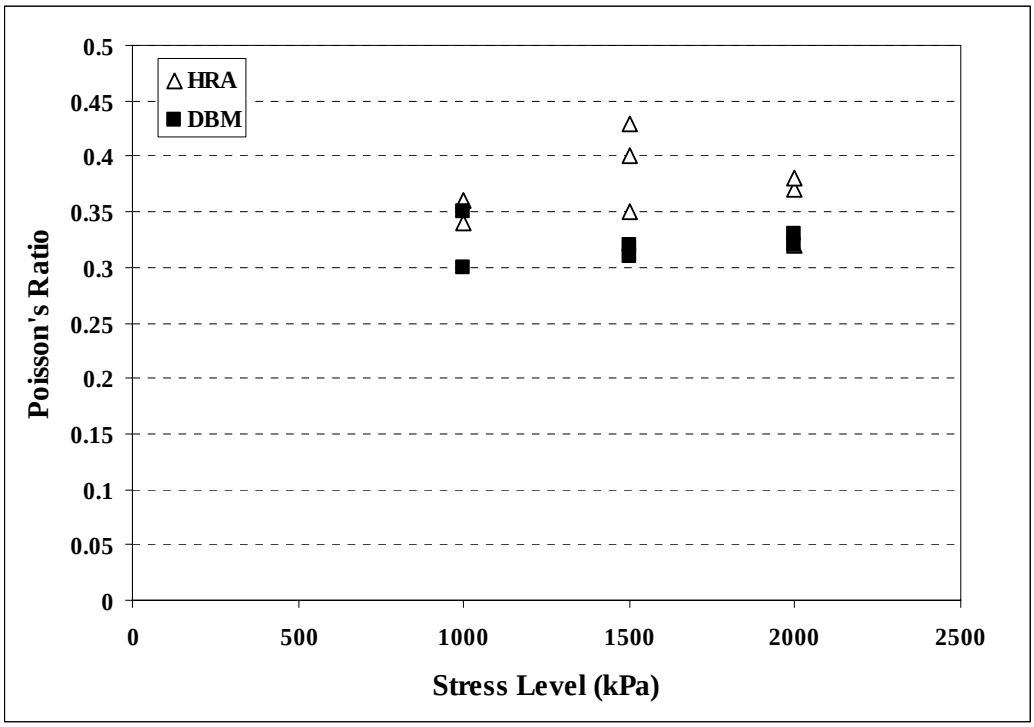

Figure 5.48 Poisson's ratio of the mixtures as a function of stress level at 20°C.

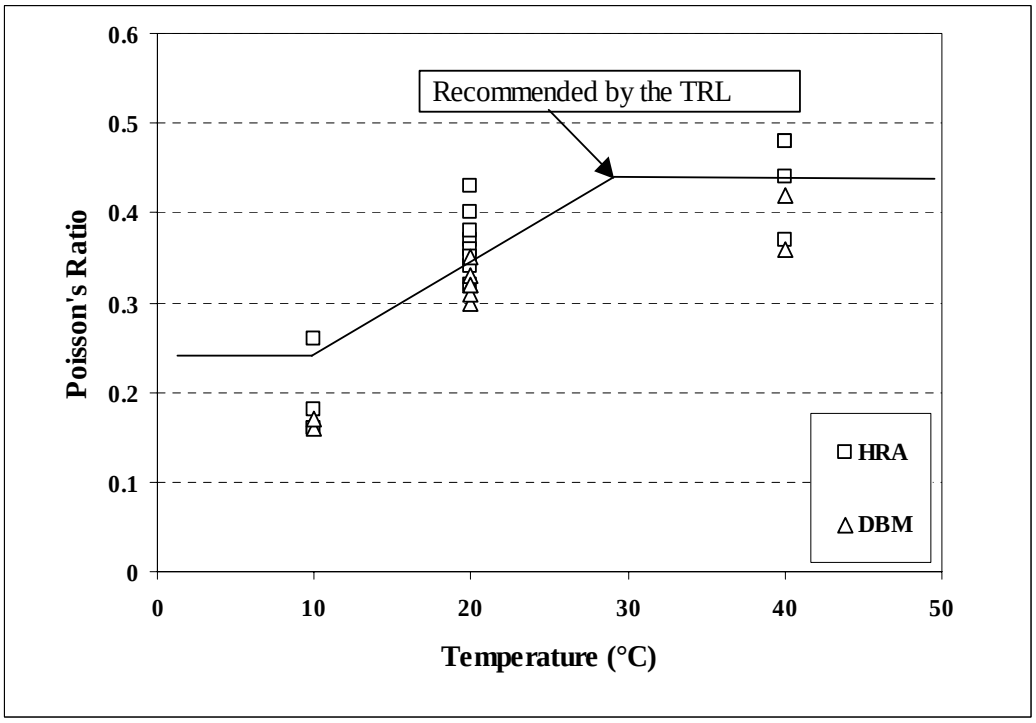

Figure 5.49 Poisson's ratio of the mixtures as a function of temperature.

5.4 Discussion

Asphaltic mixtures resist permanent deformation by resistance of the binder to shear deformation and interparticle friction due to aggregate interlock. The contribution of each mechanism depends on the volume fraction of aggregate and bitumen, the gradation, size, shape and surface texture of the aggregate and the properties of bitumen. Mixtures with little aggregate to aggregate contact have binder dominated behaviour with similar steady-state deformation behaviour to that of the bitumen. Because of the sensitivity of bitumen to temperature, the resistance to deformation of these types of mixtures is more sensitive to temperature compared to the mixtures with aggregate to aggregate contact. For example, a DBM mixture, when compared with a HRA, has continuously graded aggregate, a higher volume fraction of aggregate and a lower volume fraction of bitumen. The aggregate to aggregate contact in the DBM results in more friction and interlocking which increases the resistance of the mixture to deformation. It was observed that while the HRA deformed significantly under a constant stress level of 60 kPa at 20°C, the strain developed in the DBM under a stress level of 250 kPa at 40°C and four days of loading was negligible. It was expected that the steady-state deformation behaviour of the mixtures would be broadly the same as that of the binder, however, as observed from the test results, the power exponent of the mixtures (2.9 for the HRA and 3.9 for the DBM) was higher than that of the binder (2.6). For the HRA, it can be assumed that there is less aggregate to aggregate contact and the steady-state deformation behaviour is mostly dominated by the binder and its power exponent is close to that of the bitumen. For the DBM, it is believed that the higher friction and interlocking due to the aggregate to aggregate contact overcome the binder dominated steady-state deformation behaviour. This is not fully understood and requires further investigation.

The volumetric behaviour of the mixtures was found to be dependent on the type of mixture and temperature. The dependency on the type of mixture is discussed in Chapter 8. It was observed that Poisson's ratio and the dilation ratio increase with increasing temperature. The lateral deformation of the mixtures is

influenced by the bond between the aggregates. At high temperatures the tensile strength of the binder decreases which results in higher lateral deformation.

5.5 Conclusions

The following conclusions can be drawn from this chapter:

- The steady-state results of the constant stress creep and constant strain rate tests were found to be complementary.

- Over the range of stress levels utilised in the uniaxial tests, the uniaxial steady-state deformation behaviour of the HRA and DBM mixtures were found to be non-linear power law creep with a power exponent of 2.9 for the HRA and 3.9 for the DBM.

- The temperature dependency of the steady-state deformation behaviour of the mixtures was found to be free volume controlled and was well captured by the WLF equation.

- The ageing of bitumen during the mixing operation was found to have no effect on the steady-state deformation behaviour of the bitumen.

- In the uniaxial creep tests, the axial strain level at the start point of the steady-state strain rate was found to be independent of applied stress level, decrease with increasing temperature and, at the same test conditions, be generally higher for the HRA than that for the DBM.

- In the constant strain rate tests, the axial strain level at the peak (steady-state) stress was found to be independent of applied strain rate, decrease with increasing temperature and, at the same test conditions, be generally higher for the HRA than that for the DBM.

- At the same test conditions, the DBM was found to be more resistant to deformation than the HRA.

- The resistance to deformation of the HRA mixture was found to be more sensitive to temperature than that of the DBM.

- The resistance to deformation of the DBM mixture was found to be more sensitive to applied axial stress level than that of the HRA.

- The peak stress in the uniaxial constant strain rate tests increases with increasing strain rate and decreasing temperature.

- At the same test conditions, the peak stress of the DBM was found to be greater than that for the HRA.

- Young modulus of the mixtures was found to increase with increasing strain rate and decreasing temperature.

- A linear relationship was found between Young's modulus and the peak stress of the mixtures.
- Both mixtures were found to dilate under uniaxial constant stress creep and constant strain rate tests.

- In the steady-state behaviour of the mixtures, the radial strain varies linearly with the axial strain with a slope which depends on temperature and type of mixture and is independent of applied axial stress level.

- For both mixtures, the volumetric strain was found to vary linearly with the shear strain with a slope known as the dilation ratio.

- The dilation ratio of the HRA was found to be temperature dependent and independent of the applied axial stress level and strain rate.

- The dilation ratio of the DBM was found to be temperature and strain rate dependent and independent of the applied axial stress level.

- For the DBM mixture, the mean value of dilation ratio was observed to be higher than that of the HRA.

- Both mixtures were observed to have the same Poisson's ratio which was found to be independent of applied axial stress level and increases with increasing temperature.

Creep Recovery Tests

6.1 Introduction

An asphaltic material behaves as a viscoelastic material in many conditions. The degree of viscoelasticity depends on the rate of loading, temperature, the stress state and the mixture composition. When a load is applied on the material and held constant, the result is development of an instantaneous time-independent deformation (elastic and plastic) followed by time-dependent deformation (delayed elastic and viscous). When the load is removed and the material is allowed to recover, the result is an instantaneous recovery followed by some time-dependent recovery (delayed elastic). After full recovery, any deformation that remains in the mixture is classified as permanent deformation. Prediction of the performance of asphaltic layers under traffic loading requires an understanding of the recovery behaviour of the asphaltic mixtures used in those layers. While the time-independent deformation (elastic and plastic) of an asphaltic material is dominated by the aggregates and bitumen, the bitumen mainly dominates the time-dependent deformation. As reviewed in Chapter 3, the research work on developing a constitutive model for asphaltic materials usually divides the deformation of the material into different components (e.g. elastic, plastic, delayed elastic and viscous). The creep recovery test is an appropriate

test method to study the strain components and recovery behaviour of asphaltic materials.

This chapter describes single and repeated creep recovery tests performed on the HRA and the DBM mixtures. The single creep recovery tests were conducted over a range of stress levels and temperatures, for a series of total accumulative strain before unloading. The repeated creep recovery tests were also conducted over a range of loading and rest times at a specified stress level and temperature. In addition to the investigation of recovery behaviour of the mixtures, the creep recovery test results are used for determination of the parameters for the non-linear viscoelastic constitutive model developed by Collop *et al.* [2003], which is explained in Chapter 8.

6.2 Single Creep Recovery Tests

Single creep recovery tests were performed to study the effect of temperature, stress level and damage accumulation on the recovery behaviour of the HRA and DBM mixtures. The tests were conducted on the mixtures over a range of axial stress levels and temperatures, as shown in Table 6.1. To investigate the effect of damage accumulation on the recovery behaviour, the creep recovery tests were performed for a series of total strains before unloading for two stress levels at 20°C.

Table 6.1 Single creep recovery test conditions

Temperature (°C)		**10**	**20**	**40**
Stress Level (kPa)	**HRA**	1500, 2000	1000, 1500, 2000	400, 500
	DBM	2000, 2500	1000, 1500, 2000	500, 750

6.3 Test Procedure

The same experimental work carried out for the uniaxial creep tests (in terms of specimen, equipment, instrumentation, friction reduction system etc.), as explained in Chapter 5, was used for the creep recovery tests.

In a single creep recovery test (see Figure 6.1), after preparation, instrumentation and preloading of the specimen, as explained in Section 5.2, the target load was quickly applied on the specimen over a period of 30 to 40 milliseconds. The applied load was held constant for a certain time such that the total axial strain occurred in the specimen was in the secondary creep region. This was because the deformation components in the secondary creep region can be well divided into the elastic, delayed elastic and viscous strain components. The load was then released over a short time equivalent to the time taken to apply the target load. This was the shortest time which gave enough data points to be logged by the machine for calculation of elastic stiffness (see Chapter 8) and short enough to assume that the response of the material is elastic [Lu, 1998]. After removing the load, the specimen was allowed to recover until the rate of recovered deformation was approximately zero. For the higher temperature of 40°C, this condition was reached shortly after unloading, while at a lower temperature of 10°C it took approximately 3 hours for the DBM. During the creep and recovery stages, the axial and radial deformations, and the load were measured and logged by a computer connected to the equipment. The data were converted to ASCII files and were transferred for data analysis.

6.4 Test Results

Figure 6.1 shows a typical creep recovery test result for the HRA mixture where the axial strain is plotted as a function of time. Similar behaviour was observed for the DBM. It can be seen from Figure 6.1 that, when the load is applied, an instantaneous (time-independent) strain develops in the specimen followed by gradually increasing (time-dependent) strains. When the load is removed, there is an instantaneous recovery (elastic strain) followed by time-dependent elastic strain (delayed elastic strain) recovery. The irrecoverable strain remains in the

specimen as permanent strain, which is comprised of the plastic and viscous components. The creep recovery test results showed that the strain developed during the short period of load application was greater than the strain recovered during the same period in which the load is removed (elastic strain). The difference between these two strains is called plastic strain [Sides *et al.*, 1985; Uzan, 1996; Lu, 1998]. In this research, which concerns the deformation of asphaltic mixtures under static loading, the plastic strain is insignificant compared to the viscous strain. It can be seen in Figure 6.1 that the plastic strain is only a small fraction of the permanent strain. Moreover, part of the plastic strain is the viscous strain developed during the short period of load application. Therefore, in this research, the instantaneous strain assumed to be comprised of elastic and the viscous strain occurring during the period of target load application.

To investigate the effect of damage accumulation on the recovery behaviour of the mixtures, a series of creep recovery tests were performed for which the mixtures were unloaded at different levels of total axial strain. For each mixture, the tests were conducted at 20°C and two different stress levels. Figure 6.2, for example, shows the creep recovery response of the HRA unloaded at different strain levels at a stress level of 1000 kPa. Figure 6.3 shows the variation of the recovered strain (comprised of instantaneous and delayed elastic) plotted against the total strain before unloading for the mixtures at the same test conditions of 1000 kPa and 20°C. As can be seen, for each mixture, the recovered strain increases with increasing total strain before unloading up to a level after which the recovered strain tends to remain constant. This behaviour is similar to what was seen for the bitumen (see Section 4.6). Similarly, all the creep recovery test results for the DBM and HRA mixtures, at different stress levels and temperatures, are summarised in Figures 6.4 and 6.5, respectively. As can be seen, within the range of test conditions utilised in this study, independent of the applied axial stress level and temperature, the recovered strain varies linearly with the total strain before unloading. This linear variation continues up to a total strain level of 0.03 for the DBM and 0.075 for the HRA, after which the recovered strain stabilises to constant values of 0.013 and 0.006 for the HRA and the DBM, respectively. Ossa [2004] found that the slope of the linear variation

decreases with increasing volume fraction of aggregates. As can be seen in Figures 6.4 and 6.5, the slope of the linear variation for the HRA mixtures is slightly higher than that for the DBM. The reason for earlier flattening out of the DBM is not fully understood, although is believed to be due to the earlier development of internal damage in the DBM compared to the HRA.

To investigate the volumetric behaviour of the mixtures during recovery, the radial strain was measured for a few specimens of each mixture. It was observed that the variation of the radial strain with time was qualitatively similar to that of the axial strain, as shown in Figure 6.1. Figure 6.6 shows a typical variation of the volumetric strain (Equation 2.13) with the shear strain (Equation 2.14) in the creep recovery tests for the HRA mixture. Similar behaviour was also observed for the DBM mixture. As can be seen, the variation in the loading path is similar to that in the uniaxial creep tests, as explained in Chapter 5, with an initial reduction in volumetric strain followed by a linear increase with increasing the shear strain. After releasing the load, the volumetric strain decreases linearly with shear strain. The slope of the line during recovery is almost the same as that of the loading path, known as the dilation ratio. Similar behaviour has been observed for the idealised asphalt mixtures studied by Ossa [2004] and soils studied by Taylor [1948].

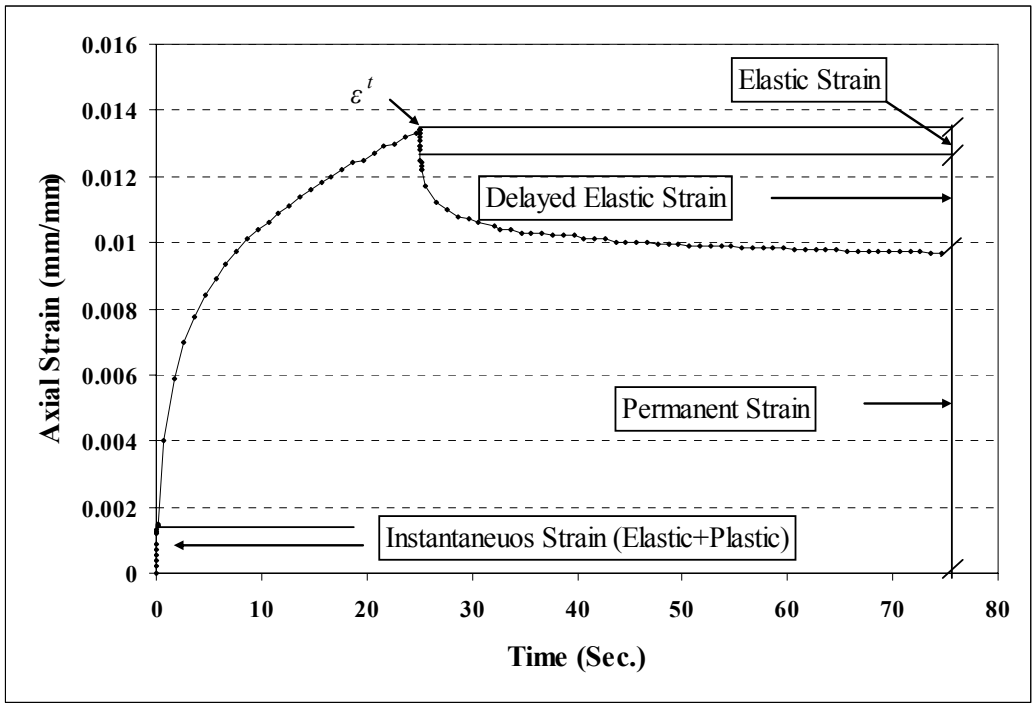

Figure 6.1 A typical creep recovery test result for the HRA30/10 AT 20°C (Axial stress level of 1000 kPa).

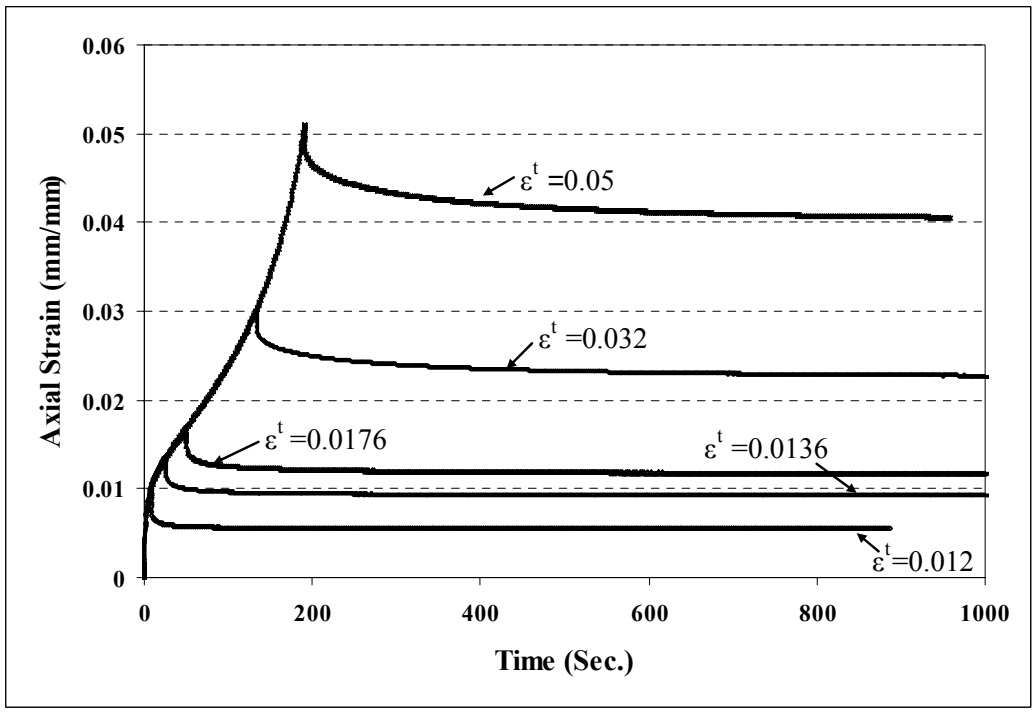

Figure 6.2 Creep recovery test results for the HRA30/10 for a series of total strain before unloading (20°C, 1000 kPa).

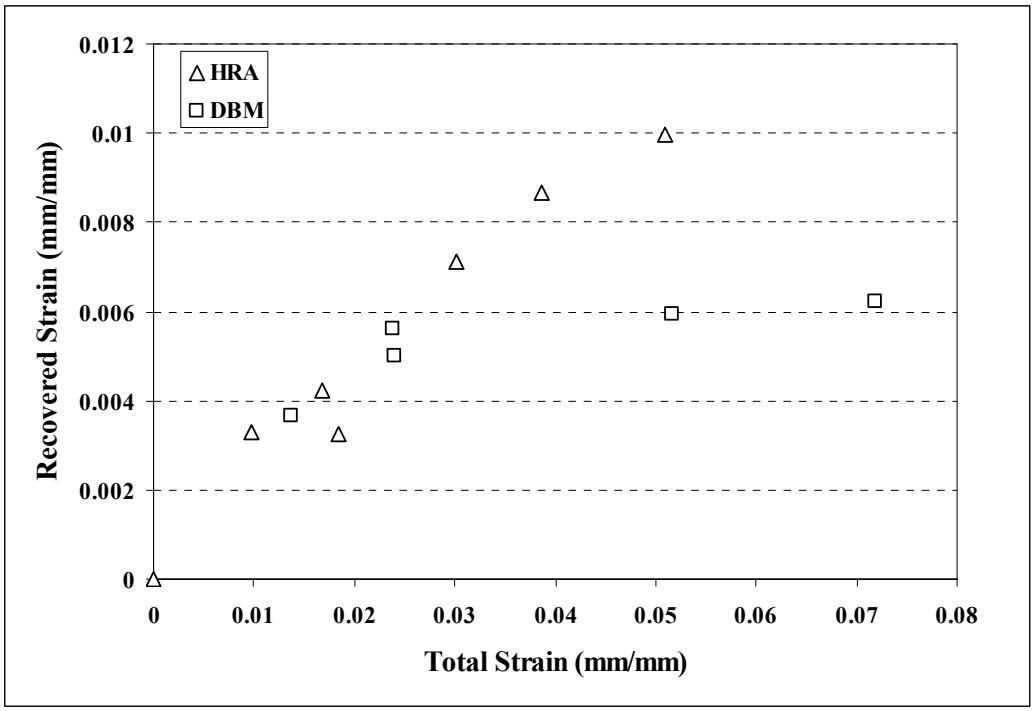

Figure 6.3 Summary of the creep recovery test results for the mixtures at 20°C (stress level of 1000 kPa).

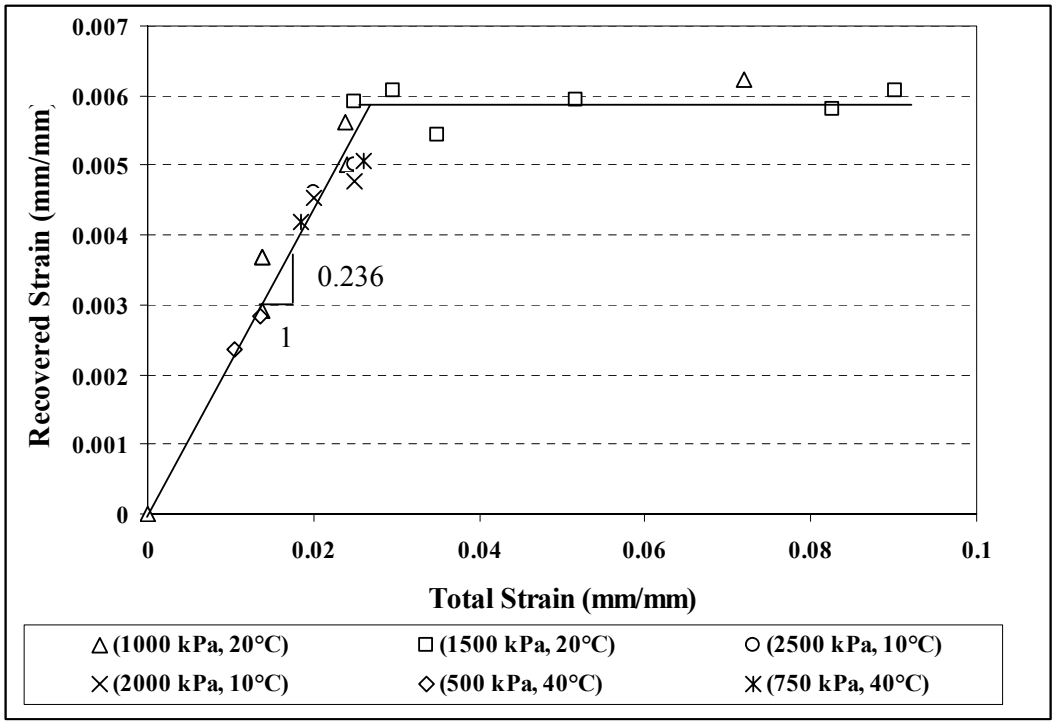

Figure 6.4 Summary of creep recovery test results for the 10mm DBM (at different temperatures and stress levels).

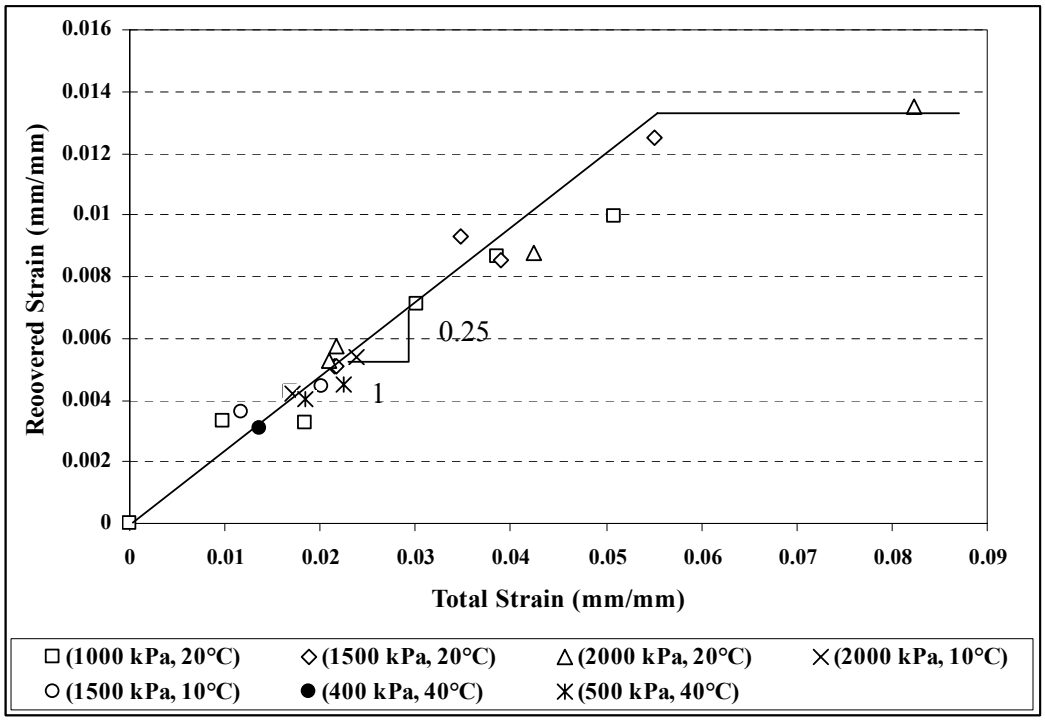

Figure 6.5 Summary of creep recovery test results for the HRA30/10 (at different temperatures and stress levels).

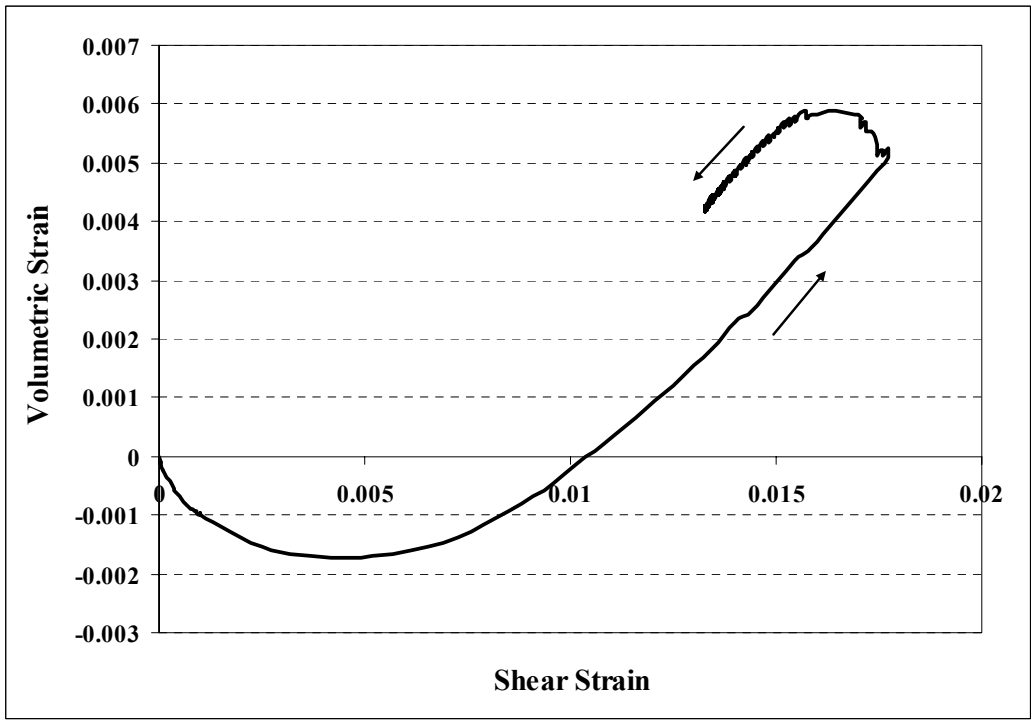

Figure 6.6 The volumetric strain against the shear strain for the HRA mixture at 20°C.

6.5 Recovery Strain Rate

The creep recovery test results showed that the rate of recovery changed for different test conditions. In order to investigate these changes, the framework developed by Ossa has been utilised (see Ossa [2004] for further details). To parameterise the recovery strain rate of the mixtures, the following definition as recovery parameter $\hat{\varepsilon}^r$, proposed by Ossa [2004] for bitumen and idealised mixtures, was used.

$$\hat{\varepsilon}^r \equiv \left(\frac{\varepsilon}{\varepsilon^{pl}} - 1 \right) \frac{1-\psi}{\psi}, \qquad \textbf{(6.1)}$$

where ε = axial strain,

ε^{pl} = permanent strain after full recovery and

ψ = the recovery constant, as defined in Section 2.5.2.

As explained in previous section, the recovery constants for the HRA and the DBM were found to be 0.25 and 0.236 respectively. The value of $\hat{\varepsilon}^r$ varies between 1 and 0 with $\hat{\varepsilon}^r$ =1 at the instant of unloading and $\hat{\varepsilon}^r$ = 0 when the strain $\varepsilon = \varepsilon^{pl}$, i.e. when there is no more recoverable strain. The recovery strain rate was calculated from experimental data and plotted against the $\hat{\varepsilon}^r$. Figure 6.7 shows the recovery strain rate of the HRA as a function of the recovery parameter $\hat{\varepsilon}^r$ for four different total strains before unloading. As can be seen, the recovery strain rate decreases with increasing total strain before unloading (damage) in the mixture. Similar behaviour was observed for the DBM. Figure 6.8 shows the recovery strain rate of the HRA at 20°C for three different stress levels. To avoid the effect of damage on the recovery rate, these three tests had almost the same total axial strain before unloading (2.1 %). As can be seen, the recovery rate is independent of the stress level. Figure 6.9 shows the recovery strain rate for the HRA and the DBM at the same test conditions (20°C, 1000 kPa) with the total strain before unloading of 1.35 % for both mixtures. As can be seen, at the same conditions the recovery rate of the DBM is slightly less than that of the HRA. The effect of temperature on the rate of recovery can be seen in

Figures 6.10 and 6.11. Figure 6.10 shows the recovery strain rate behaviour of the HRA mixture at three different temperatures, with almost the same total strain before unloading and different stress levels. Figure 6.11 shows the recovered strain as a function of time since releasing the load for the tests shown in Figure 6.10. The figures clearly show that the rate of recovery increases with increasing temperature.

The recovery strain rate of the mixtures was found to be captured by the WLF equation (for details see Ossa *et al.* [2005]). The recovery rate of asphaltic mixtures needs further study and modelling.

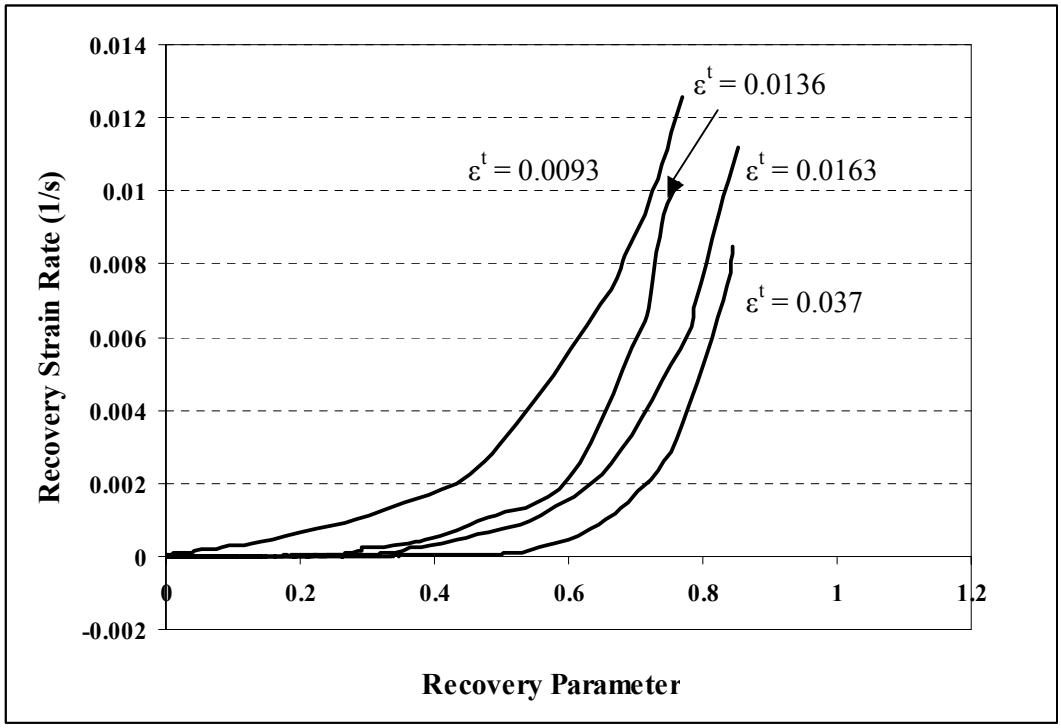

Figure 6.7 Recovery strain rate against recovery parameter for different total strains level before unloading ε^t for the HRA (20°C, 1000 kPa).

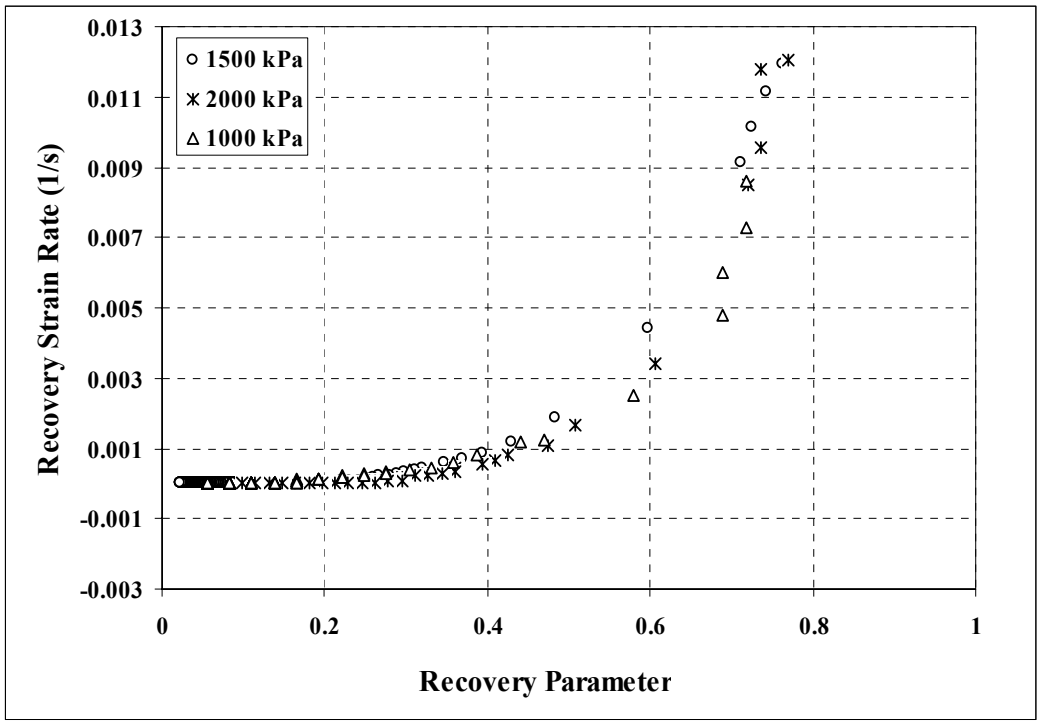

Figure 6.8 Recovery strain rate against recovery parameter for the HRA at different axial stress levels at 20°C.

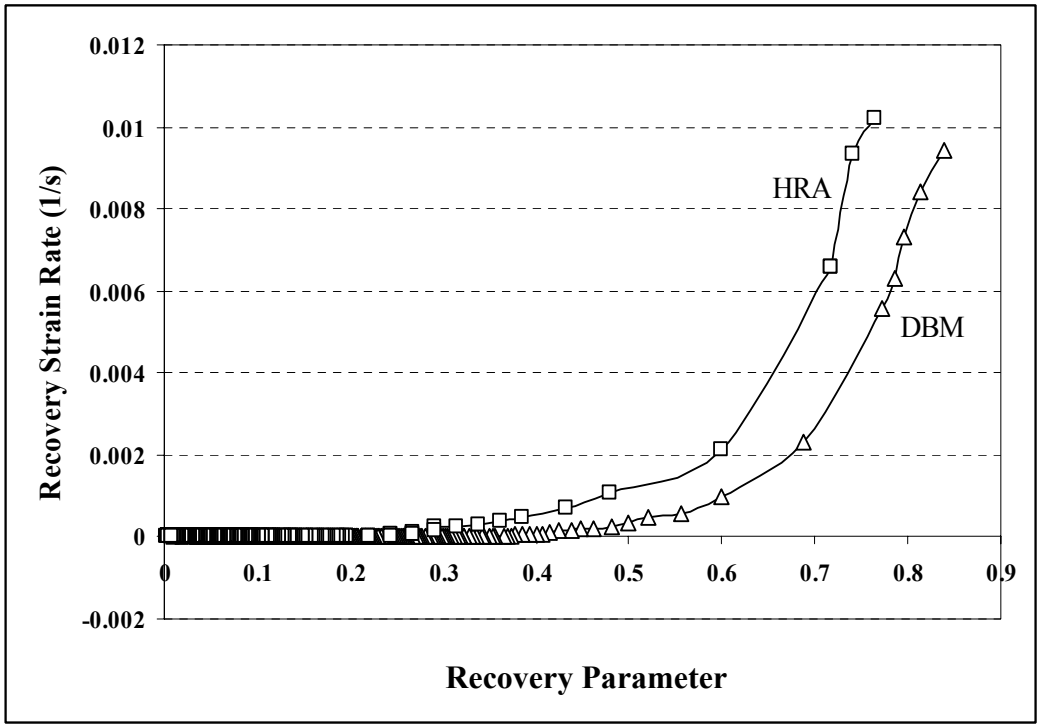

Figure 6.9 Recovery strain rate against recovery parameter for the mixtures at the same test condition of 1000 kPa and 20°C.

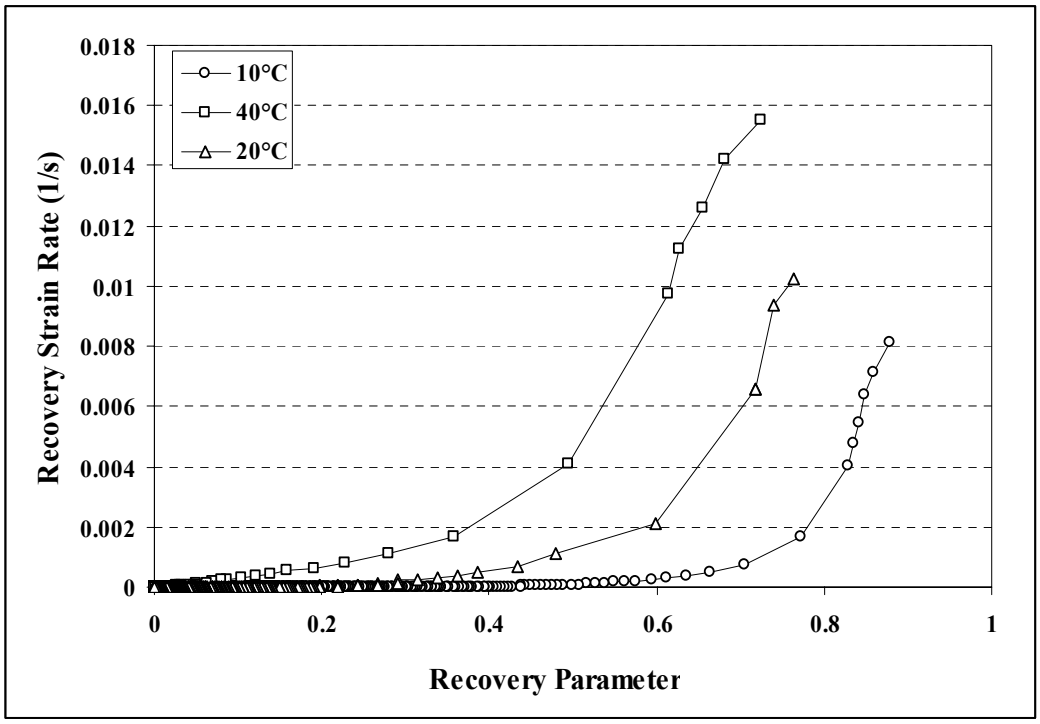

Figure 6.10 Recovery strain rate against recovery parameter for the HRA at different temperatures.

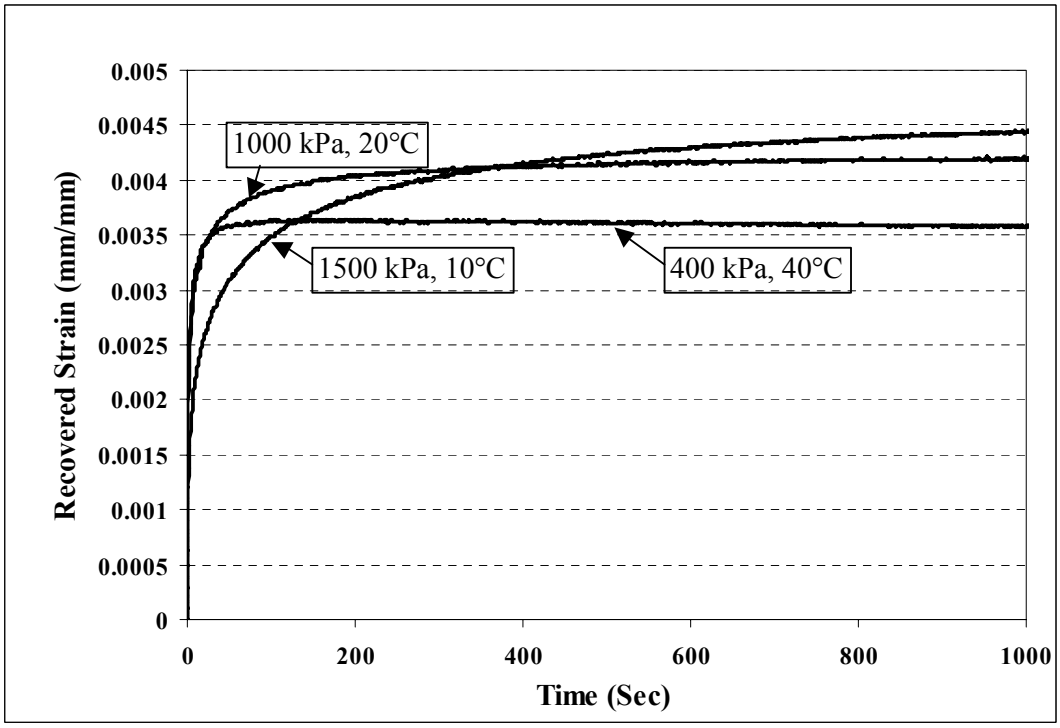

Figure 6.11 Recovered strain after unloading for the HRA at different temperatures.

6.6 Repeated Creep Recovery Tests

In order to simulate a load history more similar to that experienced in a real pavement, repeated creep recovery tests, comprising intermittent identical compressive stress pulses with a square shape in the time domain, as shown in Figure 6.12, were performed on the asphaltic mixtures. The aim was to investigate the change in the creep and recovery behaviour of the mixtures due to the application of repeated cycles of load and unloading. The results were also used to study the variation of the constitutive model parameters with the damage accumulation in the mixtures which will be discussed in Chapter 8.

The same experimental work as utilised for the single creep recovery tests was used for the repeated creep recovery tests. For each cycle, the axial stress σ was applied on the specimen and held constant for a time period of ΔL after which the stress was released and the specimen was allowed to recover for a time period of ΔR. The rate of loading and unloading was chosen to be the same, as used in single creep recovery tests, such that the target load be applied and removed over a short time between 30 to 40 milliseconds. The test was continued by repeating the cycles until specimen failure. The axial strain and load were logged during the tests by the computer connected to the equipment. The test was carried out using the following test conditions:

<u>HRA mixture</u>

- Stress level of 1000 kPa,
- 3 recovery times ΔR (50, 100 and 1500 sec),
- 2 loading times ΔL (30 and 60 sec).

<u>DBM mixture</u>

- Stress level of 1500 kPa,
- 3 recovery times ΔR (50, 100 and 1500 sec),
- 2 loading times ΔL (60 and 120 sec).

The temperature dependency of the creep and recovery behaviour of the mixtures is dominated by the binder, which was studied by the uniaxial creep and single creep recovery tests, as explained before. Therefore, the repeated creep recovery tests were performed at only 20°C. Figure 6.13 and 6.14 show the results of the repeated creep recovery tests for the DBM and the HRA mixtures, respectively, where the axial strain is plotted against time for different recovery times ΔR. Assuming the maximum strain at each cycle as a data point, it can be seen that the curve for each test has a similar shape to that for the continuous creep curve with a primary, secondary and tertiary creep region. These figures show that the permanent strain is accumulated in the specimen due to the viscous strain and part of the recoverable strain (elastic and delayed elastic) which can not be recovered during the recovery time in each cycle. The results also clearly show that, for the same accumulated loading time, the accumulated permanent strain decreases with increasing the recovery time ΔR. This is because larger fractions of the creep strain are recovered during the rest times between the pulses.

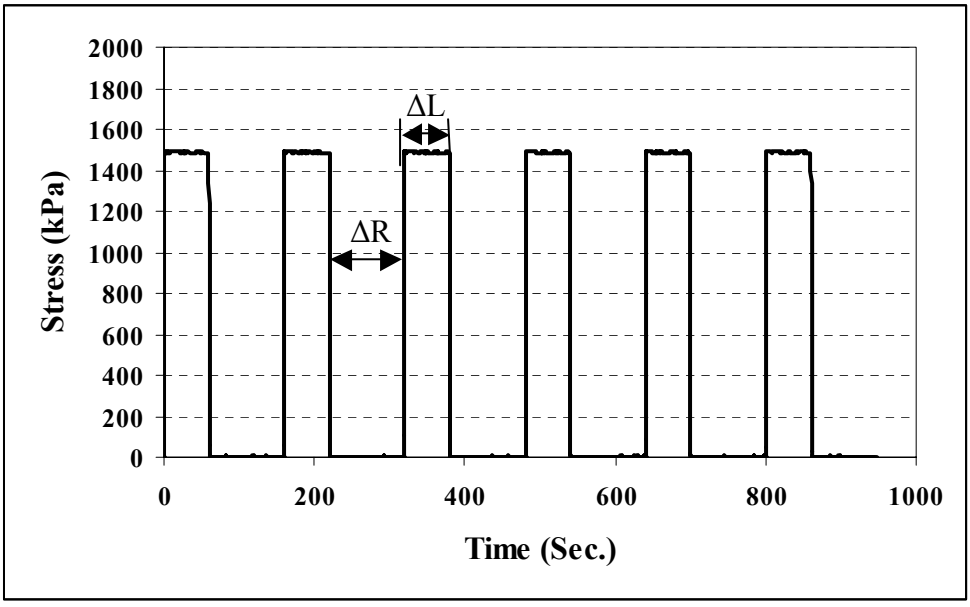

Figure 6.12 A section of the stress time history in the repeated creep recovery tests.

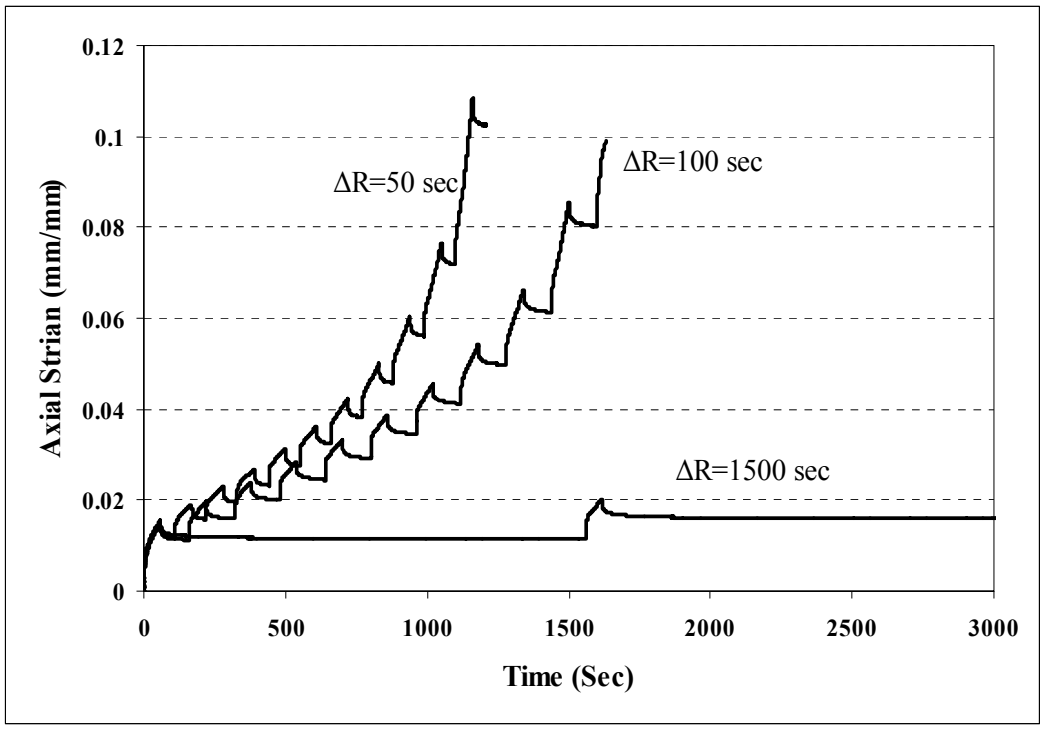

Figure 6.13 Repeated creep recovery test results of the 10 mm DBM for different recovery times at 20°C and 1500 kPa.

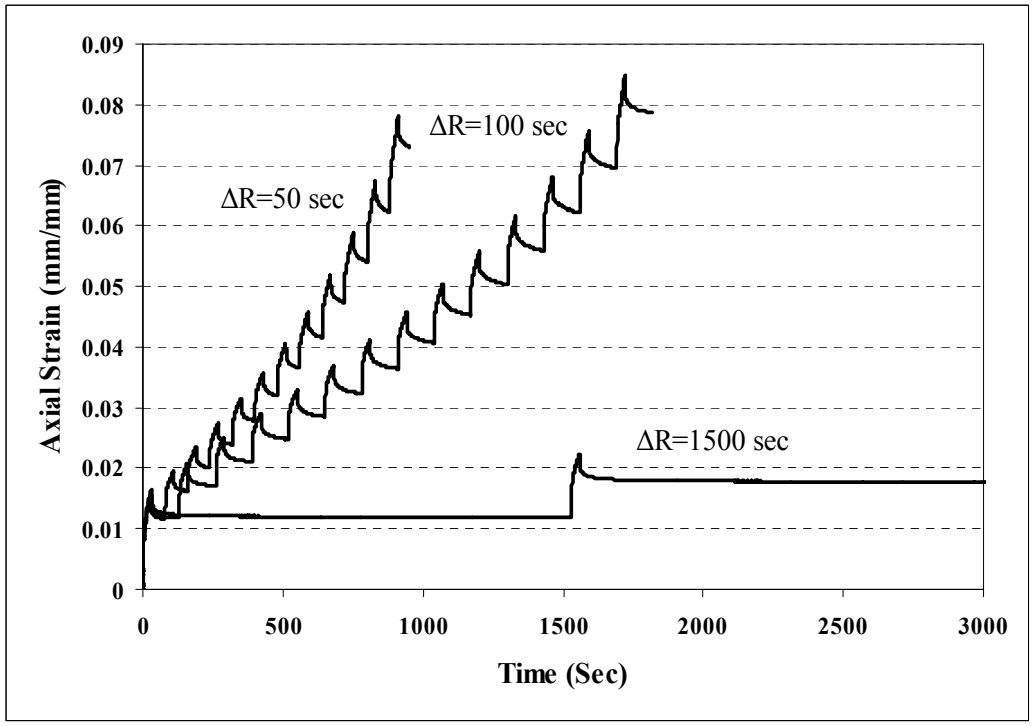

Figure 6.14 Repeated creep recovery test results of the HRA30/10 for different recovery times at 20°C and 1000 kPa.

Figure 6.15 shows the results for the DBM at two different loading times ΔL and the same recovery time ΔR of 50 seconds. As can be seen the permanent strain increases with increasing the loading time ΔL.

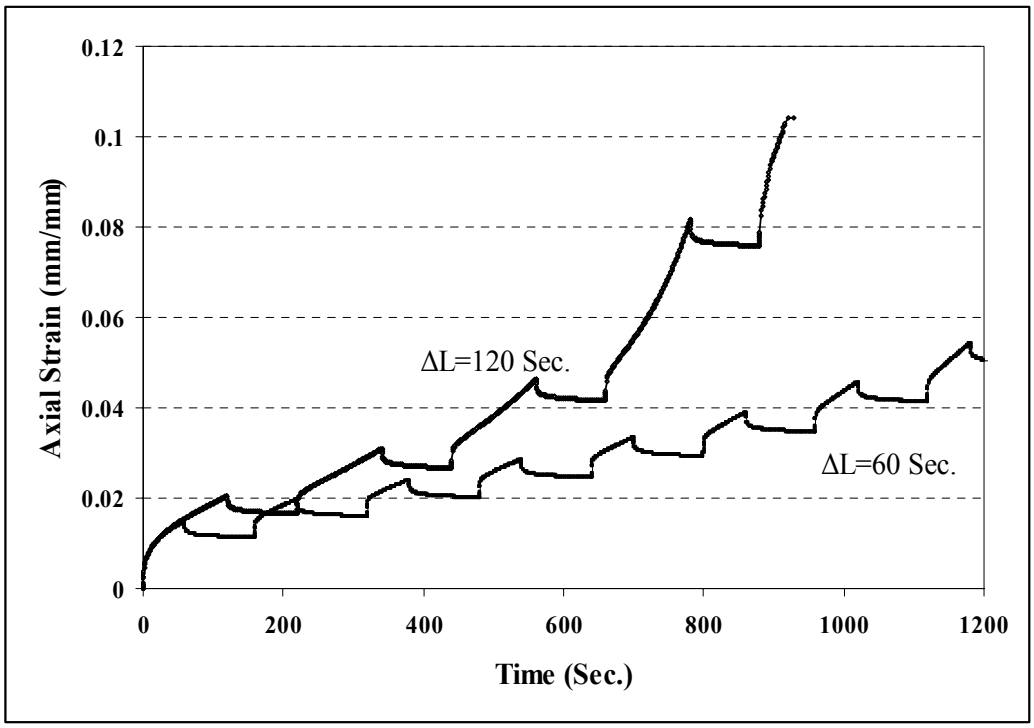

Figure 6.15 Repeated creep recovery test results of the DBM for different loading times at 20°C and 1500 kPa (ΔR=100 Sec.).

Figure 6.16 shows the creep recovery behaviour of the DBM mixture at different cycles, where the strain at the beginning of each cycle has been taken to be zero. It can be seen from this figure that there is a clear difference between the behaviour at the first cycle and cycles 2, 3 and 4, particularly, in terms of the permanent strain developed at each cycle. The reason for this is not fully understood, although it is thought to be due to the densification of the mixture, compression of the lubrication system and the restructuring within the specimen[1]. It can also be seen that the creep and recovery behaviour in the cycles 2, 3 and 4 are very similar. These three cycles correspond to the secondary creep region. By accumulation of damage in the specimen the creep and recovery behaviour tends to change with the permanent and recovered strains increase with increasing

[1] This effect is caused by the thickening of the bitumen films in the direction normal to the applied load and the thinning of the films in the direction of the applied load [Dunhill, 2002 and Read, 1996].

damage in the specimen (cycles 7, 8, 9 and 10 in the Figure 6.16). These cycles correspond to the tertiary creep region, where the strain rate increases with increasing damage in the specimen.

The repeated creep recovery tests revealed that the total strain, permanent and recovered strain (elastic + delayed elastic strain) corresponding to each cycle are affected by the recovery time ΔR. Figures 6.17, 6.18 and 6.19 show, respectively, the total, permanent and recovered strain of each cycle for the HRA mixture at different recovery times (ΔR =50, 100, 1500 sec). As explained before, these data are for the tests performed at 20°C, with an axial stress of 1000 kPa and a loading time of 30 sec. The same behaviour was observed for the DBM mixture for which the results for ΔR =50 sec are presented in Figure 6.20. As can be seen in Figures 6.17 and 6.18, up to the cycle 8, the total and permanent strains occurred in each cycle are almost similar for different recovery times. However, after Cycle 8, they decrease with increasing recovery time. This can be attributed to the healing of the mixtures during the rest times between the load pulses. When an asphaltic mixture heals, it returns to its original position and the microcracks, formed in the mixture due to the load application, meld back together [Kim *et al.*, 1989]. A longer recovery time results in a greater healing. Therefore, with the same accumulated loading time, the specimen with more recovery time heals more (less damaged), and, consequently, has a higher stiffness and less total and permanent strains. Figure 6.19 shows that, for the recovery time of ΔR = 1500 seconds, the recovered strain does not change significantly with number of cycle. However, for the recovery times of 50 and 100 seconds, it increases with increasing the number of cycles. This is due to the accumulation of the recoverable strains (elastic and delayed elastic) which have not recovered during the short recovery times of 50 seconds and 100 seconds. Whereas, in the tests with the recovery time ΔR =1500 seconds the recoverable strains are almost fully recovered.

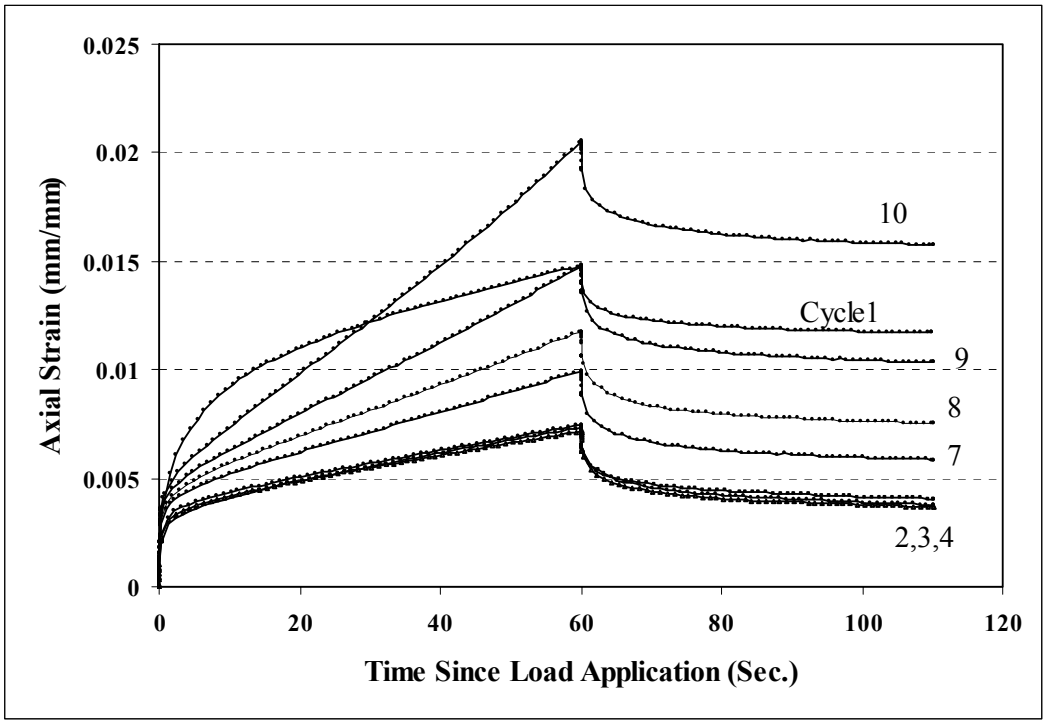

Figure 6.16 Creep and recovery response of the DBM at different cycles in a repeated creep recovery test (ΔL=60 Sec., ΔR=50 Sec.).

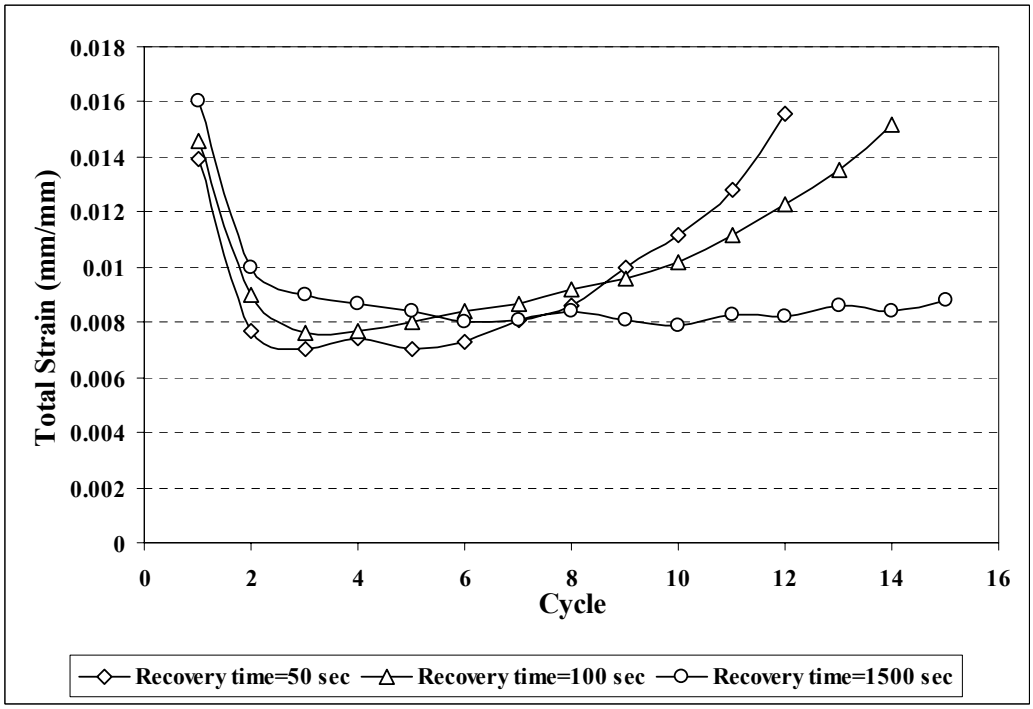

Figure 6.17 The total strain occurred in each cycle of the repeated creep recovery tests on the HRA.

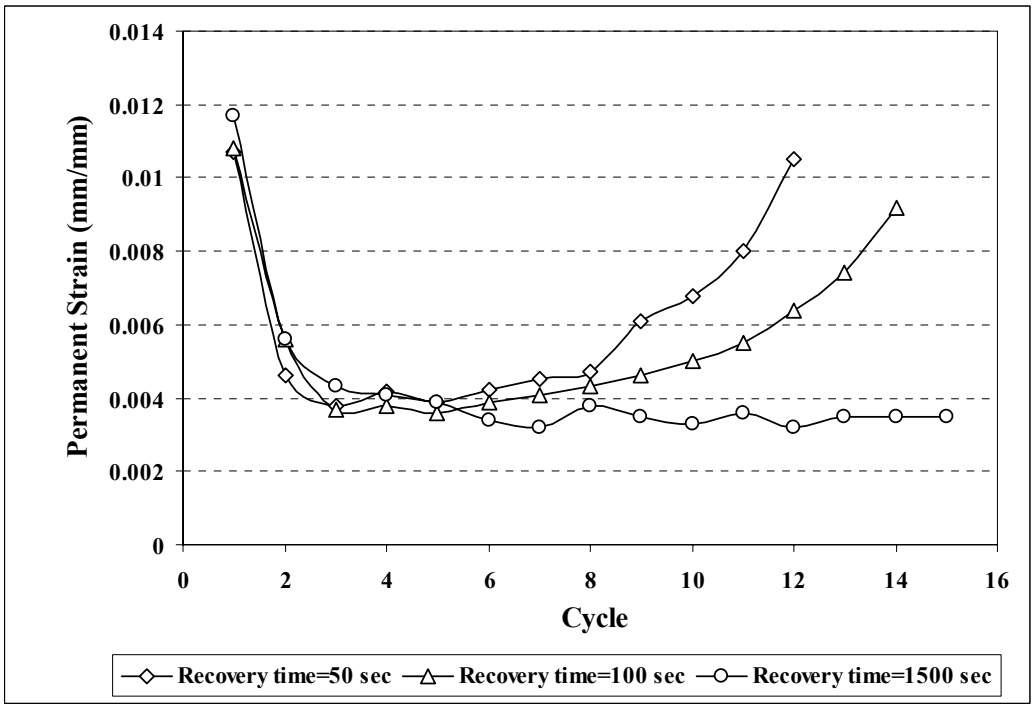

Figure 6.18 The permanent strain associated with each cycle of the repeated creep recovery tests on the HRA.

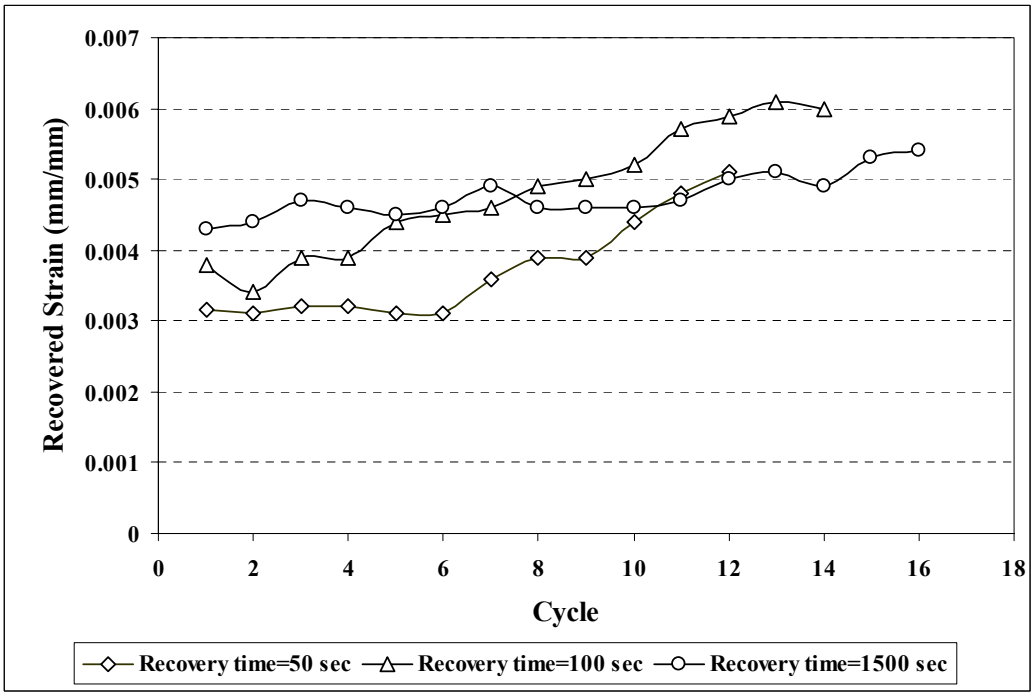

Figure 6.19 The recovered strain associated with each cycle of the repeated creep recovery tests on the HRA.

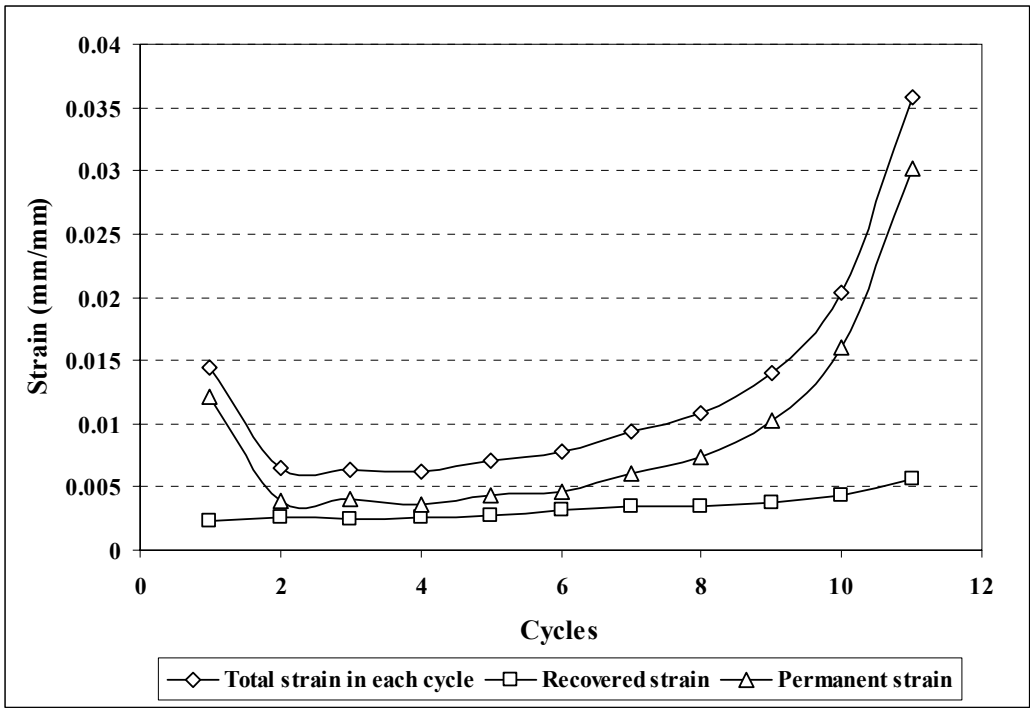

Figure 6.20 The total, recovered and permanent strain associated with each cycle of the repeated creep recovery tests on the DBM (ΔR=50sec).

Figure 6.21 shows the total strain plotted against the accumulated loading time for the HRA mixture for different values of ΔR and ΔL in the repeated creep recovery tests. The result of uniaxial creep test at the same stress level and temperature (1000 kPa, 20°C) is also included in this figure. The data points shown in the figure are the axial strain values prior to unloading and the accumulated loading time from the beginning of the tests (see Figure 6.13). As can be seen in the figure, for each test, the data points have created a curve similar to the continuous creep curve with the primary, secondary and tertiary creep regions. It can be seen from the figure that, within experimental error, independent of loading and recovery time, the slope of the secondary region (the steady-state strain rate) for all the tests is similar. It can also be seen that, while the specimen with the recovery time ΔR =1500 sec. is in the secondary creep region, the specimen with the recovery time ΔR = 50 sec. is in the tertiary creep region and the specimen with no recovery time (uniaxial creep test) has completely failed. In a similar way, Figure 6.22 shows the permanent strain plotted against the accumulated loading time for the HRA mixture at different

test conditions where the data points are the strains after recovery at each cycle. Similar observations, as explained for Figure 6.21, can also be seen in this figure.

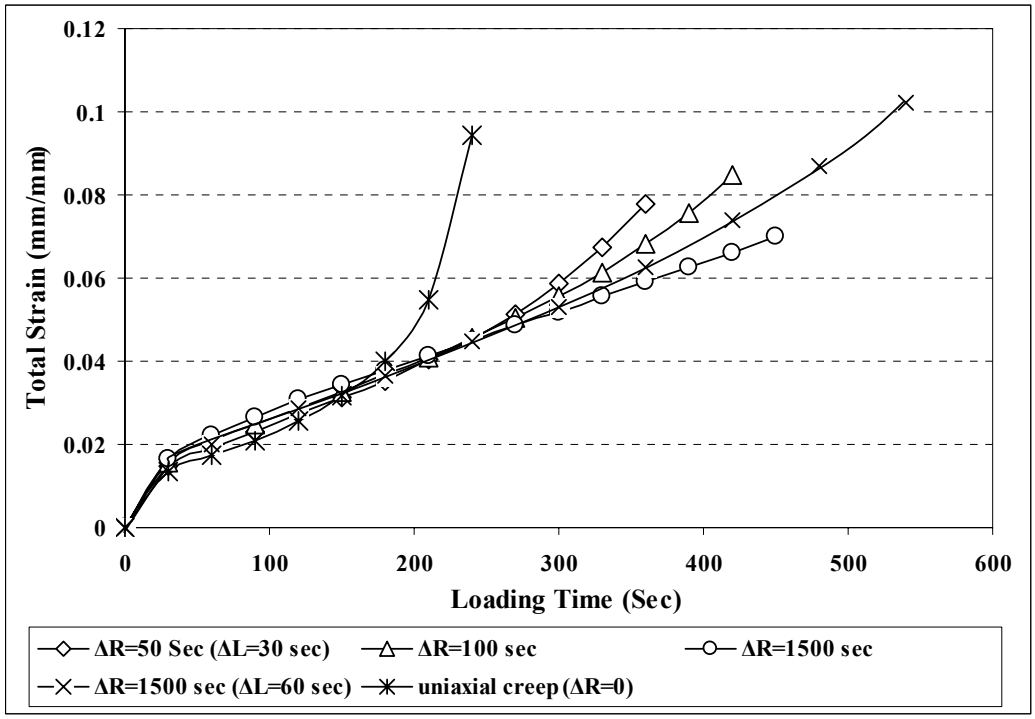

Figure 6.21 Total strain against the accumulated loading time for the HRA.

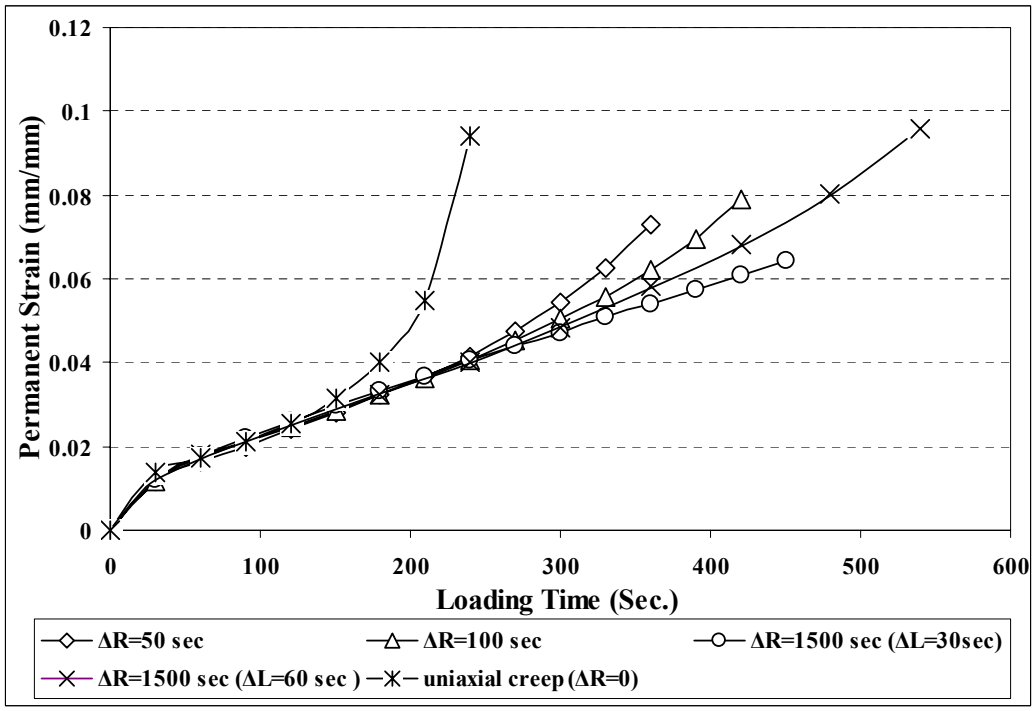

Figure 6.22 Permanent strain against the accumulated loading time for the HRA.

6.7 Conclusions

The following conclusions can be drawn from the single and repeated creep recovery tests:

- Within the range of test conditions utilised for the single creep recovery tests, the recovered strain of the HRA and DBM mixtures was found to be independent of the temperature and applied axial stress level and dependent on the type of mixture and the total strain before unloading.

- The recovered strain increases linearly with increasing the total strain before unloading, with a slightly higher slope for the HRA compared to the DBM. The linear variation continues up to a level (approximately 0.03 for the DBM and 0.06 for the HRA) after which the recovered strain remains constant.

- During recovery, the volumetric strain of the mixtures decreases linearly with the shear strain with the same slope as during creep, known as dilation ratio.

- The rate of recovery of the mixtures decreases with increasing the total strain before unloading and decreasing temperature and is independent of applied axial stress level.

- At the same test conditions, the rate of recovery for the HRA mixture was found to be greater than that for the DBM mixture.

- In the repeated creep recovery tests, the permanent strain associated with each cycle increases with decreasing recovery time ΔR and increasing the loading time ΔL.

- In the repeated creep recovery tests, with the same accumulated loading time, the specimen with longer recovery time heals more and, consequently, is stiffer than the specimen with shorter recovery time.

- More healing due to the higher recovery time reduces the elastic, delayed elastic and viscous strains.

- In the repeated creep recovery tests, taking the strains prior to unloading and after recovery at the end of the rest time for each cycle, and plotting each against the accumulated loading time makes a curve similar to the creep curve with the primary, secondary and tertiary creep regions. The slope of the steady-state region of the created curves is independent of the loading time ΔL and the recovery time ΔR. For these curves the tertiary creep region starts at a strain level which increases with increasing recovery time.

Triaxial Tests

7.1 Introduction

In a real pavement, asphaltic mixtures are under three dimensional states of stress. The state of triaxial stresses in the asphaltic mixtures within the upper layers has a significant effect on the deformation behaviour of the pavement. In the majority of research carried out on the deformation behaviour of asphaltic mixtures, uniaxial tests, usually in compression, have been performed. Nevertheless, triaxial testing has long been used for understanding the general behaviour of asphaltic mixtures, as discussed in Chapter 2.

The triaxial test is one of the important test procedures adopted for studying soils and asphaltic mixtures. The test is called triaxial because it is assumed that the three principal stresses are known and controlled. In soil mechanics, the triaxial compression test is performed under controlled drainage conditions to measure the shear strength of a soil. A specimen encased in a rubber membrane is placed in a triaxial cell and subjected to a confining pressure followed by an axial load until failure. The Mohr diagram is commonly used for interpreting the results and determination of soils shear strength. Asphaltic mixtures, which are composed of aggregate, bitumen and air voids, to some extent, are analogous to soils which are composed of soil particles, water and air voids. Hence, the triaxial test can

also be used for studying asphaltic mixtures. Early uses of triaxial tests for asphaltic mixtures were similar to that for soil mechanics in which the behaviour of the materials was interpreted by a Mohr envelope (see Murali [2004]).

The steady-state deformation behaviour of idealised asphaltic mixtures under triaxial conditions was investigated by Deshpande *et al.* [1999], Collop *et al.* [2001] and Ossa [2004]. They found that the steady-state deformation behaviour of the idealised mixtures with more than 64% volume fraction of aggregate strongly depends on the deviatoric and hydrostatic stresses. For a constant stress ratio, defined as the mean stress divided by deviatoric stress, the steady-state axial creep behaviour of the mixtures was found to have the same form as that of the pure bitumen. The aggregate was found to have a stiffening effect which increased with increasing the volume fraction of aggregate.

In this chapter, the static triaxial creep tests performed on the HRA30/10 and 10 mm DBM mixtures are described. With the aim of understanding the steady-state deformation and volumetric behaviour of the mixtures under triaxial stress states, the mixtures were tested over a range of deviatoric stresses and stress ratios at 35°C. First the experimental work for development of the test is explained followed by the discussion of the test results. The experimental data are also used for determination of the non-linear viscoelastic constitutive model which is described in Chapter 8.

7.2 Experimental Work

7.2.1 Test Equipment

Figure 7.1 shows a photograph of the triaxial testing set-up. It consists of three main parts, a servo-control hydraulic machine for applying the axial load (as explained in Chapter 5 for the uniaxial tests) a cell which is placed in the temperature-controlled cabinet fitted on the hydraulic machine, and the equipment for applying and measuring the confining pressure. The servo control machine consists of an INSTRON loading frame, a 100 kN servo-hydraulic

actuator, moving in the upward direction, an axially mounted load cell and a temperature-controlled cabinet with a -5˚C to 50˚C operating range, supplied and installed by Cooper Research Technology Ltd.

Figure 7.2 shows a picture of the cell used in this research with a maximum confining pressure capacity of 1700 kPa, supplied by Wykeham Farrance Ltd. This cell is a standard type, which is commonly used in soil mechanics. The cell had been designed for testing the specimens with 100 mm diameter and 200 mm height. Some extra parts were designed to make it suitable for the specimen of this study with 100 mm in height and diameter. As can also be seen in Figure 7.2, the cell consists of an aluminium base, cell chamber, submersible piston, valves and some fittings for connecting to the pressure gauge, air pressure supply and the LVDT for measuring radial strain.

The axial load was applied to the specimen through the submersible piston connecting the cell to the upper ram of the hydraulic machine. The load cell, mounted axially on the hydraulic machine, monitored the load and provided the feedback signal for the hydraulic actuator which moved upwards until the target load was achieved.

The axial deformation of the specimen was measured from the load line displacement of the actuator which is measured by an LVDT mounted on the actuator. The radial deformation of the samples at mid-height was measured by a calibrated LVDT mounted on the collar (as used for uniaxial tests) loaded through a sealed hole out of membrane (see later for details). The cable for the radial LVDT passed through a hole in the bottom of the triaxial cell base and was sealed by glue.

Analogue outputs from the axial and radial LVDTs, and the load cell were fed into a personal computer through an analogue to digital converter. The Software logged the data which could be converted to ASCII files.

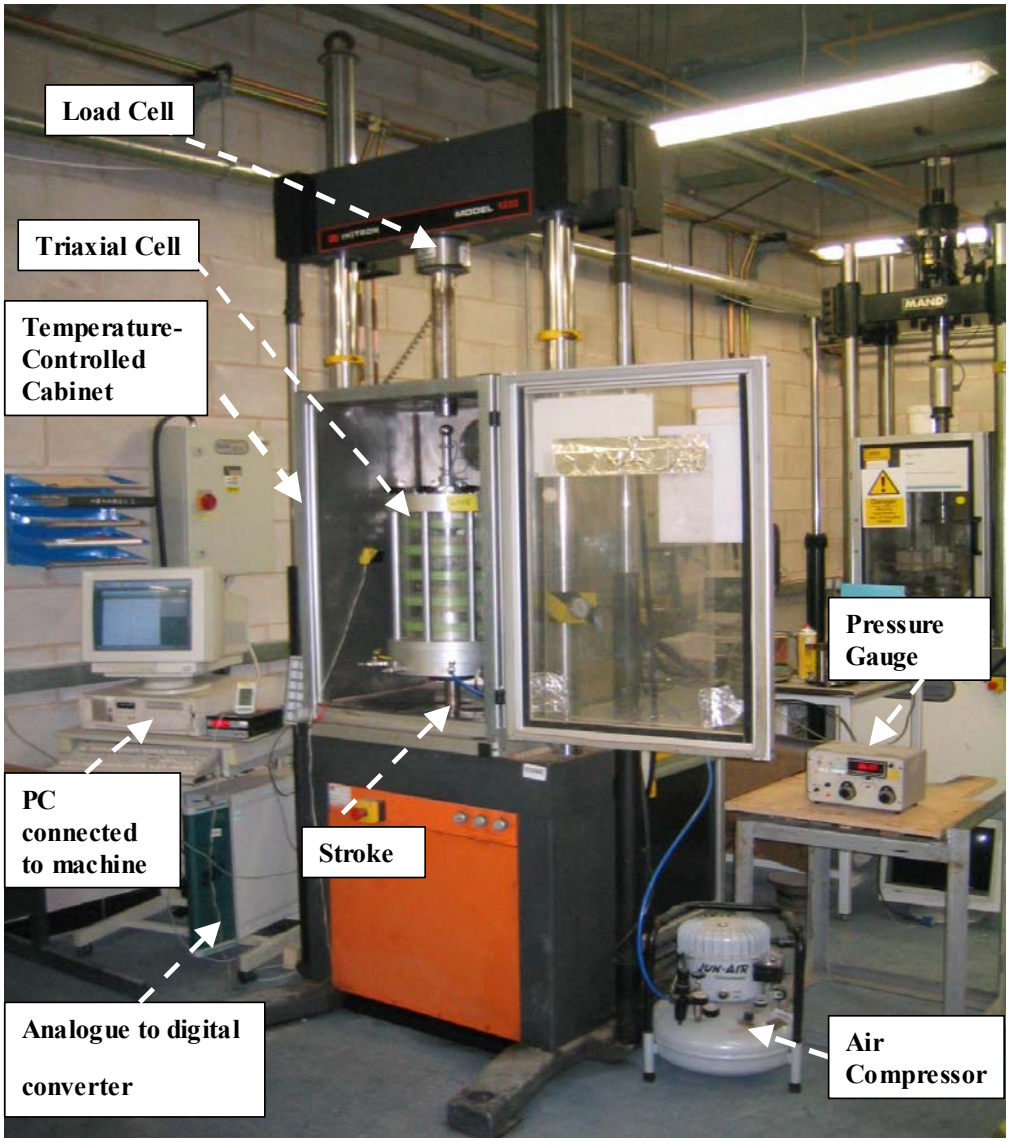

Figure 7.1 The triaxial test set-up.

Figure 7.2 The cell for the triaxial test.

7.2.2 Specimen Preparation

Cylindrical specimens (as used for uniaxial tests) were used for triaxial testing. To prepare a specimen for testing, it was first checked to ensure that it has a uniform height on all sides. This step was necessary to ensure that the specimen will not slide during the test. Next, two pips were glued at the mid-height of the specimen, diametrically opposite each other for holding the collar on which the LVDT for measuring the radial deformation is mounted. An impervious latex membrane, 100 mm in diameter and 330 mm in height, was used to seal the specimens from the pressurised air inside the cell. Without stretching the membrane, its centre at mid-height was marked diametrically opposite each other. A soldering iron with a fine tip was used to puncture the membrane in order to make holes for the screws passing through them that screwed into the threaded holes of the pips (see Figure 7.3). To seal the holes in the membrane, plastic washers were used between the membrane and the screw such that the membrane was sandwiched between the washers and the screw. A small hole

was made on the top of the screws for holding the studs of the collar. Visual inspection of the membrane during testing proved to be effective for sealing the specimen

7.2.3 Testing Procedure

The prepared specimen was placed between two polished chrome platens with a diameter of 110 mm. A friction reduction system, as used for the uniaxial tests, comprised of an interlayer plastic film lubricated with a soft soap, was placed at each of the specimen platen interfaces. The collar with the radial LVDT was fitted to the specimen by putting its studs in the holes made on top of the screws at each side (Figure 7.3). A rubber band with appropriate stiffness was used to hold the collar in position so that it was firmly located on the specimen. The stiffness of the rubber band was checked to ensure that it imparted enough stress to the collar to hold it in position without causing depression in the specimen at the points of contact between the specimen and pips. Visual inspection of the specimens after testing did not show any depression in the contact point.

The membrane surrounding the specimen was fastened to the top and bottom platens by rubber O-rings (Figure 7.4). The top and bottom platens were checked to prevent eccentric loading of the specimen. After locating the specimen on the cell base, the chamber was placed onto the base and the screws were fastened tightly to avoid any air leaking out of the cell. The whole cell was then raised by a lifting machine and placed in the temperature-controlled cabinet set at the testing temperature. Figure 7.5 schematically shows the test set-up in the temperature-controlled cabinet. The set-up was left at least for 12 hours in the cabinet to ensure uniform temperature in the specimen.

The target confining pressure was applied by the air compressor through adjusting the pressure by a regulator on the compressor and reading the pressure on the pressure gauge. The target pressure once achieved was maintained manually by adjusting the regulator on the compressor if necessary.

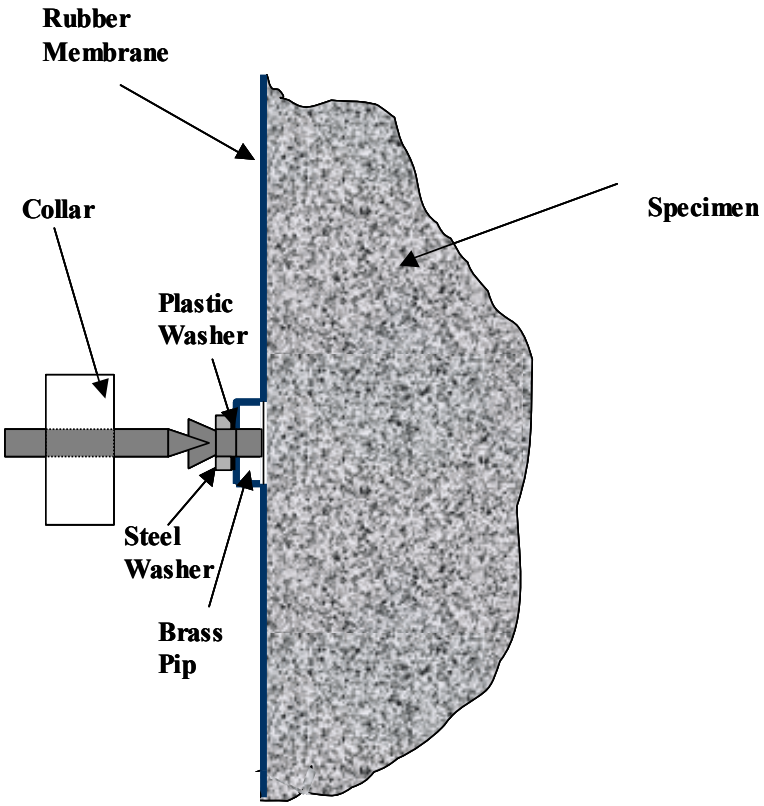

Figure 7.3 Schematic detailed showing of the arrangement for radial strain measurements.

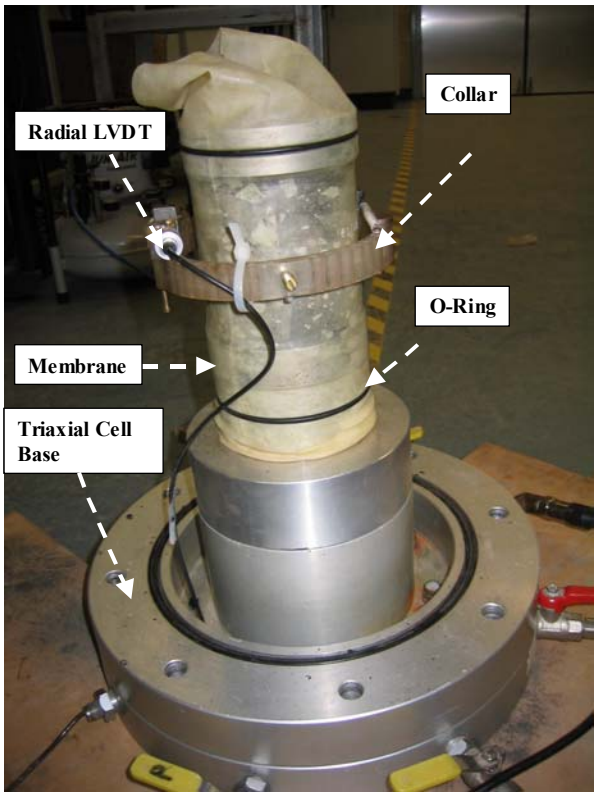

Figure 7.4 The specimen instrumentation for the triaxial test.

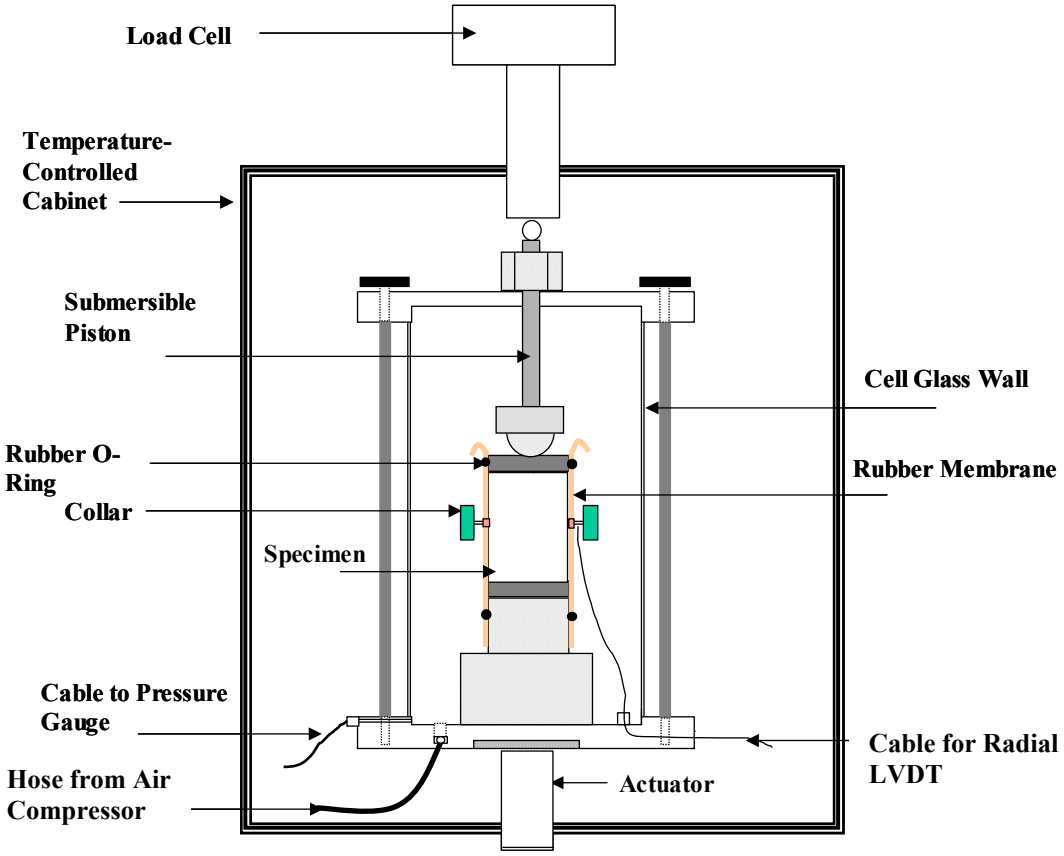

Figure 7.5 Schematic of the triaxial cell.

After the target confining pressure value was achieved, a preloading stress equal to 0.2 kN was applied for 60 seconds. The preloading stress was for seating the platens on the specimen and was immediately followed by the target axial stress. Due to the difference between the cross-sectional area of the submersible piston at top and bottom, a value of load equal to the test confining pressure times the difference in cross sectional area was added to the applied target load. After applying the target axial load, while maintaining a constant confining pressure, the axial and radial deformations were measured by the LVDTs and the axial load was measured by the load cell. All data were logged by the computer connected to the equipment for the duration of the test.

Figure 7.6 shows the principal stresses acting on the specimen in the triaxial test. As can be seen, because of axial symmetry of the arrangement, two of the princpal stresses are the same and equal to the confining stress. The third principal stress is equal to the sum of the confining stress and the deviator stress,

which is applied by the hydraulic machine. Hence, the principal stresses can be given by:

$$\sigma_{33} = \frac{Q}{A} + p$$

and **(7.1)**

$$\sigma_{22} = \sigma_{11} = p$$

where Q = applied axial load

A = cross-sectional area of the specimen

p = confining stress

The mean stress σ_m and the deviator stress σ acting on the specimen are given by:

$$\sigma_m = \frac{\sigma_{33} + \sigma_{11} + \sigma_{22}}{3} = p + \frac{Q}{3A}, \quad \textbf{(7.2)}$$

$$\sigma = \sigma_{33} - \sigma_{11} = \frac{Q}{A}, \quad \textbf{(7.3)}$$

The triaxial tests were performed at 35˚C to avoid the problems associated with handling the specimens at higher temperatures, as the softening point of the binder was 46˚C. Another reason for choosing this temperature was to get meaningful difference in the response at different confining stresses. Earlier trial tests at lower temperatures showed that the difference in response at different confining pressures was not significant.

The triaxial tests were performed over a range of confining and deviator stresses, as summarised in Table 7.1. The stress conditions were characterised by the stress ratio, $\eta = \sigma_m / \sigma$, defined by Deshpande [1997]. For each stress ratio, the tests were performed at 3 deviator stress levels within the range over which the mixtures showed non-linear behaviour in uniaxial creep tests (see Section 5.3.2). While the HRA mix was tested to a maximum stress ratio of η=0.7, the DBM

mixture could only be tested to a maximum stress ratio of 0.56 (see discussion at the end of this chapter). It was expected that the temperature dependency of the mixtures under triaxial stress would be dominated by the bitumen and is the same as that of uniaxial tests, as explained in Section 5.3.2. The temperature sensitivity of bitumen is a result of the activation energy of the bitumen molecules or the free volume in the bitumen molecular structure and, hence, is not expected to be dependent on the stress state [Deshpande *et al.*, 1999].

Table 7.1 Triaxial test conditions.

Deviator Stress (kPa)						
Mixture / **Stress Ratio**	**HRA30/10**			**10 mm DBM**		
0.33	300	500	700	500	750	1000
0.46				500	750	1000
0.56	300	500	700	500	750	1000
0.7	300	500	700			

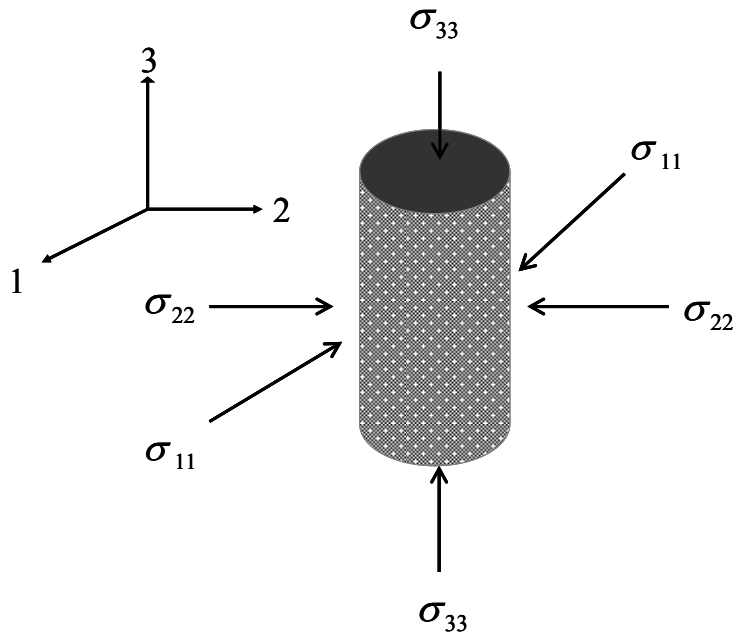

Figure 7.6 Schematic showing the triaxial tests co-ordinate system.

7.3 Test Results

Figures 7.7 and 7.8 show typical results from the triaxial tests for the HRA and DBM mixtures, respectively, where the axial strain is plotted against the time elapsed since the target axial and confining stress application. Each figure shows the creep curves at the same deviator stress and increasing series of confinement. It can be seen from this figures that the curves for different confining pressures are similar in shape with three distinct creep regions, as explained in Chapter 5. The primary creep region is characterised by a decreasing strain rate, the secondary creep region comprises an almost constant strain rate, and in the tertiary creep region the strain rate is increasing rapidly. The figures also show that the stiffness of the mixtures increases with increasing the confinement.

The triaxial tests at different stress ratios showed that confinement affected the damage accumulation in the mixtures. Figure 7.9 shows a photograph of two DBM specimens, one tested with no confinement (uniaxial) and the other at a stress ratio of 0.56, both under the same deviator stress. As can be seen, while both specimens have the same axial strain, the specimen tested with no confinement has more cracks than the specimen tested with confinement. It can be seen in Figures 7.7 and 7.8 that, at the same axial strain in the tertiary region, the related strain rate is lower for a higher stress ratio. In the next chapter, the effect of stress ratio on damage will be studied by the damage related parameters of the non-linear viscoelastic model.

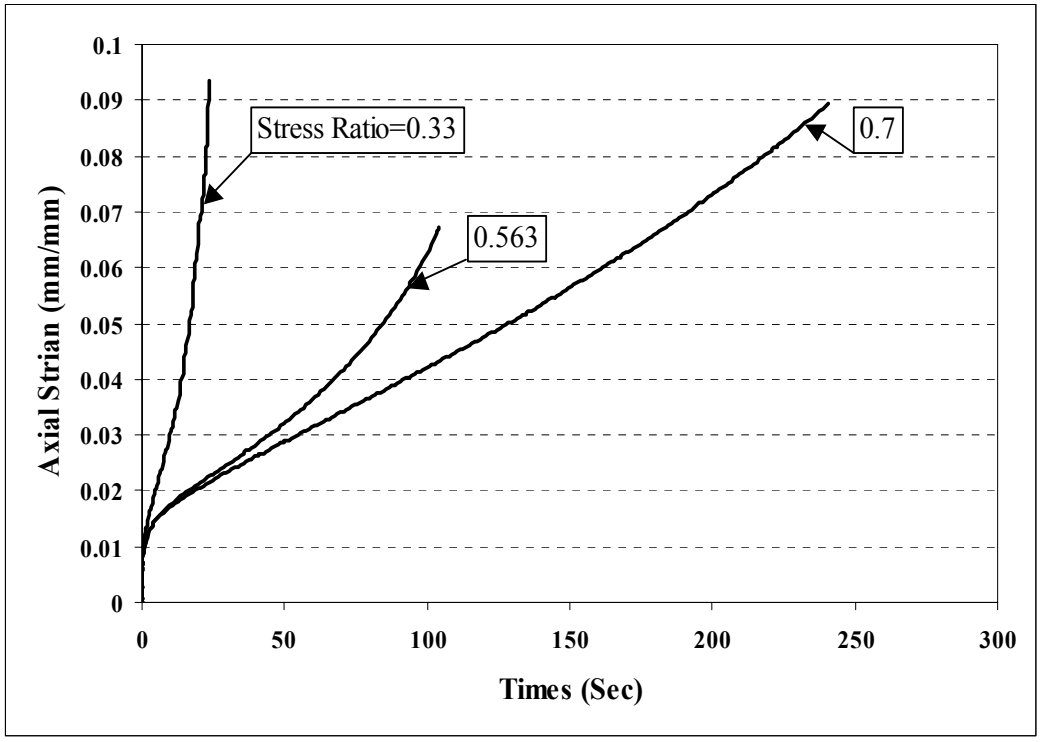

Figure 7.7 Triaxial creep response of the HRA30/10 at 35°C (different stress ratios and a constant deviatoric stress of 700 kPa).

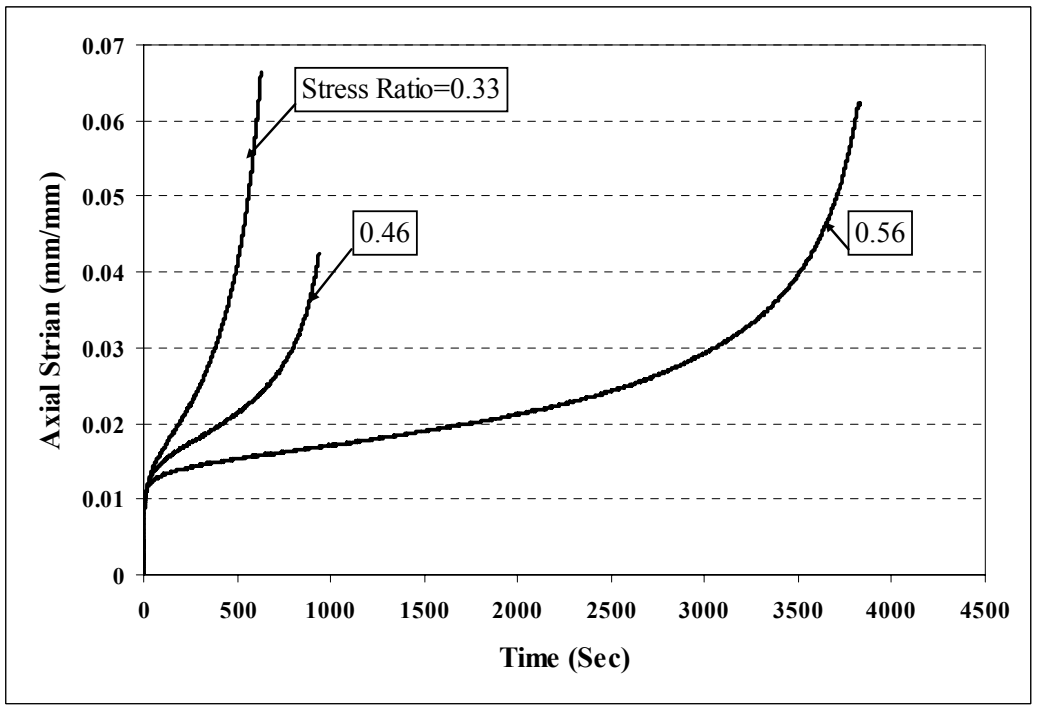

Figure 7.8 Triaxial creep response of the 10 mm DBM at 35°C (different stress ratios and a constant deviatoric stress of 750 kPa).

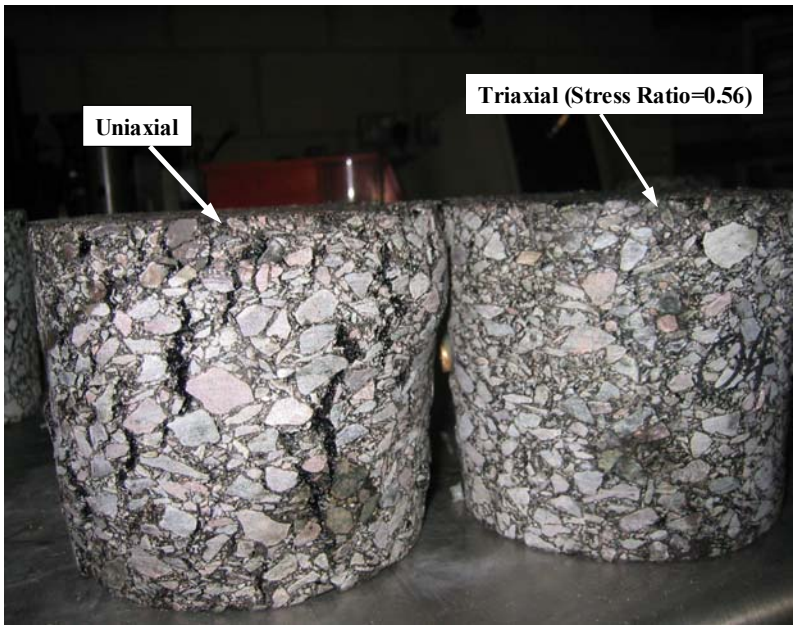

Figure 7.9 The specimen failure in uniaxial and triaxial tests.

Similar to the uniaxial creep tests, the slope of the secondary creep region was defined as the steady-state strain rate. Figures 7.10 and 7.11 summarise the triaxial steady-state behaviour of the HRA and DBM mixtures, respectively, over a range of deviator stresses σ and stress ratios η, where the steady-state strain rate $\dot{\varepsilon}$ is plotted against the stress σ on a double logarithmic scales. For both mixtures, it can be seen that, for a constant stress ratio η, the curves have the same shape as the curve for uniaxial behaviour (η=1/3). The same behaviour was observed for the idealised asphalt mixtures studied by Deshpande *et al.* [1999] and Ossa [2004]. Therefore, as for the uniaxial behaviour (Section 5.3.2), the modified Cross model [Cheung, 1995] (Equation 7.4) with the stiffening factor S [1] as a function of the applied stress ratio was fitted to the experimental data in Figures 7.10 and 7.11. The solid lines shown in the figures are the predictions of the model.

[1] S is defined as the ratio of the steady-state deformation rate of the mixtures at a specified stress ratio to the steady-state deformation rate at the stress ratio of 0.33 (uniaxial).

$$\frac{\sigma}{\sigma_0} = \frac{S\dot{\varepsilon}}{\dot{\varepsilon}_0}\left[\frac{1}{1+\left(\frac{S\dot{\varepsilon}}{\dot{\varepsilon}_0}\right)^m}\right], \qquad \textbf{(7.4)}$$

where $\dot{\varepsilon}_0$, σ_0 and m = the material constants, as given in Table 7.2 for the two mixtures

σ = the steady-state deviator stress

$\dot{\varepsilon}$ = the steady-state strain rate

S = the stiffening factor, which describes the stiffening effect of confinement.

It can be seen that the mixtures exhibit non-linear power law creep behaviour at high stress levels with the power exponent of 4.5=1/(1-0.779) for the DBM and 2.93 =1/(1-0.659) for the HRA. This is consistent with the uniaxial creep results where it was observed that the power exponent of the DBM is more than that of the HRA. The small difference between the power exponent of the DBM from triaxial and uniaxial test results is attributed to experimental error.

From Figures 7.10 and 7.11 it can be seen that S increases with increasing the stress ratio η. Figure 7.12 summarises the effect of the stress ratio on the steady-state strain rate for mixtures. The figure shows that the stiffening effect of the stress ratio is higher for the DBM than that for the HRA mixture. This is because the confinement has more effect on the movement of the aggregates with more interlock, which is the case for the DBM.

Measurement of radial strain in the triaxial tests showed that variation of the radial strain with time was qualitatively similar to that of the axial strain. Figure 7.13 shows typical variations of the radial strain with axial strain for the HRA mixture at selected test conditions. As can be seen, similar to what was observed

in the uniaxial creep tests (see Section 5.3.3), in the steady-state behaviour of the mixtures, the radial strain varies linearly with the axial strain with a slope which was observed to be independent of the applied deviatoric stress and stress ratio. Similar results were obtained for the DBM.

Figure 7.14 shows the typical variation of the volumetric strain (Equation 2.13) with the shear strain (Equation 2.14) for the HRA mixture. The curves in the figure are for different deviator stresses and stress ratios as shown in the figure. For all of the triaxial tests conducted on the HRA and the DBM mixtures, it was observed that, after an initial reduction, the volumetric strain increases linearly with the shear strain. The slope of the line is the dilation ratio (Equation 5.5), which was found to be independent of the applied deviator stress and stress ratio. For the DBM mixture, the dilation ratio varies between 1.3 and 1.5, and for the HRA, mixture it varies between 1.1 and 1.3. This variation is likely because of experimental errors such as non-uniform deformation of the specimen (bulging) and the accuracy of the instrument for measuring the radial strain.

Table 7.2 The modified Cross model parameters

Parameter	**HRA**	**DBM**
σ_0 **(MPa)**	0.041	0.051
$\dot{\varepsilon}_0$ **(1/s)**	2.669×10^{-7}	5.67×10^{-11}
m	0.659	0.779

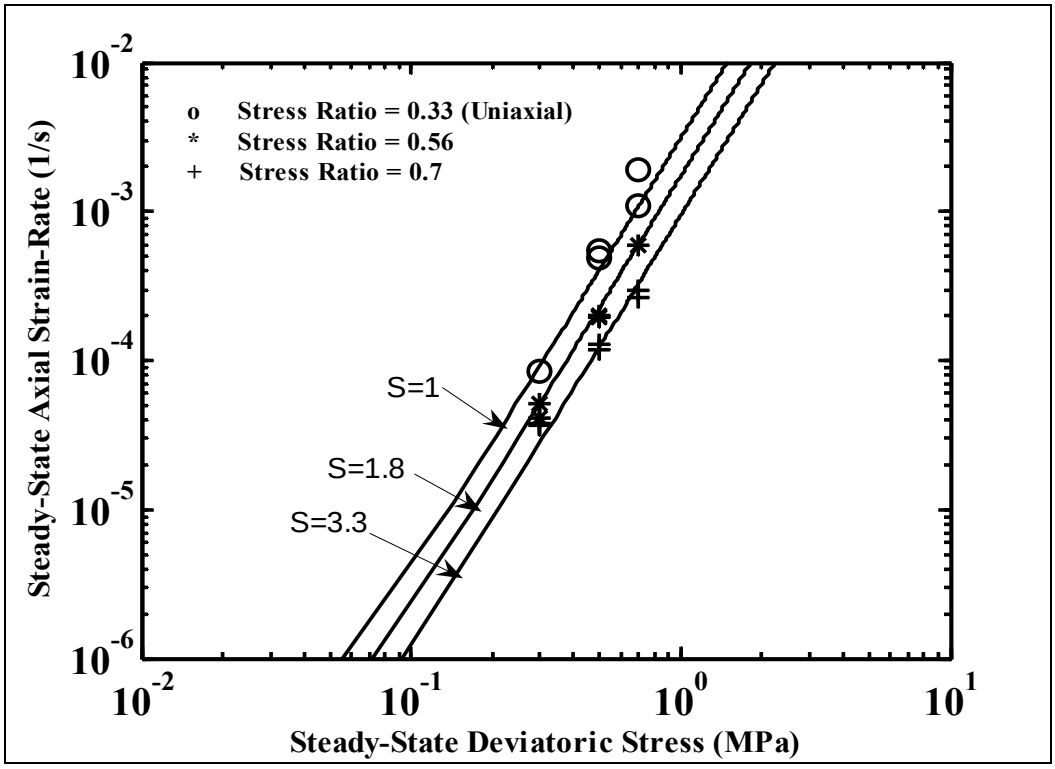

Figure 7.10 The monotonic steady-state behaviour of the HRA at different stress ratios.

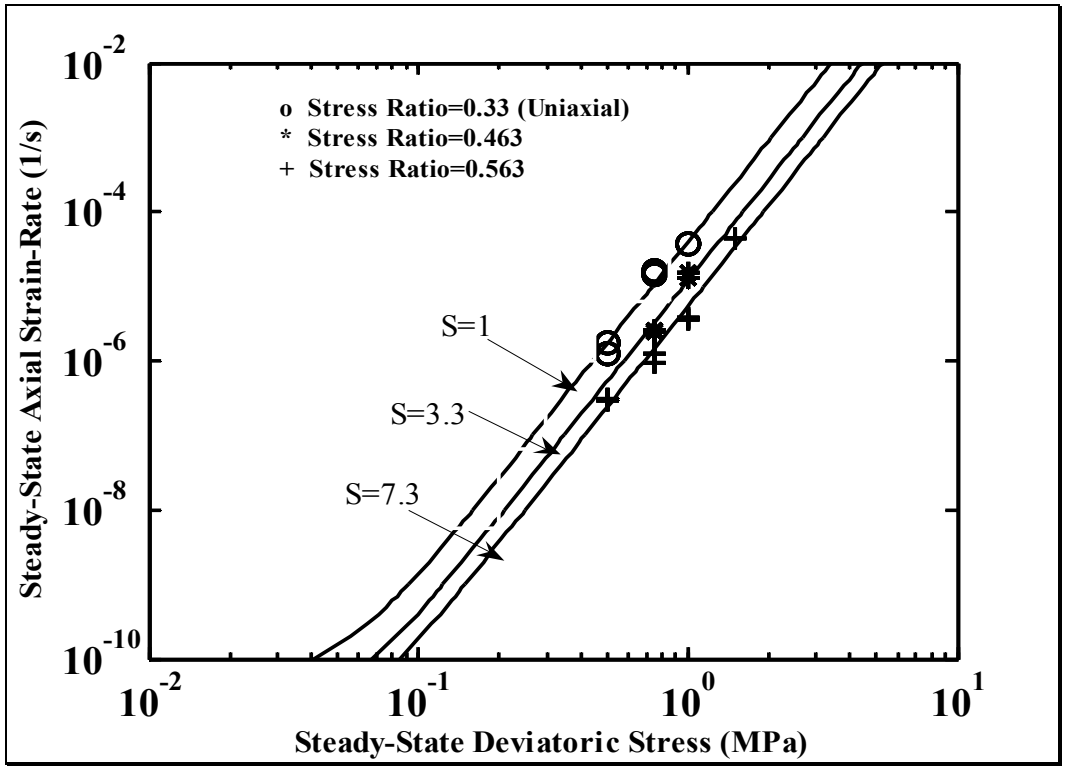

Figure 7.11 The monotonic steady-state behaviour of the DBM at different stress ratios.

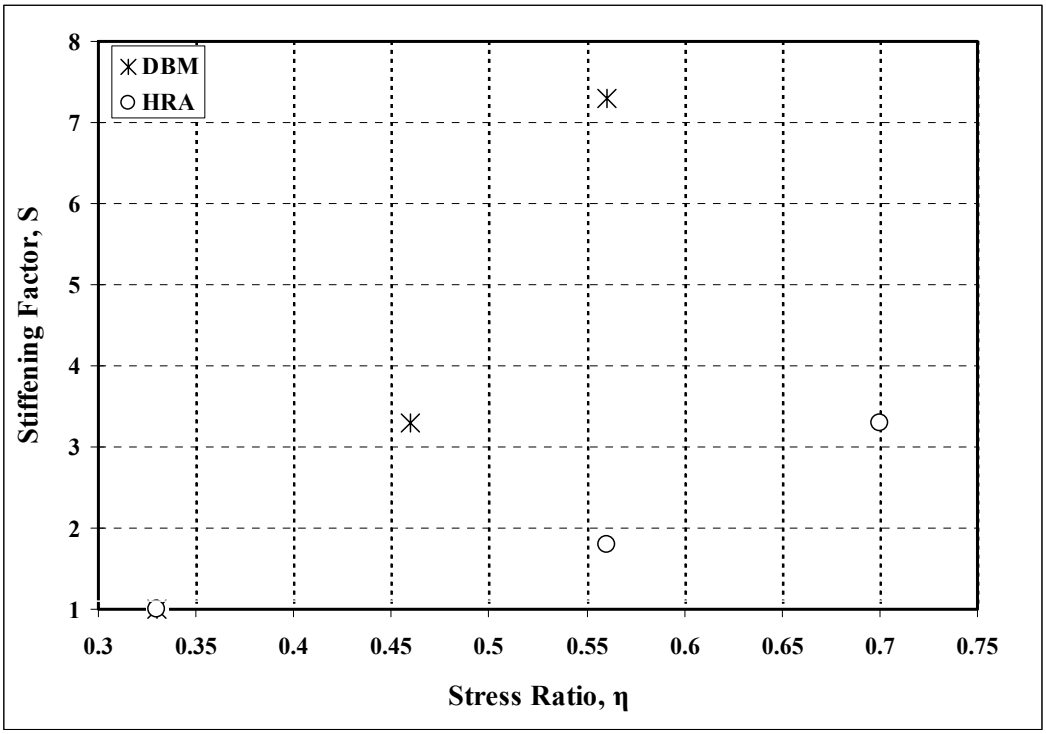

Figure 7.12 Stiffening factor of the mixtures.

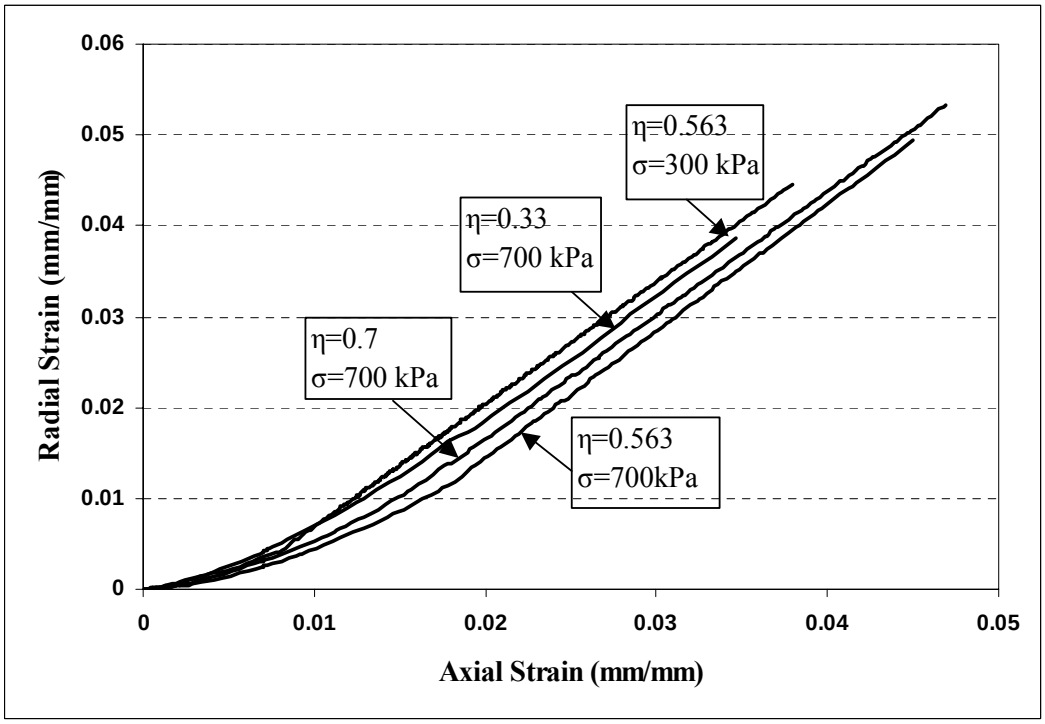

Figure 7.13 Variation of the radial strain with axial strain for the HRA30/10 at different deviator stress levels and stress ratios.

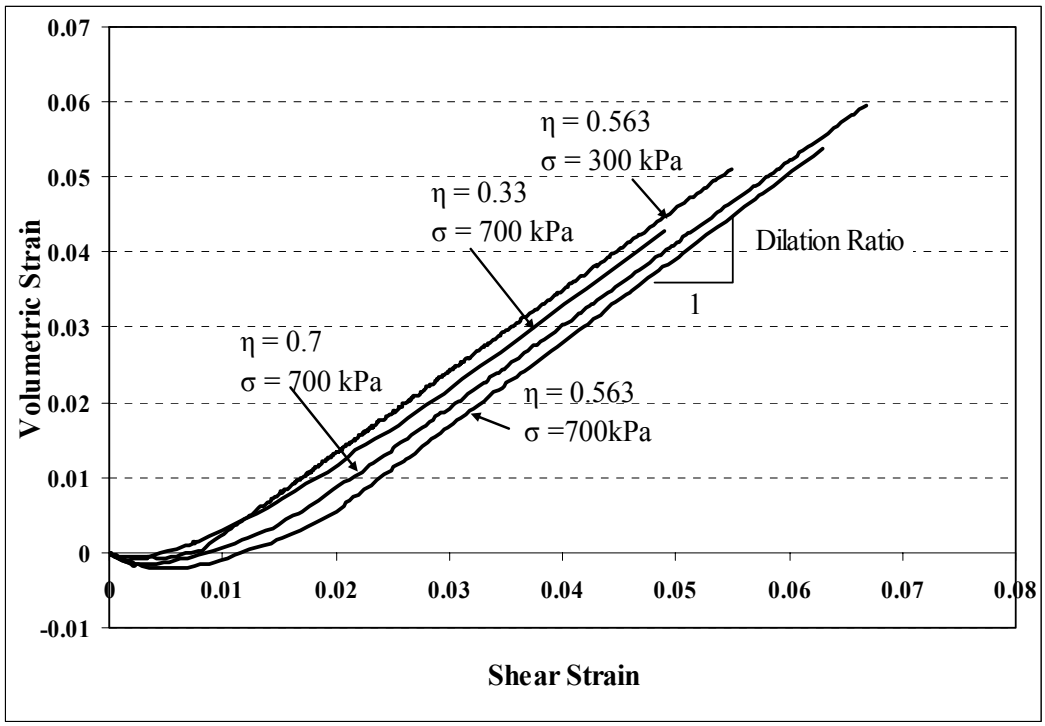

Figure 7.14 The volumetric strain against the shear strain for the HRA30/10.

7.4 Discussion

The shear strength of a dry sand was explained by Taylor [1948] to be due to the frictional resistance between the particles as they slip during shear distortion, and interlocking which requires work to be done to cause volume increase during shear distortion. In a similar way, Deshpande [1997] proposed that the shear strength of an asphaltic mixture is provided by the viscosity of the bitumen (assuming that no frictional contact exists between the particles), and aggregate interlock. As an example, consider a shear box test [Taylor, 1948], schematically shown in Figure 7.15, where the gaps between the particles are filled with bitumen. As the relative displacement of the two halves of the shear box is increased by dx, the particles need to ride up on each other and, therefore, the thickness is increased in y direction by an amount dy. The quantity dy/dx is an indication of the particles dilation which represents the internal kinematic constraints imposed by the particles. The dilation is a measure of the particles interlocking. If the normal stress σ is increased whilst keeping the shear stress τ constant, a point will be reached where the work done by the compressive stress σ cannot be provided by the positive work done by the shear stress τ. After this

critical stress ratio σ/τ, no further deformation is possible and "lock up" occurs due to the particles interlocking. Deshpande *et al.* [1999] found that the lock up phenomenon is controlled by the dilation ratio D. They developed the following model (Equation 7.5) for the shear strain rate $\dot{\varepsilon}_S$ of an idealised asphaltic mixture as a function of aggregate and bitumen properties and their proportions.

$$\dot{\varepsilon}_S = \frac{\left[\eta D sign(\sigma)+1\right]^n \dot{\varepsilon}_0}{(\frac{1}{2}kD^2+\frac{3}{2}\mu)^{\frac{n+1}{2}}\left[1-(c+V_\upsilon)\right]^{\frac{n-1}{2}}}\left(\frac{|\sigma|}{\sigma_0}\right)^n \times sign(\sigma) \quad , \qquad \textbf{(7.5)}$$

where $\dot{\varepsilon}_0, \sigma_0$ and n = the constants related to the steady-state deformation behaviour of the bitumen, as explained before

c = the volume fraction of aggregates,

Vν = air void content

k and μ = bulk and shear modulus of the mixtures (see Deshpande [1997] for details)

σ = deviator stress,

D = the dilation ratio and

η = the stress ratio.

As can be seen in the equation, when the stress ratio increases, the term $\left[\eta D sign(\sigma)+1\right]^n$ decreases, because of the negative sign of the deviatoric stress σ. When the stress ratio reaches a critical value given by η=*-1/D*, the term $\left[\eta D sign(\sigma)+1\right]^n$ =0 and lock up occurs. The equation also shows that, for a mixture with the same volume fraction of aggregate and air voids, subjected to the same stress ratio, the stiffening factor which is inversely related to the shear strain increases by increasing the dilation ratio *D*. The DBM mixture with a higher dilation ratio was found to have higher stiffening factor than the HRA mixture. Thus, the dilation ratio is a critical factor which controls the deformation behaviour of asphaltic mixtures and should be taken into consideration when designing aggregates for asphaltic mixtures. For improving

mixture design, further research work needs to be undertaken to understand the relationship between the dilation ratio and aggregate properties like particle size and shape, gradation and volume fraction of aggregate.

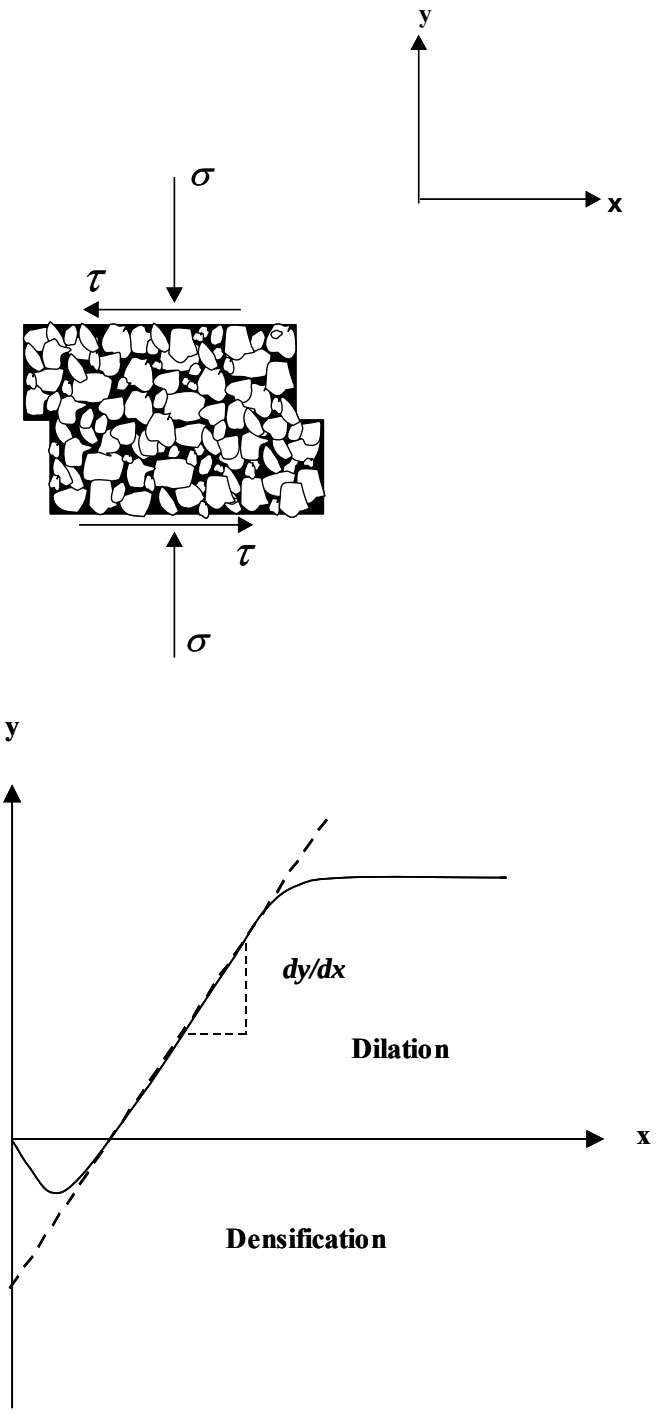

Figure 7.15 Direct shear box.

The dilation ratio of the DBM and the HRA mixtures was found to be about 1.4 and 1.25 at the triaxial test temperature. Therefore, as explained in the previous paragraph, the critical stress ratio for the DBM and the HRA is predicted to be 0.71 and 0.8, respectively. At a stress ratio higher than the critical stress ratio, because of lock up, the specimen undergoes localised deformation and fails in a weak plane which cannot be controlled. In this study, some triaxial tests were performed on the HRA mixture at stress ratios of 0.8 and 1 and on the DBM mixture at a stress ratio of 0.8, which did not give meaningful results. It was observed that, at the same test conditions, one specimen failed very soon after starting the test while the other took a long time without a significant deformation. Considering the variation of dilation ratio for the mixtures, the HRA mixture was tested at the stress ratios of 0.33 (uniaxial), 0.563 and 0.7, and the DBM was tested at the stress ratios of 0.33, 0.463, and 0.563.

7.5 Conclusions

The following conclusions can be drawn from this chapter:

- Under triaxial stress states variation of the axial and the radial strain with time was observed to be similar to those under uniaxial stress states.

- The triaxial steady-state deformation behaviour of the HRA and the DBM mixtures was found to be similar to the uniaxial steady-state deformation behaviour with non-linear power law creep viscous behaviour over the range of utilized stress levels, and was well captured by the modified Cross model.

- At the same temperature and deviatoric stress, the steady-state strain rate of a mixture was found to decrease with increasing stress ratio.

- The stiffening effect of the confining stress was found to be greater for the DBM mixture than for the HRA.

- Both the HRA and DBM mixtures were observed to dilate under triaxial stress with the volumetric strain varied linearly with the shear strain. The slope, defined as the dilation ratio, was found to be independent of the stress ratio.

- In the triaxial tests performed at the stress ratios higher than the critical stress ratio (0.8 for the HRA and 0.71 for the DBM), both mixtures were observed to lock up.

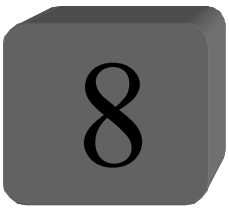

8 Determination of Model Parameters

8.1 Introduction

This chapter describes the non-linear viscoelastic constitutive model, developed by Collop *et al.* [2003], and presents determination of the model parameters necessary for characterisation of the creep and recovery behaviour of the 10 mm DBM and HRA30/10 mixtures. Results of uniaxial creep, creep recovery and triaxial tests are used to determine the model parameters. After determination of the parameters, the constitutive model is verified by fitting to the test results which have not been used in the process of parameters determination.

8.2 The Constitutive Model

As discussed in Chapter 3, in a joint research between the University of Nottingham and Delft University of technology, a non-linear viscoelastic constitutive model was developed by Collop *et al.* [2003] to model the quasi-static permanent deformation of asphalt mixtures. The following paragraphs provide a detailed explanation of the constitutive model.

The approach was based around the Burger's mechanical model (Figure 8.1) comprising elastic, delayed elastic and viscous elements, for which the strains and strain rates are additive and the stress is the same for the elements. The elastic and delayed elastic components are linear and the viscous component contains a stress-based non-linearity and is sensitive to confinement and temperature. To account for the accumulation of damage in viscous deformation, a Continuum Damage Mechanics (CDM) formulation was introduced in the formulation of the viscous component.

The creep and recovery behaviour of an asphaltic mixture, explained in Chapters 5 and 6, can be simulated by the mechanical model arrangement shown in Figure 8.1. This mechanical model, known as generalised Burger's model, is comprised of a number of Voigt elements in series with a viscous dashpot and an elastic spring. When a stress σ is applied to this combination, the spring in series deforms instantaneously in proportion to the applied stress and the inverse of the elastic modulus of the spring E_0 (Equation 8.1). However, neither the dashpot in series nor the dashpots in the Voigt elements can move in the same short period of time. When the stress is held constant, the Voigt elements deform in proportion to the applied stress σ, elastic modulus of the springs and the viscosity of the dashpots in the Voigt elements (Equation 8.2), and the dashpot in series deforms gradually proportional to the applied stress and the viscosity of the dashpot λ_{inf} (Equation 8.3).

Each Voigt element in the model can deform up to a certain level of strain. There is no limit to the deformation of the dashpot in series. The total strain of the arrangement (Equation 8.4) is the sum of the strains related to the spring in series (elastic strain $\varepsilon_{el}(t)$), the Voigt elements (delayed elastic strain $\varepsilon_{de}(t)$) and the dashpot in series (viscous strain $\varepsilon_v(t)$). For simulation of the deformation of the asphaltic mixtures using this model arrangement, the parameters of the model (i.e. the elastic modulus of the springs and viscosity of the dashpots) must be determined from the experiments on the mixtures. The methodology for determination of these parameters from experimental data is explained in this

chapter. For the model arrangement shown in Figure 8.1, the elastic, delayed elastic, viscous and total strain are calculated from the following equations.

$$\varepsilon_{el}(t) = \frac{\sigma}{E_0}, \tag{8.1}$$

$$\varepsilon_{de}(t) = \sigma \sum_{i=1}^{N} \frac{1}{E_i}\left(1 - \exp(-\frac{t}{\tau_i})\right), \tag{8.2}$$

$$\varepsilon_{v}(t) = \frac{\sigma}{\lambda_{\inf}} t, \tag{8.3}$$

$$\varepsilon(t) = \varepsilon_{el}(t) + \varepsilon_{de}(t) + \varepsilon_{v}(t) \ , \tag{8.4}$$

where τ_i = the relaxation time of the *i*'th Voigt element ($\tau_i = \lambda_i / E_i$).

λ_i and E_i = the viscosity of the dashpot and the elastic modulus of the spring, respectively, in the *i*'th Voigt element.

E_0 = the elastic modulus of the elastic element (the spring in series)

N = number of Voigt elements in the generalised Burger's model

$\lambda_{\inf}$ = the viscosity of the viscous element (the dashpot in series)

t = time.

For the model arrangement shown in Figure 8.1, when the applied stress σ is released at a time t_0 after its application, the spring in series regains its original length. Under the tension effect of the springs in the Voigt elements, the dashpots parallel with the springs return to their original length, and the dashpot in series remains permanently deformed. The strain level after releasing the stress at time t_0 is obtained from the following equation:

$$\varepsilon(t) = \varepsilon_{\sigma}^{t} + \varepsilon_{-\sigma}^{(t-t_0)}, \tag{8.5}$$

where, ε_{σ}^{t} is the strain at time t due to the stress σ applied at the $t=0$ given by:

$$\varepsilon_{\sigma}^{t} = \frac{\sigma}{E_0} + \frac{\sigma.t}{\lambda_{\inf}} + \sigma\sum_{i=1}^{N}\frac{1}{E_i}\left(1-\exp(-\frac{t}{\tau_i})\right). \qquad \textbf{(8.6)}$$

$\varepsilon_{-\sigma}^{(t-t_0)}$ is the strain at time t due to removing the stress σ at time t_0. Removing the stress is equal to application of a negative stress $-\sigma$, therefore:

$$\varepsilon_{-\sigma}^{(t-t_0)} = -\frac{\sigma}{E_0} - \frac{\sigma(t-t_0)}{\lambda_{\inf}} - \sigma\sum_{i=1}^{N}\frac{1}{E_i}\left(1-\exp(-\frac{t-t_0}{\tau_i})\right). \qquad \textbf{(8.7)}$$

Substituting Equations 8.6 and 8.7 into Equation 8.5 gives the strain after releasing the stress as:

$$\varepsilon(t) = \frac{\sigma.t_0}{\lambda_{\inf}} + \sigma\sum_{i=1}^{N}\frac{1}{E_i}\exp(-\frac{t}{\tau_i})\left(\exp(\frac{t_0}{\tau_i})-1\right). \qquad \textbf{(8.8)}$$

The formulations of the model were presented in incremental form to be implemented into the CAPA-3D. Three-dimensional expressions of the incremental formulations for the three components are as follows [Collop *et al.,* 2003]:

$$\Delta\varepsilon_{el} = C_{el}\Delta\sigma, \qquad \textbf{(8.9)}$$

$$\Delta\varepsilon_{de} = \sum_{i=1}^{N}\left\{{}^{t}\varepsilon_{de}^{i}(\exp(-\frac{\Delta t}{\tau_i})-1) + \Delta t e^{-\Delta t/2\tau_i}C_{de}^{i}({}^{t}\sigma + \frac{\Delta\sigma}{2})\right\}, \qquad \textbf{(8.10)}$$

$$\Delta\varepsilon_{v} = \Delta t C_{v}({}^{t}\sigma + \frac{\Delta\sigma}{2}), \qquad \textbf{(8.11)}$$

where $\Delta\varepsilon_{el}$, $\Delta\varepsilon_{de}$ and $\Delta\varepsilon_{v}$ = elastic, delayed elastic and viscous strain increments with time increment Δt, respectively.

$\Delta\sigma$ = the stress increment

${}^{t}\sigma$ = stress at time t

${}^{t}\varepsilon_{de}^{i}$ = the delayed elastic strain in the i'th Voigt element at time t.

$$C_{el} = \frac{1}{E_0}\begin{bmatrix} 1 & -\nu^{el} & -\nu^{el} & 0 & 0 & 0 \\ -\nu^{el} & 1 & -\nu^{el} & 0 & 0 & 0 \\ -\nu^{el} & -\nu^{el} & 1 & 0 & 0 & 0 \\ 0 & 0 & 0 & 2(1+\nu^{el}) & 0 & 0 \\ 0 & 0 & 0 & 0 & 2(1+\nu^{el}) & 0 \\ 0 & 0 & 0 & 0 & 0 & 2(1+\nu^{el}) \end{bmatrix}, \quad \textbf{(8.12)}$$

where ν^{el} = the elastic Poisson's ratio

C_{de}^{i} and C_{ν} = similar to the C_{el} with ν^{el} replaced by ν_i^{de} and ν^{v}, respectively, and E_0 replaced by λ_i and $\lambda_{\inf}$, respectively.

ν_i^{de} and ν^{v} are Poisson's ratio equivalents for the delayed elastic and viscous components respectively. Because of the framework used in this model, it is not possible to use the values of elastic Poisson's ratio and equivalent of delayed elastic and viscous Poison's ratio more than 0.5.

Based on the experimental data on the idealised asphalt mixtures, the following formulations were proposed for the $\lambda_{\inf}$ [Collop *et al.*, 2003].

$$\lambda_{\inf} = \lambda_{uni}(T)\left(\frac{\sigma_e}{\sigma_0}\right)^{1-n} 10^{B(\eta+1/3)}(1-D)^{\beta} \qquad (\sigma_e > \sigma_0),$$

$$= \lambda_{uni}(T)10^{B(\eta+1/3)}(1-D)^{\beta} \qquad (\sigma_e \le \sigma_0), \quad \textbf{(8.13)}$$

where σ_e = the Von Mises equivalent stress, as defined in Equation (2.10)

T = temperature

n, B, β and σ_0 = material constants, determined from test results

D = damage variable

λ_{uni} = the uniaxial viscosity of the mixture, measured from uniaxial compression tests data

η = the stress ratio ($\eta = \sigma_m / \sigma_e$), where σ_m is the mean stress ($\sigma_m = \frac{1}{3}\sigma_{kk}$) and σ_{kk} was defined in Equation (2.9).

The constants in Equation 8.13 were determined by fitting to the experimental data for an idealised mixture studied by Collop *et al.* [1999].

The damage variable *D* was used to account for the dramatic increase in strain rate, which is observed in tertiary creep stage in the creep tests. That is, the equivalent viscosity is reduced by damage accumulation. For the fully damaged material, the value of *D* is 1 and for undamaged material the magnitude of *D* is 0. The three-dimensional formulation of the damage factor *D* was given by:

$$\frac{dD}{dt} = \left(\frac{\sigma_e}{\widetilde{C}}\right)^{\nu} \frac{1}{(1-D)^{\mu}} \quad , \tag{8.14}$$

which after integrating can be written as:

$$D(t) = 1 - \left[1 - \left(\frac{\sigma_e}{\widetilde{C}}\right)^{\nu} (\mu+1)t\right]^{\frac{1}{\mu+1}}, \tag{8.15}$$

where $\widetilde{C}, \nu, \mu$ are the material constants. The incremental formulation of the damage factor was presented as:

$$\Delta D = {}^{t+\Delta t}D - {}^{t}D \cong (1 - {}^{t}D) - \left[\left(1 - {}^{t}D\right)^{\mu+1} - (\mu+1)\left(\frac{{}^{t}\sigma_e + \Delta\sigma_e/2}{\widetilde{C}}\right)^{\nu} \Delta t\right]^{\frac{1}{(\mu+1)}}. \tag{8.16}$$

Substitution Equation 8.15 into Equation 8.13, Equation 8.4 can be rewritten in a way that allows taking into account the damage accumulation effect on the dramatic decrease of the viscosity of the dashpot in series $\lambda_{\inf}$.

$$\varepsilon(t) = \frac{\sigma}{E_0} + \frac{\sigma \cdot t}{\lambda_{uni}(T)\left(\frac{\sigma}{\sigma_0}\right)^{1-n} 10^{B(\eta+1/3)}(1-D(t))^{\beta}} + \sigma\sum_{i=1}^{N}\frac{1}{E_i}\left(1 - \exp(-\frac{t}{\tau_i})\right). \tag{8.17}$$

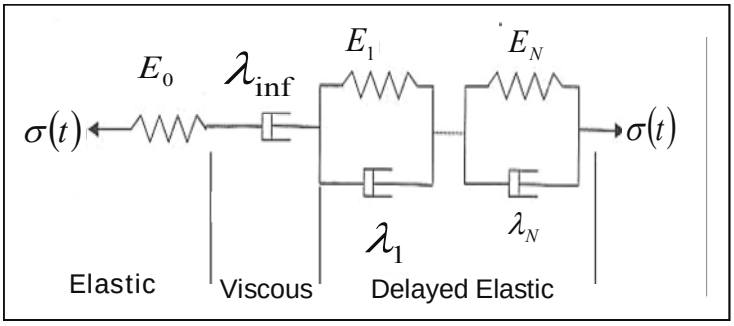

Figure 8.1 Mechanical arrangement of the model.

8.3 Determination of the Model Parameters

The constitutive model explained in above section is used for characterisation of the creep and recovery behaviour of the 10 mm DBM and HRA30/10 mixtures. A methodology is presented for determination of the model parameters necessary for implementation of the model into the CAPA-3D. The parameters associated with the elastic, delayed elastic, and viscous elements, and damage accumulation in the mixtures (i.e. $E_0, \nu^{el}, \lambda_i, E_1, \nu^{de}, \sigma_0, \nu^v, \lambda_{uni}, B, n, \widetilde{C}, \nu, \mu, \beta$) are determined in this chapter.

For this research, the generalised Burger's model with one Voigt element was used for simulation of the creep and recovery behaviour of the mixtures. For the generalised Burger's model with one Voigt element, using Equation 8.4, the formulation for the total strain can be written as:

$$\varepsilon(t) = \frac{\sigma}{E_0} + \frac{\sigma \cdot t}{\lambda_{\inf}} + \frac{\sigma}{E_1}\left(1 - \exp(-\frac{tE_1}{\lambda_1})\right), \qquad \textbf{(8.18)}$$

where E_1 and λ_1 =elastic modulus of the spring and viscosity of the dashpot in the Voigt element respectively.

The viscosity of the dashpot in series $\lambda_{\inf}$ is calculated as $\lambda_{\inf} = \sigma / \dot{\varepsilon}$, where σ is the applied stress level, and $\dot{\varepsilon}$ is the viscous strain rate. Considering a creep curve for the mixtures, the strain rate is constant in the secondary creep region and increases rapidly in the tertiary creep region. For the primary creep region, it

can be assumed to be similar to that in the secondary region. Therefore, the viscosity λ_{inf} remains constant up to the tertiary creep region, after which decreases with increasing damage in the mixtures. Therefore, the viscosity of the dashpot in series can be written as:

$$\lambda_{\text{inf}} = \lambda_{\text{inf}\,0}.(1-D(t))^{\beta}, \qquad \textbf{(8.19)}$$

where $D(t)$ = variation of damage variable with time (Equation 8.15).

$\lambda_{\text{inf}\,0}$ = the constant value of the viscosity in the primary and secondary creep regions

β = material constant.

Therefore, substitution of Equation 8.15 and 8.19 into Equation 8.18 gives the total strain of the generalised Burger's model with one Voigt element as:

$$\varepsilon(t) = \frac{\sigma}{E_0} + \frac{\sigma \cdot t}{\lambda_{\text{inf}\,0}\left[1-\left(\frac{\sigma_e}{\widetilde{C}}\right)^{\nu}(\mu+1).t\right]^{\frac{\beta}{\mu+1}}} + \frac{\sigma}{E_1}\left(1-\exp(-\frac{tE_1}{\lambda_1})\right) \quad . \qquad \textbf{(8.20)}$$

For Equation 8.20, the values for the elastic modulus of the spring in series E_0, explained in the following section, and the creep exponent of the steady state deformation behaviour n, as explained in previous chapters, are calculated separately and used for determination of the rest of parameters. Moreover, For reducing the parameters, it has been suggested that the parameter β and υ equal n and $n+1/2$, respectively [Collop *et al.*, 2003]. For determination of the parameters corresponding to the delayed elastic, viscous and damage accumulation in Equation 8.20 (i.e. $\lambda_1, E_1, \lambda_{\text{inf}\,0}, \widetilde{C}, \mu$), using Matlab, the equation was fitted to experimental data. The values of the parameters were changed manually until a good fit was obtained, which was evaluated visually and quantified using an R-squared value. Figure 8.2 shows an example of the fitting where the formulation for total strain in creep (Equation 8.20) is fitted to an uniaxial creep test result for the DBM, and Figure 8.3 shows an example of

fitting to the loading path of the creep recovery test results where Equation 8.20 with $D(t)$=0 is fitted to a creep recovery test result for the HRA.

8.3.1 Elastic Parameter E_0

The parameters of the constitutive model related to the elastic behaviour are Poisson's ratio ν^{el} and elastic modulus of the spring in series E_0. Poisson's ratio of the mixtures was presented in detail in Chapter 5, this section concentrates on the determination of the elastic modulus E_0 from the experimental data.

Upon application of a stress, the spring in series (see Figure 8.1) will experience an instant strain that is recovered instantly after releasing the stress. In an idealised creep recovery test, the instantaneous strain after load application will be equal to the instantaneous recovered strain after load removal. However, for the asphalt mixtures, as seen in Chapter 6, the instantaneous strain after load application was higher than the instantaneous strain recovered after releasing the load (see Figure 6.1). This difference is thought to be due to the plastic strain caused by aggregate movement, densification, the deformation of friction reduction system and the viscous deformation occurred in the short period in which the load varies from zero to the target load. Therefore, the elastic modulus of the spring E_0 was calculated from the unloading path in the creep recovery test results. As shown in Figure 8.4, the elastic modulus was taken as the slope of the straight line from a plot of axial strain versus stress during the short period of time in which the stress varies from the target stress to zero in the creep recovery tests. In this figure the strain prior to unloading has been taken as zero.

Ideally, to obtain the elastic modulus of the spring E_0, the unloading time should be short enough so that the time dependent recovery deformation (delayed elastic) can be ignored. Achieving a target load at a very short time depends on the accuracy of the loading system and the software which controls the machine. Based on the data logging software used in the tests and the data points required for calculation of the elastic modulus, the shortest loading and unloading time was estimated to be around 40 milliseconds.

Figure 8.5 shows the elastic modulus E_0 for the DBM mixture at different temperatures and stress levels. As can be seen in the figure for the DBM, which similar behaviour was observed for the HRA, the elastic modulus of the mixtures is independent of the stress level and only depends on the temperature.

Figure 8.6 shows the elastic modulus E_0 as a function of temperature. The solid lines represent the WLF equation (Equation 8.21) fitted to the experimental data. As can be seen, the temperature dependency of the parameter for the mixtures is well captured by the WLF equation.

$$E_0 = A \exp \frac{-2.303.c_s^1.(T - T_s)}{c_s^2 + (T - T_s)}, \qquad \textbf{(8.21)}$$

where T = temperature in Celsius degree

E_0 = the elastic modulus in GPa

A = material constant with values of 17400 GPa and 21000 GPa for the HRA and DBM mixtures, respectively

T_s = the reference temperature with a value of -60°C

c_s^1 and c_s^2 = universal constants with the values defined in Section 5.3.2.

Results from the single creep recovery tests, unloaded at different strain levels, along with the repeated creep recovery test results, revealed that the elastic modulus of the mixtures decreases with increasing damage in the mixtures. Figure 8.7 shows the elastic modulus E_0 as a function of the accumulated strain in the mixtures. As can be seen, up to a certain level of strain, the elastic modulus remains almost constant, after which it reduces with increasing accumulated strain or damage in the mixtures. The figure clearly shows that the reduction of the elastic modulus for the DBM mixture occurs at a lower strain level than that for the HRA. Moreover, the reduction of the elastic modulus with accumulated strain is linear with approximately the same slope for both mixtures. The reduction of the elastic modulus is thought to be due to the development of cracks and internal damage in the mixtures. As discussed before, because of continuous grading and thinner binder films in the DBM mixture the internal

cracks develop at a lower axial strain level than in the HRA. The following equations can be used for determination of the elastic modulus E_0 (in GPa) for the mixtures at 20°C. Developing an equation as a function of temperature and damage needs further experimental work at different temperatures.

$$E_0^{DBM} = \begin{cases} 2.97 & \varepsilon_t \le 0.03 \\ -21.3\varepsilon_t + 3.6 & \varepsilon_t > 0.03 \end{cases} \quad \textbf{(8.22)}$$

$$E_0^{HRA} = \begin{cases} 1.9 & \varepsilon_t \le 0.043 \\ -20.7\varepsilon_t + 2.79 & \varepsilon_t > 0.043 \end{cases} \quad \textbf{(8.23)}$$

where ε_t is the total accumulated strain in the mixtures.

As explained in Chapter 7, the axial strain of the specimens in triaxial tests was measured by the LVDT on the actuator. This LVDT can not accurately measure the instant deformation of the specimen as the instrument used in the uniaxial tests does. Therefore, the possible effect of confinement on the elastic modulus E_0 cannot be presented. Further experimental work is required to use some instruments in the triaxial cell for measuring the instantaneous deformation of the specimen.

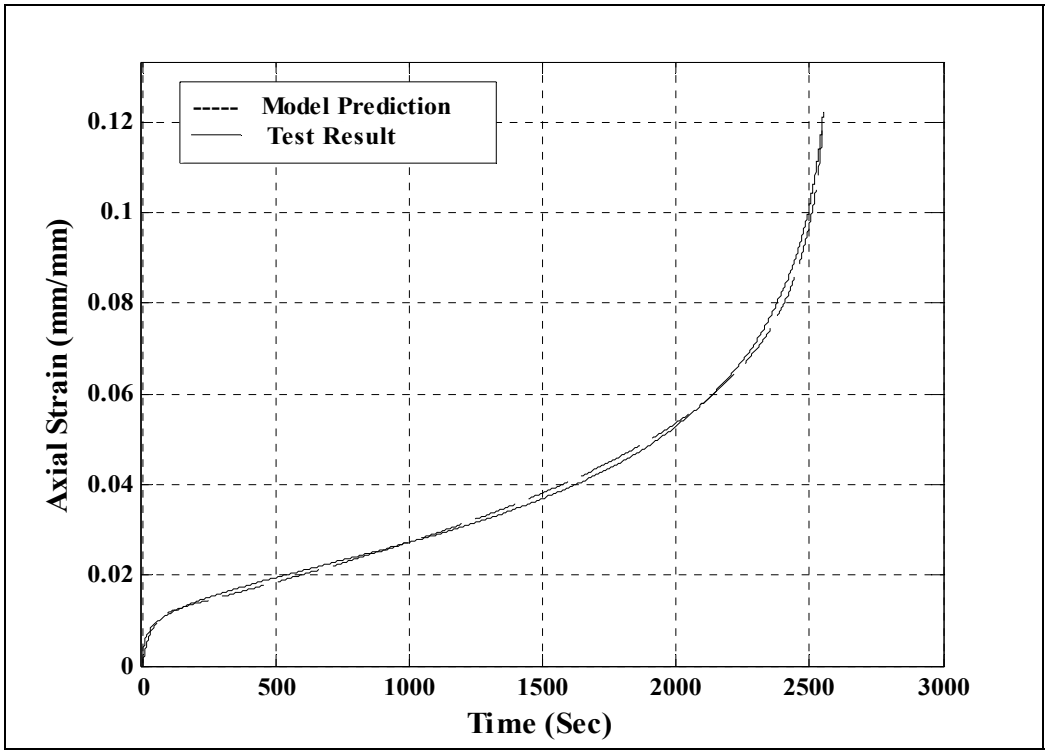

Figure 8.2 A typical fitting of the constitutive model to the static uniaxial creep test result for the DBM at 20°C (σ =2000 kPa).

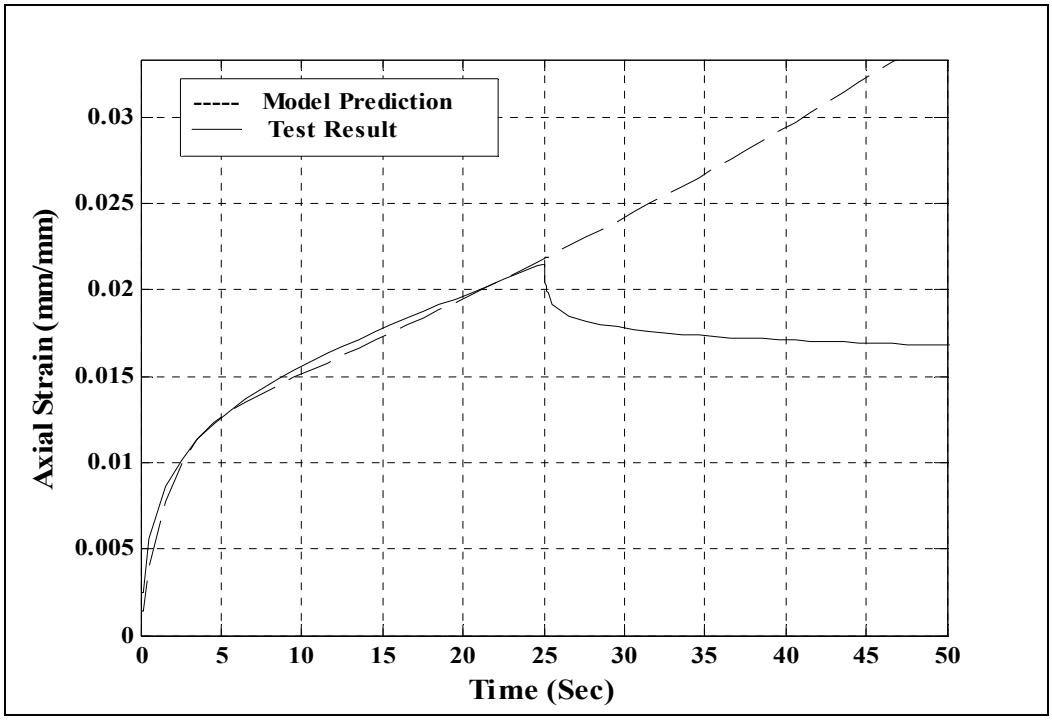

Figure 8.3 A typical fitting of the model to the loading path of a creep recovery test result for the HRA30/10 at 20°C (σ =1500 kPa).

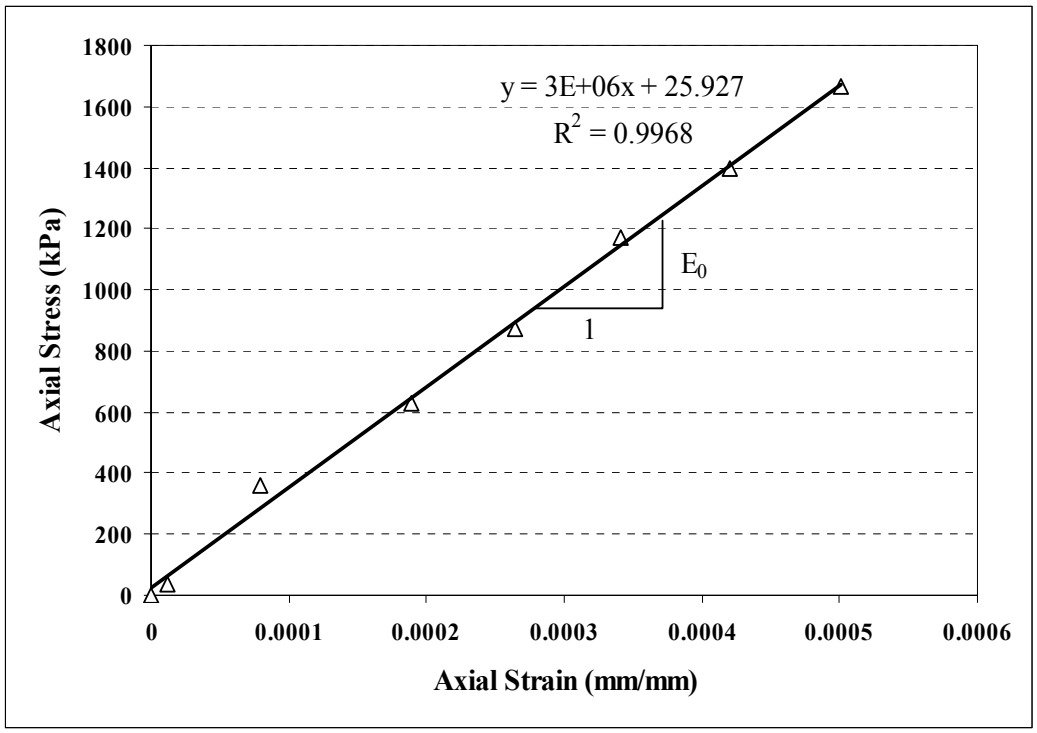

Figure 8.4 Calculation of the elastic modulus E_0 for the HRA at 20°C (stress level of 2000 kPa).

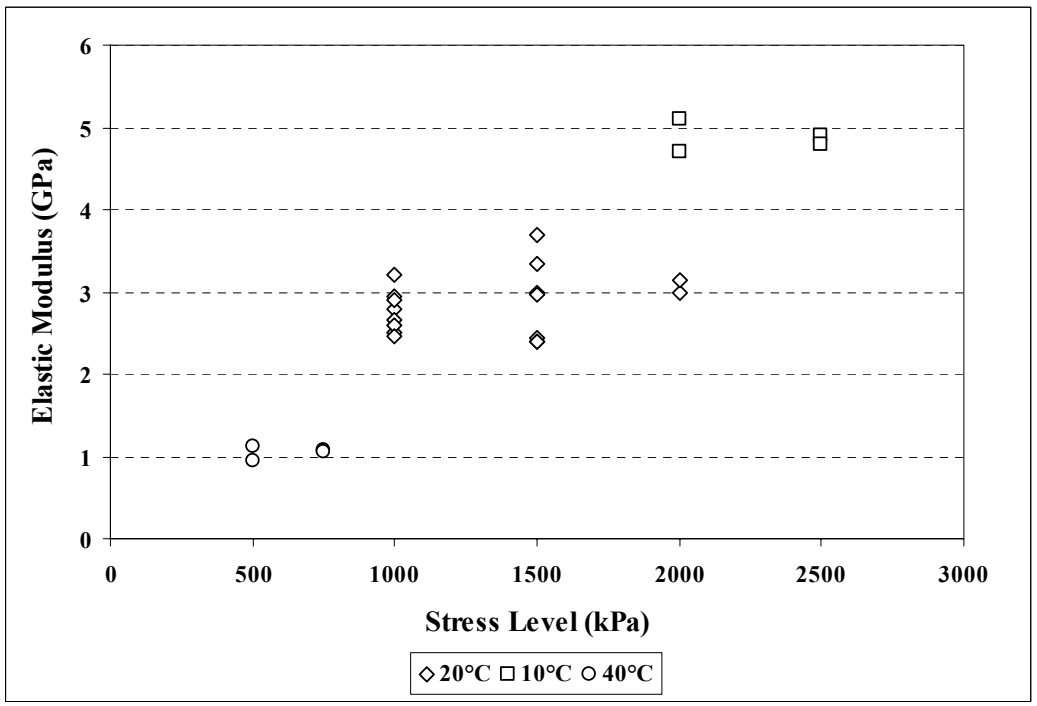

Figure 8.5 Elastic modulus E_0 for the 10 mm DBM.

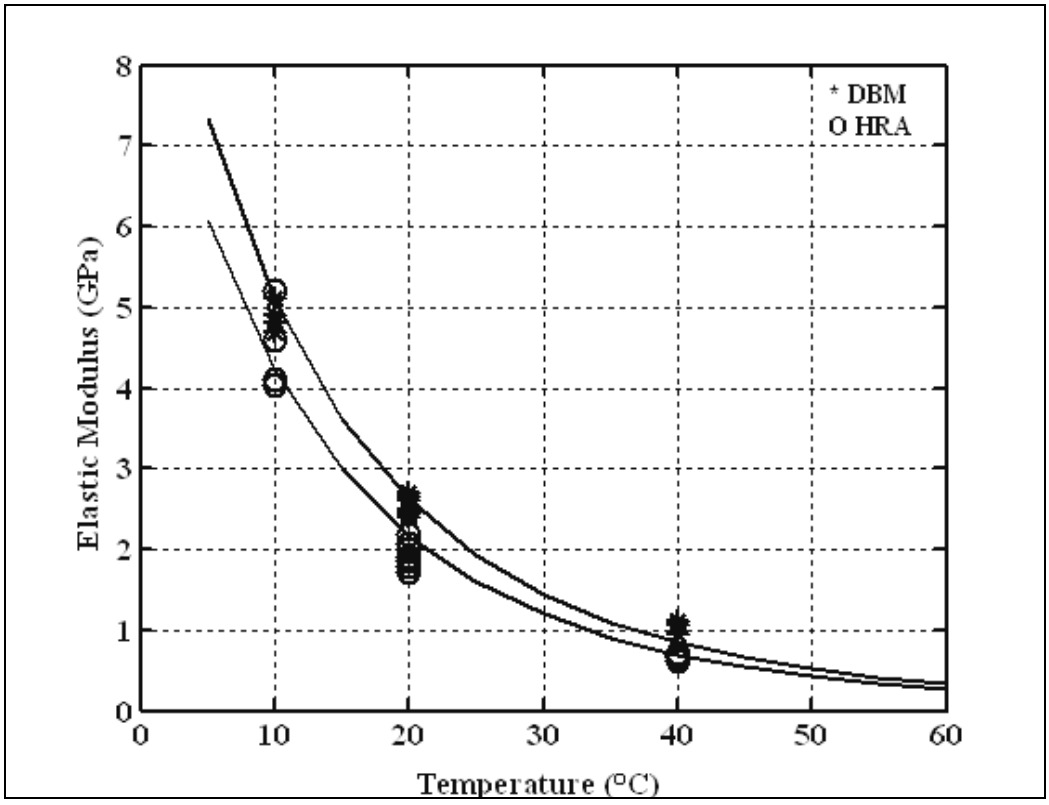

Figure 8.6 Elastic modulus E_0 of the mixtures as a function of temperature.

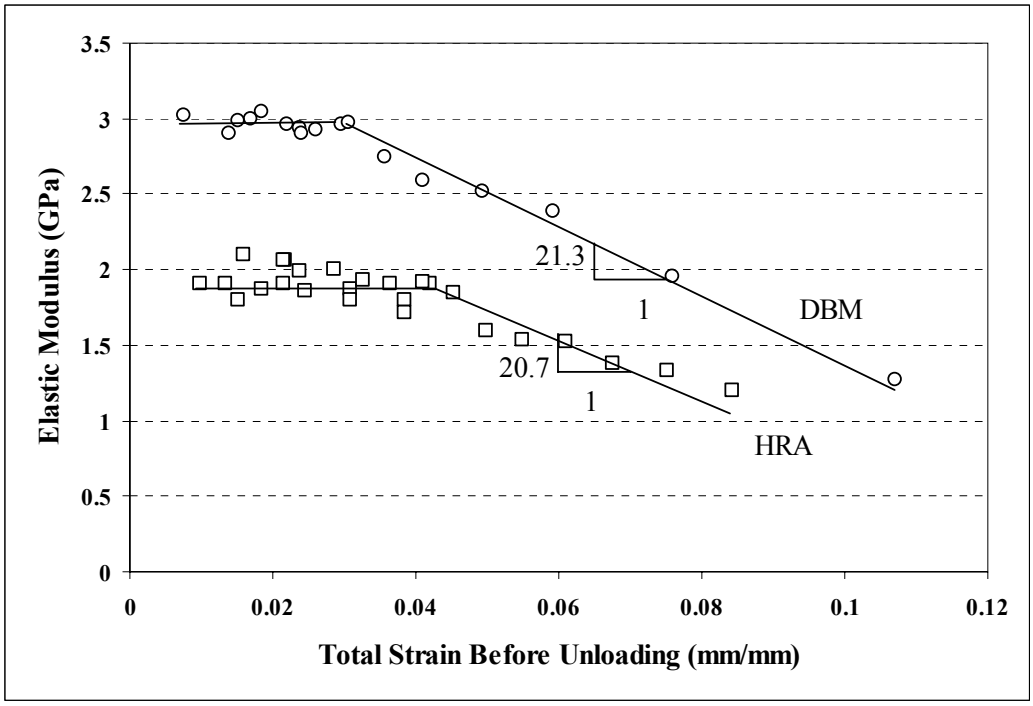

Figure 8.7 Elastic modulus E_0 of the mixtures as a function of accumulated strain in the mixtures.

8.3.2 Delayed Elastic Parameters

In this section, the parameters corresponding to the delayed elastic behaviour of the mixtures E_1 and λ_1 determined from the fitting process and ν^{de} determined from test results are described in detail.

Model Parameter E_1

From fitting the formulation of total strain (Equation 8.20) to the triaxial test results and determination of the parameters it was found that the parameter E_1 does not change with stress ratio. This can be seen in Figure 8.8 where the parameter E_1 is plotted against the applied deviator stress level at different stress ratios for the HRA and DBM mixtures. As the instrumentation for measuring the axial strain in the triaxial tests was different from that for the uniaxial tests, the values of the E_1 from triaxial tests were not consistent with those from uniaxial and, therefore, the results for the triaxial tests are shown separately in Figure 8.8.

Figures 8.9 and 8.10 summarise the parameter E_1, obtained from fitting to the uniaxial test results, versus the applied deviator stress level at different temperatures for the HRA30/10 and 10 mm DBM mixtures, respectively. Using multivariable curve fitting technique in Matlab, Equations 8.24 and 8.25 were found to well represent the E_1 as a function of temperature and deviator stress level for the HRA and the DBM mixture, respectively.

$$E_1^{HRA} = -23.5 + 0.097\sigma + 1.09T, \qquad \textbf{(8.24)}$$

$$E_1^{DBM} = -98.7 + 0.164\sigma + 1.85T, \qquad \textbf{(8.25)}$$

where E_1 = the elastic modulus of the spring in Voigt element in MPa

σ = the applied deviator stress level in kPa

T = temperature in Celsius degree.

The values predicted by the above equations are shown in Figures 8.9 and 8.10 by the solid lines.

General observations from the values of E_1 for the mixtures can be summarised as follows. These observations can also be seen in Figures 8.9 and 8.10.

- At the same temperature and applied deviator stress level, the value of E_1 for the DBM is higher than that for the HRA mixture.
- For both mixtures, the elastic modulus E_1 increases with increasing the deviator stress level.
- The rate of increase with the applied deviator stress level (gradient) is almost uniform at different temperatures with a higher gradient for the DBM mixture.
- For both mixtures, the elastic modulus E_1 is independent of the stress ratio.
- The elastic modulus E_1 increases with increasing temperature.
- The elastic modulus E_1 for the DBM mixture is more sensitive to temperature than that for the HRA.

In order to study the effect of accumulated strain (damage) on the parameters, the formulation for total strain (Equation 8.20) was fitted to the creep data in the loading path of each cycle in the repeated creep recovery test results and the parameters were determined. Figures 8.11 and 8.12 show the parameter E_1 as a function of the accumulated strain and recovery times ΔR for the HRA and DBM mixtures, respectively. It can be seen that, for both mixtures, the value of the parameter increases to a maximum value followed by decreasing with increasing strain (damage) accumulation. The figures show that, for both mixtures, the maximum value and the rate of reduction depend on the recovery time. Further work is required to model this behaviour.

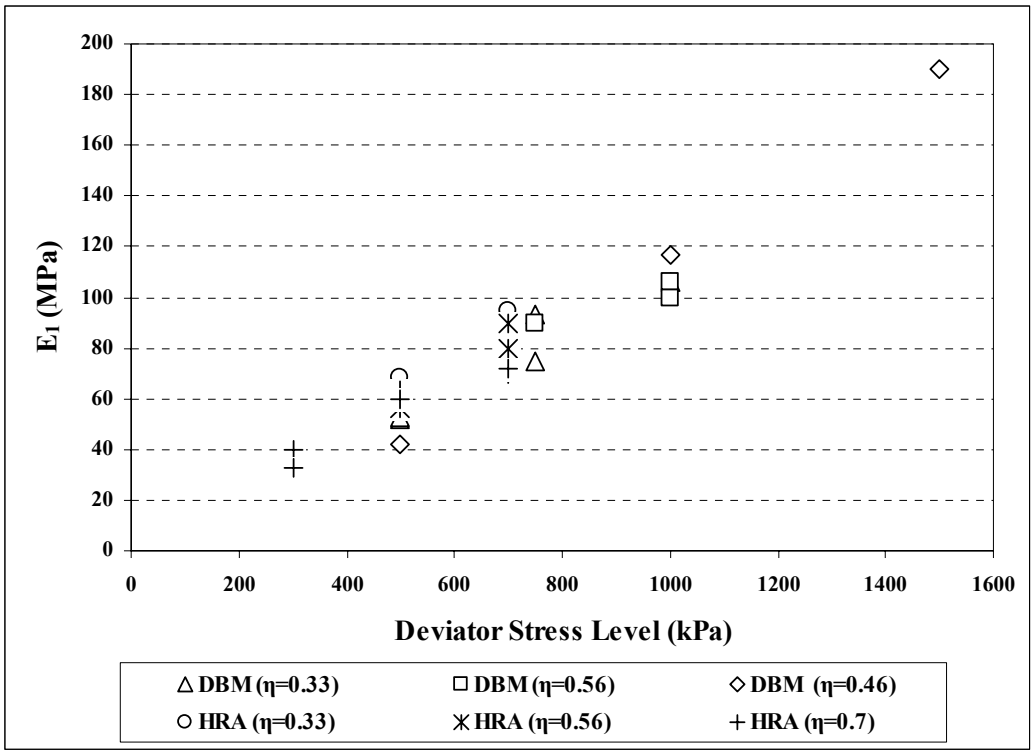

Figure 8.8 The model parameter E_1 as a function of the applied deviator stress level and stress ratio.

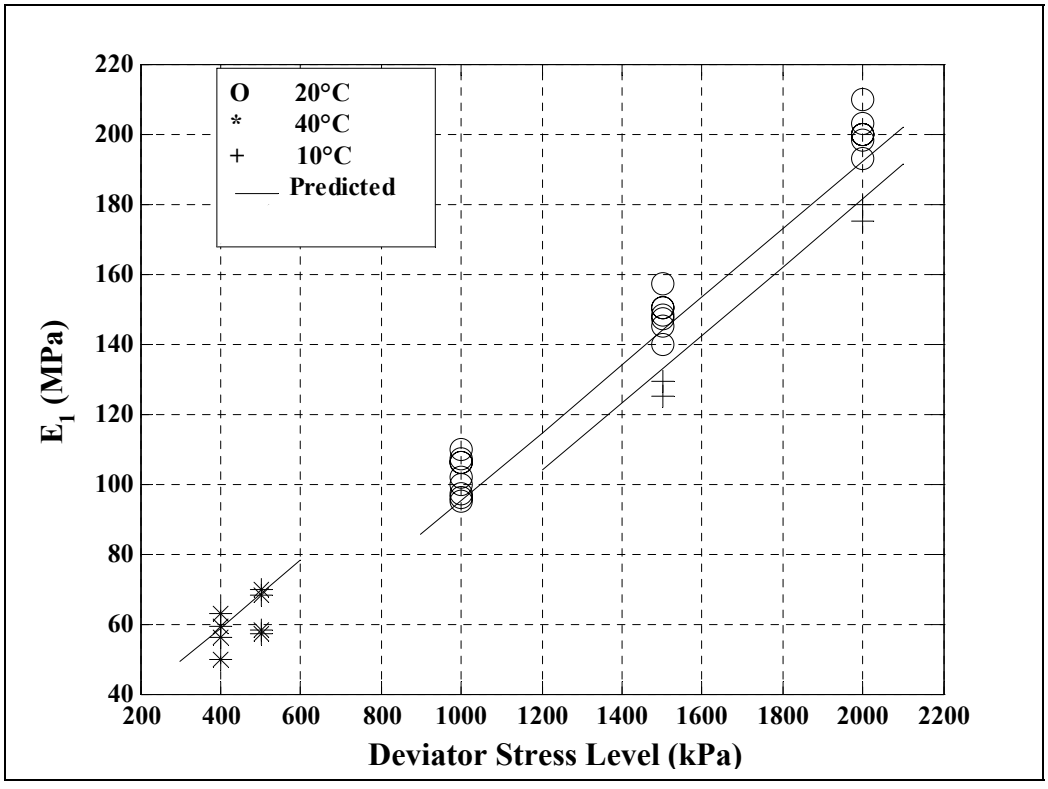

Figure 8.9 The model parameter of E_1 as a function of the applied deviator stress level and temperature for the HRA30/10 in uniaxial tests.

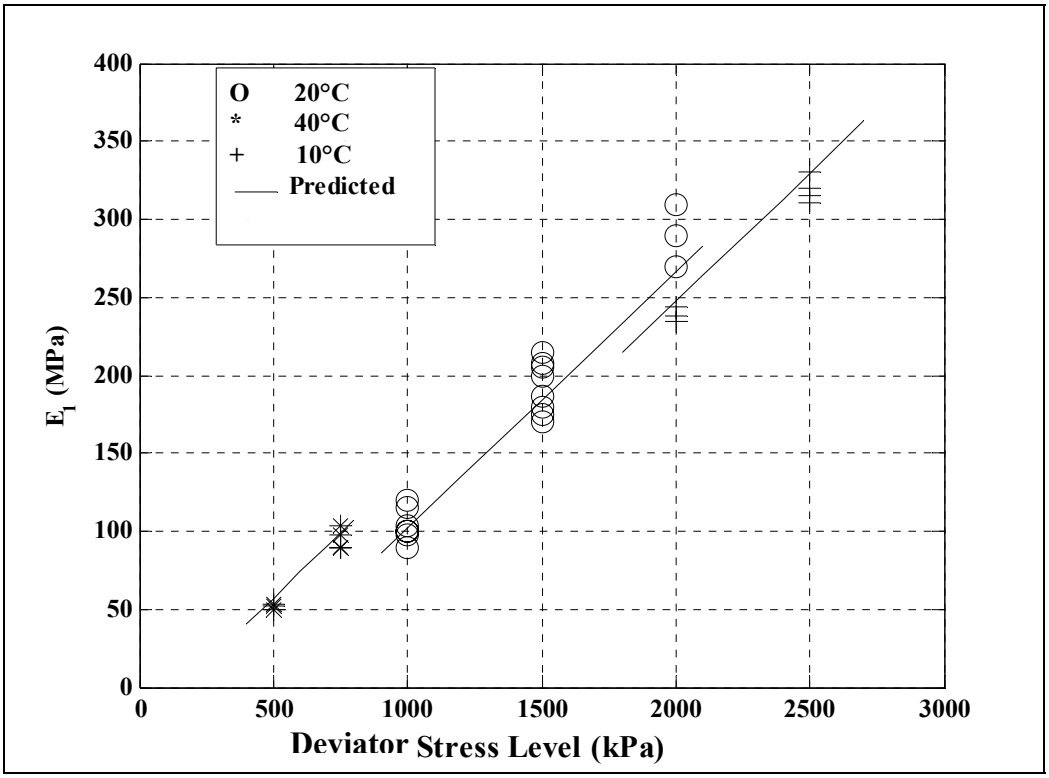

Figure 8.10 The model parameter E_1 as a function of deviator stress level and temperature for the 10 mm DBM.

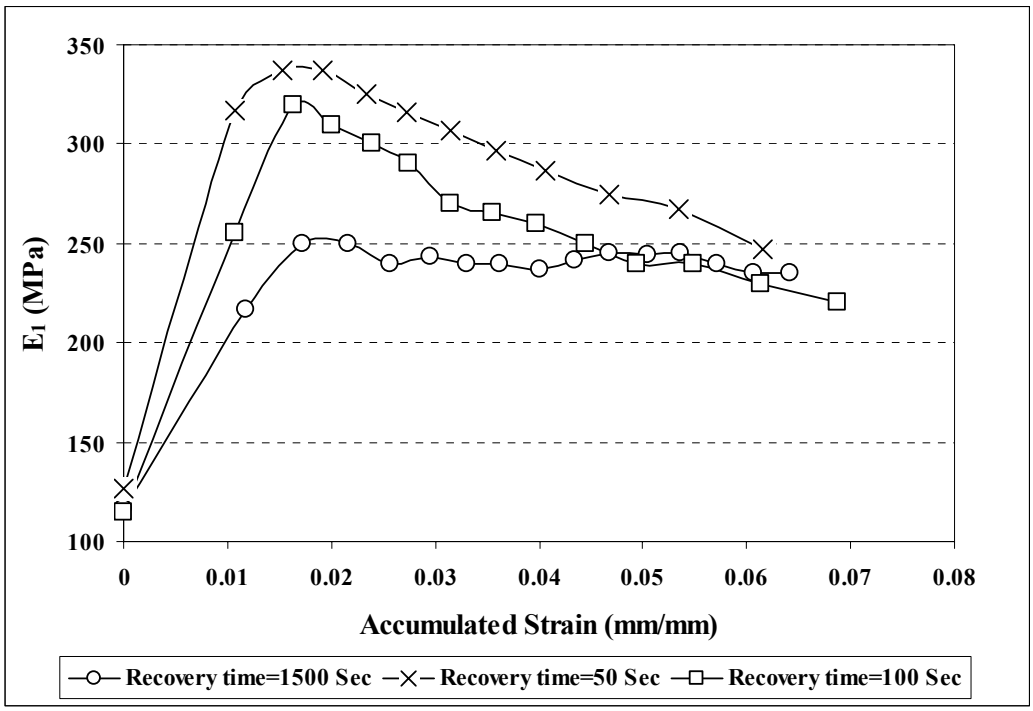

Figure 8.11 Variation of the model parameter E_1 with the accumulated strain and recovery time ΔR in the repeated creep recovery tests for the HRA30/10.

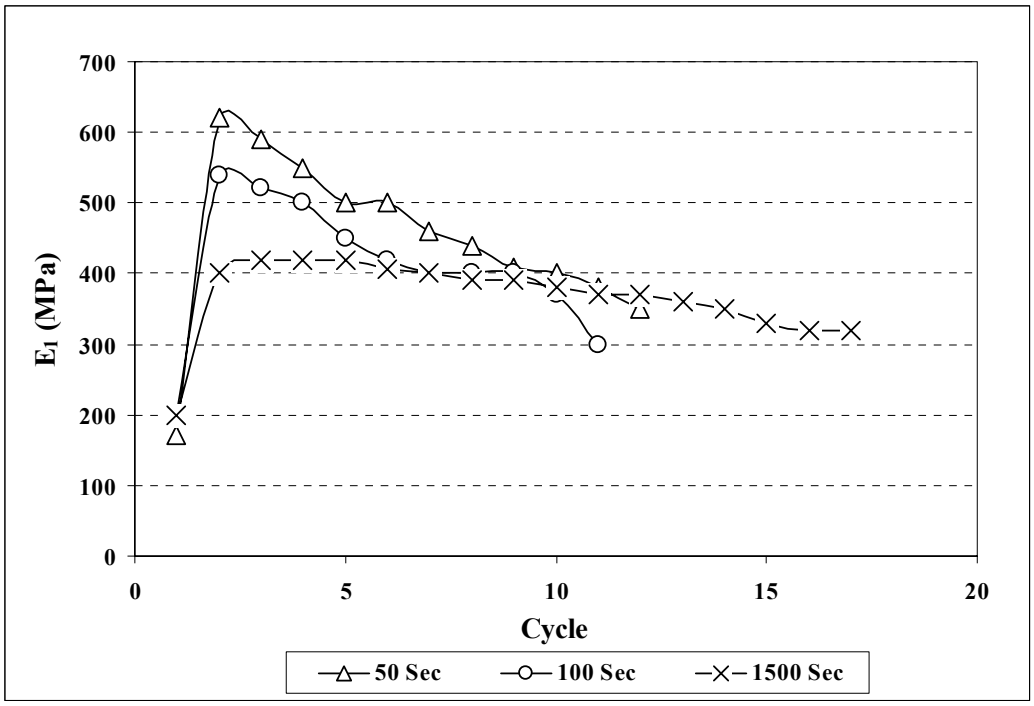

Figure 8.12 Variation of the model parameter E_1 with the accumulated strain and recovery time ΔR in the repeated creep recovery tests for the 10 mm DBM.

Model Parameter λ_1

Figures 8.13 and 8.14 summarise the parameter λ_1, determined from the fitting process, as a function of the applied deviator stress level, temperature and stress ratio for the HRA and DBM mixtures, respectively. Using multivariable fitting technique in Matlab, Equations 8.26 and 8.27 were found to well predict the parameter λ_1 for the HRA and the DBM mixture, respectively.

$$\log \lambda_1^{HRA} = (10.94.T^{-0.3768} - 0.33482.\sigma - 0.241/\eta - 0.0595), \qquad \textbf{(8.26)}$$

$$\log \lambda_1^{DBM} = (12.98.T^{-0.144} - 0.54927.\sigma - 0.37198/\eta - 3.194), \qquad \textbf{(8.27)}$$

where λ_1 = viscosity of the dashpot in Voigt element in MPa.s

η = stress ratio, and

T and σ were defined before. The solid lines shown in Figures 8.13 and 8.14 are the predictions using above equations.

As can be seen in Figures 8.13 and 8.14:

- For both mixtures, λ_1 decreases with increasing applied deviator stress levels and temperatures with a higher rate of decrease for the DBM than for the HRA.
- For both mixtures, λ_1 increases with increasing stress ratio.
- At the same temperature and applied deviator stress level, the parameter λ_1 for the DBM is higher than that for the HRA
- For the DBM, λ_1 is more sensitive to the confinement than that for the HRA mixture.

Figures 8.15 and 8.16 show variation of the parameter λ_1 with accumulated strain at different recovery times for the HRA and DBM mixtures, respectively. As can be seen in the figures, the variation with the accumulated strain is similar to that found for E_1. The figures also show that the rate of reduction depends on the recovery time, with a lower rate of reduction for higher recovery time. Comparing Figure 8.15 with 8.16 reveals that the rate of reduction with accumulated strain is higher for the DBM compared to that for the HRA mixture. This difference in behaviour can be related to more development of microcracks in the DBM than in the HRA.

The delayed elastic parameters of the model (E_1, λ_1) are related to the delayed elastic strain and the relaxation time. The delayed elastic strain of the model arrangement (Figure 8.1) with one Voigt element is calculated from Equation 8.2 as:

$$\varepsilon_{de} = \frac{\sigma}{E_1}\{1 - \exp(-\frac{tE_1}{\lambda_1})\}. \qquad \textbf{(8.28)}$$

The maximum delayed elastic strain of the model arrangement with one Voigt element is $\frac{\sigma}{E_1}$.

As can be seen, the total delayed strain depends only on the E_1 and the applied deviator stress level, and the relaxation time $\tau = \lambda_1 / E_1$ depends on both λ_1 and E_1. Using the parameters determined from the fitting process, the total delayed elastic strain values were calculated from Equation 8.28. Consistent with the axial strain level at the beginning of the secondary creep region in uniaxial creep test results, as explained in Section 5.3.1, the total delayed elastic strain of the mixtures was found to:

- Be independent of applied deviator stress level.
- Decrease with increasing temperature.
- Be higher for the HRA than for the DBM.
- Be independent of stress ratio.

Figures 8.17 and 8.18 show variation of the relaxation time with the applied deviator stress level and temperature for the HRA and DBM mixtures, respectively. The values of relaxation time in the figures were calculated from $\tau = \lambda_1 / E_1$, using the parameters E_1 and λ_1 determined from the fitting process. As can be seen in Figures 8.17 and 8.18, at the same test conditions, the relaxation time of the DBM is higher than that of the HRA mixture.

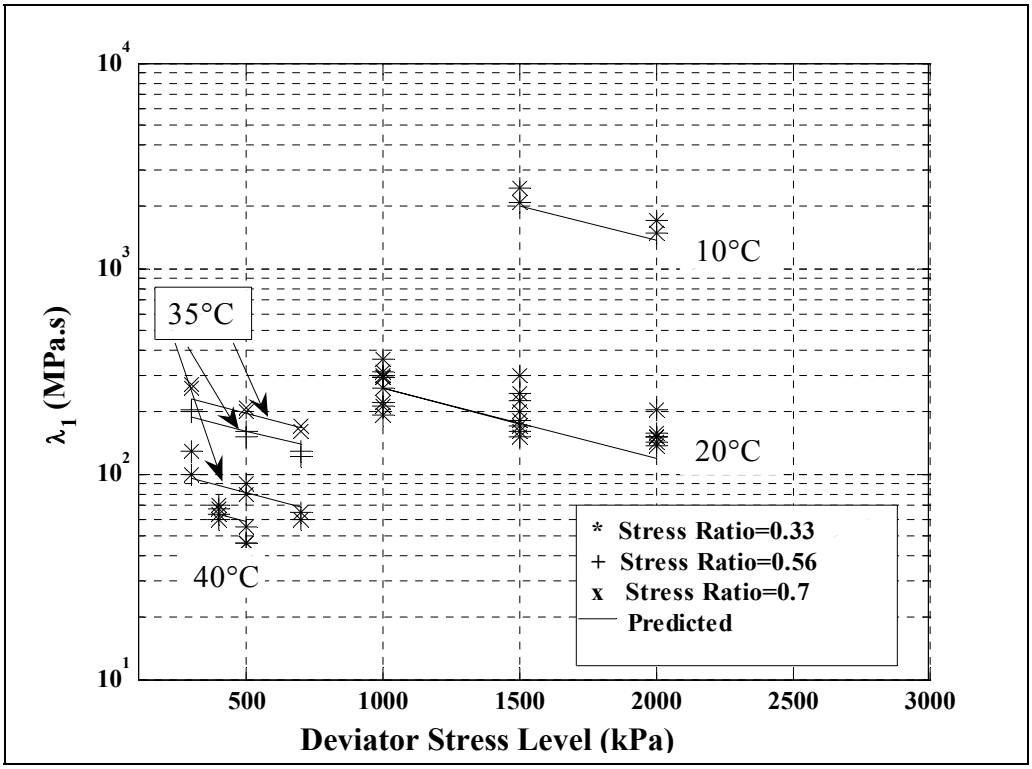

Figure 8.13 The model parameter λ_1 as a function of deviator stress level and temperature for the HRA30/10.

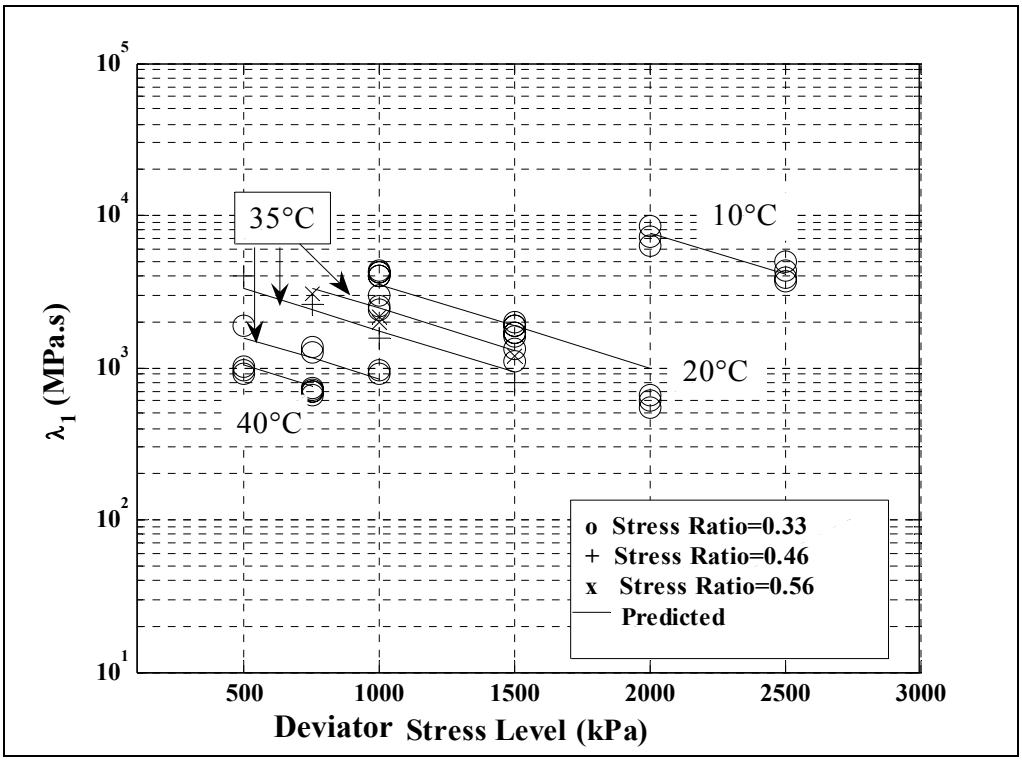

Figure 8.14 The model parameter λ_1 as a function of deviator stress level and temperature for the 10 mm DBM.

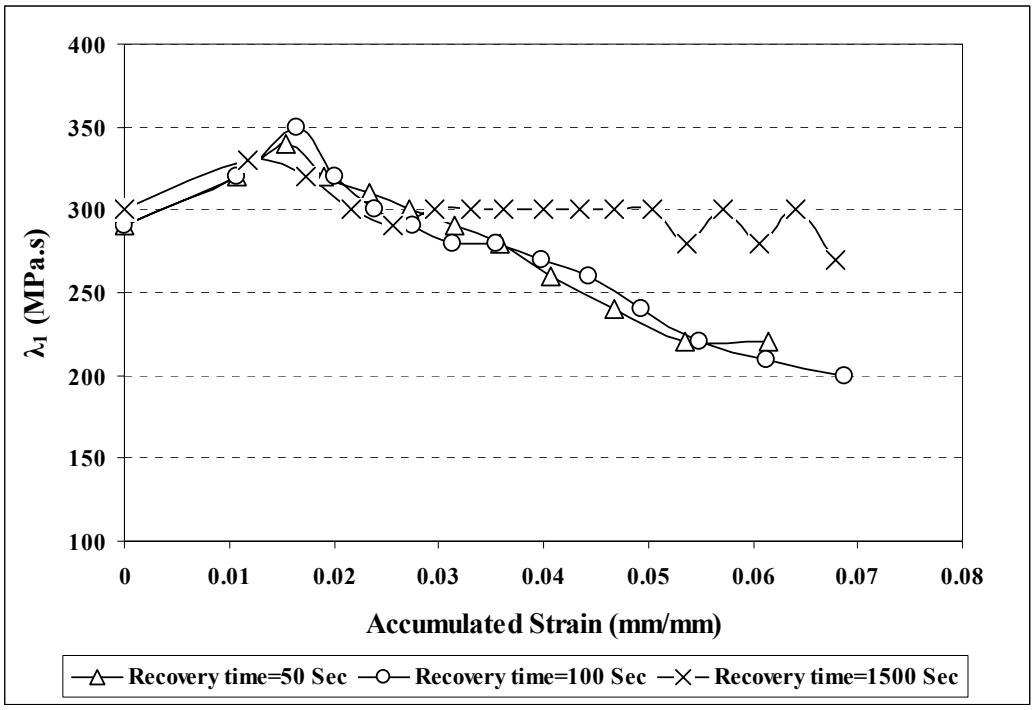

Figure 8.15 Variation of the model parameter λ_1 as a function of accumulated strain and recovery time for the HRA30/10.

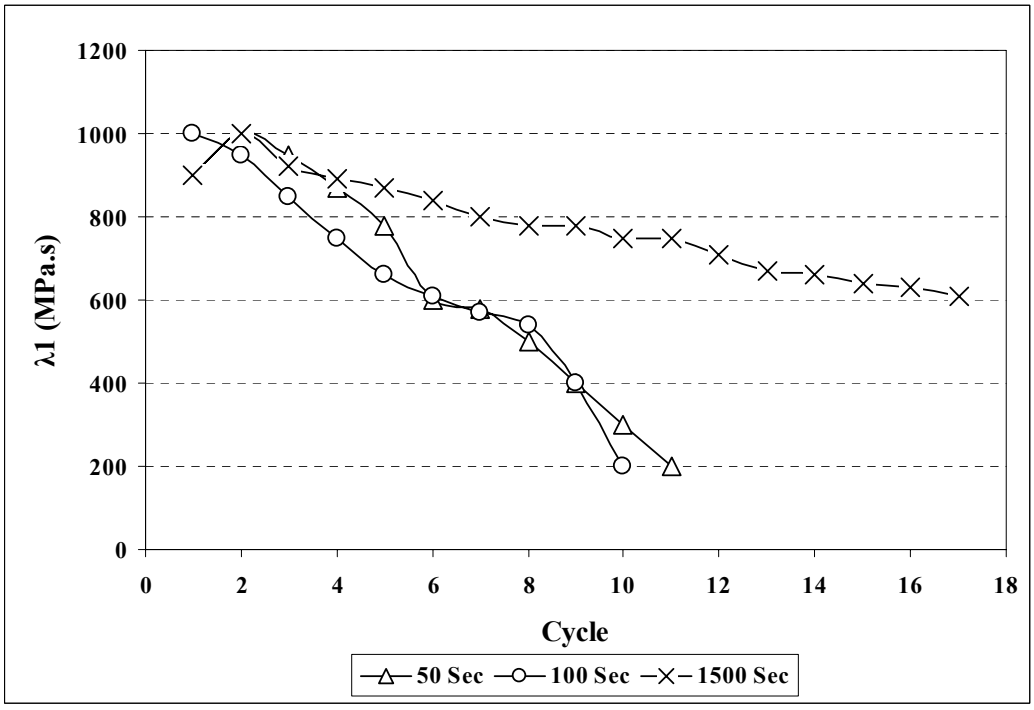

Figure 8.16 Variation of the model parameter λ_1 as a function of accumulated strain and recovery time for the 10 mm DBM.

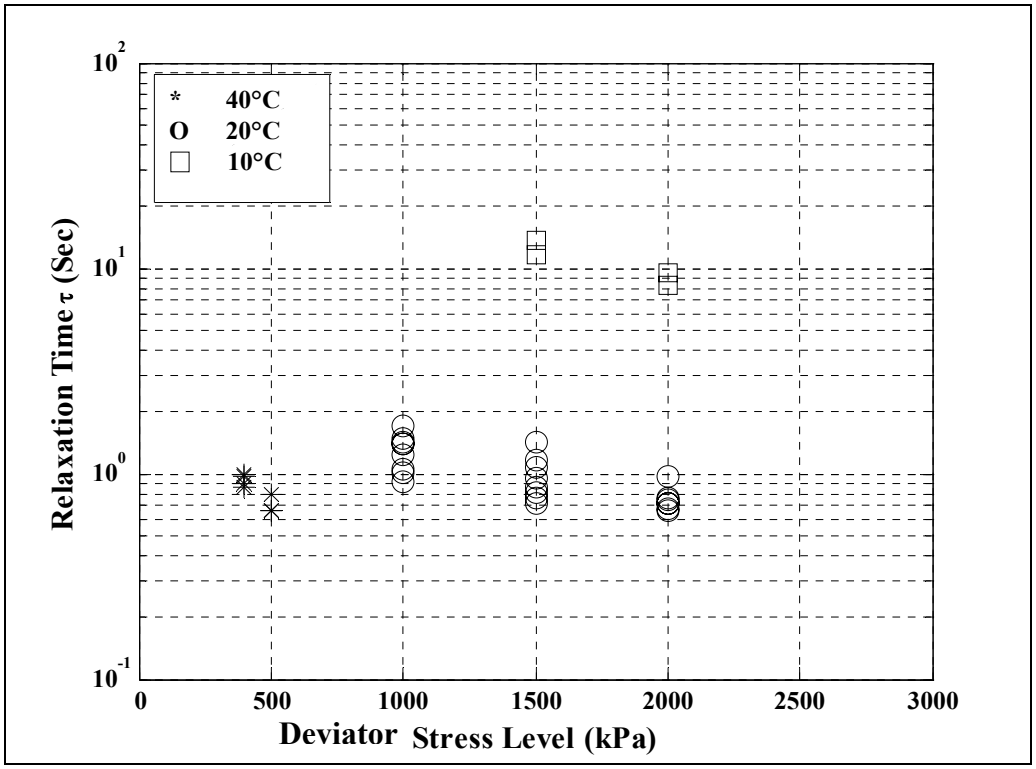

Figure 8.17 The relaxation time of the HRA30/10 as a function of the applied deviator stress level and temperature.

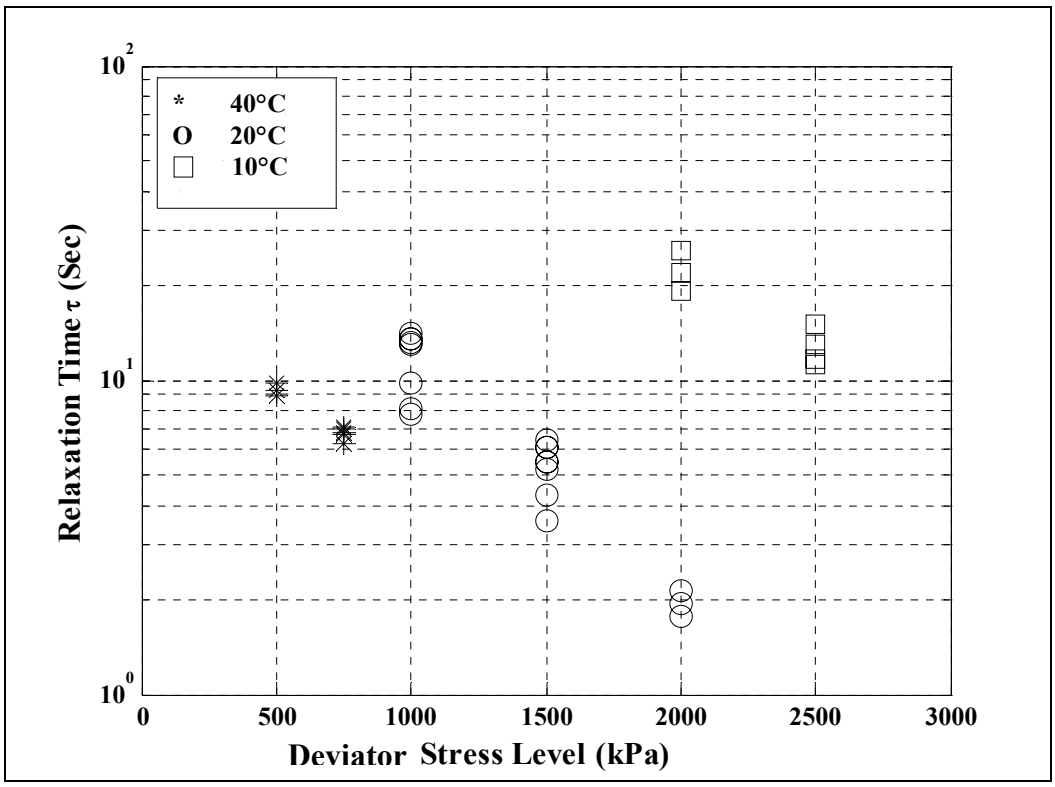

Figure 8.18 The relaxation time of the DBM as a function of the applied deviator stress level and temperature.

Model Parameter ν^{de}

As noted earlier in Section 8.2, implementation of the constitutive model into the CAPA-3D requires the parameters ν^{el} (elastic Poisson's ratio), ν^{de} and ν^{v} (equivalent Poisson's ratio for delayed elastic and viscous components) (see Equations 8.9 to 8.12). It was also noted that dilation is not possible in the constitutive model, which means that the maximum value of the parameters ν^{el}, ν^{de} and ν^{v} is 0.5.

Variation of the ratio of radial to axial strain in a creep test was presented in Figure 5.38. It was seen that the plot of this ratio against time was similar to the creep curve with the primary, secondary and tertiary creep regions. The ratio of radial to axial strain upon load application (as the elastic region) is known as Poisson's ratio. In the primary region the ratio of radial to axial strain increases with time at a decreasing rate. This corresponds to the delayed elastic behaviour, and will be called the equivalent Poisson's ratio for delayed elastic component ν^{de} in this study. In the secondary region of variation, the ratio increases linearly with time which corresponds to the viscous behaviour and is called equivalent Poisson's ratio for viscous component.

For each creep test, ν^{de} was calculated as the average of the ratios of radial to axial strain in the primary region, discarding the elastic part corresponding to the elastic Poisson's ratio. Figure 8.19 shows a summary of the calculations where the parameter ν^{de} is plotted as a function of temperature for the HRA and DBM mixtures. It was found that the parameter does not change with stress level. The data points for each temperature are the average of the values calculated at different stress levels. Similar to ν^{el}, ν^{de} increases with increasing temperature. The figure also shows that the values for the DBM are higher than those for the HRA which is equivalent to higher dilation for the DBM. The equations shown in the figure can be used for an estimation of the parameter for the mixtures as a function of temperature. As can be seen in the figure, some of the values for the

parameter are greater than 0.5. Therefore, they can not be used in the simulation by the model and are replaced with the value of 0.5.

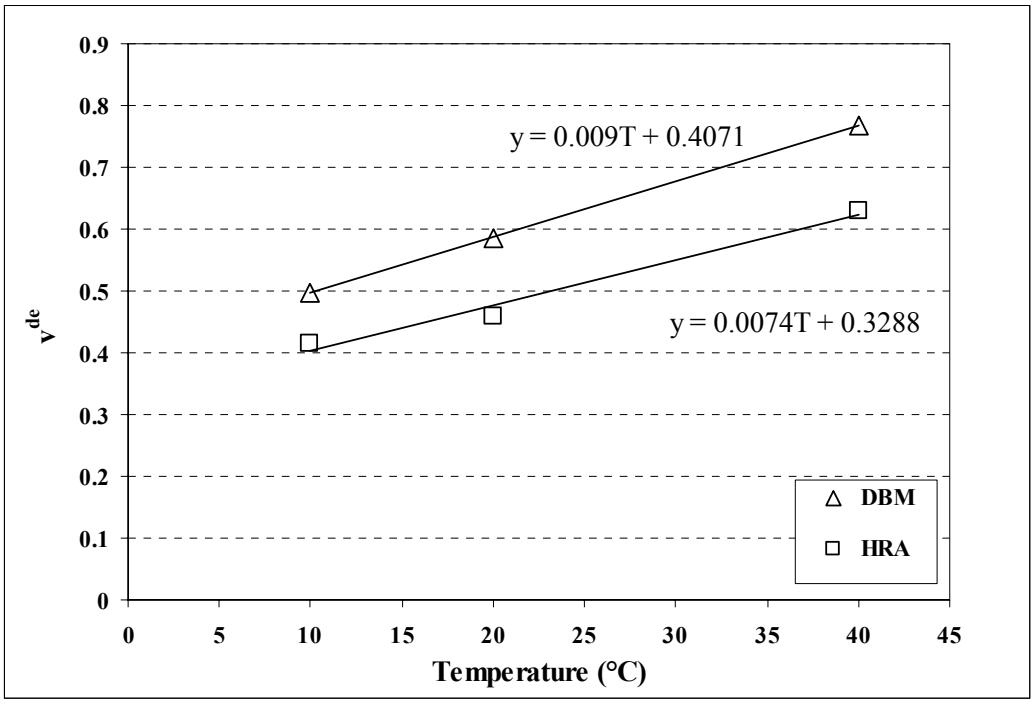

Figure 8.19 Model parameter ν^{de} as a function of temperature.

8.3.3 Viscous Parameters

Model Parameter λ_{inf0}

The value of $\lambda_{\inf 0}$ in Equation 8.20 was obtained for all test conditions by the fitting technique, as explained earlier. Figures 8.20 and 8.21 show the parameter plotted as a function of the applied deviator stress level, temperature and stress ratio for the HRA and DBM mixture, respectively. As can be seen, the parameter $\lambda_{\inf 0}$:

- Decreases with increasing temperature and applied deviator stress level.
- Increases with increasing stress ratio.
- For the DBM, at the same test conditions, is higher than that for the HRA.
- For the DBM is more sensitive to the applied deviator stress level and stress ratio (confinement) than that for the HRA.

- For the HRA is more sensitive to temperature than that for the DBM.

Equations 8.29 and 8.30 were found to well predict the viscous parameter $\lambda_{\inf 0}$ for the HRA and DBM, respectively.

$$\log \lambda_{\inf 0}^{HRA} = (-0.107T - 1.95\log\sigma + 16.62(\eta + 1/3)), \quad \textbf{(8.29)}$$

$$\log \lambda_{\inf 0}^{DBM} = (-0.0961T - 3.2\log\sigma + 13.2(\eta + 1/3)), \quad \textbf{(8.30)}$$

where $\lambda_{\inf 0}$ = viscosity of the dashpot in series, corresponding to the primary and secondary creep regions,

and T, σ and η were defined before. In these equations, the viscosity is in MPa.s, temperature is in Celsius and the deviator stress level is in MPa. Comparing these equations with Equation 8.13, it is resulted that the parameter B in Equation 8.13, independent of temperature, deviator and confining stress level is 16.62 and 13.2 for the HRA30/10 and 10mm DBM mixture respectively. The values predicted by the equations are shown in Figures 8.20 and 8.21 by the solid lines.

Model Parameter n

Parameter n in the formulations of the constitutive model corresponds to the stress-based non-linearity of the steady-state strain rate. It is actually the slope of the straight lines that represent the steady-state viscous strain rate versus the deviator stress level plotted on double logarithmic scales (see Figures 5.32 and 5.33). As seen before, the slope of the lines for the HRA and DBM mixtures, also known as the creep exponent of the steady-state deformation behaviour was found to be 2.9 and 3.9, respectively. The slope of the lines in Figure 8.20 and 8.21 is *(1-n)*.

As seen in Chapter 5, the higher creep exponent for the DBM indicates that the strain rate of the mixture is more sensitive to the applied stress level compared to that for the HRA. The reason for this is not fully understood, but it is thought to be associated with the structure of the DBM mixture in which there is more

aggregate to aggregate contact and less bitumen film thickness. It is well documented that HRA mixture is stronger against cracking than the DBM in which a thinner film of bitumen is between the aggregates. When the aggregates lose their bond by bitumen, the major stress bearing system will be the aggregate contact, which is more sensitive to stress level than the bitumen in HRA.

Model Parameter ν^{v}

As for ν^{de}, the value of equivalent Poisson's ratio for viscous component ν^{v} for each test was calculated as the average of the ratio of radial to axial strain values in the secondary creep region. Figure 8.22 summarises ν^{v} as a function of temperature. As the parameter ν^{v} was observed to be independent of the applied stress, each data point in the figure is the average of the values calculated from the replicate tests at different stress levels. It can be seen that, the parameter increases linearly with increasing temperature. Figure 8.22 shows that the values for the DBM are higher than those for the HRA which is due to higher dilation of the DBM mixture. The equations shown on the figure can be used for calculation of the parameter ν^{v}. As explained before, the values of Poisson's ratio greater than 0.5 can not be used in the model. Therefore, the value of the parameter ν^{v} used for simulation of the permanent deformation of the mixtures by the constitutive model is 0.5.

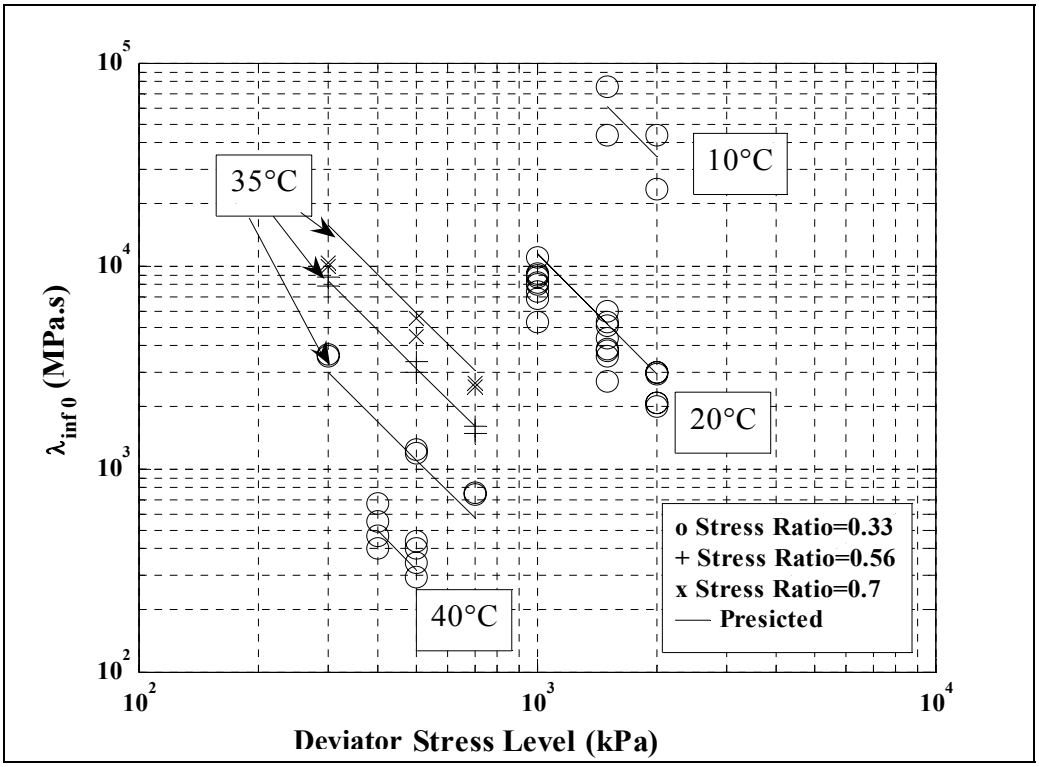

Figure 8.20 Model parameter $\lambda_{\inf 0}$ as a function of the applied deviator stress level and temperature for the HRA30/10.

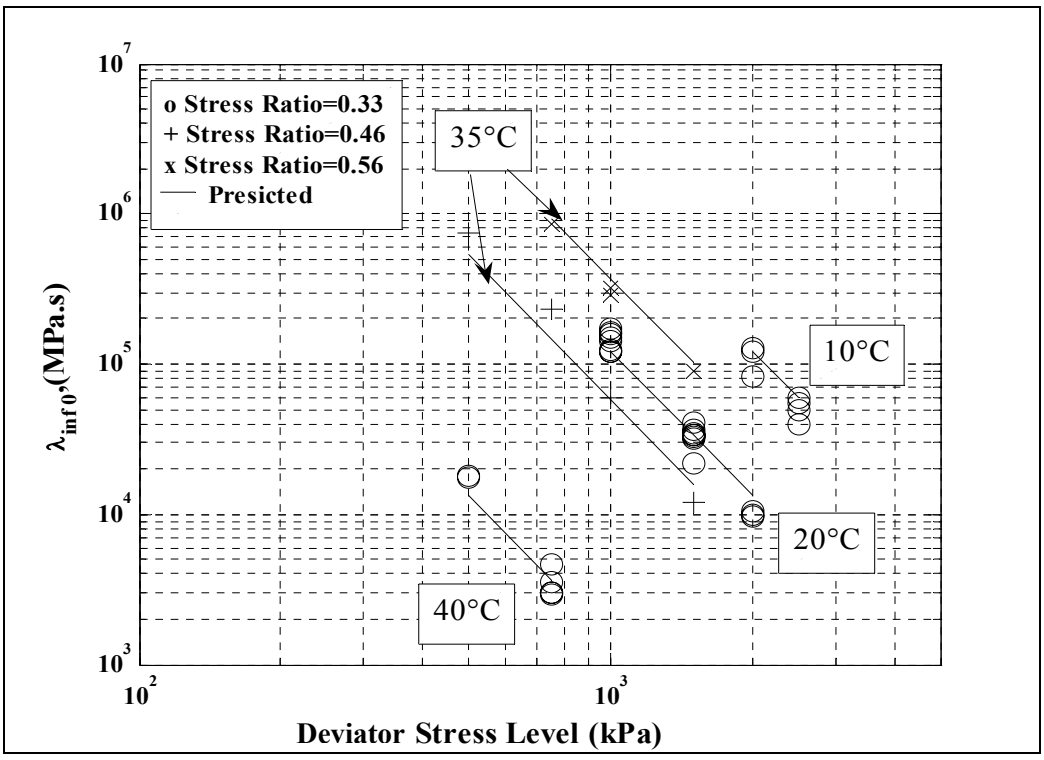

Figure 8.21 Model parameter $\lambda_{\inf 0}$ as a function of the applied deviator stress level and temperature for the 10 mm DBM.

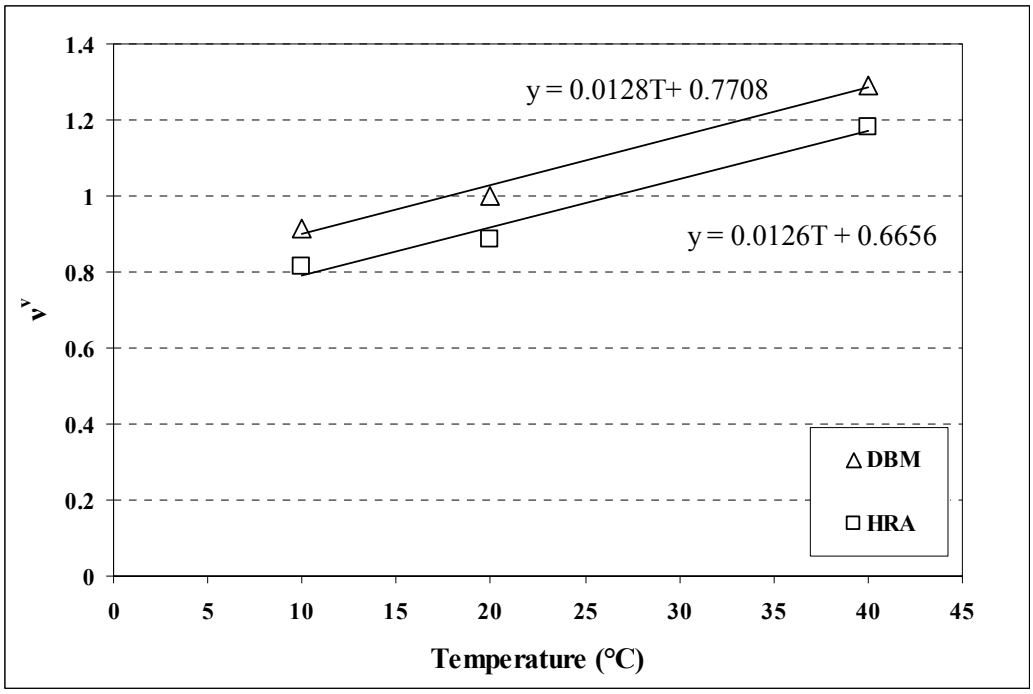

Figure 8.22 Model parameter ν^{v} as a function of temperature.

8.3.4 Damage Parameters

The parameters $\widetilde{C}$ and μ in Equation 8.20 correspond to the effect of damage accumulation on the viscous strain. As explained earlier, they were obtained by fitting the formulation for total strain (Equation 8.20) to the uniaxial creep tests data. It was observed that the parameters do not change with the applied deviator stress level and only vary with temperature.

Figure 8.23 shows the parameter $\widetilde{C}$ plotted as a function of temperature for the HRA and DBM mixtures. As can be seen, the parameter decreases with increasing temperature. The figure also shows that while, at lower temperatures, the values for the HRA are higher than those for the DBM, at higher temperatures, the values for the DBM become higher than those for the HRA mixture. This means that the damage accumulation of the HRA mixture is more sensitive to temperature than that of the DBM mixture. Although the values for this parameter were highly scattered, Equations 8.31 and 8.32 can be used for determination of the parameter for the HRA and the DBM mixture, respectively.

$$\widetilde{C}^{HRA} = 53480T^{-2.41}, \qquad \textbf{(8.31)}$$

$$\widetilde{C}^{DBM} = 6271.3T^{-1.61}. \quad \textbf{(8.32)}$$

Figure 8.24 shows the parameter μ as a function of temperature for the HRA and DBM mixtures. For both mixtures, it decreases linearly with increasing temperature. The figure also shows that the values for the DBM are higher than those for the HRA. The following equations can be used for determination of μ for the HRA and DBM mixtures, respectively.

$$\mu^{HRA} = -0.068T + 7.36, \quad \textbf{(8.33)}$$

$$\mu^{DBM} = -0.0865T + 15.273. \quad \textbf{(8.34)}$$

As explained in Chapter 7, visual examination of the specimens in the triaxial tests showed that the confinement is effective on the crack and damage development in the specimens (see Fig. 7.9). The values of the parameters $\widetilde{C}$ and μ, obtained by fitting the formulation for the total strain (Equation 8.20) to the triaxial creep tests data, showed that they vary with confinement. Figure 8.25 and 8.26 show the parameters $\widetilde{C}$ and μ, respectively, as a function of stress ratio (confinement). It can be seen from these figures that the damage accumulation in the DBM mixture is more sensitive to the confinement than that in the HRA. The formulations shown in the figures can be used for determination of the parameters as a function of stress ratio at 35°C. However, because of the limitation of triaxial creep test data, in terms of range of temperatures and that all the triaxial tests were not continued until failure, a relationship for the parameters, as a function of temperature and stress ratio cannot be obtained here. More experimental work by undertaking triaxial tests over a range of temperatures and stress ratios can be used for obtaining such relationships.

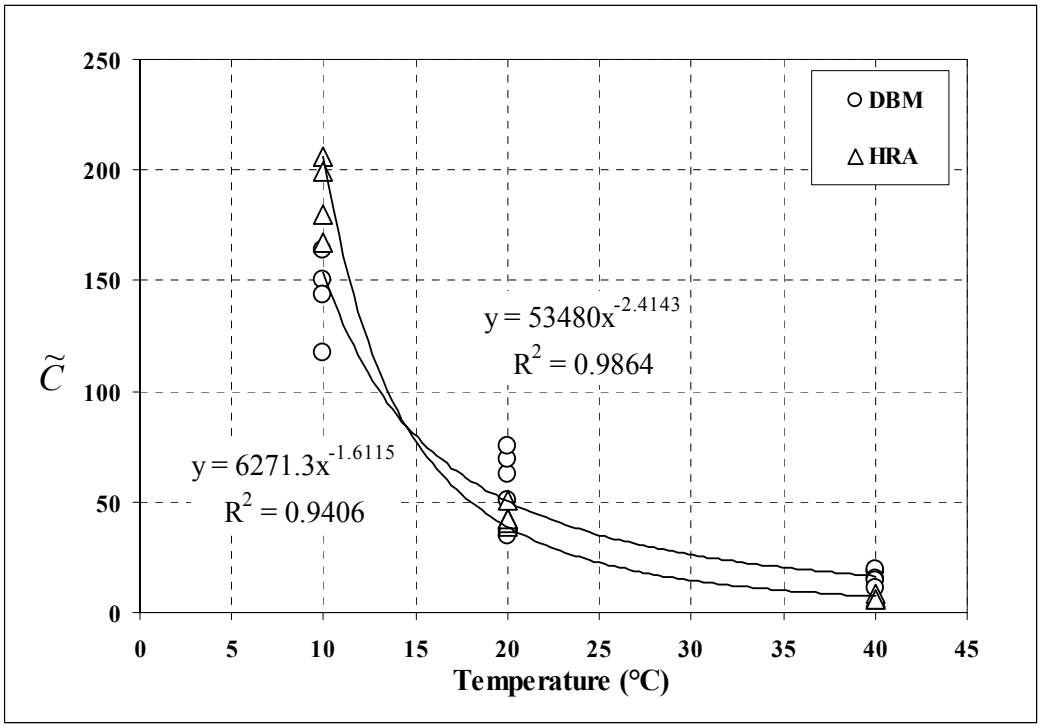

Figure 8.23 Model parameter $\widetilde{C}$ as a function of temperature.

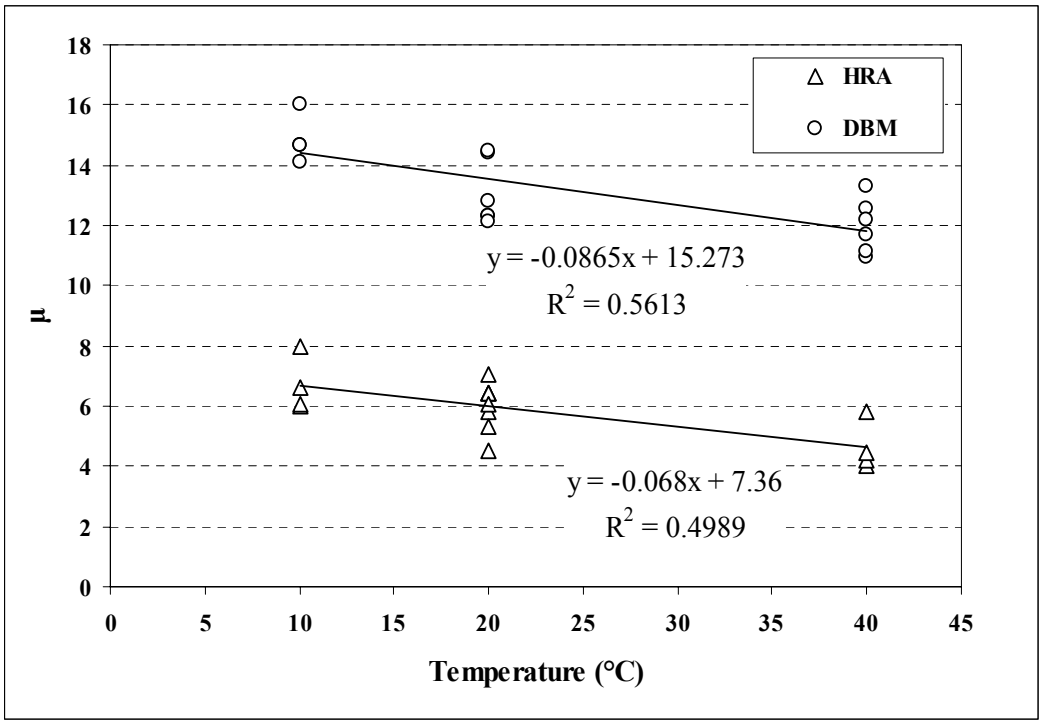

Figure 8.24 Model parameter μ as a function of temperature.

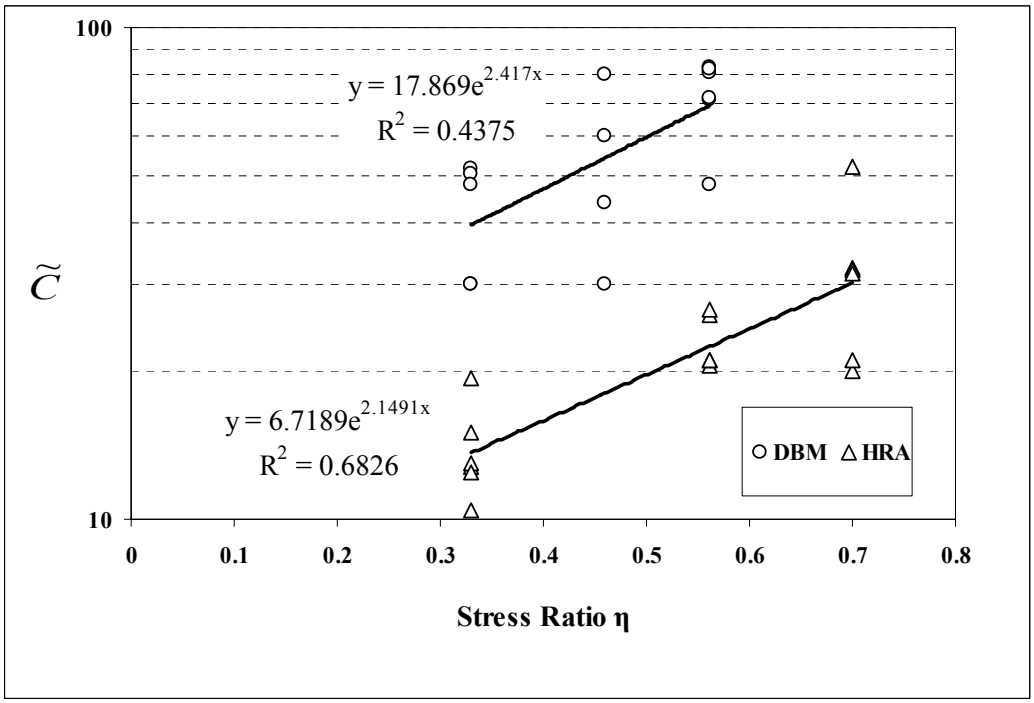

Figure 8.25 Model parameter $\widetilde{C}$ as a function of stress ratio.

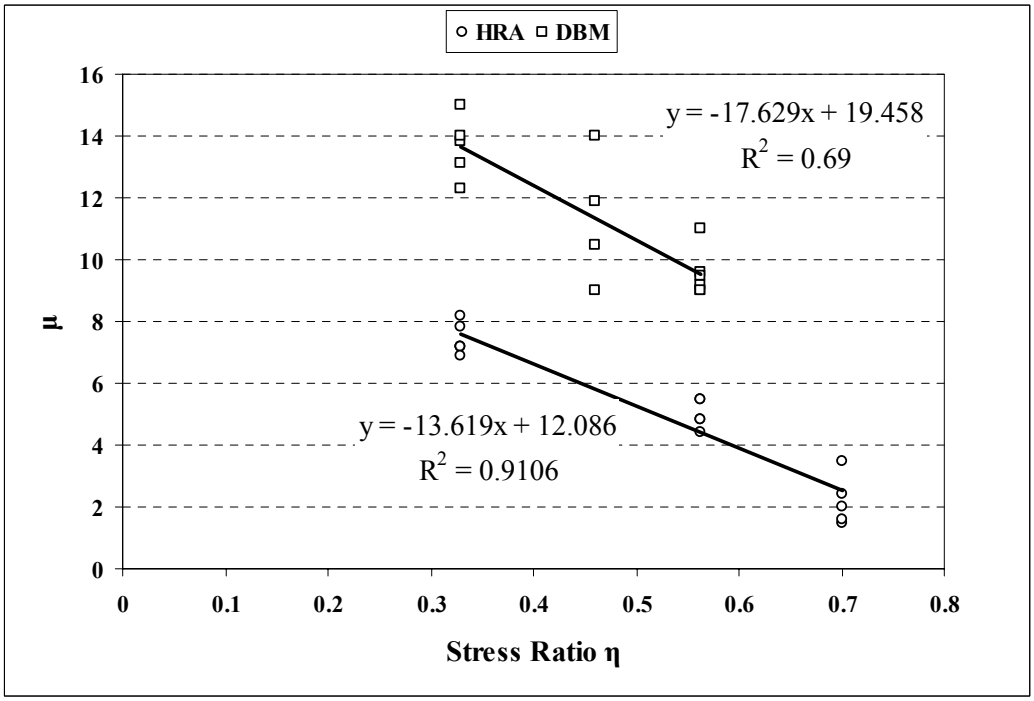

Figure 8.26 Model parameter μ as a function of stress ratio.

8.4 Verification of the Constitutive Model

To verify the constitutive model, the uniaxial creep response of the HRA and DBM mixtures at specified test conditions were predicted and compared with the test results at the same test conditions. The selected test results had not been used in the fitting process for determination of the parameters. Equation 8.20 was used for prediction of creep behaviour by the model, where the values for the model parameters were calculated from Equations 8.21 to 8.34 developed for different parameters. Figures 8.27 and 8.28 show the predicted and test results for the HRA and DBM mixture, respectively. It can be seen that the model can reasonably predict the creep response of the HRA and, with some discrepancies, that of the DBM mixture. Part of the discrepancies between the predicted responses and test results is due to experimental errors such as the effect of air void content variation in different specimens and instrumentation. For the DBM mixture, in this research, more scattered results have been observed. As explained before, the deformation behaviour of the DBM is dominated by the aggregate interlock compared to the HRA which its behaviour is dominated by the mortar of bitumen, filler and sand. The aggregate interlock in the DBM mixture is expected to result in a higher variation in different specimens compared to the mortar in different specimens of the HRA. Therefore, more scattered results were anticipated for the DBM and, as can be seen in Figure 8.28, more difference between the model prediction and the actual response of the mixture.

Figure 8.29 shows a typical single creep recovery test result along with the creep and recovery strains predicted by the constitutive model. Equation 8.20 with no damage effect was fitted to the loading path and using the obtained parameters, shown in Figure 8.29, Equation 8.8 was used for prediction of the recovered strain. It can be seen that the model significantly underpredicts the strains in unloading path. The same behaviour was observed by Stevenson *et al.* [2004]. This is thought to be due to the densification of the mixtures, which remains in the mixture as permanent strain and is not accounted for by the model formulation. While the permanent deformation of the mixtures occurs as a result of viscous deformation and densification, the permanent deformation of the

model is only corresponding to the viscous element. It will be seen later in this section that, the model can more accurately predict the permanent strain of the mixtures after densification. Another difference between recovered strain predicted by the model and the test result is that the rate of recovery for the test is less than that for the model. The reason for this difference is not fully understood, however, it is thought to be due to the effect of aggregate structure and damage of the mixture to decelerate the recovery of the binder in the mixture. The model can more accurately predict the recovered strain by using the parameters as shown in Figure 8.30. Using those parameters in Equation 8.20 with no damage effect, the strain in loading path was predicted. As can be seen, while the recovery response is well fitted by the model, there is an obvious difference between the test result and the response predicted by the model in the loading path.

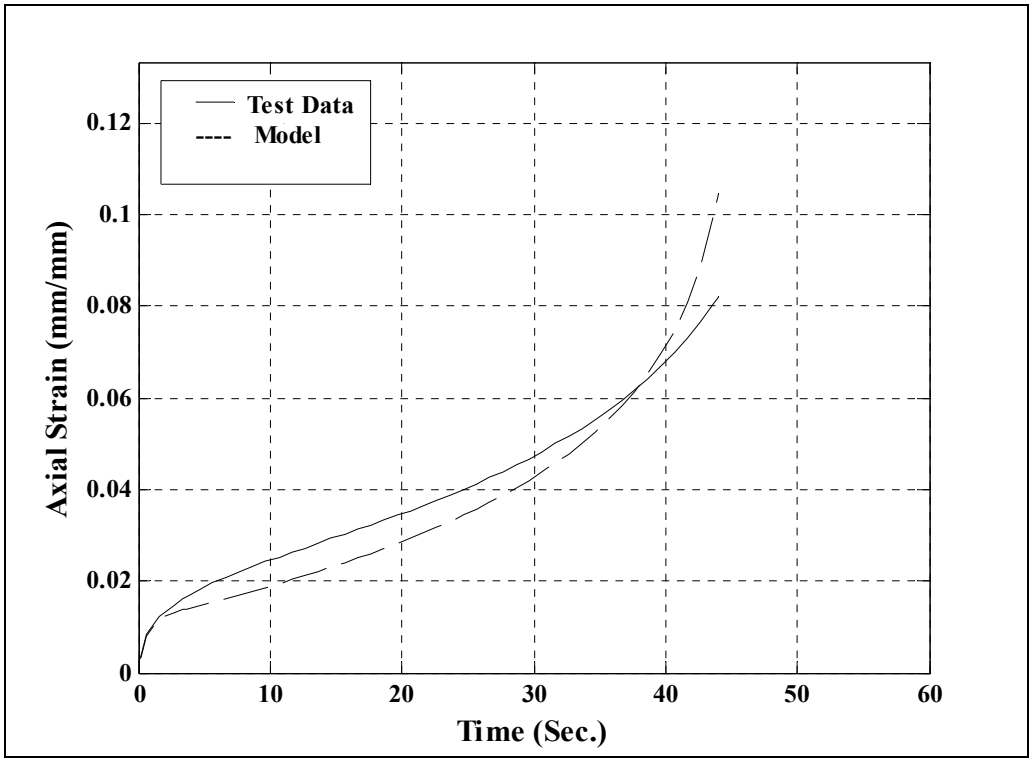

Figure 8.27 Prediction of the uniaxial creep response of the HRA at 20°C (axial stress of 2000 kPa) by the constitutive model.

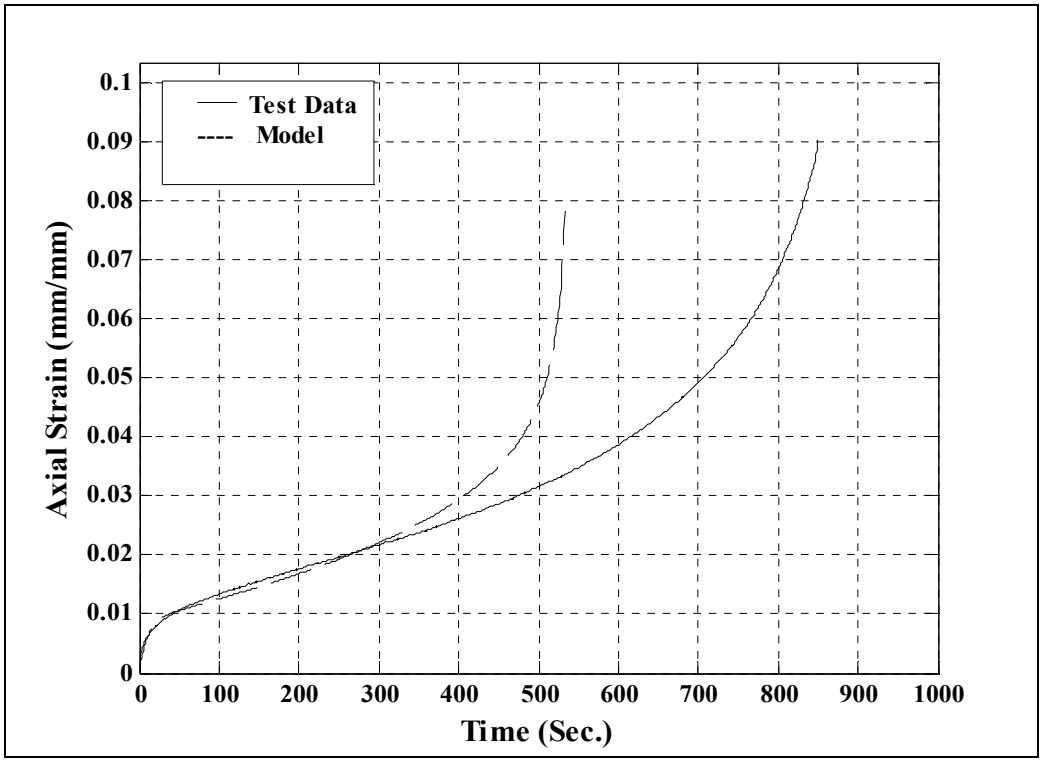

Figure 8.28 Prediction of the uniaxial creep response of the DBM at 20°C (axial stress level of 1500 kPa) by the constitutive model.

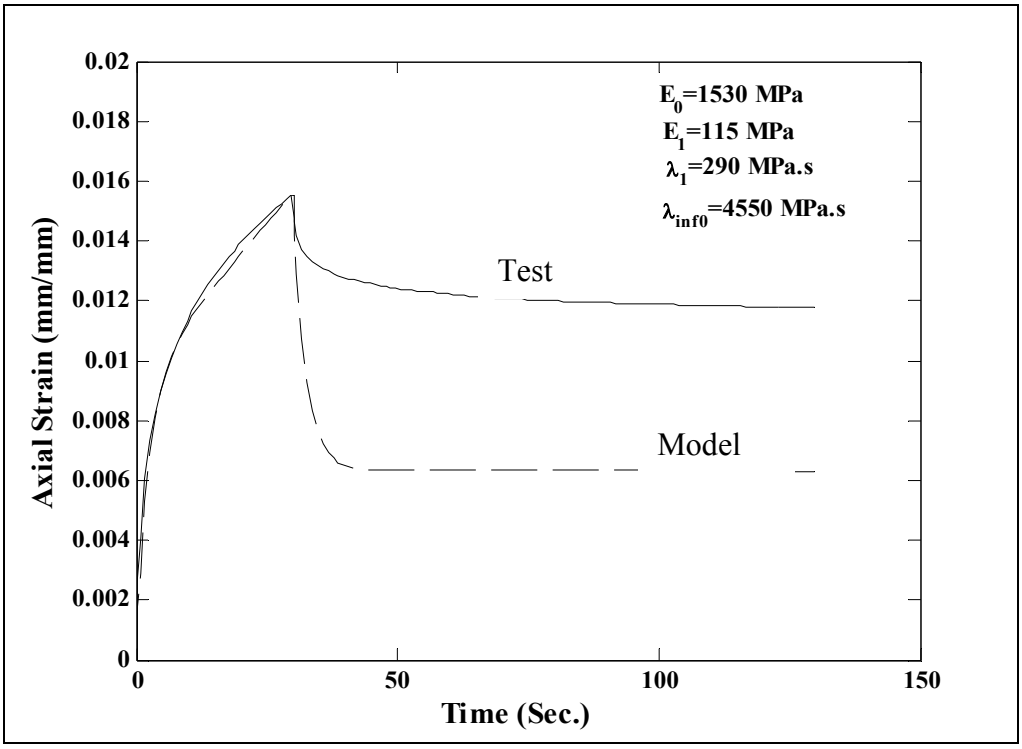

Figure 8.29 A typical recovery response of the model for the HRA at 20°C (axial stress level of 1000 kPa) with the parameters determined from fitting to the loading path.

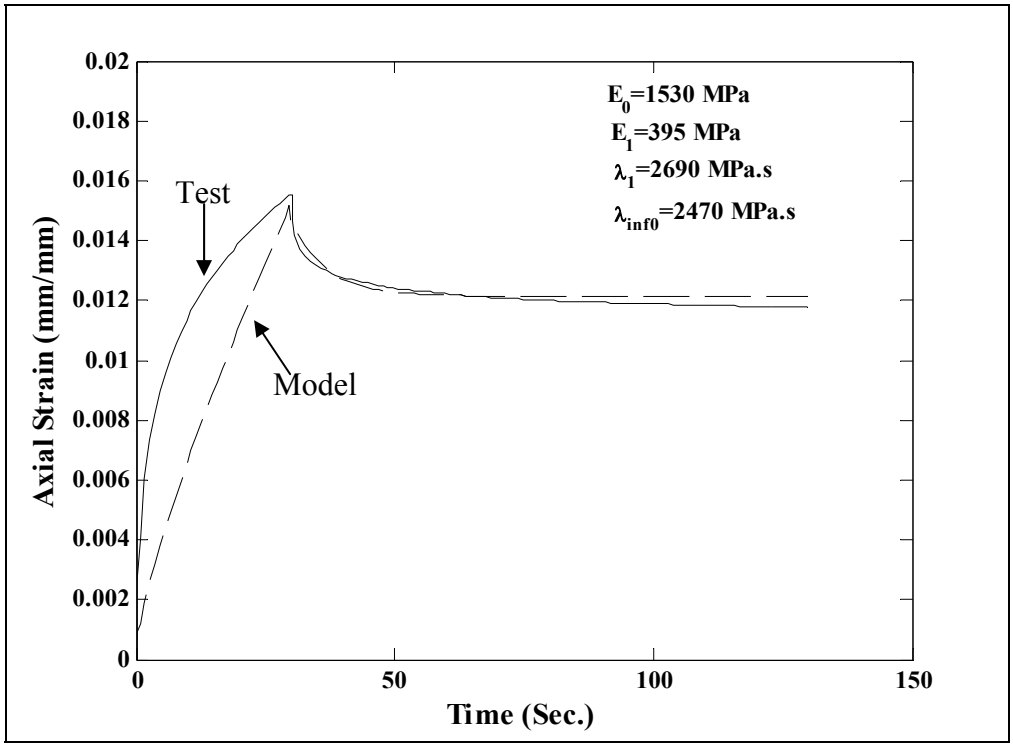

Figure 8.30 A typical creep and recovery response of the model for the HRA at 20°C (axial stress level of 1000 kPa) with the parameters determined from fitting to the unloading path.

Figures 8.31 and 8.32 show typical repeated creep recovery test results for the HRA and DBM mixtures, respectively, at selected test conditions, where the axial strain is plotted as a function of time. As can be seen in the figures, for the DBM mixture, the results after the first cycle, and for the HRA, the results after the second cycle are presented. For the DBM, most of the densification occurred during the first cycle, and for the HRA, it occurs during the first and second cycles. It can be assumed that the densification of the DBM, with a loading time of 60 seconds in each cycle (see Section 6.6), has completed in the first cycle, and that of the HRA, with a loading time of 30 seconds in each cycle, has completed after two cycles. As no formulation was developed for the model parameters as a function of damage accumulation, the model parameters for each cycle were determined by fitting Equation 8.20 (without the damage related constants) to the loading path and used for prediction of the strain in the unloading path using Equation 8.8. The dashed lines in the figures show the model response. It can be seen that, after densification of the mixtures, the model can reasonably predict the recovered strain. However, as can be seen in Figures

8.31 and 8.32, there are some discrepancies between the predicted values and test results, which are attributed to the rate of recovery predicted by the model. As can be seen, the model can not well predict the rate of recovery for the mixtures, where the rate of recovery predicted by the model is higher than that of the test results. This difference was seen to increase with increasing damage accumulation in the mixtures.

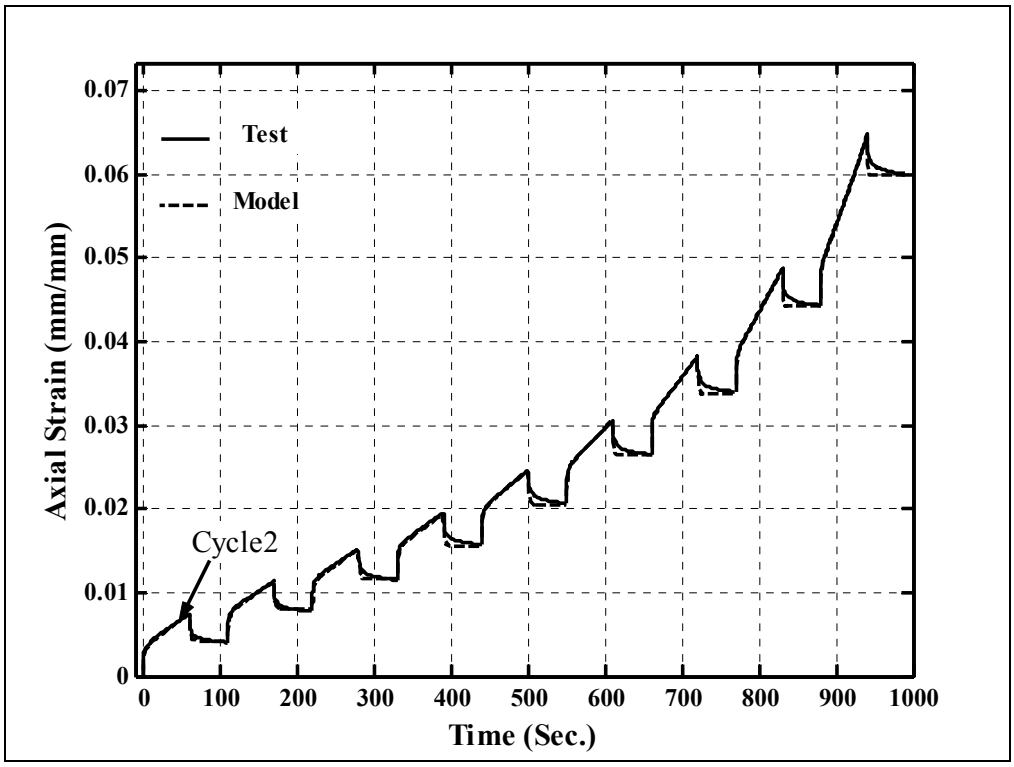

Figure 8.31 A typical repeated creep recovery test result for the DBM at 20°C (axial stress of 1500 kPa) and its response predicted by the model.

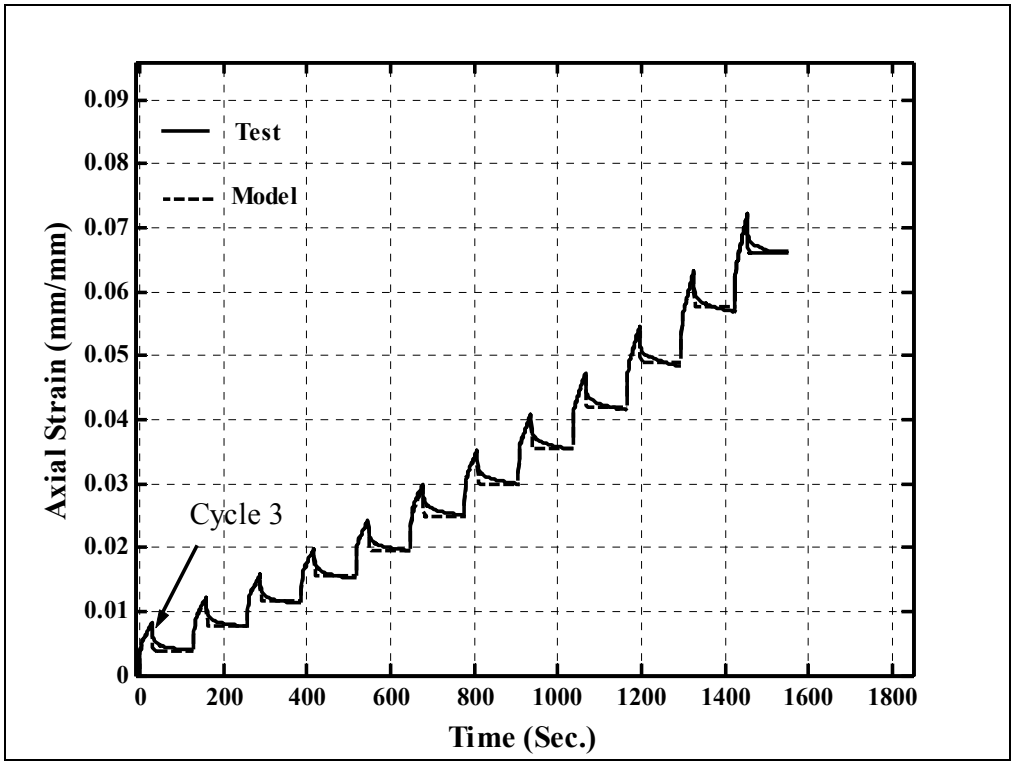

Figure 8.32 A typical repeated creep recovery test result for the HRA at 20°C (axial stress of1000 kPa) and its response predicted by the model.

8.5 Discussion

Several differences and similarities were found between the parameters of the constitutive model for characterisation of the HRA and the DMB mixtures. As the same binder was used for both mixtures, the differences are expected to be due to the structure of the mixtures. The higher volume fraction of aggregate and continuous aggregate grading of the DBM create more interlock resulting in thinner binder films between aggregate particles which give it different creep and recovery characteristics. This results in earlier damage and crack development in the DBM mixture and the steady-state behaviour is reached at a lower axial strain level. Moreover, the structure of the DBM mixture results in a higher stiffness and dilation ratios, and more sensitivity of its stiffness to applied deviator stress level and confinement. The HRA behaviour is dominated by mortar of binder, filler and sand which makes it more sensitive to temperature.

The constitutive model was seen to capture reasonably well the static uniaxial and triaxial creep behaviour of the mixtures. The parameters of the model change with densification of the mixtures and damage accumulation, depending on the

recovery time ΔR. Therefore, it is not appropriate to use the model with the constants determined from the static tests for prediction of the creep and recovery behaviour of the mixture under repeated loading condition. More experimental work needs to be undertaken to establish a quantitative relationship between the parameters, the densification, damage level in the mixtures and the recovery time.

8.6 Conclusions

The following conclusions can be drawn from this chapter:

- The constitutive model was found to predict reasonably well the static creep behaviour of the mixtures.

- The elastic parameter E_0 was found to be independent of applied axial stress level, decrease with increasing temperature and damage in the mixture. The variation of the parameter with temperature was well captured by the WLF equation.

- The delayed elastic parameter E_1 was found to increase with increasing applied deviator stress level and temperature and be independent of stress ratio. At the same test conditions, the value of the parameter for the DBM is higher than that for the HRA mixture. It was also found that the parameter increases with densification of the mixtures and starts to decrease with increasing damage in the mixtures.

- The equivalent of Poisson's ratio for the delayed elastic and viscous components v^{de} and v^{v} increases linearly with increasing temperature. The values higher than 0.5 for these parameters must be replaced by 0.5.

- The delayed elastic parameter λ_1 decreases with increasing applied deviator stress level and temperature and increases with increasing stress ratio. Its variation with densification and damage was found to be similar to that for the parameter E_1.

- The relaxation time of the mixtures τ was found to increase with increasing stress ratio and decrease with increasing temperature and applied deviator stress level.

- The viscous parameter λ_{inf0} decreases with increasing temperature and applied deviator stress level and increases with increasing stress ratio.

- The parameter *n*, which shows the stress-based non-linearity of the steady-state viscous strain of the mixtures, was found to be 3.9 and 2.9, respectively, for the DBM and HRA mixtures.

- The damage related parameters $\widetilde{C}$ and μ were found to be independent of applied deviator stress level and decrease with increasing temperature. The parameter $\widetilde{C}$ increased and the μ decreased with increasing stress ratio.

- The parameters of the model for the DBM mixture were found to be more sensitive to applied deviator and confining stress level than those for the HRA which were more sensitive to temperature.

- Before fully densification of the mixtures, the recovered strain predicted by the model is higher than real recovered strain of the mixtures.

- The recovered strain of the mixtures, after their densification, was found to be well predicted by the constitutive.

- The rate of recovery predicted by the model is higher than that occurred in the tests.

- Ignoring the dilation behaviour of the mixtures causes inaccuracies for prediction of asphaltic mixtures in real pavements.

9 Summary, Conclusions and Recommendations

9.1 Summary

Permanent deformation of asphaltic mixtures in the upper layers of flexible pavements can have a major contribution in the rutting. With the objective of improving the current understanding of the permanent deformation behaviour of asphaltic mixtures, the compressive deformation behaviour of two generic types of asphaltic mixtures traditionally used in the UK Pavements have been studied. These were continuously graded 10 mm dense bitumen macadam (DBM) and a gap graded hot rolled asphalt (HRA). The approach used for this study was to experimentally investigate the deformation behaviour of these mixtures under conditions that the loading time is considerably longer that for the typical traffic (e.g. a parking pavement). This study can be extended to investigate the permanent deformation behaviour of asphaltic mixtures under typical traffic loading. The main properties of the mixtures affecting the permanent deformation under static or slow moving loading conditions are the viscous deformation behaviour, the volumetric response and the recovery behaviour, which were investigated in this research. The viscous deformation is the dominant component of the deformation under static loading. The volumetric

response of asphaltic mixtures under static loading is an important issue affecting the rut profile. It has also been found that the dilation behaviour of asphaltic mixtures can be related to their resistance to permanent deformation. The test results have been used to determine the parameters of a non-linear viscoelastic constitutive model and for its verification.

In this chapter a summary of the research detailed in previous chapters is presented along with the main conclusions of this study and recommendation for future work.

9.1.1 Review of Permanent Deformation Behaviour of Asphaltic Mixtures: Chapter 2

A review of the relevant literature concerned with the permanent deformation of asphaltic materials was provided in this chapter.

The permanent deformation of asphaltic mixtures, well compacted during construction, has been found to be mainly due to the shear deformation associated with the bitumen. The shear deformation of asphaltic mixtures is influenced by the properties of the binder (stiffness, grade etc.) and aggregates (grading, shape, texture, size, etc.), their proportion in the mixture, loading and temperature. The extent of the aggregate and binder effect on the shear deformation of asphaltic mixtures depends on the stiffness of the binder. At a low binder stiffness, the continuously graded mixtures show a higher resistance to permanent deformation, and at a high binder stiffness, the gap graded asphaltic mixtures, which relies on the binder/filler mortar, present a higher resistance to permanent deformation. Characterisation of the permanent deformation behaviour of asphaltic mixtures relies, at least in part, on the understanding of the steady-state deformation behaviour of mixtures. The steady-state deformation behaviour of bitumen and idealised asphaltic mixtures has been extensively studied in a series of research projects at the universities of Cambridge and Nottingham, which were reviewed in Section 2.5. It has been found that the steady-state deformation behaviour of pure bitumen and idealised mixtures is linear at low stress levels and non-linear at higher stress levels. At temperatures

well above the glass transition, the steady-state deformation behaviour of bitumen and idealised mixtures is captured satisfactorily by the modified Cross model, developed by Cheung [1995].

The idealised asphaltic mixtures with high volume fraction of aggregate (more than 65%) were found to dilate under compressive loading. The dilation ratio of the mixtures was found to increase with increasing the volume fraction of aggregate and be independent of the applied deviatoric stress level, temperature and confining stress.

An element of asphaltic material in a flexible pavement undergoes repeated axial, radial and shear stresses under moving traffic loads. Simulation of the realistic response of asphaltic mixtures needs test equipment that can apply the realistic states of stress and environmental conditions. This equipment would be very complicated and has not been developed yet. Static and cyclic uniaxial and triaxial tests, in tension, compression and shear (usually in compression) and wheel tracking tests over a wide range of loading and environmental conditions have been used for investigation of the deformation behaviour of asphaltic mixtures which were reviewed in Section 2.6.

9.1.2 Review of Constitutive Modelling of Rutting: Chapter 3

In this chapter, constitutive models of permanent deformation of asphaltic mixtures used for simulation of pavement rutting were reviewed.

A successful pavement design method requires simulation of pavement materials response under realistic loading and environmental conditions. The constitutive models for simulation of the response of pavement material are formulations which relate the stress and strain in the material over a range of conditions. These relationships are used for analysis of the pavement and prediction of its performance (e.g. deformation and fatigue cracking). Because of the problems associated with the development and implementation of complex models, earlier models used for simulation of asphaltic materials were simple linear elastic or viscoelastic in nature. Assuming linear behaviour for asphaltic materials, various

methods are used for prediction of the rutting of flexible pavements, as reviewed in this chapter. Although asphaltic materials display elastic behaviour under short loading times and/or low temperatures, their behaviour under traffic loading conditions is generally more complex. Assuming linear elastic or viscoelastic behaviour for the asphaltic mixtures results in inaccurate pavement design which can impose costs to highway authorities and users. Due to the availability of advanced numerical methods and developments in computer technology, application of non-linear viscoelastic and elasto-visco-plastic models for simulation of the behaviour of asphaltic mixtures has recently increased.

9.1.3 Binder Testing: Chapter 4

In this chapter, results from constant stress creep and single creep recovery tests on the 70/100 Pen grade bitumen, used as the binder in the mixtures under study, were presented. Using the Dynamic Shear Rheometer (DSR), static shear creep tests were performed over a range of stress levels and temperatures. It was found that the steady-state deformation behaviour of the bitumen is power law creep with the creep exponent of 1 at low stress levels (<100 kPa), indicating linear viscous behaviour, and 2.6 at high stress levels (>500 kPa), indicating non-linear viscous behaviour. At the intermediate stress levels (100 kPa> and <500 kPa), the steady-state deformation behaviour was transition from linear to non-linear viscous behaviour. Using the DSR, single creep recovery tests were performed on the bitumen over a range of shear stress levels and a series of total strains before unloading at 20°C. The results showed that the recovered strain increases with increasing the strain level prior to unloading. This behaviour continues up to a level of the strain prior to unloading after which the recovered strain flattens towards a constant value. The level of the accumulated strain prior to unloading, after which the recovered strain becomes constant, was found to increase with increasing the applied shear stress level. Moreover, it was found that, at the same test conditions, the recovered strain increases with increasing the applied shear stress level.

9.1.4 Uniaxial Tests on Asphaltic Mixtures: Chapter 5

In this chapter the quasi-static uniaxial deformation behaviour of the HRA30/10 and 10 mm DBM mixtures was studied. Constant stress creep tests over a range of stress levels and temperatures, and constant strain rate tests over a range of strain rates and temperatures were conducted on the mixtures. The experimental work for manufacturing test specimens and test set-up and test procedure was detailed. The axial and radial strains and axial stress level were recorded during testing until the specimen failure. The test results were used to investigate the steady-state deformation behaviour and volumetric response of the mixtures and their comparison. Steady-state results from the constant stress creep and the constant strain rate tests were found to be complementary. The deformation behaviour of the two mixtures was found to have some differences and similarities which were attributed to the structure and composition of the mixtures. The steady-state deformation behaviour of the mixtures was found to be well captured by the modified Cross model, developed by Cheung [1995], with linear behaviour at low stress levels (<50 kPa for the HRA and 100 kPa for the DBM) and non-linear power law creep behaviour at high stress levels (>400 kPa). The creep exponent of the HRA and DBM mixtures was found to be 2.9 and 3.9 respectively. The short-term ageing of the bitumen during the mixing operation was found to have no influence on the power exponent of the bitumen. The temperature dependency of the mixtures was found to be well captured by the WLF equation. The axial strain level, at which the mixtures reach the steady-state strain rate, was found to: (i) be generally higher for the HRA, (ii) decrease with increasing temperature and (iii) be independent of applied axial stress level.

Both mixtures were found to dilate under constant stress creep and constant strain rate deformation. After some reduction in volume at the beginning of loading, the volumetric strain was found to increase linearly with the shear strain with a slope, known as the dilation ratio, which was found to be strain rate (only for the DBM) and temperature dependent and independent of applied axial stress level. The mean values of dilation ratio for the HRA and DBM mixtures were found to be 1.2 and 1.4 respectively.

Calculation of Poisson's ratio from the radial and axial strains measurements at the beginning of the tests showed that both mixtures have the same Poisson's ratio which was found to be independent of the applied axial stress level and increases with increasing temperature.

9.1.5 Creep Recovery Tests: Chapter 6

In this chapter the uniaxial creep recovery behaviour of the HRA30/10 and 10 mm DBM mixtures was studied. Single creep recovery tests over a range of stress levels, temperatures and for a series of total strains prior to unloading, and repeated creep recovery tests over a range of loading and recovery times were conducted on the mixtures. The same specimen and test set up, as used in the uniaxial tests, was used in the creep recovery tests. The results were used to investigate the elastic and delayed elastic deformation of the mixtures. The results were also used for determination of model parameters and its verification. The single creep recovery tests on the mixtures revealed that, within the range of test conditions utilised in this study, the recovered strain of the mixtures is independent of temperature and applied axial stress level and depends on the type of mixture and the accumulated strain prior to unloading. The variation of the recovered strain with the accumulated strain before unloading was found to be linear with a slope of 0.25 for the HRA and 0.23 for the DBM. This linear variation continued up to a level of strain before unloading (approximately 0.03 for the DBM and 0.06 for the HRA) after which the recovered strain flattened towards a constant value. It was found that the volumetric strain of the mixtures during the recovery decreases linearly with the shear strain with the same slope as that during creep (dilation ratio). The rate of recovery of the mixtures was found to decrease with increasing accumulated strain and decreasing temperature, and be independent of applied axial stress level. At the same test conditions, the rate of recovery for the HRA mixture was found to be higher than that for the DBM mixture.

From the repeated creep recovery tests it was found that the permanent strain in each cycle increases with decreasing recovery time and increasing loading time in the loading history. Healing of the mixtures, which occurs during the rest

period of each cycle was found to affect the behaviour of the mixtures under repeated cycles of loading and unloading. The healing of the mixtures was found to increase with increasing the recovery time. Plots of the accumulated axial strain prior to unloading and permanent strain against the accumulated loading time were observed to be similar to the static creep curve with the primary, secondary and tertiary creep regions. The slope of the secondary creep region was found to be independent of the loading and recovery times. However, the axial strain level at the beginning of the tertiary creep region increases with increasing recovery time.

9.1.6 Triaxial Tests: Chapter 7

In this chapter, the quasi-static triaxial deformation behaviour of the HRA30/10 and 10 mm DBM mixtures were studied. Static triaxial tests over a range of deviatoric stresses and stress ratios were conducted on the mixtures at 35°C. The axial and radial strains and deviatoric and confining stress levels of specimen confined by air pressure in a triaxial cell were recorded during testing. The test results were used to investigate the steady-sate deformation behaviour and volumetric response of the mixtures under triaxial stress states. The test results also were used for determination of the constitutive model parameters.

Under triaxial stress states, variation of the axial and radial strain with time was observed to be qualitatively similar to that under uniaxial stress states. The triaxial steady-state deformation behaviour of the mixtures was found to be well captured by the modified Cross model with the addition of a stiffening factor which was found to be a function of the applied stress ratio. Over the range of test conditions applied in this study, the triaxial steady-state deformation behaviour of the mixtures was found to be non-linear power law creep. The power exponent of the mixtures was found to be independent of stress ratio. The confining stress was found to have a stiffening effect on the mixtures, where, at the same temperature and deviator stress for a mixture, the steady-state strain rate was found to decrease with increasing stress ratio. The stiffening effect of the confining stress on the DBM mixture was found to be higher than that on the HRA.

Both the HRA and DBM mixtures were observed to dilate under triaxial stress states. The dilation ratio was found to be independent of stress ratio and depends only on the type of mixture.

Both mixtures were found to lock up in triaxial tests performed at a stress ratio higher than a critical value for each mixture. The critical stress ratio of the HRA and DBM was found to be 0.8 and 0.71, respectively.

9.1.7 Determination of Model Parameters: Chapter 8

In this chapter, using the experimental data from tests conducted on the 10 mm DBM and HRA30/10 mixtures, the parameters of the non-linear viscoelastic constitutive model, developed by Collop *et al.* [2003], were determined. The constitutive model was found to well simulate the axial deformation of the mixtures under static uniaxial and triaxial loading.

The elastic modulus E_0 was found to be independent of the applied axial stress level, and decrease with increasing temperature. For each mixture, up to a level of accumulated damage in the mixture, E_0 remains constant. After that level, due to the development of internal cracks in the mixtures, it decreases with increasing the accumulated damage in the mixture. The variation of the parameter with temperature was well captured by the WLF equation.

The delayed elastic parameter E_1 was found to increase with increasing applied deviatoric stress level and temperature and was found to be independent of stress ratio. At the same test conditions, the value of this parameter for the DBM is higher than that for the HRA. It was also found that this parameter increases with densification of the mixtures after which starts to decrease with increasing damage and cracks in the mixtures. The equivalent of Poisson's ratio for the delayed elastic component v^{de} increases linearly with increasing temperature. The values of the parameter for the DBM were higher than those for the HRA. The values of this parameter greater than 0.5 can not be used for the simulation by the constitutive model and must be replaced with 0.5. The delayed elastic parameter of λ_1 was found to decrease with increasing the applied deviatoric stress level and

temperature and increase with increasing stress ratio. Its variation with densification and damage was found to be similar to that for the parameter E_1, as explained above. The relaxation time of the mixtures τ was found to increase with increasing the stress ratio and decrease with increasing temperature and the applied deviator stress level.

The viscous parameter λ_{inf0} was found to decrease with increasing temperature and applied deviatoric stress level and increases with increasing stress ratio. The equivalent Poisson's ratio for viscous component v^v was found to increase linearly with temperature. The values of the parameter for the DBM were higher than those for the HRA. Over the range of test conditions applied in the uniaxial tests all the values of this parameter were greater than 0.5, which must be replaced with 0.5 in simulation by model. The parameter n, which shows the stress-based non-linearity of the steady-state viscous strain rate of the mixtures, was found to be 3.9 and 2.9 for the 10 mm DBM and HRA30/10 mixtures, respectively. The damage related parameters of $\tilde{C}$ and μ were found to be independent of applied deviator stress level and decrease with increasing temperature. The parameter $\tilde{C}$ increases and the μ decreases with increasing stress ratio.

The parameters of the model for the DBM mixture were more sensitive to the applied deviatoric and confining stress level than those for the HRA which were more sensitive to temperature.

Using the formulations developed for the parameters of the model, the axial strain of the mixtures under uniaxial creep was well predicted. The constitutive model was found to over predict the recovered strain of the mixtures before densification. After densification, the recovered strain was well predicted by the model, although there were some discrepancies due to over prediction of the rate of recovery by the model. The model parameters were found to change with the damage accumulation in the mixtures which can be a disadvantage for the model, unless further work be carried out to find accurate relationship between the parameters and damage. Another disadvantage of the model is that it can not

simulate the dilation of the mixtures. This means that the volume change of the mixtures, which could have a major contribution to the permanent deformation, is not considered and therefore permanent deformation of pavements can not be well predicted by this model, unless further work be carried out to modify the model.

9.2 Concluding Remarks

1. The steady-state deformation behaviour of pure bitumen is linear at low stress levels (<100kPa for the bitumen under study) and non-linear power law creep with a power exponent of approximately 2.6 at high stress levels (>500 kPa).
2. The delayed elastic strain of a pure bitumen increases with increasing the accumulated strain prior to unloading. This behaviour continues up to a certain level of accumulated strain prior to unloading, after which the delayed elastic strain remains constant.
3. At the same conditions, the delayed elastic strain of pure bitumen increases with increasing the applied stress level.
4. The steady-state results of constant stress creep and constant strain rate tests are complementary.
5. The steady-state deformation behaviour of the HRA and DBM mixtures is well captured by the modified Cross model, with its temperature dependency well captured by WLF equation.
6. The stress-based non-linearity of the steady-state viscous behaviour of the mixtures is power law creep with a higher power exponent for the DBM.
7. The stiffness of the DBM mixture (resistance to permanent deformation) is more sensitive to the applied stress level (confining and deviatoric) compared to that of the HRA, which is more sensitive to temperature.
8. Short-term ageing of bitumen occurred during mixing operation does not affect its steady-state deformation behaviour.
9. After initial reduction of volume, both the HRA and DBM mixtures dilate under constant stress and strain rate loading where the volumetric strain increases linearly with shear strain, with a slope termed as dilation ratio.

10. The dilation ratio increases with increasing the volume fraction of aggregate and temperature and is independent of deviatoric and confining stress.
11. Similar to pure bitumen, the delayed elastic strain of the mixtures increases with increasing the accumulated strain prior to unloading. This behaviour continues up to a certain level of the accumulated strain prior to unloading, after which the recovered strain remains constant.
12. The value of the accumulated strain, after which the recovered strain is constant, was found to decrease with increasing the volume fraction of aggregate with a lower value for the DBM than that for the HRA.
13. At the same conditions, the delayed elastic strain of asphaltic mixtures increases with decreasing volume fraction of aggregate.
14. The rate at which the delayed elastic strain is recovered decreases with increasing the accumulated strain prior to unloading and volume fraction of aggregate, increases with increasing temperature and is independent of applied axial stress level.
15. Under a repeated identical cycles of loading and unloading the creep and recovery behaviour of asphaltic mixtures change with the number of cycle.
16. Under a repeated loading and unloading cycles, the permanent strain occurred in a cycle decreases with increasing recovery time in the loading history.
17. The triaxial steady-state deformation behaviour of the mixtures under study is similar to that of the uniaxial with a stiffening effect of confining stress.
18. The stiffening effect of the confinement increases with increasing dilation ratio.
19. Beyond a certain level of stress ratio, which was found to equal, approximately, to the inverse of dilation ratio, the mixtures lock up, where no strain develop in the mixtures and it undergoes localised deformation and fails in a weak plane that can not be controlled.
20. Although, the non-linear constitutive model, developed based on Burger's mechanical arrangement, can well simulate the axial strain under uniaxial

and triaxial creep loading; however, it is not suitable for simulation of the mixtures' behaviour under cyclic loading and unloading.

21. The model does not consider the densification of mixtures, and therefore, before fully densification of the mixtures, the recovered strain is over predicted.
22. After fully densification of the mixtures, the model can well predict the permanent and recovered strain of the mixtures, however, it can not well predict the rate of recovery.
23. The parameters of the model, change with mixture condition and need further study to develop formulations to determine them as a function of mixture condition (e.g. densification, damage accumulation and ageing).
24. The model does not consider the dilation of mixture and is not suitable to predict the volumetric change of mixtures which is an important issue in the permanent deformation of flexible pavements.

9.3 Application of Research in Practice

The constitutive model explained in this research, with some simplifications, can be used for analysis of asphaltic pavements under static loading (e.g. parking pavements). Using the parameters determined for the mixtures (HRA30/10 and 10 mm DBM in this study), or using the same methodology for their determination for other types of mixtures, the model can be implemented in a finite element program (e.g. CAPA-3D) to analyse the pavement and predict the permanent deformation under static loading. The results of this research can not be directly used by engineers in practice for prediction of the permanent deformation of typical road pavements. However, by considering some important aspects of deformation behaviour, this research improves the understanding of the permanent deformation behaviour of asphaltic mixtures. This is a step forward and can be extended by further research work for development of more accurate constitutive model to predict the permanent deformation of asphaltic mixtures under realistic traffic loading. Prediction of the permanent deformation of asphaltic mixtures is essential for prediction of rutting which can be included in pavement design methods and used by pavement management systems for management of pavement maintenance.

9.4 Recommendations for Future Work

9.4.1 Deformation Behaviour of Binder and Asphaltic Mixtures

In this research, the deformation behaviour of one type of bitumen and two types of asphaltic mixtures were investigated. The deformation behaviour of other materials like polymer-modified binders, the mixtures with polymer-modified binders and other types of asphaltic mixtures (i.e. Stone Mastic Asphalt, Porous Asphalt etc.) is a topic which merits further study. The steady-state deformation behaviour, creep recovery, triaxial deformation and volumetric behaviour of the mixtures may change with the type of bitumen and aggregate properties which can be studied in future research.

Another recommendation for future research is the investigation of the deformation behaviour of pure bitumen and asphaltic mixtures beyond the range of test conditions utilized in this research. The creep recovery behaviour of pure bitumen was investigated at 20°C in this research and is recommended to be investigated at lower and higher temperatures. The static uniaxial deformation behaviour of the mixtures at the temperatures lower than 10°C and higher than 40°C, which the mixtures may undergo in real conditions, could also be investigated. Investigation of the deformation behaviour of the mixtures at lower stress levels, which the behaviour of the mixtures is predicted to be linear, needs further work. The deformation behaviour of the mixtures under compressive stress conditions was investigated. Investigation of the deformation behaviour under tensile stress is recommended.

Unlike pure bitumen, the recovery behaviour of the asphaltic mixtures was observed to be independent of the applied axial stress level and the recovered strain varied linearly with the total strain before unloading. This is because the range of stress levels applied on the mixtures in the creep recovery tests were narrower than that applied for the pure bitumen. Therefore, it is anticipated that the recovery behaviour of the mixtures shows stress dependency, if it be investigated over a wider range of stress levels than that used in this study.

The repeated creep recovery tests on the mixtures were conducted at 20°C and one stress level for each mixture. The effect of recovery time on the creep and recovery behaviour of the mixtures can be investigated by conducting the repeated creep recovery tests over a wide range of temperatures and stress levels. Investigation of the creep recovery behaviour of the mixtures under tensile loading is also recommended.

In this research, the static triaxial deformation behaviour of the mixtures in compression was studied at 35°C. It is anticipated that the stiffening effect of the confining stress is temperature dependent. Therefore, investigation of the triaxial deformation behaviour of the mixtures over a wide range of temperatures is recommended. Moreover, to have a stress state closer to that experienced in reality, the triaxial deformation behaviour of the mixtures could be studied under cyclic deviator and confining stresses. For application of tensile stress in triaxial tests, development of equipment and performing the static or cyclic triaxial tests in tension will improve the understanding of the realistic behaviour of the asphaltic mixtures. It is also recommend that single and cyclic creep recovery tests be conducted on the mixtures to find out how the confinement affects their recovery behaviour.

As seen in this research, the dilation ratio of the asphaltic mixtures influenced the stiffening effect of the confining stresses on the steady-state deformation behaviour of the mixtures. To improve asphaltic mixtures design, investigation of the dilation ratio of asphaltic mixtures and finding the relationships between the dilation ratio and the aggregate properties like particle size, shape, gradation and volumetric proportion needs more consideration.

9.4.2 Recommendation for the Constitutive Modelling

In this research, the methodologies for determination of the parameters for the constitutive model were explained. The testing programme in this research constitutes the minimum for determination of the parameters for simulation of static uniaxial and triaxial deformation of the mixtures in compression. Determination of the material parameters from tensile uniaxial and triaxial loading conditions is recommended. As observed in this research, the material

parameters of the model varied with densification level and accumulated damage in the mixtures. It is also anticipated that the parameters will change with the binder ageing occurred during the life of the pavement. In addition to the variation of the model parameter with temperature, stress level and confinement, application of the model for simulation of the realistic behaviour of asphaltic mixtures needs accurate relationships between the model parameters and densification, accumulated damage and ageing in the mixtures.

The constitutive model was seen to reasonably predict the response of the mixtures under long loading and recovery times, where the strain in each cycle is large. However, the asphaltic mixtures in the pavement are subject to short loading and recovery times where the induced strain in each cycle is small. Therefore, it is suggested that the model be evaluated for prediction of the response under realistic loading conditions.

In this research the Burger's mechanical model with one Voigt element was utilized. Application of the model with more Voigt elements merits further research.

Although the constitutive model well predicts the creep response of the mixtures, some discrepancies, especially before full densification of the mixtures, was observed between the real recovery response and that simulated by the model. The discrepancies were in terms of rate of recovery and level of recovered strain. More research work is recommended on the modification of the model for a better prediction of the recovery response of asphaltic mixtures. The model was also seen that can not simulate the dilation behaviour of asphaltic mixtures. Modification of the model for considering this property merits further work.

The constitutive model was verified by prediction of the creep behaviour of the mixtures using the element testing data which had not been used in the process of determination of the model parameters. It is recommended that the model be validated by prediction of the deformation of a test pavement made from the mixtures studied in this research. Using the parameters determined in this research, the incremental formulation of the constitutive model can be used in FE codes to analyse the pavement and predict its response.

REFERENCES

Abdulshafi, A., Majidzadeh, K., 'Combo viscoelastic-plastic modelling and rutting of asphalt mixtures.' Transportation Research Record 968, Asphalt Mixtures and Performance, TRB, 1968, pp 19-31.

Airey, G. D., 'Rheological Characteristics of polymer modified and aged bitumens.' Ph.D. Thesis, School of Civil Engineering, the University of Nottingham, 1997.

Anon., 'Bituminous Pavements; Materials, Design and Evaluation.' Residential Course Lecture Notes, Department of Civil Engineering, University of Nottingham, Nottingham, UK, 2000.

Barksdale, R D., 'Compressive stress pulse times in flexible pavements for use in dynamic testing.' Highway Research Record, No.345, Highway Research Board, 1971, pp 32-34.

Barksdale, R D., 'Laboratory evaluation of rutting in base course materials.' 3rd Conference on the Structural Design of Asphalt Pavements, London, 1972, pp 161-174.

Battiato, G., Ronco, F. and Verga, C., 'Moving loads on a viscoelastic double layer: Prediction of recoverable and permanent deformation.' 4th International Conference on the Structural Design of Asphalt Pavements, Ann Arbor, 1977, pp 459-466.

Blab, R. and Harvey, J. T., 'Viscoelastic rutting with improved loading assumptions.' Proc. 9th International Conference on Asphalt Pavements, Copenhagen, Denmark, Volume I, Paper 1, 2002.

Bolk, H. J. N. A. and Van De Loo, P. j., 'The Creep test: a routine method for the design of stable mixes.' Proc. of Eurobitume seminar, the challenge of the future for asphalt roads, London, 1978, pp 121-127.

Bonaure, F., Gest G., Gravois A. and Uge P., 'A new method of predicting the stiffness of asphalt paving mixtures.' Journal of Association of Asphalt Paving Technologists, Vol. 46, 1977, pp 64-104.

British Standards Institution, 'Coated macadams for roads and other paved areas.' BS 4987: Part1, London, 2003.

British Standards Institution, 'Sampling and examination of bituminous mixtures for roads and other paved areas.' Methods of test for the determination of density and compaction,1989.

British Standards Institution. 'Hot rolled asphalt for roads and other paved areas'. BS 594:Part1, London, 2003.

Brodrick, B. V., 'The development and performance of a wheel tracking facility and in-situ instruments for pavement experiments.' MPhil thesis, University of Nottingham, Nottingham, UK, 1977.

Brown, E. R., 'Density of asphalt concrete-How much is needed?' 69th Annual Meeting of the Transportation Research Board, Washington DC, 1990.

Brown, E. R. and Foo, K. Y., 'Comparison of unconfined and confined creep tests for hot mix asphalt.' Journal of Materials in Civil Engineering **6**(2), 1994, pp 307-326.

Brown, S. F., 'Improved framework for predicting permanent deformation in asphalt layers.' Transportation Research Record, No. 537, Pavement and Soil Characteristics, TRB, 1975, pp 18-30.

Brown, S. F., 'Laboratory testing for use in the prediction of rutting in asphalt pavements.' Transportation Research Record, No. 616, Transportation Research Board, Washington D.C., 1976, pp 22-27.

Brown, S. F., 'Material Characteristics for Analytical Pavement Design.' In: **Pell, P. S.**, Ed. 'Developments in Highway Pavement Engineering-1.'London, Applied Science Publishers LTD., 1978a.

Brown, S. F., 'Stiffness and fatigue requirements for structural performance of asphalt mixes.' Eurobitume Conference, London, 1978b.

Brown, S. F. and Bell, C. A., 'The validity of design procedures for the permanent deformation of asphalt pavements.' Proc. 4th Int. Conf. on the Structural Design of Asphalt Pavements, Ann Arbor, 1977, pp 467-482.

Brown, S. F., Austin, G. and Overy, R., 'An instrumented triaxial cell for cyclic loading of clay.' ASTM Geotech. Test, J.3, No. 4, 1980, pp 145-152.

Brown, S. F. and Brunton, J. M., 'An Introduction to the analytical design of bituminous pavements.' 3rd Edition, University of Nottingham, 1986.

Brown, S. F. and Cooper, K. E., 'A fundamental study of stress-strain characteristics of bituminous material.' J. of Association of Asphalt Paving Technologists, Vol. 49, 1980.

Brown, S. F. and Cooper, K. E., 'The mechanical properties of bituminous materials for road bases and base courses.' J. of Association of Asphalt Paving Technologists, Vol. 53, 1984.

Brown, S. F. and Gibb, J. M., 'Validation of experiments for permanent deformation testing of bituminous materials.' Journal of Association of Asphalt Paving Technologists, Vol. 65, 1996, pp 255-289.

Brown, S. F. and Snaith, M. S., 'The permanent deformation characteristics of a dense bitumen macadam subjected to repeated loading.' Journal of Association of Asphalt Paving Technologists, Vol. 43, 1974, pp 224-252.

Burmister, D. M., 'The theory of stresses and displacements in layered systems and applications to the design of airport runways.' Highway Research Board, No. 23, 1943, pp 126-144.

Chehab, G. R., Kim, Y. R., Schapery, R. A., Witzack, M., Bonaquist, R., 'Characterisation of asphalt concrete in uniaxial tension using a viscoelastoplastic model.' Journal of Asphalt Paving Technologists, Vol.72, 2003.

Cheung, C. Y., 'Mechanical behaviour of bitumens and bituminous mixes.' Ph.D. Thesis, University of Cambridge, Cambridge, 1995.

Cheung, C. Y. and Cebon, D., 'Experimental study of pure bitumen in tension, compression and shear.' Journal of Rheology 41(1), 1997, pp 45-73.

Cheung, C. Y. and Cebon, D., 'Deformation mechanisms of pure bitumen.' Journal of Materials in Civil Engineering 9(3), 1997, pp 117-129.

Claessen, A. I. M., Edwards, J. M., Sommer, P. and Uge P., 'Asphalt pavement design - The Shell method.' Proc. 4th Int. Conf. on the Structural Design of Asphalt Pavement, Ann Arbor, 1977, pp 39-74.

Collop, A. C., Cebon, D. and Hardy, M. S., 'Viscoelastic approach to rutting in flexible pavements.' Journal of Transportation Engineering Vol. 121, 1995, pp 88-29.

Collop, A. C., Airey, G. D., and Khanzada, S., 'Creep testing of bitumens using the dynamic shear Rheometer.' Journal of Pavement Engineering 3(2), 2002, pp 107-116.

Collop, A. C., Scarpas, A., Kasbergen, C. and de Bondt, A., 'Development and finite element implementation of a stress dependent elasto-visco-plastic constitutive model with damage for asphalt.' Proc. of 82nd TRB Annual Meeting, Washington D.C., U.S., 2003.

Collop, A. C. and Khanzada, S., 'Permanent deformation behaviour of idealised bituminous mixtures.' Proc. 3rd European symposium on performance and durability of bituminous materials and hydraulic stabilised composites, Leeds UK, 1999, pp 47-58.

Collop, A. C. and Khanzada, S., 'Permanent deformation in idealised "Sand Asphalt" bituminous mixtures.' The International Journal of road Materials and Pavement Design 2(1), 2001, pp 7-28.

Croney, D. and Croney, P., 'Design and performance of road pavements'. 3rd Edition, McGraw-Hill, 1998.

Department of the Environment and Road Research Laboratory., 'Road Note 29-A Guide to the Structural Design of Pavements for New Roads: 3rd Edition.' HMSO, 1970.

Deshpande, V., 'Steady-state deformation behaviour of bituminous mixes.' Ph.D. Thesis, University of Cambridge, Cambridge, 1997.

Deshpande, V. and Cebon, D., 'Steady-state constitutive relationship for idealised asphalt mixes.' Journal of Mechanics of Materials 31(4), 1999, pp 271-297.

Dormon, G. M. and Metcalf, C .T., 'Design curves for flexible pavements based on the layered elastic theory.' Highway Research Board Record, No. 71, 1965, pp 69-84.

Drescher, A., Kim, J. R. and Newcomb, D. E., 'Permanent deformation in asphalt concrete.' Journal of Materials in Civil Engineering 5(1), 1993.

Dunhill, S., 'Modelling the deterioration mechanisms of UK lightly trafficked roads.' Nottingham: School of Civil Engineering, The University of Nottingham, Report nr Report PGR 99031, 1999.

Dunhill, S., 'Quasi-static characterisation of asphalt mixtures.' Ph.D. Thesis, University of Nottingham, Nottingham, 2002.

Eisenmann, J. and Hilmer, A., 'Influence of wheel load and inflation pressure at asphalt pavements - experiments and theoretical investigations.' Proc. 6th Int. Conf. on the Structural Design of Asphalt Pavements, Ann Arbor, 1987, pp 392-403.

Erkens, S.M.J.G., 'Asphalt concrete response -determining, modelling and predicting.' Ph.D Thesis, Delft University of Technology, Delft Netherlands, 2002.

Erkens, S.M.J.G., (S.M.J.G.Erkens@citg.tudelft.nl), re: question, 18 August 2003, Email to: Hasan Taherkhani (evxht@nottingham.ac.uk).

Gibb, J. M., 'Evaluation of resistance to permanent deformation in the design of bituminous paving mixtures.' Ph.D. Thesis, University of Nottingham, Nottingham, UK,1996.

Hadipour, K. and Anderson, K. O., 'An evaluation of permanent deformation and low temperature characteristics of some recycled asphalt concrete mixtures.' J. of Association of Asphalt Paving Technologists, Vol. 57, 1988, pp 615-645.

Harvey, J., Guada, I. And Long, F., 'Effects of material properties, specimen geometry, and specimen preparation variables on asphalt concrete tests for rutting.' J. of Association of Asphalt Paving Technologists, Vol. 69, 2000.

Harvey, J., Weissman, S., Long, F. and Monismith, C. L., 'Tests to evaluate the stiffness and permanent deformation characteristics of asphalt/binder-aggregate mixes, and their use in mix design and analysis.' J. of Association of Asphalt Paving Technologists, Vol. 70, 2001, pp 573-598.

Harvey, J., Guada, I., Monismith, C., Bejarano, M. and Long, F., 'Repeated simple shear test for mix design: A summary of recent field and accelerated test experience in California.' Proc. 9th International Conference on Asphalt Pavements, Copenhagen, 2002.

Henderson, N, (rheology@vilastic.com). Creep Recovery, 3 June 2005, Email to: Hasan Taherkhani (evxht@nottingham.ac.uk).

Hensley, J., 'Establishing hot mix asphalt mixing and compaction temperatures at the project.' Asphalt Institute, Available at: http://www.asphaltinstitute.org/upload/Establishing_HMA_Mixing_Temp_Project_Level.pdf (25/09/2005),1998.

Heukelom, W. and Herrin, M., 'Road design and dynamic loading.' J. of Association of Asphalt Paving Technologists, Vol. 42, 1964, pp 92-125.

Hills, J. F., 'The creep of asphalt mixes.' J. Of the Institute of Petroleum, 59(570), 1973.

Hills, J. F., Brien, D. and Van de Loo, P. J., 'The correlation of rutting and creep tests on asphalt mixes.' Journal of institute of petroleum, London, UK, 1974, pp 74-001.

Hofstra, A. and Klomp, A. J. G., 'Permanent deformation of flexible pavements under simulated road traffic conditions.' Proc. 3rd Int. Conf. on the Structural Design of Asphalt Pavements, London, UK, 1972, 613-621.

Honrych, P., Kerzreho, J-P. and Salasca, S., 'Prediction of the behaviour of a flexible pavement using finite element analysis with non-linear elastic and viscoelastic models.' Proc., 9th International Conference on Asphalt Pavements, Copenhagen, 2002.

Hopman, P. C., Pronk, A. C., Kunst, P. A. J. C., Molenaar, A. A. A. and Molenaar, J. M. M., 'Application of the viscoelastic properties of asphalt concrete.' Proc. 7th Int. Conf. on the Structural Design of Asphalt Pavements, Nottingham, UK, 1992, pp 73-88.

Huang, Y. H., 'Stresses and displacements in viscoelastic layered systems under circular loaded areas.' Proc. 2nd International Conference on the Structural Design of Asphalt Pavements, Ann Arbor, 1967, pp 225-244.

Huang, Y. H., 'Pavement Analysis and Design.' New Jersey, Prentice Hall, 1993.

Huschek, S., 'Evaluation of rutting due to viscous flow in asphalt pavements.' Proc. 4th Int. Conf. on the Structural Design of Asphalt Pavements, Ann Arbor, 1977, pp 497-508.

Kenis, W. J., 'Predictive design procedures - A design method for flexible pavements using the VESYS structural subsystem.' Proc. 4th Int. Conf. on the Structural Design of Asphalt Pavements, Ann Arbor, 1977, pp 100-110.

Khanzada, S., 'Permanent Deformation in Bituminous Mixtures.' Ph.D thesis, University of Nottingham, Nottingham, UK, 2000.

Kim, Y. R. and Little, D. N., 'Evaluation of healing in asphalt concrete by means of the theory of nonlinear viscoelasticity.' Transportation Research Record 1228, Washington, D.C., Transportation Research Board, 1989, pp 198-210.

Kirwan, R. W., Snaith, M. S. and Glynn, T. E., 'A computer based subsystem for the prediction of pavement deformation.' Proc. 4th Int. Conf. on the Structural Design of the Asphalt Pavements, Ann Arbor, 1977, pp 509-518.

Long, F., Govindjee, S. and Monismith, C. L., 'Permanent deformation of asphalt concrete pavements: development of a nonlinear viscoelastic model for mix design and analyses.' Proc. 9th International Conference on Asphalt Pavements, Copenhagen, 2002.

Lu, Y., 'Temperature dependent visco-elasto-plastic evaluation of flexible pavements.' Ph.D. Thesis, South Bank University, London, UK, 1998.

McLean, D. B. and Monismith, C. L., 'Estimation of permanent deformation in asphalt concrete layers due to repeated loading.' Transportation Research Record, No 510, TRB, 1977, pp 14-30.

Monismith, C. L., Alexander, R. L. and Secor, K. E., 'Rheologic behaviour of asphalt concrete.' Journal of Association of Asphalt Paving Technologists, Vol. 35, 1966, pp 400-450.

Monismith, C.L., 'Rutting prediction in asphalt concrete pavements.' Transportation Research Record, No. 616, Soil Mechanics: Rutting in Asphalt Pavements, Embankments on Varved Clays, and Foundations, TRB, 1976, pp 2-8.

Monismith, C. L. and Secor, K. E., 'Viscoelastic behaviour of asphalt concrete pavements.' Proc. of the 1st international conference on the structural design of asphalt pavements, 1962, pp 476-498.

Monismith, C. L. and Tayebali, A. A., 'Permanent deformation (rutting) considerations in asphalt concrete pavement sections.' J. of Association of Asphalt Paving Technologists, Vol. 57, 1988.

Morris, J., Haas, R. C. G., Reily, P. and Hignell, E., 'Permanent deformation in asphalt pavements can be predicted.' J. of Association of Asphalt Paving Technologists, Virginia, 1974.

Murali Krishnan, J. and Rajagopal, K. R., 'Triaxial testing and stress relaxation of asphalt concrete.' Mechanics of Materials, Vol. 36, 2004, pp 849-864.

Nair, K., Smith, W. S. and Chang, C. Y., 'Applicability of a linear viscoelastic characterisation for asphalt concrete.' Proc. 3rd international conference on the structural design of asphalt pavements, Michigan, 1962.

Newcomb, D. E., Struop-Gardiner, M., Olson, R. and Teig, J., 'Traffic densification of asphalt concrete pavement.' Transportation Research Record, Nation Research Council, Washington D.C., TRB, 1997, pp 1-9.

Nunn, M. E., 'Prediction of permanent deformation in bituminous pavement layers.' Transport and Road Research Laboratory. Report nr 29.1986.

Nunn, M. E., Brown. A. and Lawrence, D., 'Standardisation trial of RLAT'. Draft Report, Transport Research Laboratory, 1999.

Ossa, E. A., Deshpande, V. and Cebon, D., 'A Phenomenological Model for the Monotonic and Cyclic Behaviour of Pure Bitumen.' Journal of Materials in Civil Engineering, ASCE, April, 2003.

Ossa E. A., Taherkhani, H. and Collop, A. C., 'Compressive deformation behaviour of asphalt mixtures.' Accepted for Journal of Association of Asphalt Paving Technologists, March 2005.

Ossa, E. A., 'Deformation behaviour of bitumen and bituminous mixes.' Ph.D. thesis, University of Cambridge, Cambridge, UK, 2004.

Owen, D.R.J. and Hinton, E., 'Finite Elements in Plasticity: Theory and Practice.' Swansea, UK, Pineridge Press Limited, 1980.

Pagen, C. A., 'Rheological response of bituminous concrete.' Highway Research Record, No. 67, 1964.

Pagen, C. A., 'Size and thermological relationships of asphaltic concrete.' Proceedings of the Association of Asphalt Paving Technologists, 1968, p 228.

Pagen, C. A., 'Dynamic structural properties of asphalt pavement mixtures.' Proceedings of the 3rd International Conference on Structural Design of Asphalt Pavements, 1972, pp 290-316.

Papazian, H. S., 'The response of linear viscoelastic materials in the frequency domain with emphasis on asphalt concrete.' Proc. 1st Int. Conference on the Structural Design of Asphalt Pavements, Ann Arbor, 1962, pp 454-463.

Pidwerbesky, B. D., Steven, B. D. and Arnold, G., 'Subgrade strain criterion for limiting rutting in asphalt pavements.' Proc. 8th Int. Conf. on the Asphalt Pavements, Seattle, 1997, pp 1529-1544.

Preston, J. N., 'The design of bituminous concrete mixes.' Ph.D. Thesis, University of Nottingham, Nottingham, UK, 1991.

Rahimzadeh, B., 'Linear and non-linear viscoelastic behaviour of binders and asphalts.' Ph.D thesis, University of Nottingham, Nottingham, UK, 2002.

Read, J. M.,' Fatigue cracking of bituminous paving mixtures.' Ph.D. Thesis, University of Nottingham, Nottingham, UK, 1996.

Romain, J. E., 'Rut depth prediction in asphalt pavements.' Proc. 3rd Int. Conf. on the Structural Design of Asphalt Pavements, London, 1972, pp 705-710.

Rowe, G. M. and Cooper, K. E., 'A practical approach to the evaluation of bituminous mix properties for the structural design of asphalt pavements.' J. of Association of Asphalt Paving Technologists, Vol. 57, 1988.

Sayegh, G., 'Viscoelastic properties of bituminous mixes.' Proc. the 2nd International Conference on Structural Design of Asphalt Pavements, 1967, pp 743-755.

Scarpas, A., 'CAPA-3D, Finite Elements System, User's manual, Parts I, II and III.' Delft University of Technology, the Netherlands, 1992.

Scarpas, A., Al-Khoury, R., Gurp, C.A.P.M and Erkens, S.M.J.G., 'Finite element simulation of damage development in asphalt concrete pavements.' International Society for Asphalt Pavements, Eighth International Conference on Asphalt Pavements, University of Washington, Seattle, Washington, 1997, pp 673-692.

Scarpas, A. and Blaauwendrad, J., 'Experimental calibration of a constitutive model for asphalt concrete.' Proceedings of the Euro-C Conference on the Computational Modelling of Concrete Structures, Bagastein, Ostenrijk, 1998, pp 193-202.

Sharma, M. G., 'Viscoelasticity and mechanical properties of polymers.' Pennsylvania, The Pennsylvania State University, 1964.

Shell International Petroleum Company Limited., 'Shell pavement design manual, asphalt pavements and overlays for road traffic.'1978.

Sides, A., Uzan, J. and Perl, M., 'A comprehensive viscoelasto-plastic characterization of sand-asphalt compressive and tensile cyclic loading.' Journal of Testing and Evaluation, 13(1), 1985, pp 49-59.

Sluys, L. J. and de Borst, R., 'Computational Methods in Nom-Linear Solid Mechanics.' Delft, Netherlands, Delft University of Technology: Faculty of Civil Engineering and Geosciences, 2002.

Sousa, J. B., Weissman, S. L., Sackman, J. L. and Monismith, C. L., 'A non-linear elastic viscous with damage model to predict permanent deformation of asphalt concrete mixes.' 72nd Annual Transportation Research Board Annual Meeting, Washington D.C., 1993.

Sousa, J. B. and Weissman, S. L., 'Modelling permanent deformation of asphalt-aggregate mixes.' J. of Association of Asphalt Paving Technologists, Vol. 63, 1994, pp 224-257.

Stevenson, J. L. and Mehta, Y. A., 'Evaluation of creep and recovery curve to characterize asphalt concrete.' Eurasphalt & Eurobitume Congress, Vienna, 2004, pp 1560-1570.

Tan, S. A., Low, B. H. and Fwa, T. F., 'Behaviour of asphalt concrete mixtures in triaxial compression.' Materials and Structures, Issue 172, 1994, pp 474-482.

Tashman, L., Masad, E., D' Angelo, J., Bukowski, J. and Harman, T., 'X-ray tomography to characterise air void distribution in superpave gyratory compacted specimens.' The International Journal of Pavement Engineering, 2002, 3(1), pp 19-28.

Taylor, D. W., 'Fundamentals of soil mechanics.' Wiley, New York, 1948.

Thrower, E. N., 'Methods of predicting deformation in road pavements.' Proc. 4th Int. Conf. on the Structural Design of Asphalt Pavements, Ann Arbor, 1977, pp 540-554.

Uzan, J., Sides, A. and Perl, M., 'Viscoelastoplastic model for predicting performance of asphalt mixtures.' Transportation Research Record 1043, TRB, 1985, pp 78-89.

Uzan, J., 'Asphalt concrete characterisation for pavement performance prediction.' J. of Association of Asphalt Paving Technologists, Vol. 65, 1996, pp 573-607.

Van de loo, P. J., 'Creep testing, a simple tool to judge asphalt mix stability.' J. of Association of Asphalt Paving Technologists, Vol. 43, 1974, pp 253-285.

Van de loo, P. J., 'Practical approach to the prediction of rutting in asphalt pavements: The Shell Method.' Transportation Research Record, No. 616, Transportation Research Board, Washington D.C., 1976, pp 15-21.

Van de loo, P. J., 'The creep test: A key tool in asphalt mix design and in the prediction of pavement rutting.' J. of Association of Asphalt Paving Technologists, Vol. 47, 1978, pp 522-557.

Van der Poel, C., 'A general system describing the visco-elastic properties of bitumen and its relation to routine test data.' J. of Applied Chemistry, Vol. 4, 1954, pp 221-236.

Westergaard, H. M., 'Theory of concrete pavement design.' Proceedings of Highway Research Board, Vol. 1, Part1, 1927, pp 175-181.

Whiteoak, C. D., 'Shell bitumen handbook.' Shell Bitumen UK, 1991.

Witczak, M. W., Bonaquist, R., Von Quintus, H. and Kalush, K., 'Specimen geometry and aggregate size effects in uniaxial compression and constant height shear tests.' J. of Association of Asphalt Paving Technologists, Vol. 69, 2000, pp 733-793.

Zhang, J., Cooley, A.L., Jr., and Kandhal, P. S., 'Comparison of fundamental and simulative test methods for evaluating permanent deformation of Hot-Mix Asphalt.' Transportation Research Record, No 1789, TRB, 2000.

Zone.ni.com, 'Measuring Position and Displacement with LVDTs' National Instruments, available at:
http://zone.ni.com/devzone/conceptd.nsf/webmain/436F6D85DCCAE19086256CEC0072932D#2 (3/07/2006).

Zyczkowski, M., 'Creep damage evolution equations expressed in terms of dissipated power.' International Journal of Mechanical Sciences, Vol. 42, 2000, pp 755-769.